Dissertation

submitted to the

Combined Faculties for the Natural Sciences and for Mathematics

of the Ruperto-Carola University of Heidelberg, Germany

for the degree of

Doctor of Natural Sciences

presented by

Erik Lötstedt, M. Sc.

born in Nacka, Sweden

Oral examination: May 7th, 2008

Laser-assisted second-order relativistic QED processes: Bremsstrahlung and pair creation modified by a strong electromagnetic wave field

Referees: **Prof. Dr. Christoph H. Keitel**

Prof. Dr. Peter Schmelcher

Zusammenfassung

Das primäre Ziel dieser Dissertation ist, das Verständnis von Laser-unterstützten relativistischen Prozessen höherer Ordnungen der Quantenelektrodynamik (QED) zu vertiefen. Dadurch wird eine Formulierung notwendig, die stark Laser-modifizierte fermionische Propagatoren benutzt. Die heute vorliegenden Laserquellen erzeugen routinemäßig elektromagnetische Felder, die stark genug sind, um Elektronen auf Geschwindigkeiten nahe der Lichtgeschwindigkeit zu beschleunigen. Im Unterschied zur Störungsentwicklung der gewöhnlichen QED, erfordert die starke Laser-Materie-Kopplung eine Behandlung aller Ordnungen. In dieser Dissertation wird der Einfluss eines starken Laserfelds auf zwei grundlegende Prozesse der QED theoretisch studiert. Der erste Prozess, Bremsstrahlung eines vom Coulombfeld eines Atomkerns gestreuten Elektrons, wird bei Anwesenheit eines Lasers im resonanten Fall berechnet. Der Wirkungsquerschnitt wird numerisch ausgewertet, mit Hilfe einer Formel, die aus den Feynman-Regeln für starke Felder folgt. Der zweite Prozess, Elektron-Positron-Paarbildung von Photon und Coulombfeld, wird für den Fall untersucht, dass die Feldstärke des Lasers kleiner als die kritische Feldstärke ist. Der totale Wirkungsquerschnitt wird dabei nicht vom Laser verändert, während der differentielle Querschnitt drastisch modifiziert wird. Schließlich wird eine detaillierte Studie und ein neuer Algorithmus für die verallgemeinerte Besselfunktion, eine spezielle Funktion, die in Laser-modifizierter QED natürlich vorkommt, präsentiert.

Abstract

The primary aim of this thesis is to advance the understanding of higher-order laser-assisted relativistic processes within quantum electrodynamics (QED), which necessitates a formulation using fully laser-dressed fermion propagators. This study is motivated by presently available laser sources which routinely produce electromagnetic fields strong enough to accelerate the electron to velocities close to the speed of light. The strong laser-matter interaction requires an all-order treatment, different from the perturbative expansion of the usual QED. In this thesis, the influence of a strong laser field on two fundamental processes of QED is studied theoretically. The first process, bremsstrahlung from an electron scattered at the Coulomb potential of a nucleus, is found to show a resonant behavior in the presence of the laser. The cross section is numerically evaluated from the formula resulting from applying the strong-field Feynman rules. The second process, electron-positron pair creation by a gamma photon and a Coulomb field is studied in the case when the laser field strength is below the critical field. Here the total cross section is unchanged by the laser, while the differential cross section is drastically modified. Finally, a detailed study and a novel evaluation algorithm of the generalized Bessel function, a special function occurring naturally in laser-modified QED, is presented.

In connection with the work on this thesis, the following articles were published in refereed journals:

- E. Lötstedt, U. D. Jentschura, and C. H. Keitel,
  Evaluation of Laser-Assisted Bremsstrahlung with Dirac-Volkov Propagators,
  Physical Review Letters **98**, 043002 (2007).

  [selected for the February 2007 issue of the "Virtual Journal of Ultrafast Science" (`http://www.vjultrafast.org`), publishers: APS, AIP]

- S. Schnez, E. Lötstedt, U. D. Jentschura and C. H. Keitel,
  Laser-Assisted Bremsstrahlung for Circular and Linear Polarization,
  Physical Review A **75**, 053412 (2007).

  [selected for the June 2007 issue of the "Virtual Journal of Ultrafast Science" (`http://www.vjultrafast.org`), publishers: APS, AIP]

Unrefereed report:

- A. Di Piazza, E. Lötstedt, K. Z. Hatsagortsyan, U. D. Jentschura, and C. H. Keitel,
  QED effects in strong laser fields,
  in "ILIAS Ion and Laser beam Interaction and Application Studies", Progress Report of the PHELIX theory group, ed. P. Mulser, T. Schlegel, (GSI, Darmstadt, Germany, 2008), in press.
  Preprint appended in Appendix C.3.

Submitted preprint:

- E. Lötstedt, U. D. Jentschura, and C. H. Keitel, *Laser Channeling of Bethe-Heitler Pairs* (2008).
  Preprint appended in Appendix C.1.

Completed preprint:

- E. Lötstedt, U. D. Jentschura, and C. H. Keitel, *Bethe-Heitler Pair Creation Assisted by a Subcritical Laser Field* (2008).
  Preprint appended in Appendix C.2.

Contents

1 Introduction **11**

1.1 Notation and conventions 16

1.1.1 Units 16

1.1.2 Dirac matrices and metric 17

2 The relativistic laser-dressed electron: classically and quantum mechanically **19**

2.1 The motion of a classical, relativistic electron in a laser field 19

2.1.1 Solution of the equations of motion by the Hamilton-Jacobi method . . 19

2.1.2 Direct numerical solution 22

2.2 The Volkov solution 23

2.2.1 Derivation of the Volkov solution 23

2.2.2 Positron Volkov states and charge symmetry 26

2.2.3 Fourier expansion of the Volkov solution and classical-quantum correspondence 26

2.2.4 Generalized Bessel functions from the Floquet ansatz 28

2.2.5 Laser dressed Green's function: the Dirac-Volkov propagator 31

3 Laser-assisted bremsstrahlung **35**

3.1 Introductory remarks 35

3.1.1 Validity of the approximations made in the description of the laser field 36

3.2 Laser-induced Compton scattering: photon emission by a laser-dressed electron 37

3.2.1 Discrete level interpretation of the Compton scattering matrix element . 41

3.2.2 Decay width of Volkov states 43

3.3 Bremsstrahlung matrix element and cross section 44

3.3.1 Matrix element for linear polarization 44

3.3.2 Gauge invariance 49

3.3.3 Differential cross section 50
3.3.4 Limit of vanishing laser field 51
3.3.5 Matrix element for circular polarization 52
3.4 Resonances in the laser-dressed propagator and unphysical infinities 53
3.4.1 Regularization by imaginary energy 54
3.4.2 Validity of the imaginary energy method and other ways of regularization 55
3.4.3 Divergence due to the infinite range of the Coulomb field 57
3.5 Numerical results for different laser intensities and photon emission angles . . . 58
3.5.1 Parameters used for evaluation 59
3.5.2 Comments on the numerical evaluation 60
3.5.3 Numerically evaluated spectra 63
3.5.4 Comparison with the free propagator 66
3.6 Comparison with the nonrelativistic laser-assisted bremsstrahlung cross section 70
3.6.1 Derivation of the first Born matrix element for laser-assisted bremsstrahlung in the dipole approximation 70
3.6.2 Demonstration of the correct nonrelativistic limit of the relativistic cross section 73

4 Laser-assisted pair creation **77**
4.1 Introduction 77
4.2 Matrix element and cross section for laser-assisted pair creation in a linearly polarized laser field 80
4.2.1 Matrix element 80
4.2.2 Regularization of the propagators 81
4.2.3 Cross section 82
4.3 Numerical results and discussion on laser-assisted pair creation: gamma photon and laser wave counter propagating 83
4.3.1 Energy cutoff 83
4.3.2 Resonances and competing processes 86
4.3.3 Apparent singularity 86
4.3.4 Angular distribution 87
4.3.5 Total cross section 87
4.4 Numerical results and discussion on laser-assisted pair creation: collinear gamma photon and laser wave 90
4.4.1 Simplification of the matrix element in the collinear geometry 90

4.4.2 Angular distribution: focusing of the produced pairs 91
4.4.3 Total cross section 94
4.4.4 Experimental realization 94

5 An essential ingredient of laser-modified QED processes: generalized Bessel functions 99
5.1 On special functions in general 99
5.2 Usual Bessel functions 100
5.2.1 Basic properties of the usual Bessel function 100
5.2.2 Saddle point approximation and cutoff properties 101
5.2.3 Miller's algorithm for numerical evaluation 102
5.3 Generalized Bessel functions 104
5.3.1 Basic properties 104
5.3.2 Saddle point approximation and cutoff properties 107
5.3.3 Generalized recursive Miller's algorithm for generalized Bessel functions 113
5.3.4 Explanation of the stability of the generalized recursive Miller's algorithm 118
5.3.5 The function S_n 120

6 Conclusions and outlook 125
6.1 General conclusions and summary of obtained results 125
6.2 Outlook 127

A Basics of strong-field QED 129
A.1 The Furry picture in the presence of a strong laser field 129
A.2 Cutkosky's rules and the optical theorem 131
A.3 Crossing symmetries 134

B Completeness and gauge invariance 137
B.1 Demonstration of the completeness property of the function $E(x, p)$ 137
B.2 Demonstration of gauge invariance 139

C Appended preprints of completed / submitted papers 143
C.1 Laser channeling of Bethe-Heitler pairs 143
C.2 Bethe-Heitler pair creation assisted by a subcritical laser field 148
C.3 QED effects in strong laser fields 158

Bibliography **163**

Acknowledgements **177**

Chapter 1

Introduction

The theory of quantum electrodynamics (QED) describes the interaction between fundamental, charged particles like the electron, and light. Founded by Dirac in the 1930's with the invention of the relativistic wave equation bearing his name, and finalized in the 1950's by Feynman, Tomonaga and Schwinger, QED remains one of the most successful scientific theories ever. Predictions made by QED agree with experiment with up to 12 significant figures [87], with further improvements, both theoretically and experimentally, to be expected. The diagrammatic technique introduced by Feynman, the "Feynman diagrams", proves to be a very powerful tool to organize the terms in the perturbative expansion of various physical quantities, such as the gyromagnetic ratio of the electron or the cross section for Compton scattering. One thing is sure: Results obtained by flawless calculations made according to the rules of QED will be believed by anyone. There is no doubt of the soundness and correctness of QED, once correctly applied.

As already mentioned, QED deals with the interaction of matter such as electrons, positrons or muons, with external fields such as photons or the Coulomb field. The textbook examples all deal with problems where the field is weak: The scattering of an electron by the field of a nucleus (Mott scattering), the scattering of a photon by a free electron (Compton scattering), creation of an electron-positron pair by absorption of two photons, to name a few. In all the preceding examples the external field is assumed to be weak, so that the main contribution to the quantum mechanical amplitude is given by the first term in the perturbation series, and the next order terms are expected to be smaller by the order of the fine-structure constant $\alpha \approx 1/137$. As a consequence, in the case of oscillating photon fields, the cross sections are independent of the amplitude of the field. Naturally, the next question to ask is what happens if the external field considered is strong. For a field sufficiently strong, it is inevitable that at some point perturbation theory will break down. If we limit our discussion to strong fields that may be produced in the laboratory, and thereby omit the astrophysically interesting case of ultra-strong magnetic fields (for example around pulsars, see calculations in [9, 12, 55] and [63, 74, 77, 79]), two types of strong fields are perceivable:
(1). The Coulomb field around heavy nuclei. In the case of the Coulomb interaction, the expansion parameter is $Z\alpha$, where Z is the nuclear charge number. For small Z this expansion makes sense, but is clearly not applicable for high-Z atoms like lead or uranium. The theory of QED in a strong nuclear field has advanced very far, see for example [78, 88, 107] for high-

precision calculations in heavy ions, or [19,75,146,168] for reviews of pair production in heavy ion collisions. Especially interesting is here the case of a Coulomb potential with charge number $Z > 1/\alpha \approx 137$, since the ground state dives into the Dirac sea, and spontaneous production of electron-positron pairs is expected. In the case of a strong Coulomb field, two types of nonlinear effects of QED that have actually been measured, apart from the high-precision measurements mentioned above, are Delbrück scattering [3, 85, 111] and photon splitting [2, 100]. Delbrück scattering is the classically forbidden scattering of a photon in the Coulomb field of a nucleus, photon splitting is the splitting of one initial photon into two photons with the same total energy in a nuclear Coulomb field.
(2). The electromagnetic field produced by a laser. Here the expansion parameter with respect to the laser field is

$$\xi = -ea/m, \tag{1.1}$$

where $e = -|e|$ is the charge of the electron, m is the electron mass and a is the peak value of the vector potential of the laser field. The peak electric field E of the laser is related to a as $E = a\omega$, where ω is the frequency, meaning that the parameter ξ describes the amount of work performed by the peak electric field of the laser over one laser period, scaled with the electron mass m. Note that we will use relativistic units such that $\hbar = c = 1$, where $\hbar$ is the reduced Planck constant and c is the speed of light, throughout this thesis, for further discussions of units and notation used we refer to section 1.1. Present-day lasers routinely reach values where ξ is of the order of unity up to $\xi = 10^2$ [106, 161], and therefore a nonperturbative approach is called for when describing the interaction between electrons and strong laser fields.

Modern lasers can be divided into two categories: (a). Low-frequency high-power lasers. Lasers of this kind have low frequency of order 1 eV, but can deliver high intensities, that is, large electric field amplitudes. The current record is an intensity of 10^{22} W/cm^2 [8, 179], which corresponds to a value of $\xi = 300$. Such high intensities has been made possible with the technique of chirped pulse amplification [119]. There are also two newly started projects: the Extreme Light Infrastructure (ELI) [65], and the European High Power laser Energy Research facility (HiPER) [80], both aiming at extreme intensities of up to order 10^{26} W/cm^2.
(b). The other class is the high-frequency, low-power laser, represented by the X-ray Free Electron Laser (X-FEL). At present intensities of order 10^{16} W/cm^2 can be achieved at a frequency of 100 eV [53]. This leads to a value $\xi = 3 \times 10^{-3}$, so that this regime can be treated with perturbation theory. According to an optimistic view in [151], with future upgrades of the FLASH facility in Hamburg, it could be possible to reach intensities as high as 10^{28} W/cm^2 at frequencies of 10 keV, if focusing to the diffraction limit of the laser beam can be achieved.

High intensities imply that the motion of the electron in the field of the laser becomes relativistic. A measure of when the transition to the relativistic regime starts is when the mean kinetic energy, or the ponderomotive energy U_p, of the electron becomes of the same order as its rest mass. For a nonrelativistic electron in an oscillating electric field $E\cos(\omega t)$ we have from Newton's equation of motion

$$m\frac{\mathrm{d}^2x}{\mathrm{d}t^2} = eE\cos(\omega t), \tag{1.2}$$

which leads to a kinetic energy, assuming the electron starts at rest,

$$U_{\mathrm{kin}} = \frac{1}{2}m\left(\frac{\mathrm{d}x}{\mathrm{d}t}\right)^2 = \frac{1}{2m}\left(\frac{eE}{\omega}\sin(\omega t)\right)^2 = \frac{m}{2}\xi^2\sin^2(\omega t). \tag{1.3}$$

The peak nonrelativistic velocity is thus ξ. Averaging Eq. (1.3) over one period of the oscillation we finally obtain the ponderomotive energy as

$$U_p = \overline{U_{\text{kin}}} = \frac{e^2E^2}{4m\omega^2} = \frac{e^2a^2}{4m} = \frac{m}{4}\xi^2. \tag{1.4}$$

The condition $U_p = m$ gives $\xi = 2$. In the relativistic regime the concept of a ponderomotive potential is not as straightforward, but can still be defined [17]. As we will see in section 2.1, here not only the electric field of the laser but also the magnetic component will contribute to the acceleration of the electron.

With these high-power lasers comes a field of research, which we may call "laser-modified" QED. The goal is to investigate how the presence of a strong laser field modifies the fundamental processes of QED, and how they depend on the laser parameters amplitude, frequency and polarization, et cetera. The laser also opens up new reaction channels, which means that processes that were forbidden by energy-momentum conservation become possible by virtue of the energy and momentum provided by the field. Laser-modified QED was initiated in the 1960's, long before the advent of powerful laser sources, with the seminal papers [38, 129, 147]. Very important is that with the experimental availability of ultra-intense laser facilities and bright prospects of pushing the intensity-limits even further, even exotic processes in laser-modified QED can be experimentally verified. We divide the processes into two groups, depending on if they can occur in absence of the field:
Laser-induced processes. Here the laser is necessary for something to happen. To this group belong among others electron-positron pair creation by a non-laser mode photon [105,129,147], photon emission by a laser-dressed electron (also called laser-induced Compton scattering) [38, 129, 138], which was only recently observed in experiment [6, 61, 97, 110, 116], pair production by a Coulomb and laser field [58, 89, 95, 96, 112, 114, 121–124, 167, 176], and splitting of a photon in a laser field [57].
Laser-assisted processes. To this group processes belong that are allowed without the laser, and are modified in its presence. All laser-assisted scattering fall in this group, such as laser-assisted Coulomb scattering (also called Mott scattering) [52, 139, 169], electron-electron scattering (or Møller scattering) [35, 36, 130, 140, 158] and laser-assisted Compton scattering (here one non-laser mode photon scatters of a laser-dressed electron, to be distinguished from laser-induced Compton scattering which is the emission of a non-laser mode photon from a laser dressed electron) [23, 131]. Also light emission in the collision of charged particles, bremsstrahlung, has been considered with an external laser field [33, 60, 90, 104, 157, 164]. Particle decay can be modified by the laser: [4, 22, 154].

For the processes that are of intrinsically quantum nature, which would not occur in classical electrodynamics [84], there appears another parameter besides ξ, called χ, that will govern the probability of the process in question. An invariant definition of χ is

$$\chi = -e\frac{\sqrt{\left|\left(F^{\text{peak}}_{\mu\nu}p^\nu\right)^2\right|}}{m^3}, \tag{1.5}$$

where $F^{\text{peak}}_{\mu\nu}$ is the peak value of the field tensor $F_{\mu\nu} = \partial_\mu A_\nu - \partial_\nu A_\mu$ and p^ν is the four-momentum of the incoming particle involved, electron or photon. For a massive particle, we

can write Eq. (1.5) in the rest frame of the particle as

$$\chi = \xi \frac{\omega}{m}. \tag{1.6}$$

Since there is no rest frame for photons, for a probing photon with momentum k' we have instead

$$\chi = 2\xi \frac{\omega}{m} \frac{\omega'}{m}, \tag{1.7}$$

in a frame where the photon with frequency ω' is counterpropagating with the laser wave with frequency ω. The physical meaning of χ is the amount of work, in units of m, that the field performs (at its peak value) over the Compton wavelength $\lambda_C = 1/m$ of the particle. We have

$$\text{Work} = \text{Force} \times \text{Distance} = ea\omega\lambda_C = \xi\omega. \tag{1.8}$$

According to the seminal work by Sauter [162] and later by Schwinger [165], pairs will be produced spontaneously out of vacuum by a static electric field. However, the production rate will be exponentially damped unless the field exceeds the so-called critical field, which in our notation corresponds to $\chi = 1$. This conclusion holds for other field-configurations as well: For the field to participate in the pair-production process, the corresponding parameter χ must be close to unity. We also note that even though ξ [see Eq. (1.1)] may be large, χ is small for particles at rest, if an optical laser is assumed. As an example, we have $\chi = 4 \times 10^{-4}$ for an infrared laser with frequency $\omega = 1$ eV, $\xi = 200$, and corresponding intensity $I = 4 \times 10^{22}$ W/cm^2. To overcome this obstacle, we note that Eq. (1.5) is valid in the rest frame of the probing particle. Therefore, if a particle beam with gamma factor γ, is used to collide head-on with the laser, the laser frequency in the rest frame of the particle beam is blue-shifted or enhanced with a factor of approximately 2γ. This was the scheme employed in the experiment performed at the Stanford Linear Accelerator Center [16, 39, 41], where an electron beam of 50 GeV was collided with a high-power, low-frequency laser. Here nonlinear Compton scattering, with up to four laser photons participating, produced high-frequency gamma rays (frequency of the order 30 GeV) which subsequently decayed inside the laser to form electron-positron pairs. In this experiment, peak values $\chi = 0.25$ and $\xi = 0.4$ were obtained. Unfortunately, this experiment remains to date the only one dealing with nonlinear pair production in a laser field. A lot of theoretical proposals for experiments of the above described type have been published, in particular for pair production by an ion beam colliding with a laser [121, 123, 124] or photon merging in the combined field of a proton's Coulomb field and a laser [56, 177].

For the theoretical treatment of laser-modified QED, we want to treat the laser-electron (or laser-positron) interaction in a nonperturbative way, that is to all orders. This is so since for $\xi > 1$, we expect the probability for one laser-mode photon to be emitted or absorbed in a certain process to be comparable to that of absorbing or emitting several laser-mode photons. The interaction with other fields, such as the Coulomb field of an atomic nucleus, or the emitted or absorbed non-laser mode photon (such as a bremsstrahlung photon) is treated with perturbation theory. This nonperturbative treatment of the laser-electron coupling is possible due to the fact that the basic system of an electron moving in the potential of a plane laser wave can be exactly solved. The analytic solution to the Dirac equation with a plane wave potential was found by Volkov in 1935 [172]. From the expression for the wave function, the Green's function can be

written down comparatively easily [113, 154]. Using the Volkov states, one obtains a concrete way to deal with laser-modified QED: Draw the usual Feynman diagram in coordinate space, and replace the free electron and positron lines with laser-dressed lines, Volkov wave functions, and replace the intermediate propagator lines with the laser-dressed Dirac-Volkov propagator. Integration over the interaction coordinates then yields the amplitude of the considered process.

In this thesis, we investigate the influence of a strong laser field on two fundamental processes of particle physics: bremsstrahlung, which is light emission by an electron scattered at a Coulomb potential and laser-assisted pair production by a high-energy photon and a Coulomb field. Following some notes on the conventions used in section 1.1, in chapter 2, we present the theoretical foundations needed for the later analysis. In particular, we review the derivation of the Volkov solution to the Dirac equation, the expression for the Dirac-Volkov propagator, and we also review the solution to the classical, relativistic equation of motion of an electron in a plane wave electromagnetic field, since it is required to understand the behavior of the quantum system. We point out the strong classical-quantum correspondence between the quantum Volkov solution and the classical solution. In particular, this correspondence can be used to derive, by physical arguments, cutoff rules for the generalized Bessel functions, by which the Volkov solution is expressed. The appendix A explains the method of calculation employed in laser-modified QED, in which the free electron lines are replaced by Volkov states and internal propagator lines are replaced with the laser-dressed Dirac-Volkov propagator.

In chapter 3 we study in detail the process of laser-assisted bremsstrahlung. In this process, a laser-dressed electron is deflected by the Coulomb field of a nucleus, emitting radiation as a result. Being described by a Feynman diagram with two vertices, the calculation of the matrix element and cross section demands proper use of the Dirac-Volkov propagator. We show that it is possible to evaluate the cross section concretely even for large values of ξ. The results presented in this thesis are the first concrete numerical evaluations of the cross section of a second-order laser-dressed QED process involving the Dirac-Volkov propagator, for relativistic laser intensities. Previous studies of second-order laser-modified processes [36, 157] were limited to the weak field ($\xi < 1$) regime.

Chapter 4 deals with the process related to laser-assisted bremsstrahlung by a crossing symmetry [see section A.3]: laser-modified pair production by a photon in a Coulomb field. Here laser-dressed electron-positron pairs are created by a high-energy photon with frequency ω_γ (where γ is a label to distinguish ω_γ from the laser frequency ω) and a Coulomb field. Especially interesting here is the fact that this process is, according to the definitions made above, either laser-induced or laser-assisted depending on the value of ω_γ. Although the formal expression for the cross section is similar to that of laser-assisted bremsstrahlung, the dynamics of the process and the numerical evaluation are quite different. We evaluate the cross section of pair production for large values of ξ, but small values of the quantum parameter χ. By numerical calculations and intuitive arguments it is shown that the total number of pairs produced is almost unchanged by the laser field, provided the gamma photon frequency is above threshold, $\omega_\gamma > 2m$. The differential cross section is however drastically changed. We find that in a specific setup of laser beam and gamma photon beam, the created electrons and positrons are strongly focused by the laser into a narrow angular region, which also facilitates experimental observation. Also here, the numerical results presented are the first for this kind of process, previously only analytical results for weak fields ($\xi \ll 1$) have been obtained [30, 31].

As they are crucial for the modeling of electrons dressed by a laser, the Bessel functions have earned themselves a chapter of their own: chapter 5. Here we review all definitions and properties of the Bessel function. In particular we study the so-called generalized Bessel function, a generalization of the usual Bessel function characteristic for description of electrons dressed by a laser field of linear polarization. Particular emphasis is placed on the numerical evaluation of the generalized Bessel functions. We present a novel recursive algorithm for calculation of generalized Bessel functions, thereby generalizing the so-called Miller's algorithm to work also for generalized Bessel functions.

1.1 Notation and conventions

1.1.1 Units

In this thesis, we will use conventional high-energy units, that is $\hbar = c = 1$. This means that all dimensionful quantities are measured on one single scale. If nothing else is stated, we take this scale to be energy, measured in MeV. We have the electron mass $m = 0.511$ MeV. Some conversion factors read:

$$\begin{aligned} (\mathrm{MeV})^2 &= 2.568 \times 10^{21} \frac{1}{\mathrm{cm}^2}, \\ \mathrm{MeV} &= 1.602 \times 10^{-13} \mathrm{J}, \\ \mathrm{MeV} &= 1.519 \times 10^{21} \frac{1}{\mathrm{s}}, \\ (\mathrm{MeV})^2 &= 0.507 \times 10^{19} |e| \frac{\mathrm{V}}{\mathrm{m}}, \\ (\mathrm{MeV})^{-1} &= 0.1973 \times 10^{-12} \mathrm{m}. \end{aligned} \tag{1.9}$$

We use the Heaviside-Lorentz conventions, so that the relation between the negative electric charge $e = -|e|$ and the fine-structure constant α reads

$$e = -2\sqrt{\pi\alpha} \approx -0.3028, \tag{1.10}$$

with $\alpha \approx 1/137.04$. A useful formula for conversion of laser intensities I is

$$\frac{I}{(\mathrm{W/cm}^2)} = 3.127 \times 10^{29} \left(\frac{a\omega}{(\mathrm{MeV})^2} \right)^2 = 8.906 \times 10^{29} \xi^2 \left(\frac{\omega}{\mathrm{MeV}} \right)^2 = 2.325 \times 10^{29} \chi^2, \tag{1.11}$$

which is valid for linear polarization. In the case of circular polarization there is an extra factor of 2. For photon wavelengths λ (not to forget the extra factor of 2π!) we have

$$\frac{\lambda}{(\mathrm{m})} = \frac{12.401 \times 10^{-13}}{\omega/(\mathrm{MeV})}. \tag{1.12}$$

1.1.2 Dirac matrices and metric

The metric used is

$$(g^{\mu\nu}) = \begin{pmatrix} 1 & 0 & 0 & 0 \\ 0 & -1 & 0 & 0 \\ 0 & 0 & -1 & 0 \\ 0 & 0 & 0 & -1 \end{pmatrix}, \tag{1.13}$$

and vector products will be written with a dot $\cdot$, so that

$$p \cdot q = p_\mu q^\mu = p^0 q^0 - \boldsymbol{p} \cdot \boldsymbol{q}. \tag{1.14}$$

Boldcase letters denote three-vectors, and summation over Greek indices (μ, ν, ...) is implied. Partial derivatives are written like

$$\partial_\mu = \frac{\partial}{\partial x^\mu}. \tag{1.15}$$

If a specific representation should be needed (like in a computer program), we use the Dirac representation of the gamma matrices:

$$\begin{gathered} \gamma^0 = \begin{pmatrix} 1 & 0 & 0 & 0 \\ 0 & 1 & 0 & 0 \\ 0 & 0 & -1 & 0 \\ 0 & 0 & 0 & -1 \end{pmatrix}, \quad \gamma^1 = \begin{pmatrix} 0 & 0 & 0 & 1 \\ 0 & 0 & 1 & 0 \\ 0 & -1 & 0 & 0 \\ -1 & 0 & 0 & 0 \end{pmatrix}, \\ \gamma^2 = \begin{pmatrix} 0 & 0 & 0 & -i \\ 0 & 0 & i & 0 \\ 0 & i & 0 & 0 \\ -i & 0 & 0 & 0 \end{pmatrix}, \quad \gamma^3 = \begin{pmatrix} 0 & 0 & 1 & 0 \\ 0 & 0 & 0 & -1 \\ -1 & 0 & 0 & 0 \\ 0 & 1 & 0 & 0 \end{pmatrix}. \end{gathered} \tag{1.16}$$

The γ's satisfy $\gamma^\mu\gamma^\nu + \gamma^\nu\gamma^\mu = 2g^{\mu\nu}$. The hat $\hat{}$ operator is used to denote the Feynman dagger, the "slash":

$$\hat{p} = \gamma^\mu p_\mu, \tag{1.17}$$

for any four-vector p. This notation is standard in Russian literature [129, 154] on high-field QED. The reason why to use the hat $\hat{}$ instead of the conventional slash is simply that slashed capital letters, which will be employed heavily later on when the theory is introduced, do not look good: compare $\not{p}$ with $\not{A}$. The bar-conjugate operation on spinors is defined as

$$\overline{\Psi} = \Psi^\dagger \gamma^0, \tag{1.18}$$

and for matrices M

$$\overline{M} = \gamma^0 M^\dagger \gamma^0. \tag{1.19}$$

Chapter 2

The relativistic laser-dressed electron: classically and quantum mechanically

In this chapter we review the properties of the system consisting of an electron plus an electromagnetic wave, the laser field. We will see that this system can be solved exactly in an analytical form, both classically and quantum mechanically. The condition is that the laser wave can be treated as a plane wave, that is, a wave that propagates in one direction only. The fact that there is such exact solutions makes it possible to develop a perturbation theory with these states as basis states, and thereby taking the interaction with the laser field into account to all orders.

2.1 The motion of a classical, relativistic electron in a laser field

The classical equations of motion for a charged particle in an electromagnetic field can be solved analytically, if the electromagnetic field is a plane wave. This problem is treated in [7, 17, 83, 98, 109]. We will review the necessary steps leading to the analytic expressions for the trajectories, momentum and energy of the electron. In particular the expression for the energy will be important for the physical interpretation of the generalized Bessel functions.

2.1.1 Solution of the equations of motion by the Hamilton-Jacobi method

The laser field is described by the vector potential

$$A^\mu = A^\mu(\phi) = (0, \boldsymbol{A}(\phi)), \qquad \phi = x^\mu k_\mu, \tag{2.1}$$

where k^μ is the wave vector, and the gauge is chosen so that $k_\mu A^\mu = 0$ (Lorenz gauge). The relativistically invariant equation of motion read

$$m\frac{\mathrm{d}^2 x^\mu}{\mathrm{d}\tau^2} = e(\partial^\mu A_\nu - \partial_\nu A^\mu)\frac{\mathrm{d}x^\nu}{\mathrm{d}\tau}, \tag{2.2}$$

where x^μ is the coordinate of the particle and τ the proper time. This equation can be solved directly [83, 109], but we will do it with another method, the Hamilton-Jacobi method, since this method employs the action functional S [see Eq. (2.8)], which appears also in the quantum mechanical solution. The relativistic Hamiltonian H of a classical charged particle with charge e and mass m coupled to the potential A^μ reads

$$H = \sqrt{m^2 + (\boldsymbol{P} - e\boldsymbol{A})^2}, \tag{2.3}$$

or squared

$$H^2 = m^2 + (\boldsymbol{P} - e\boldsymbol{A})^2, \tag{2.4}$$

where $\boldsymbol{P}$ is the canonical three-momentum of the particle. The canonical four-momentum is given by $P^\mu = (H, \boldsymbol{P})$. Note however that P^μ is not a gauge-invariant quantity. The physical, gauge invariant momentum is the kinetic momentum $\mathfrak{p}^\mu = P^\mu - eA^\mu$. The derivative of the classical action S should satisfy

$$\partial^\mu S = (-H, -\boldsymbol{P}) = -P^\mu, \tag{2.5}$$

which inserted into equation (2.4) lead to

$$(\partial_\mu S + eA_\mu)\,(\partial^\mu S + eA^\mu) = m^2. \tag{2.6}$$

This equation is now solved with the ansatz that the the action can be split up into one field-free part and one field-dependent part, depending only on the laser phase ϕ:

$$S = -p_\mu x^\mu + \tilde{S}(\phi). \tag{2.7}$$

Here p^μ is determined by the initial conditions. It is interpreted as the momentum at infinity, that is, the asymptotic momentum of the particle in absence of the field, where $\tilde{S}(\phi) = 0$. As a four-momentum, p^μ should satisfy $p^2 = m^2$. Equation (2.6) with the ansatz (2.7) can be integrated, with the solution

$$\begin{aligned}\tilde{S}(\phi) &= \frac{-1}{2p\cdot k}\int_{\phi_0}^{\phi} \mathrm{d}\phi' \left(m^2 - [-p_\mu + eA_\mu(\phi')]\,[-p^\mu + eA^\mu(\phi')]\right) \\ &= \frac{1}{2p\cdot k}\int_{\phi_0}^{\phi} \mathrm{d}\phi' \left(p_\mu p^\mu - m^2 + e^2 A^\mu(\phi')A_\mu(\phi') - 2eA_\mu(\phi')p^\mu\right),\end{aligned} \tag{2.8}$$

with ϕ_0 given by the initial conditions, the initial phase of the laser. The derivative of the total action S with respect to the asymptotic momentum p^μ equals the (constant) initial position $-x_{0\mu}$,

$$\begin{aligned}\frac{\partial S}{\partial p^\mu} &= -x_{0\mu} \\ &= -x_\mu + \int_{\phi_0}^{\phi} \mathrm{d}\phi' \left[\frac{k_\mu}{2(p\cdot k)^2}\left(2eA_\nu(\phi')p^\nu - e^2A^\nu(\phi')A_\nu(\phi')\right) + \frac{1}{p\cdot k}\left(p_\mu - eA_\mu(\phi')\right)\right],\end{aligned} \tag{2.9}$$

so that the trajectories of the particle are given by

$$x_\mu = x_{0\mu} + \int_{\phi_0}^{\phi} \mathrm{d}\phi' \left[\frac{k_\mu}{2(p\cdot k)^2} \left(2eA_\nu(\phi')p^\nu - e^2 A^\nu(\phi')A_\nu(\phi') \right) + \frac{1}{p\cdot k}\left(p_\mu - eA_\mu(\phi') \right) \right]. \tag{2.10}$$

For the instantaneous canonical four-momentum we have

$$\begin{aligned} P_\mu =& -\partial_\mu S \\ =& p_\mu + \frac{k_\mu}{2p\cdot k}\left(2eA_\nu(\phi)p^\nu - e^2 A^\nu(\phi)A_\nu(\phi) \right), \end{aligned} \tag{2.11}$$

from which it is easily verified that the kinetic momentum $\mathfrak{p}_\mu = P_\mu - eA_\mu$ is gauge invariant under $A_\mu \to A_\mu + \lambda k_\mu$, with an arbitrary function λ (the gauge should remain in the Lorenz gauge). Specializing on a laser wave of the form

$$A_\mu(\phi) = a_\mu \cos\phi, \tag{2.12}$$

we get for the trajectories, with $\phi_0 = k\cdot x_0 = 0$,

$$x_\mu = x_{0\mu} + \left(\frac{p_\mu}{p\cdot k} - \frac{e^2a^2}{4(p\cdot k)^2}k_\mu \right)\phi + \left(\frac{ep\cdot a}{(p\cdot k)^2}k_\mu - \frac{ea_\mu}{p\cdot k} \right)\sin\phi - \frac{e^2a^2}{8(p\cdot k)^2}k_\mu \sin(2\phi). \tag{2.13}$$

Note that the trajectory is not given as an explicit function $x(t)$, but rather as a function of the laser phase ϕ. The phase ϕ is proportional to the proper time τ of the particle like $\phi = k\cdot\frac{\mathrm{d}x(0)}{\mathrm{d}\tau}\tau$, which can be seen by multiplying Eq. (2.2) by k^μ and integrating, using $k\cdot A = 0$. For the energy-momentum four-vector P_μ we get

$$P_\mu = p_\mu + \frac{k_\mu}{2p\cdot k}\left(2ea\cdot p\cos\phi - e^2a^2\cos^2\phi \right), \tag{2.14}$$

with the phase average

$$\overline{P}_\mu = p_\mu - \frac{e^2a^2}{4p\cdot k}k_\mu. \tag{2.15}$$

Of interest for the cutoff properties of the quantum Volkov solution is the solutions to the equation $\frac{\partial P_0}{\partial\phi} = 0$, since this will tell us the maximum and minimum of the instantaneous energy of the particle. The solutions are

$$\cos\phi = \pm 1; \qquad \cos\phi = \frac{\alpha}{8\beta} \text{ if } |\alpha| \le 8|\beta|, \tag{2.16}$$

with the corresponding energies

$$P_0 = p_0 - 2\omega\beta + \omega(-2\beta \pm \alpha), \qquad P_0 = p_0 - 2\omega\beta + \omega\frac{32\beta^2 + \alpha^2}{16\beta}, \tag{2.17}$$

where we have introduced the parameters

$$\alpha = \frac{ea\cdot p}{k\cdot p}, \qquad \beta = \frac{e^2a^2}{8k\cdot p}, \tag{2.18}$$

and written Eq. (2.17) on a form so that to facilitate comparison with the quantum Volkov solution in section 2.2 [See Eq. (2.47)]. In the nonrelativistic limit when $k \cdot p \approx \omega m$ we can express the ponderomotive energy as $U_p = 2\omega|\beta|$ [See Eq. (1.4)]. Note that $\beta \leq 0$, always, since $a^2 = a_\mu a^\mu \leq 0$ and $k \cdot p = E\omega - \boldsymbol{p} \cdot \boldsymbol{k} > 0$, and that the minimal and maximal energies given by Eq. (2.17) are independent of ω. Another remark is that since $\beta \leq 0$, it might seem that $P_0 < m$ is possible. Careful inspection shows that this is not the case, we always have that $P_0^{\text{min}} \geq m$ for both the case when $P_0^{\text{min}} = p_0 - 4\omega\beta - \omega|\alpha|$ and the case when $P_0^{\text{min}} = p_0 + \omega\frac{\alpha^2}{16\beta}$.

2.1.2 Direct numerical solution

In the previous subsection, the expression Eq. (2.13) was derived, providing an expression for the coordinates of a laser-dressed electron as a function of the invariant phase ϕ. If an expression for the orbit as an explicit function of the time t in some frame is searched for, there is no exact solution, but the equations of motion have to be integrated numerically. This approach also allows for inclusion of other forces besides the Lorentz force of the laser field, such as a Coulomb field. The classical equation of motion for a relativistic particle reads

$$m\frac{\mathrm{d}}{\mathrm{d}t}\frac{\dot{\boldsymbol{r}}}{\sqrt{1-\left(\frac{\dot{\boldsymbol{r}}}{c}\right)^2}} = \boldsymbol{F}, \tag{2.19}$$

where $\boldsymbol{F}$ is the force acting on the particle. Here we write explicitly the factor c (the speed of light) to better see which terms are important in the non-relativistic limit. To put this equation on a computer, we want to have it on the form $\frac{\mathrm{d}}{\mathrm{d}t}\dot{\boldsymbol{r}} = \ddot{\boldsymbol{r}} = f(\dot{\boldsymbol{r}}, \boldsymbol{r})$. If we let $\boldsymbol{r} = (x, y, z)$ and $\boldsymbol{F} = (F_x, F_y, F_z)$, we get a system of equations for the acceleration vector $\ddot{\boldsymbol{r}}$: (we ignore the y-component, since we want to look at the laser case, then there will only be two force components, one in the laser propagation direction and one in the laser polarization direction)

$$\begin{aligned}
\frac{\dot{x}}{c^2}(\ddot{x}\dot{x} + \ddot{z}\dot{z}) + \ddot{x}\left(1 - \frac{\dot{x}^2}{c^2} - \frac{\dot{z}^2}{c^2}\right) &= \frac{F_x}{m}\left(1 - \frac{\dot{\boldsymbol{r}}^2}{c^2}\right)^{3/2}, \\
\frac{\dot{z}}{c^2}(\ddot{x}\dot{x} + \ddot{z}\dot{z}) + \ddot{z}\left(1 - \frac{\dot{x}^2}{c^2} - \frac{\dot{z}^2}{c^2}\right) &= \frac{F_z}{m}\left(1 - \frac{\dot{\boldsymbol{r}}^2}{c^2}\right)^{3/2}.
\end{aligned} \tag{2.20}$$

This is solved to yield

$$\begin{aligned}
m\ddot{x} &= \frac{\left(1 - \frac{\dot{\boldsymbol{r}}^2}{c^2}\right)^{3/2} + \frac{\dot{x}^2\dot{z}^2}{c^4}\sqrt{1 - \frac{\dot{\boldsymbol{r}}^2}{c^2}}}{1 - \frac{\dot{z}^2}{c^2}}F_x - \frac{\dot{x}\dot{z}}{c^2}\sqrt{1 - \frac{\dot{\boldsymbol{r}}^2}{c^2}}\,F_z, \\
m\ddot{z} &= \left(1 - \frac{\dot{z}^2}{c^2}\right)\sqrt{1 - \frac{\dot{\boldsymbol{r}}^2}{c^2}}\,F_z - \frac{\dot{x}\dot{z}}{c^2}\sqrt{1 - \frac{\dot{\boldsymbol{r}}^2}{c^2}}\,F_x.
\end{aligned} \tag{2.21}$$

In the case with a monochromatic laser field with electric (and magnetic) field amplitude $|\boldsymbol{E}| = |\boldsymbol{B}| = E_0$, frequency ω, propagating in the z-direction and linearly polarized in the x-direction we have

$$F_x = eE_0\cos(\omega t - \omega z/c)(1 - \dot{z}/c), \qquad F_z = eE_0\cos(\omega t - \omega z/c)(\dot{x}/c). \tag{2.22}$$

2.2 The Volkov solution

That the Dirac equation, coupled to an electromagnetic plane wave, possesses an exact analytic solution was first found by Volkov over 70 years ago [172]. The Volkov solution is remarkable in several ways. Firstly, analytical solutions to the Dirac equation are rare, especially for field configurations that are realizable in the laboratory. (See [7] for other fields for which the Dirac equation is solvable, most of them quite exotic.) Secondly, the Volkov solution is strongly connected to the solution to the classical equations of motion, given by Eq. (2.8). As we will see, the phase of the Volkov wave function is given by the classical action. Usually this kind of quasi-classicality of a wave function is the result of some approximation, but here it is the exact wave function (apart from the spin term). The Volkov solution forms the foundation for laser-modified QED, since it provides the basis set from which the scattering theory is developed. Knowing the wave function for arbitrary momentum, it is subsequently an easy task to construct the propagator.

2.2.1 Derivation of the Volkov solution

In this section we follow [24], but we note that other, algebraic, approaches also exist [7, 128]. The starting point is the Dirac equation coupled to an electromagnetic plane wave, described by the four-vector potential $A(\phi)$ as in Eq. (2.1):

$$\left(i\hat{\partial} - e\hat{A}(\phi) - m\right)\psi(x) = 0, \tag{2.23}$$

where $\psi(x)$ is a spinor, a 4×1 complex matrix. The vector potential $A^\mu(\phi)$ depends on the coordinates only through $\phi = k \cdot x$ and satisfies the Lorenz gauge condition

$$\partial \cdot A = k \cdot \frac{\mathrm{d}A}{\mathrm{d}\phi} = 0, \tag{2.24}$$

which implies $k \cdot A = 0$. Here we assumed that A is on the general form

$$A^\mu(\phi) = a_1^\mu f_1(\phi) + a_2^\mu f_2(\phi). \tag{2.25}$$

Taking $a_2 = 0$ gives linear polarization, and $a_1^2 = a_2^2$ corresponds to circular. Note also that we in general do not assume $A^\mu = (0, \boldsymbol{A})$, since we want to keep open the possibility of making gauge transformations later. It turns out that with the present direct approach of solution, it is easier to work with the squared Dirac equation. Thus, by applying $\left(i\hat{\partial} - e\hat{A}(\phi) + m\right)$ to both sides of Eq. (2.23) we end up with

$$\left(-\partial^2 - 2ieA \cdot \partial + e^2A^2 - m^2 - ie\hat{k}\frac{\mathrm{d}\hat{A}}{\mathrm{d}\phi}\right)\psi(x) = 0. \tag{2.26}$$

This is just like the Klein-Gordon equation [24] with an extra matrix term, arising from the spin-laser interaction. The standard way of obtaining the Volkov solution is now to make the

ansatz $\psi(x) = e^{-ip\cdot x}F(\phi)$, analogous to the classical case in Eq. (2.7). Inserting this ansatz into Eq. (2.26) and integrating yields the sought Volkov solution:

$$\psi_p(x) = \sqrt{\frac{m}{EV}}\left(1 + \frac{e\hat{k}\hat{A}(\phi)}{2k\cdot p}\right)u(p)\exp\left(-ip\cdot x - i\int_{\phi_0}^{\phi}\left[\frac{ep\cdot A(\phi')}{k\cdot p} - \frac{e^2A^2(\phi')}{2k\cdot p}\right]\mathrm{d}\phi'\right), \tag{2.27}$$

where p is a four-vector labeling the solution, $\sqrt{\frac{m}{EV}}$ is a normalization factor containing $E = p^0$, the quantization volume V, and $u(p)$ is so far an arbitrary column vector of four complex numbers. The phase ϕ_0 depends on the initial conditions. We note that the initial phase ϕ_0 only gives rise to a constant phase in the wave function, which will cancel when forming the absolute value squared, thus being unimportant for the evaluation of any measurable quantities such as cross sections. Now, we are searching for a solution to the first-order Dirac equation, and not the square one. To single out the required solutions, we demand

$$(\hat{p} - m)u(p) = 0, \qquad p^2 = m^2, \tag{2.28}$$

which can be seen by letting $A \to 0$ in Eq. (2.27). The spinors $u(p)$ are normalized according to

$$\bar{u}(p)u(p) = 1. \tag{2.29}$$

Eq. (2.28) has two linearly independent solutions, called spin up and spin down. If we label these by $r = 1, 2$, then the sum over spin satisfies

$$\sum_{r=1,2} u_r(p)\bar{u}_r(p) = \frac{\hat{p} + m}{2m}, \tag{2.30}$$

which is all that we need, since we will always calculate spin-averaged or spin-summed quantities in this thesis. We then interpret p as the four-momentum of the particle outside the field, or the momentum at infinity, where the field is zero. We also observe that Eq. (2.27) allows solutions ψ_{-p} with negative zeroth component p^0. These negative-energy solutions will correspond to positrons when we treat pair creation in chapter 4, see also the discussion in subsection 2.2.2.

We close this subsection with giving the expression for the Volkov state in a laser of linear polarization, since this is the laser polarization we will work with in this thesis. Assuming

$$A^\mu(\phi) = a^\mu\cos\phi, \tag{2.31}$$

and taking the initial phase $\phi_0 = 0$, we have

$$\psi_p(x) = \sqrt{\frac{m}{QV}}\left(1 + \frac{e\hat{k}\hat{a}\cos\phi}{2k\cdot p}\right)u(p)\exp\left(-iq\cdot x - i\frac{ea\cdot p}{k\cdot p}\sin\phi + \frac{e^2a^2}{8k\cdot p}\sin(2\phi)\right). \tag{2.32}$$

Note that a^μ is a four-vector. If we take a^μ in the radiation gauge $a^\mu = (0, \boldsymbol{a})$, we have $a^2 = -\boldsymbol{a}^2$. With the absolute value $|a|$ of a_μ we always mean $|a| = \sqrt{|a^2|}$. Here we have defined the effective four-momentum q of the Volkov state as

$$q \equiv p + \frac{e^2|a|^2}{4k\cdot p}k, \tag{2.33}$$

which satisfies

$$q^2 = m^2 + \frac{e^2|a|^2}{2} \equiv m_*^2, \tag{2.34}$$

with m_* called the effective mass, and $Q = q^0$ the effective energy. We remark that $k \cdot p = k \cdot q$ and $a \cdot p = a \cdot q$. The effective momentum q is also called the average momentum, and corresponds to the phase-average value of P^μ [see Eq. (2.15)] from section 2.1. Note the choice of normalization factor in Eq. (2.32). With this choice, the Volkov states are normalized with respect to the effective four-momentum q:

$$\int \mathrm{d}^3x \psi^\dagger_{q,r}(x)\psi_{q',r'}(x) = \frac{1}{V}\delta(\boldsymbol{q} - \boldsymbol{q}')\delta_{rr'}, \tag{2.35}$$

where r, r' label the spin. The validity of the normalization condition (2.35), which is not self-evident, is discussed further in subsection 2.2.5.

Volkov wave functions for circular polarization of the laser

Since we present results in chapter 3 also for circular polarization of the laser field, we give here the expression for the Volkov wave function in a circularly polarized laser, without further discussion. The laser vector potential is here given as

$$A^\mu(\phi) = a_1^\mu \cos\phi + a_2^\mu \sin\phi, \tag{2.36}$$

with polarization vectors $a_{1,2}$ satisfying

$$a_1 \cdot a_2 = 0, \qquad a_1^2 = a_2^2 = -\tilde{a}^2. \tag{2.37}$$

Circular polarization is particular in the sense that the electric (and magnetic) field is constant in time, $A^2 = -\tilde{a}^2$. The Volkov solution is, with initial phase $\phi_0 = 0$ (see also [163]),

$$\begin{aligned}\psi_p^{\text{circ}}(x) = \sqrt{\frac{m}{QV}} &\left(1 + \frac{e\hat{k}\,(\hat{a}_2\cos\phi + \hat{a}_2\sin\phi)}{2k\cdot p}\right) u(p) \\ &\times \exp\left(-ip\cdot x - i\frac{e^2\tilde{a}^2}{2k\cdot p} - i\frac{ea_1\cdot p}{k\cdot p}\sin\phi + i\frac{ea_2\cdot p}{k\cdot p}\cos\phi)\right),\end{aligned} \tag{2.38}$$

where an unimportant constant phase factor has been dropped. The main difference is that there is no term proportional to $\sin(2\phi)$ in the exponential in Eq. (2.38). This means that when expanding the wave function $\psi_p^{\text{circ}}(x)$ into a sum of plane waves [see subsection 2.2.3], the coefficients are usual Bessel functions, instead of generalized Bessel functions as one gets in the linear polarization case. Another difference is that the effective mass is larger [compare Eq. (2.34)],

$$m_*^{\text{circ}\,2} = \left(p + \frac{e^2\tilde{a}^2}{2k\cdot p}k\right)^2 = m^2 + e^2\tilde{a}^2, \tag{2.39}$$

which can be explained by the larger average value of A^2. For the same peak value $\tilde{a}_0$ of the vector potential $A^\mu(\phi)$ we have

$$\overline{|A^2|} = \tilde{a}_0^2\overline{\cos^2\phi} = \tilde{a}_0^2/2 \tag{2.40}$$

for linear polarization, but

$$\overline{|A^2|} = \tilde{a}_0^2 \tag{2.41}$$

in the circular case.

2.2.2 Positron Volkov states and charge symmetry

To start with, we write down explicitly the negative energy solution to Eq. (2.23), obtained by letting $p \to -p$ in Eq. (2.27),

$$\psi_p^{\text{neg}}(x) = \sqrt{\frac{m}{|E|V}}\left(1 - \frac{e\hat{k}\hat{A}(\phi)}{2k\cdot p}\right) v(p) \exp\left(ip\cdot x - i\int_{\phi_0}^{\phi}\left[\frac{ep\cdot A(\phi')}{k\cdot p} + \frac{e^2A^2(\phi')}{2k\cdot p}\right]\mathrm{d}\phi'\right), \tag{2.42}$$

which is still a solution of Eq. (2.23), but only if the spinor now satisfies $(\hat{p}+m)v(p) = 0$. How does one know that the negative energy solution ψ_p^{neg} of the Dirac equation (2.23) actually has negative charge? The positive energy positron wave function $\psi_p^c(x)$ should be a positive energy solution to the Dirac equation with the charge reversed

$$\left(i\hat{\partial} + e\hat{A}(\phi) - m\right)\psi_p^c(x) = 0. \tag{2.43}$$

The transformation from the negative energy solution of Eq. (2.23) to the positive energy solution of Eq. (2.43) is provided by applying the charge conjugation operator C to the negative energy solution, so that $\psi_p^c = C\left(\psi_p^{\text{neg}}\right)$ [28]. In the Dirac representation of the gamma matrices, we have $C(\psi) = i\gamma^2\psi^*$. To within a constant phase factor, we have for the constant spinors u and v

$$C(u) = v, \qquad C(v) = u. \tag{2.44}$$

Now, applying the operation C to the negative energy solution (2.42), noting in particular that $\gamma^2\hat{k}^*\hat{A}^* = \hat{k}\hat{A}\gamma^2$, we obtain (up to a constant phase)

$$\begin{aligned} C(\psi_p^{\text{neg}}) =& \sqrt{\frac{m}{|E|V}}\left(1 - \frac{e\hat{k}\hat{A}(\phi)}{2k\cdot p}\right) \\ &\times u(p)\exp\left(-ip\cdot x - i\int_{\phi_0}^{\phi}\left[-\frac{ep\cdot A(\phi')}{k\cdot p} - \frac{e^2A^2(\phi')}{2k\cdot p}\right]\mathrm{d}\phi'\right), \end{aligned} \tag{2.45}$$

which is equal to the solution (2.27) with the replacement $e \to -e$, and indeed solves Eq. (2.43). The conclusion is that the operation C on the wave function combined with the shift $A(x) \to -A(x)$ leaves the Dirac equation invariant.

2.2.3 Fourier expansion of the Volkov solution and classical-quantum correspondence

As will be evident from the discussion in chapter 3, to evaluate a scattering matrix element, the initial and final wave functions have to be harmonic plane waves, that is, the dependence on the

coordinates should be of the form $e^{-ib\cdot x}$, for some momentum vector b and the coordinate x. The Volkov solution (2.32) is of the form $e^{-iq\cdot x}f(k\cdot x)$, a product of two plane waves, of which only the first has the required x-dependence. However, by Fourier's theorem, we can expand the Volkov wave function into its harmonic components. To this end we employ a special case of the generating function for the generalized Bessel function $A_0(n,\alpha,\beta)$:

$$e^{-i\alpha\sin\theta+i\beta\sin(2\theta)}=\sum_{s=-\infty}^{\infty}A_0(s,\alpha,\beta)e^{-is\theta}, \tag{2.46}$$

to yield

$$\psi_p(x)=\sqrt{\frac{m}{QV}}\sum_{s=-\infty}^{\infty}\left(A_0(s,\alpha,\beta)+\frac{e\hat{k}\hat{a}}{2k\cdot p}A_1(s,\alpha,\beta)\right)u(p)\exp\left[-i(q+sk)\cdot x\right], \tag{2.47}$$

where α and β were defined in Eq. (2.18), and

$$A_1(s,\alpha,\beta)=\frac{1}{2}\left(A_0(s+1,\alpha,\beta)+A_0(s-1,\alpha,\beta)\right). \tag{2.48}$$

The generalized Bessel function $A_0(s,\alpha,\beta)$ is defined and described in detail in chapter 5. The interpretation of the expansion (2.47) is clear: The quantum Volkov state is a superposition of plane waves with well-defined four-momenta $q^\mu+sk^\mu$, corresponding to the absorption of s number of laser-mode photons from the laser wave, if s is positive, and emission of $|s|$ number of photons into the laser field is s is negative. We can speak of a momentum spectrum composed of one continuous part, the effective momentum q^μ, plus one discrete part, sk^μ. The constant increase in momentum represented by the addition $e^2|a|^2k^\mu/(4k\cdot p)$ to p^μ in the definition (2.33) corresponds to the interaction with the laser without any net absorption of photons, making the electron heavier. Note from Eq. (2.34) that $m_*\geq m$. Every plane wave component is multiplied with its corresponding amplitude $A_0(s,\alpha,\beta)$ [for now disregarding the spin term $\frac{e\hat{k}\hat{a}}{2k\cdot p}A_1(s,\alpha,\beta)$], whose square $\left[A_0(s,\alpha,\beta)\right]^2$ gives the instantaneous probability of finding the laser-dressed electron in that particular momentum state. For consistency, this implies $\sum_s\left[A_0(s,\alpha,\beta)\right]^2=1$, which is indeed one of the characteristic properties of the generalized Bessel function. Since the sum over s in the expansion (2.47) extends from $-\infty$ to $+\infty$, the electron can, in the quantum case, acquire arbitrarily large energies in the laser field. However, beyond a certain value of $s=s_{\text{max,min}}$ (different for negative and positive s), the generalized Bessel function shows a sharp decrease in amplitude, so that the probability of absorbing (or emitting) $s>s_{\text{max}}$ ($s>|s_{\text{min}}|$) laser-mode photons is effectively zero. The actual dependence of $s_{\text{max,min}}$ on α and β follows directly from the maximally and minimally allowed classical energy, using the results from Eq. (2.17), noting that $q^\mu=\overline{P}^\mu$:

$$\begin{aligned}
s_{\text{max}}=&2|\beta|+|\alpha|,\\
s_{\text{min}}=&-2|\beta|-\frac{\alpha^2}{16|\beta|},\quad \text{if } 8|\beta|>\alpha,\\
s_{\text{min}}=&-|\alpha|+2|\beta|,\quad \text{if } 8|\beta|\leq\alpha,
\end{aligned} \tag{2.49}$$

which is valid for negative β. The general case and the mathematical proof of the cutoff rule are shown in chapter 5. This classical-quantum correspondence is illustrated in the two figures

Fig. 2.1 and Fig. 2.2. Concluding this subsection on the Fourier expansion of the Volkov state, we have seen that the four-momentum spectrum of the quantum Volkov state consists of two parts, one continuous [the effective momentum q] and one discrete [the sk^μ in the exponent of Eq. (2.47)]. However, the probability to occupy an energy state with energy greater or smaller than the classically allowed value is very small [factorially small, as we shall see in chapter 5].

2.2.4 Generalized Bessel functions from the Floquet ansatz

There is another direct, physical way to see where the generalized Bessel functions come from. The result of this approach defines $A_0(s,\alpha,\beta)$ in terms of a recurrence relation and a normalization condition. In section 5.3, we use this recurrence relation for fast and accurate numerical evaluation of the generalized Bessel function. We begin with inserting the Floquet ansatz [17, 166]

$$\psi_{\text{Floquet}}(x) = e^{-iq\cdot x}\sum_s A_s e^{-isk\cdot x}, \qquad q^2 = m_*^2, \tag{2.50}$$

where the coefficients A_s are independent of x, into the Klein-Gordon equation with an external laser field of linear polarization $A_\mu(x) = a_\mu\cos(k\cdot x)$,

$$\begin{aligned} 0 &= \left[-\partial^2 - 2ieA\cdot\partial + e^2A^2 - m^2\right]\psi_{\text{Floquet}}(x) \\ &= \left[-\partial^2 - 2ie\cos(k\cdot x)a\cdot\partial + \frac{e^2a^2}{2}\cos(2k\cdot x) - m_*^2\right]\psi_{\text{Floquet}}(x). \end{aligned} \tag{2.51}$$

We take the Klein-Gordon equation, since our goal is to obtain the properties of $A_0(s,\alpha,\beta)$, and we therefore neglect the spin of the electron, the inclusion of which would be an unnecessary complication. Eq. (2.51) leads to a relation for the coefficients A_s,

$$\sum_s\left[2\frac{eq\cdot a}{k\cdot q}\cos(\phi) - \frac{e^2a^2}{2k\cdot q}\cos(2\phi) - 2s\right]A_s e^{-is\phi} = 0. \tag{2.52}$$

Multiplying Eq. (2.52) with $e^{-in\phi}$, and integrating $\int_{-\pi}^{\pi}\mathrm{d}\phi$ leads to the recurrence relation for $A_0(s,\alpha,\beta)$,

$$\begin{aligned} 2sA_0(s,\alpha,\beta) = {}& \alpha\left[A_0(s+1,\alpha,\beta) + A_0(s-1,\alpha,\beta)\right] \\ & - 2\beta\left[A_0(s+2,\alpha,\beta) + A_0(s-2,\alpha,\beta)\right], \end{aligned} \tag{2.53}$$

if $ea\cdot q/(k\cdot q)$ and $e^2a^2/(8k\cdot q)$ are identified with α and β, and A_s with $A_0(s,\alpha,\beta)$. For the wave functions (2.50) constructed from the solution to the recurrence relation (2.53) to solve the Klein-Gordon equation (2.51), we must demand $A_0(s,\alpha,\beta)$ to be normalizable. This is expressed by the condition

$$\sum_s A_0^2(s,\alpha,\beta) = 1, \tag{2.54}$$

a special case of the general sum rule Eq. (5.21).

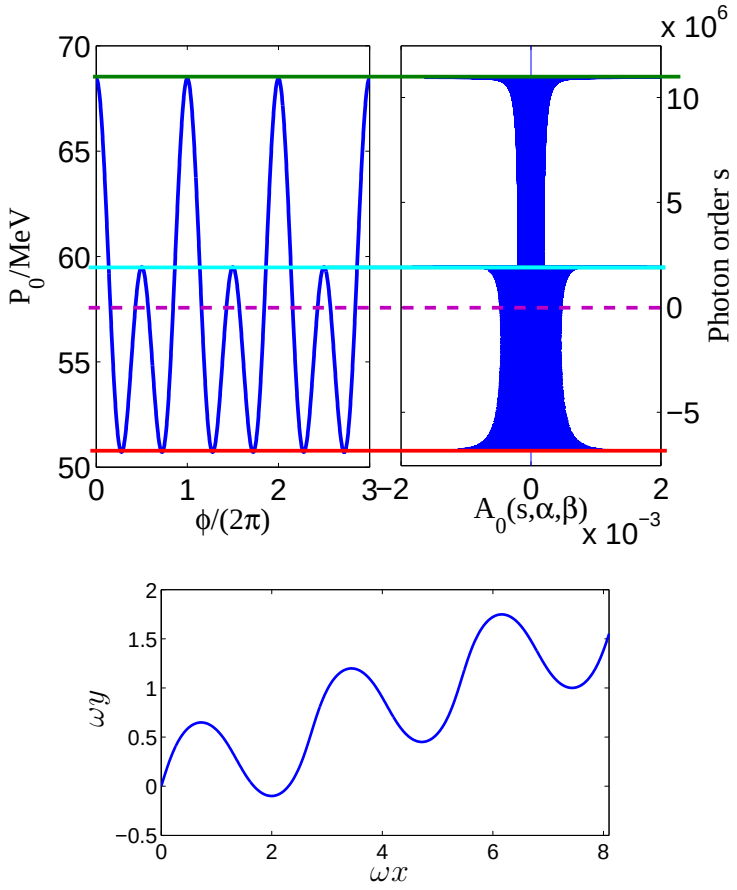

Figure 2.1: An illustration of the correspondence between the classical solution and the cut-off of the generalized Bessel functions, which are used to expand the quantum mechanical Volkov solution in a Fourier series. In this figure, the asymptotic momentum $\boldsymbol{p}$ of the electron makes an angle $\theta = 80°$ with the laser field polarization vector $\boldsymbol{a} = (0, |a|, 0)$, so that $\boldsymbol{p} = |\boldsymbol{p}|(\sin\theta, \cos\theta, 0)$, and the asymptotic energy $E = p_0 = 100m = 51.1$ MeV. The laser wave propagates in the negative x-direction, $\boldsymbol{k} = (-\omega, 0, 0)$, the laser frequency is $\omega = 1$ eV, and $\xi = 100$, which corresponds to an intensity $I = 8.9 \times 10^{21}$ W/cm^2. The upper graph shows the correspondence between the classical energy $P_0(\phi)$ from Eq. (2.14) as a function of the laser phase ϕ and the generalized Bessel function $A_0(s, \alpha, \beta)$ from Eq. (2.47). The laser and electron parameters here give $\alpha = 4.47 \times 10^6$ and $\beta = -3.22 \times 10^6$. The red line corresponds to the lowest possible value of $P_0(\phi)$, $P_0^{\text{min}} = E - \frac{\omega\alpha^2}{16|\beta|} = 50.7$ MeV, which amounts to emission of $|s| = 2\beta + \frac{\alpha^2}{16|\beta|}$ photons into the laser. The purple dashed line corresponds to the time averaged energy $\overline{P}_0 = E + 2\omega|\beta| = 57.5$ MeV, the effective energy [See Eq. (2.15)]. It is clear that the effective energy corresponds to not absorbing any photons at all, that is $s = 0$. A transition to another "plateau" in $A_0(s, \alpha, \beta)$ is visible at the light blue line, which corresponds exactly to the local maxima in P_0. The peak value of the amplitude of $A_0(s, \alpha, \beta)$ is lower here, since the electron spends less time on average in levels over the light blue one. Finally, the green line is the maximal classical energy $P_0^{\text{max}} = E + 4\omega|\beta| + |\alpha| = 68.5$ MeV, corresponding to absorption of $s = 2|\beta| + |\alpha|$ photons. The lower picture shows the corresponding classical trajectory from Eq. (2.13). Here the trajectory of the particle is plotted as implicit function of ϕ in the x-y plane, in units of the dimensionless parameters ωx and ωy.

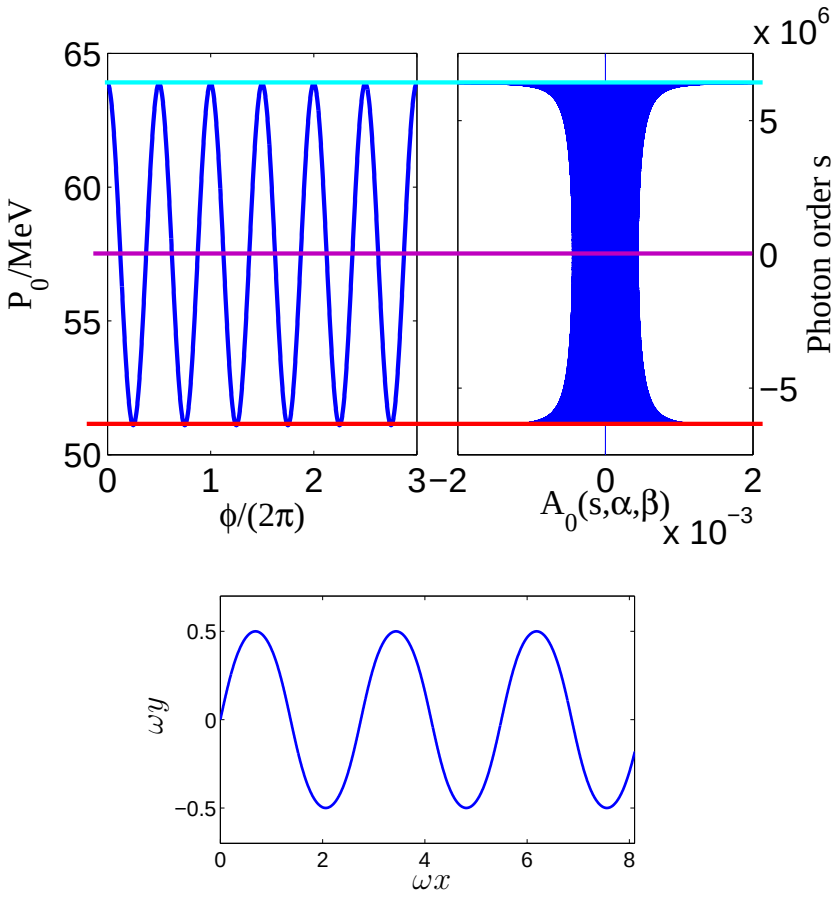

Figure 2.2: Another illustration of the classical-quantum correspondence of the Volkov state. The same parameters as in Fig. 2.1 are used, except that here $\theta = \pi/2$, which means $\boldsymbol{p} = |\boldsymbol{p}|(1,0,0)$. This gives $\alpha = 0$ and $\beta = 3.19 \times 10^6$. There is now no momentum component of $\overline{P}_\mu$ in the polarization direction, and therefore no plateau structure in $A_0(s,\alpha,\beta)$. A vanishing average momentum in the polarization direction is reflected also in the trajectory, shown in the lower panel. In the upper graph, the purple line going through $s = 0$ corresponds to the effective energy $\overline{P}_0 = E + 2\omega|\beta| = 57.5$ MeV. It follows that $P_0^{\text{max}} = E + 4\omega\beta = 63.9$ MeV (the light blue line), and $P_0^{\text{min}} = E = 51.1$ MeV (the red line). In this particular case the generalized Bessel function simplifies to the usual Bessel function: $A_0(s,0,\beta) = J_{-s/2}(\beta)$ for even s, and is zero otherwise.

2.2.5 Laser dressed Green's function: the Dirac-Volkov propagator

There are many representations for the electron's Green's function in the presence of an electromagnetic wave, also called the Dirac-Volkov propagator. In early attempts [38,149], the Green's function was found by direct solution of the inhomogeneous Dirac equation. The form presented in these references is however not well suited for application and can not easily be used for calculation of actual matrix elements. Another approach is the so-called operator method of writing the electron propagator, which is very powerful when making calculations involving closed electron loops [9–11, 57]. We use an elegant and useful way, described in [113, 154], of writing the laser-dressed Green's function of the electron, suitable for applications in scattering theory. Following this method, we introduce the Volkov solution without the free spinor, the so-called E-function [113, 154], which is still a 4×4 matrix:

$$E(p,x) = \left[1 + \frac{e\hat{k}\hat{A}(\phi)}{2k\cdot p}\right] \exp\left(-ip\cdot x - i\int_0^\phi \left[\frac{ep\cdot A(\tilde{\phi})}{k\cdot p} - \frac{e^2A^2(\tilde{\phi})}{2k\cdot p}\right] \mathrm{d}\tilde{\phi}\right). \tag{2.55}$$

We also define the adjoint by

$$\begin{aligned}\bar{E} &= \gamma^0 E(p,x)^\dagger \gamma^0 \\ &= \left[1 + \frac{e\hat{A}(\phi)\hat{k}}{2k\cdot p}\right] \exp\left(ip\cdot x + i\int_0^\phi \left[\frac{ep\cdot A(\tilde{\phi})}{k\cdot p} - \frac{e^2A^2(\tilde{\phi})}{2k\cdot p}\right] \mathrm{d}\tilde{\phi}\right).\end{aligned} \tag{2.56}$$

If we consider momenta off the mass shell, that is, we do not demand $p^2 = m^2$, we can show the following properties of the E's:

$$\left(i\hat{\partial} - e\hat{A}(\phi)\right) E(p,x) = E(p,x)\hat{p}, \tag{2.57}$$

$$-i\partial_\mu \bar{E}(p,x)\gamma^\mu - e\bar{E}(p,x)\hat{A}(\phi) = \hat{p}\bar{E}(p,x), \tag{2.58}$$

$$\frac{1}{(2\pi)^4}\int \mathrm{d}^4x \bar{E}(p,x)E(p',x) = \delta(p-p'), \tag{2.59}$$

and

$$\frac{1}{(2\pi)^4}\int \mathrm{d}^4p E(p,x)\bar{E}(p,x') = \delta(x-x'). \tag{2.60}$$

A couple of remarks concerning the above properties. The identities (2.57) and (2.58) follow, together with the definition (2.28) of the spinor, from the fact that the Volkov solution (2.27) solves the Dirac equation. Eqs. (2.57) and (2.58) are also easy to check explicitly. The orthogonality identity (2.59) is a very important property of the Volkov solutions, if they are going to be used as a basis for perturbation theory. It can be seen to hold in a number of ways. The handwaving argument, found in [24], is first to observe that Eq. (2.59) holds for $A = 0$. The field is turned on adiabatically, "slowly", from $\phi = -\infty$, which does not alter the value of the integral (2.59). In other words, the orthogonality integral only depends on the behavior of the function $E(p,x)$ at infinity, where the field is assumed to be turned off. An elegant proof using change of variables can be found in [154, chapter 1, section 2], and recently a mathematically rigorous proof was published in [180]. The property (2.60) is more difficult, and it seems that there is no published proof of completeness of the Volkov states. There is no doubt, however, that it is true. In section B.1 we present a proof by direct integration of the left side of Eq. (2.60), which is the first published proof of this property, to the author's knowledge.

The property (2.60) of $E(p,x)$ means that we can easily write down a solution G, a Green's function, to the equation

$$(i\hat{\partial} - e\hat{A} - m)G(x,x') = \delta(x-x'). \tag{2.61}$$

By using the properties (2.57) and (2.60), it is easy to show that

$$\begin{aligned} G(x,x') =& \frac{1}{(2\pi)^4}\int \mathrm{d}^4p E(p,x)\frac{\hat{p}+m}{p^2-m^2+i\varepsilon}\bar{E}(p,x') \\ =& \frac{1}{(2\pi)^4}\int \mathrm{d}^4p \left[1+\frac{e\hat{k}\hat{A}(\phi)}{2k\cdot p}\right]\frac{\hat{p}+m}{p^2-m^2+i\varepsilon}\left[1+\frac{e\hat{A}(\phi')\hat{k}}{2k\cdot p}\right] \\ & \times \exp\left(-ip(x-x') - i\int_{\phi'}^{\phi}\left[\frac{ep\cdot A(\tilde{\phi})}{k\cdot p} - \frac{e^2A^2(\tilde{\phi})}{2k\cdot p}\right]\mathrm{d}\tilde{\phi}\right), \end{aligned} \tag{2.62}$$

where ε is small and positive. This choice of boundary condition corresponds to the "Feynman boundary condition" [66, 67], exactly as in the case without the laser field [141]. With this choice of boundary conditions, pair production is accurately accounted for, by ensuring that waves with negative energy p_0 are propagated backwards in time. That the sign of p_0 [or q_0, see Eq. (2.33)] can be used to distinguish particle and antiparticle states even if the energy is not conserved, is due to the fact that a plane wave can not produce pairs of its own [154]. See the discussion in chapter 4. In the limit $A \to 0$, the Dirac-Volkov propagator $G(x,x')$ naturally goes to the free electron propagator $G_{\text{free}}(x,x')$ [141],

$$G_{\text{free}}(x,x') = \frac{1}{(2\pi)^4}\int \mathrm{d}^4p \frac{\hat{p}+m}{p^2-m^2+i\varepsilon}e^{-ip(x-x')}. \tag{2.63}$$

Eq. (2.62) can be rewritten using the expansion into generalized Bessel functions, assuming linear polarization $A = a\cos\phi$, as

$$\begin{aligned} G(x,x') =& \frac{1}{(2\pi)^4}\int \mathrm{d}^4p \sum_{s,s'=-\infty}^{\infty}\left(A_0(s,\alpha,\beta) + \frac{e\hat{k}\hat{a}}{2k\cdot p}A_1(s,\alpha,\beta)\right)\frac{\hat{p}+m}{p^2-m^2+i\varepsilon} \\ & \times \left(A_0(s',\alpha,\beta) + \frac{e\hat{a}\hat{k}}{2k\cdot p}A_1(s',\alpha,\beta)\right)\exp\left(-iq_p\cdot(x-x') - ik\cdot(sx-s'x')\right), \end{aligned} \tag{2.64}$$

where

$$q_p = p - \frac{e^2a^2}{4k\cdot p}k \tag{2.65}$$

and

$$\alpha = \frac{ea\cdot p}{k\cdot p}, \quad \beta = \frac{e^2a^2}{8k\cdot p}. \tag{2.66}$$

The Green's function is thus the free propagator inserted between the Volkov-like functions E and $\bar{E}$.

To make the dependence on the integration variable in the exponential simple, we make the change of variables

$$q = p - \frac{e^2a^2}{4k\cdot p}k. \tag{2.67}$$

The Jacobian of this transformation is

$$\begin{aligned} J =& \det\left(\frac{\partial q^\mu}{\partial p^\nu}\right) = \det\left(\delta^{\mu\nu} + \frac{e^2a^2k^\nu k_\alpha \delta^{\alpha\mu}}{4(k\cdot p)^2}\right) = \epsilon^{\mu\nu\alpha\beta}\frac{\partial q^0}{\partial p^\mu}\frac{\partial q^1}{\partial p^\nu}\frac{\partial q^2}{\partial p^\alpha}\frac{\partial q^3}{\partial p^\beta} \\ =& \epsilon^{\mu\nu\alpha\beta}\left(\delta^{0\mu} + \frac{e^2a^2k^\mu k_\gamma\delta^{\gamma 0}}{4(k\cdot p)^2}\right)\left(\delta^{1\nu} + \frac{e^2a^2k^\nu k_\gamma\delta^{\gamma 1}}{4(k\cdot p)^2}\right) \\ & \times\left(\delta^{2\alpha} + \frac{e^2a^2k^\alpha k_\gamma\delta^{\gamma 2}}{4(k\cdot p)^2}\right)\left(\delta^{3\beta} + \frac{e^2a^2k^\beta k_\gamma\delta^{\gamma 3}}{4(k\cdot p)^2}\right) \\ =& 1. \end{aligned} \tag{2.68}$$

Here $\epsilon^{\mu\nu\alpha\beta}$ is the usual anti-symmetric symbol with $\epsilon^{0123} = 1$. The last step can be seen most easily by choosing an explicit coordinate system, letting $k = (\omega, \omega, 0, 0)$. We then have

$$\mathrm{d}p^0\mathrm{d}p^1\mathrm{d}p^2\mathrm{d}p^3 = J^{-1}\mathrm{d}q^0\mathrm{d}q^1\mathrm{d}q^2\mathrm{d}q^3 = \mathrm{d}q^0\mathrm{d}q^1\mathrm{d}q^2\mathrm{d}q^3. \tag{2.69}$$

Written in the new integration variable, and noting that $k\cdot p = k\cdot q$ and $a\cdot p = a\cdot q$, the expression for the propagator reads (renaming $q \to p$)

$$\begin{aligned} G(x,x') =& \frac{1}{(2\pi)^4}\int \mathrm{d}^4p \sum_{s,s'=-\infty}^{\infty}\left(A_0(s,\alpha,\beta) + \frac{e\hat{k}\hat{a}}{2k\cdot p}A_1(s,\alpha,\beta)\right)\frac{\hat{p} + \frac{e^2a^2}{4k\cdot p}\hat{k} + m}{p^2 - m_*^2 + i\varepsilon} \\ & \times\left(A_0(s',\alpha,\beta) + \frac{e\hat{a}\hat{k}}{2k\cdot p}A_1(s',\alpha,\beta)\right)\exp\left(-ip\cdot(x-x') - ik\cdot(sx - s'x')\right). \end{aligned} \tag{2.70}$$

We see that the poles are shifted to the effective mass shell, $p^2 = m_*^2$.

With the all the building blocks constructed, the Volkov states (2.27) as basis functions and the propagator (2.62), we can proceed to write down laser-modified matrix elements and calculate cross sections. However, due to the numerous infinite sums over Bessel functions, the actual evaluation of cross sections is numerically quite involved.

Chapter 3

Laser-assisted bremsstrahlung

3.1 Introductory remarks

Bremsstrahlung is the process where a charged particle, in our case an electron, collides with a nucleus, decelerates and thereby emits radiation. If the nucleus is heavy enough, it can be treated as an external field, which means that the interaction of the electron with the nucleus can be approximated with the scattering of an electron in a time-independent external potential. This approximation means that only energy will be conserved in the process, as the nucleus can absorb any momentum from the electron. The relativistic quantum mechanical problem of bremsstrahlung in a Coulomb field in the first Born approximation was solved some 70 years ago by Bethe and Heitler [25], and the problem is now a standard problem in QED textbooks [141]. The Born approximation means that the interaction with the external nuclear Coulomb field is treated in first-order perturbation theory, and is valid if $Z\alpha \ll v$. Here Z is the atomic charge number, α is the fine-structure constant, and v is the velocity of the electron. The most important feature for the laser-free bremsstrahlung spectrum is that it is non-resonant. The total (or differential) cross section σ is a smooth function of ω_b, where ω_b is the angular frequency of the emitted radiation, decreasing approximately as $\sigma \propto \omega_b^{-1}$ until the cutoff at $\omega_b = E_i - m$, where E_i is the energy of the initial electron. The maximal energy that can be carried away by the photon is obviously $E_i - m$, since the electron must keep at least an amount of energy equal to its rest mass after the collision. At the cutoff, all kinetic energy of the initial electron is transformed into the emitted photon. Explicit formulas for the Bethe-Heitler cross section with different degrees of freedom integrated out, like the direction of the final electron, can be found in [72], and [93] provides a large collection of cross section formulas in different approximations.

If the whole system of incoming and outgoing electron and stationary nucleus is placed in a background laser field, we call the process laser-assisted bremsstrahlung. The modification of the bremsstrahlung spectrum by the presence of an external laser field has been studied previously by several authors, mainly in the nonrelativistic regime. The most important result is that of Karapetyan and Fedorov [90], who study laser-assisted bremsstrahlung in the non-relativistic regime, in first Born approximation and dipole approximation for the laser field. Here resonances at ω_b equals integer multiples of the laser frequency ω are found in the limit

of large laser intensities. It should be stressed that this is not the same kind of Green's function resonances that we find in our work (see section 3.4). In section 3.6, the relativistic formulas employed in this work are compared to and found to agree, within the regimes of validity, with the formula of [90]. Other articles that go beyond the first Born approximation include [181], where a low laser frequency approximation is developed, the recent [68], and [42] includes a numerical approach to the problem by solving the Schrödinger equation. In [59, 60] the formulas of Zhou and Rosenberg [181] and Karapetyan and Fedorov [90] are compared by numerical means. An interesting contribution is [44] where the problem is treated in dipole approximation for the laser-electron coupling, but beyond the first Born approximation: Here distinct resonances where the bremsstrahlung frequency equals an integer multiple of the laser frequency are found, as a consequence of an extended Coulomb singularity. This should be compared with the discussion in subsection 3.4.3, where a divergence due to the Coulomb field is found, even in the Born approximation.

To find a resonant behavior of the propagator similar to our results, one has to go beyond the dipole approximation for the laser. This is done for the nonrelativistic case in [99], where indeed resonant peaks are found. The fully relativistic formula was presented for the first time in [156, 157], however, without performing any numerical calculations, and even limiting the analytical investigations to the weak-field case where $\xi \ll 1$. We also mention further studies by the same author, treating the generalization to a two-color laser [159, 160].

In this chapter, we start in section 3.2 with reviewing the simplest of all laser-modified QED diagrams, laser-induced Compton scattering. This process is fundamental to the understanding of laser-assisted bremsstrahlung. In section 3.3 we use the theoretical building blocks of chapter 2 and appendix A to write down the matrix element and the resulting cross section of laser-assisted bremsstrahlung. Our main results [104, 164] are presented in section 3.5, preceded by a detailed discussion about the fundamentally interesting question about the Green's function resonances in section 3.4. In section 3.6, we explain why the nonrelativistic treatment does not result in any resonances, and we also check that the nonrelativistic result is recovered from the relativistic formula in the appropriate limit.

3.1.1 Validity of the approximations made in the description of the laser field

To be able to write down transition matrix elements between Volkov states, we make certain approximations, as is always the case when trying to describe Nature by means of a physical model. In this subsection we discuss the different approximations and their limitations. A similar discussion can be found in [113, 154].

Approximation of a plane wave of infinite extent

In this and all following chapters, we approximate the laser field $A^\mu(x)$ with a monochromatic plane wave laser field of infinite extent,

$$A^\mu(x) = a^\mu \cos(k \cdot x), \tag{3.1}$$

for linear polarization. Consequently, for our calculations to be valid, the involved particles should spend a large number of laser cycles, at least say 10, inside the laser field. In some cases, there are other constraints, like the radiation time, coming from the particular process involved (see the discussion regarding Compton scattering in subsection 3.4.2). Provided that the laser pulse is long enough, the plane wave approximation is a good one, since more realistic Gaussian beams are close to plane waves near the focus [161, 170], and in fact any electromagnetic field looks like a plane wave in the rest frame of a relativistic particle [154]. For example, an electric field $\boldsymbol{E}_{\text{lab}} = [f(x^\mu), 0, 0]$ in the lab frame transforms under a Lorentz transformation Λ in the x^3 direction [to the rest frame of a relativistic particle with velocity $\boldsymbol{v} = (0, 0, |\boldsymbol{v}|)$, gamma factor γ] to the combined electric and magnetic fields [84]

$$\boldsymbol{E}_{\text{rf}} = [\gamma f(y^\mu), 0, 0], \qquad \boldsymbol{B}_{\text{rf}} = [0, -\gamma|\boldsymbol{v}| f(y^\mu), 0], \tag{3.2}$$

where $y^\mu = (\Lambda^{-1})^\mu{}_\nu x^\nu = (\gamma x^0 + \gamma|\boldsymbol{v}|x^3, x^1, x^2, \gamma x^3 + \gamma|\boldsymbol{v}|x^0)$, so that if $|\boldsymbol{v}| \approx 1$, we have $|\boldsymbol{E}_{\text{rf}}| \approx |\boldsymbol{B}_{\text{rf}}|$ and $\boldsymbol{E}_{\text{rf}} \cdot \boldsymbol{B}_{\text{rf}} \approx 0$, close to a plane wave field configuration.

External classical field approximation

The laser field used in our model is assumed to behave as a classical external field. This implies that an arbitrary amount of energy and momentum can be taken from or emitted into the field without changing it. Evidently, this approximation breaks down if a large number of laser photons, enough to deplete the laser field considerably, is absorbed form the laser field during the process under consideration. To get a feeling for the photon densities involved, consider the photon number density in a typical strong laser field, $N/V = \xi^2\omega m^2/e^2 \approx 4 \times 10^{28}$ photons/cm^3, if $\xi = 10$ and $\omega = 1$ eV is assumed. Therefore, in for example a pulse of $\tau = 1$ ps duration, focused to an area of 100 squared wavelengths, we have $N = 100\xi^2 m^2\tau/(\omega e^2) \approx 2 \times 10^{21}$ photons. Now, as discussed in sections 3.2, 3.3, and 4.2, the largest number of photons absorbed during a laser-dressed QED process is controlled by the parameter $\beta = \xi^2 m^2/(8k \cdot p)$, entering as argument of the generalized Bessel functions [For the definition, see Eq. (3.6) in the case of Compton scattering, Eq. (3.33) for bremsstrahlung and Eq. (4.8) for the pair creation case]. The maximal value of β is obtained for a relativistic particle moving in the same direction as the propagation direction of the laser wave. However, even for a particle energy $E = 100m$, much larger than we consider in this thesis, we have for the same parameters as considered above that $\beta \approx \xi^2 E/(4\omega) \approx 1.3 \times 10^9$, much smaller than the number of photons contained in one laser pulse.

3.2 Laser-induced Compton scattering: photon emission by a laser-dressed electron

Laser-induced Compton scattering is the simplest of all laser-induced QED processes. The first theoretical treatments of this problem can be found in [38, 105, 129]. Recently, the process was numerically investigated in [138], and [15] provides a comprehensive treatment. In [30, 125, 126], the process is treated in a two-color laser. We treat the case of linear polarization of the

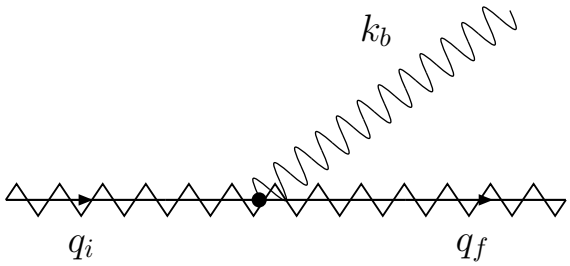

Figure 3.1: Feynman diagram for laser-induced Compton scattering. The incoming (effective four-momentum q_i) and outgoing (effective four-momentum q_f) electron is denoted by a zig-zag line on top of a straight line to stress that it is dressed by a strong laser. The emitted photon has four-momentum k_b. The Feynman diagrams in this thesis were drawn with the help of the program JaxoDraw [27].

laser here. One initial Volkov state classified by effective momentum q_i spontaneously emits a photon with four-momentum k_b and ends up with final effective four-momentum q_f. The Feynman diagram is shown in Fig. 3.1. To compute the matrix element M for this process, we employ the wave function of the emitted photon

$$A^{\mu}_{b,\lambda}(x) = \frac{1}{\sqrt{2\omega_b V}} \epsilon^{\mu}_{b,\lambda} e^{ik_b \cdot x}, \tag{3.3}$$

where $\lambda = 1,\ 2$ labels the two polarization directions and $\epsilon_{b,\lambda}$ is the polarization vector satisfying $\epsilon^2_{b,1} = \epsilon^2_{b,2} = -1$ and $\epsilon_{b,2} \cdot \epsilon_{b,2} = 0$. Note the plus sign in the exponential in Eq. (3.3), photon emission is the process we wish to describe. That this in fact is the correct sign will be clear from the four-momentum conserving delta function [see Eq. (3.5)]. This is consistent with the expression for momentum mode k_b of the second-quantized electromagnetic field $A^{\mu}_{\text{quant.}}(x)$ of a plane wave [141],

$$A^{\mu}_{\text{quant.}}(x) = \frac{1}{\sqrt{2\omega_b V}} \sum_{\lambda} \epsilon^{\mu}_{b,\lambda} \left(a_{\boldsymbol{k}_b,\lambda} e^{-ik_b \cdot x} + a^{\dagger}_{\boldsymbol{k}_b,\lambda} e^{ik_b \cdot x} \right), \tag{3.4}$$

where $a_{\boldsymbol{k}_b,\lambda}$ is the creation operator and $a^{\dagger}_{\boldsymbol{k}_b,\lambda}$ is the annihilation operator of a photon with three-momentum $\boldsymbol{k}_b$ and polarization state labeled with λ. Since we are only interested in photon creation, only the term with $a^{\dagger}_{\boldsymbol{k}_b,\lambda}$ in expression (3.4) should be retained. Using now the Volkov state in its Fourier expanded form (2.47), we are able to perform the required space-time integration over the interaction coordinate x with the result [38, 129]

$$\begin{aligned} M &= e \int \mathrm{d}^4 x \bar{\psi}_{q_f}(x) \hat{A}_{b,\lambda} \psi_{q_i}(x) \\ &= \frac{e(2\pi)^4}{\sqrt{2Q_i Q_f \omega_b V^3}} \sum_{n=-\infty}^{\infty} \bar{u}_{r_f}(p_f) \Big[A_0(n,\alpha,\beta) \hat{\epsilon}_{b,\lambda} + \left(\frac{e\hat{a}\hat{k}\hat{\epsilon}_{b,\lambda}}{2k \cdot q_f} + \frac{\hat{\epsilon}_{b,\lambda}\hat{k}\hat{a}e}{2k \cdot q_i} \right) A_1(n,\alpha,\beta) \\ &\qquad - \frac{e^2 a^2 k \cdot \epsilon_{b,\lambda} \hat{k}}{2k \cdot q_f k \cdot q_i} A_2(n,\alpha,\beta) \Big] u_{r_i}(p_i) \delta(nk + q_i - q_f - k_b). \end{aligned} \tag{3.5}$$

Here $r_{i,f}$ labels the spin state of the initial (final) electron, and

$$\alpha = \frac{ea\cdot q_i}{k\cdot q_i} - \frac{ea\cdot q_f}{k\cdot q_f}, \qquad \beta = \frac{e^2a^2}{8}\left(\frac{1}{k\cdot q_i} - \frac{1}{k\cdot q_f}\right). \tag{3.6}$$

We note several things. The matrix element (3.5) is gauge invariant under the gauge transformation under both $\epsilon_{b,\lambda} \to \epsilon_{b,\lambda} + \Lambda_1 k_b$ and $a \to a + \Lambda_2 k$ for arbitrary constants $\Lambda_{1,2}$. The a-invariance is easy to see, and the $\epsilon_{b,\lambda}$-invariance can be proven directly from Eq. (3.5) by using the recursion relation (5.23) of the generalized Bessel function $A_0(n,\alpha,\beta)$, or more elegantly by the same method as in section B.2. Gauge invariance can for example be used to transform $\epsilon_b \to \epsilon_b - \frac{\epsilon_b\cdot k}{k_b\cdot k}k_b$, so that $k\cdot\epsilon_b = 0$ and the term containing $A_2(n,\alpha,\beta)$ in Eq. (3.5) vanishes. More important however, is that gauge invariance makes it possible to use the relation [141]

$$\sum_{\lambda=1,2}(\epsilon_{b,\lambda}\cdot M)^2 = -M^2 \tag{3.7}$$

for photon sums in squared matrix elements. Taking the square of M and multiplying with the final phase space volume $\mathrm{d}^3q_f\mathrm{d}^3k_bV^2(2\pi)^{-6}$, averaging over the initial spin r_i and summing over final electron spin r_f and polarization λ of the photon we obtain the differential rate per unit time $\mathrm{d}W$ [129]

$$\begin{aligned}
\mathrm{d}W &= \sum_{n=1}^{\infty}\int \frac{e^2m^2\mathrm{d}^3q_f\mathrm{d}^3k_b}{4(2\pi)^2Q_iQ_f\omega_b}\delta(nk+q_i-q_f-k_b) \\
&\quad\times\left[-A_0^2(n,\alpha,\beta) + \xi^2\left(1+\frac{(k\cdot k_b)^2}{2k\cdot q_fk\cdot q_i}\right)\left(A_1^2(n,\alpha,\beta) - A_0(n,\alpha,\beta)A_2(n,\alpha,\beta)\right)\right] \\
&= \frac{e^2\omega_b}{16\pi^2}\sum_{n=1}^{\infty}\mathrm{d}\Omega_b\frac{1}{q_i\cdot k_b^{\mathrm{dir}} + nk\cdot k_b^{\mathrm{dir}}} \\
&\quad\times\Bigg[-2m^2A_0^2(n,\alpha,\beta) \\
&\qquad + |a|^2e^2\left(2+\frac{(k\cdot k_b)^2}{k\cdot q_ik\cdot q_f}\right)\left(A_1^2(n,\alpha,\beta) - A_0(n,\alpha,\beta)A_2(n,\alpha,\beta)\right)\Bigg],
\end{aligned} \tag{3.8}$$

where in the last step we used the delta function to integrate over $\mathrm{d}^3q_f\mathrm{d}\omega_b$, so that

$$\omega_b = \frac{nk\cdot q_i}{q_i\cdot k_b^{\mathrm{dir}} + nk\cdot k_b^{\mathrm{dir}}}, \tag{3.9}$$

and $q_f = nk + q_i - k_b$. By k_b^{dir} we mean the ω_b-independent four-vector $k_b^{\mathrm{dir}} = k_b/\omega_b = (1, \boldsymbol{k}_b/|\boldsymbol{k}_b|)$. Eq. (3.9) is sometimes called the nonlinear Compton formula [38,138], because the frequency of the emitted photon depends on q_i, the effective momentum, and therefore on ξ, the intensity. For $\xi \ll 1$ we have $q_i \approx p_i$ and Eq. (3.9) goes to the normal Compton formula [141] for the emitted frequency, since only terms with $n = 1$ contribute to the sum in Eq. (3.8) in this limit. The rate (3.8) is differential in the solid angle $\Omega_b = \mathrm{d}\theta\sin\theta\mathrm{d}\phi$ of the emitted photon

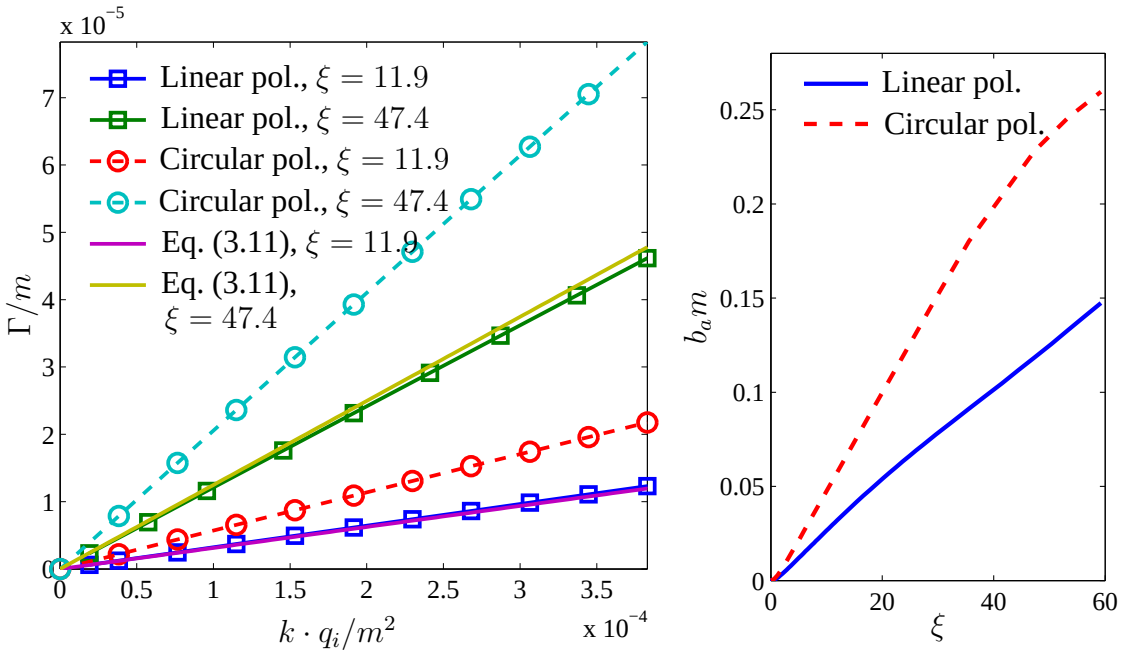

Figure 3.2: The dependence of the mass operator Γ of the electron in the laser on the parameters $k \cdot q_i$ and $\xi = |ea|/m$. In the right graph, the dependence on the proportionality constant b_a on ξ is shown, with $\Gamma = b_a k \cdot q_i$. The same value of ξ for linear and circular polarization implies that we compare laser fields with the same peak value of the electric field. The laser intensity, however, differ by a factor of $1/2$ between circular and linear polarization of the same value of ξ.

(by fixing the direction of the emitted photon and the order n, both the photon energy ω_b and the four-momentum q_f of the final electron are decided by energy-momentum conservation). The vector $\boldsymbol{k}_b$ is written in terms of the angles θ and ϕ as $\boldsymbol{k}_b = \omega_b(\cos\phi\sin\theta, \sin\phi\sin\theta, \cos\theta)$. Important for the discussion in subsection 3.2.2 is the total rate W, integrated over the solid angle Ω_b of the emitted photon:

$$W = \int \mathrm{d}W = \int_0^\pi \mathrm{d}\theta \sin\theta \int_0^{2\pi} \mathrm{d}\phi \frac{\mathrm{d}W}{\mathrm{d}\Omega_b}. \tag{3.10}$$

The total rate (3.10) can by gauge and Lorentz invariance only be a function of the invariants $k \cdot q_i$ and $\xi = |ea|/m$. We have evaluated the function $\Gamma = \frac{Q_i}{m}W$, also called the mass operator (see subsection 3.2.2) for different values of these parameters, with the results shown in Figure 3.2. Here we also show results for circular polarization of the laser, which were evaluated from an expression similar to Eq. (3.8) [105, 164]. For small values of ξ, these graphs agree with the approximate formulas of Becker and Mitter [113], and we have also checked for consistency with the results in [105].

The evaluation is made as follows: For each n, we choose to evaluate Γ in the special center-of-mass frame where $\boldsymbol{q}_i + n\boldsymbol{k} = \boldsymbol{q}_f + \boldsymbol{k}_b = 0$. Note that this frame is not physical, since it is different for every n, but it simplifies the evaluation of the total rate. If we in addition choose $\boldsymbol{k}$ to point in

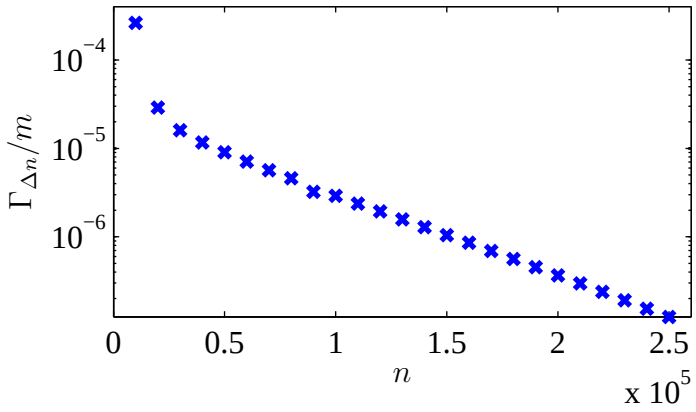

Figure 3.3: Illustration of the slow exponential convergence of the partial sums involved in the calculation of Γ. Shown in the graph above is the quantity $\Gamma_{\Delta n}$ (to be defined below) as a function of n. The function $\Gamma_{\Delta n}$ is defined as follows. First, let the nth total rate for laser-induced Compton scattering be $W_n = \int \mathrm{d}W_n$, where $\mathrm{d}W_n$ is the nth term in the sum in Eq. (3.8). Then, let $\Gamma_{\Delta n} = \frac{Q_i}{m} \sum_{n'=n-\Delta}^{n} W_{n'}$. Here $\Delta = 10^4$. The total value of Γ is then given as $\Gamma = \sum_n \Gamma_{\Delta n}$. The other parameters used for the calculation are $k \cdot q_i/m^2 = 1.53 \times 10^{-3}$, $\xi = 47.4$.

the negative x-direction, i.e. $k = (\omega, -\omega, 0, 0)$, this implies $k \cdot q_i/\omega = Q_i + \sqrt{Q_i^2 - m_*^2} = Q_i + n\omega$ so that $\omega = (k \cdot q_i)^2/\sqrt{(nk + q_i)^2} = (k \cdot q_i)^2/\sqrt{(n\omega + Q_i)^2} = (k \cdot q_i)^2/\sqrt{2nk \cdot q_i + m_*^2)}$. Moreover, by energy conservation (3.9) we have $\omega_b = nk \cdot q_i/(Q_i + n\omega) = n\omega$ in this special frame. We now have to perform the integration over the solid angle of $\boldsymbol{k}_b$. Numerically, the sum over n in Eq. (3.8) is a quite demanding task when ξ is large. To reach convergence, a number of terms of order $\sim 10^5$ has to be summed. The convergence rate is exponential, although very slowly exponential, as illustrated in Fig. 3.3.

Surprisingly, the function Γ is linear in $k \cdot q_i$ for values of $k \cdot q_i$ of the order 10^{-4} MeV^2 or smaller. Indeed, in [129], they find a linear dependence on $k \cdot q_i$ if the inequality chain $1 \ll e|a|/m \ll m^2/(k \cdot q_i)$ is satisfied (limit of a crossed field) according to

$$\Gamma = k \cdot q_i \frac{5e^3|a|}{8\sqrt{3}\pi m^2}. \tag{3.11}$$

We see from our graphs that Eq. (3.11) gives the slope for $|a| = 20$ MeV, but differs slightly for $|a| = 80$ MeV.

3.2.1 Discrete level interpretation of the Compton scattering matrix element

A nice interpretation of the Compton scattering amplitude is as a spontaneous decay from one discrete Volkov level to another. Recall that the Volkov state can be thought of as a superposition of states with definitive four-momentum, with generalized Bessel functions as coefficients (see

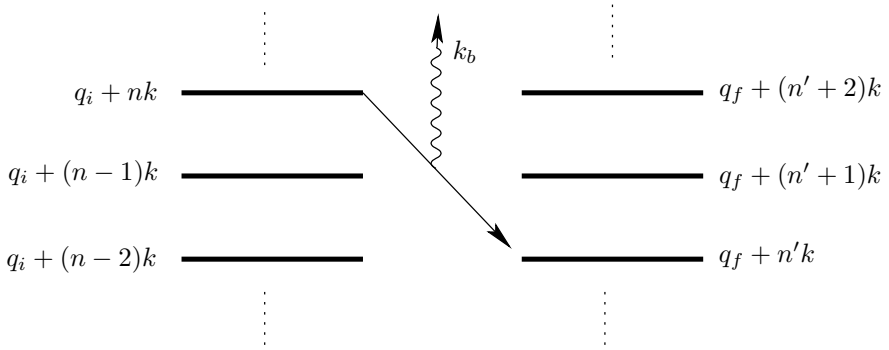

Figure 3.4: Laser-induced Compton scattering in a level-transition picture, introduced in subsection 3.2.1. The electron in state with momentum $q_i + nk$ decays by emitting a photon k_b to a state with momentum $q_f + n'k$. The difference $\Delta n = n - n'$ is dictated by energy-momentum conservation, and to obtain the total amplitude, one must sum over all allowed Δn.

subsection 2.2.3),

$$\psi(x) = \sum_n \psi_n(x) = \sum_n A_0(n, \alpha, \beta) e^{-i(q+nk)\cdot x}, \tag{3.12}$$

where we have dropped the spin terms for simplicity. In this picture, an initial state n with momentum $q_i + nk$ can decay spontaneously to a final state n' with momentum $q_f + n'k$, emitting a photon with momentum $k_b = (\omega_b, \boldsymbol{k}_b)$ in the process, as illustrated in Fig. 3.4. Consequently, only the difference $\Delta n = n - n'$ is constrained by four-momentum conservation:

$$q_i + nk - k_b = q_f + n'k, \tag{3.13}$$

which leads to the demand

$$\frac{k_b \cdot q_i}{k \cdot q_f} = \Delta n. \tag{3.14}$$

In other words, the fraction $k_b \cdot q_i/(k \cdot q_f)$ has to be integer valued. If we let the amplitude of each level in the initial Volkov state be $A_0(n, \alpha, \beta)$, and the amplitude of the levels in the final Volkov state $A_0(n', \alpha', \beta')$, then the total amplitude M for the transition is expressed as the product of the level amplitudes, summed over all possible transitions

$$\begin{aligned} M &= \sum_{n,n'} A_0(n, \alpha, \beta) A_0(n', \alpha', \beta') \delta(q_i - q_f - k_b + [n - n']k) \\ &= \sum_{\Delta n} A_0(\Delta n, \alpha - \alpha', \beta - \beta') \delta(q_i - q_f - k_b + \Delta n k), \end{aligned} \tag{3.15}$$

by the summation formula (5.21). Eq. (3.15) gives, apart from the spin terms, the essential physics of the full amplitude (3.5). We see that for very small frequencies $\omega_b < \omega$, the transition must go to the same level ($n = n'$) of the final state, $q_i \approx q_f$, and the transition amplitude is approximately one,

$$M \approx \sum_n A_0(n, \alpha, \beta)^2 \delta(q_i - q_f) = \delta(q_i - q_f). \tag{3.16}$$

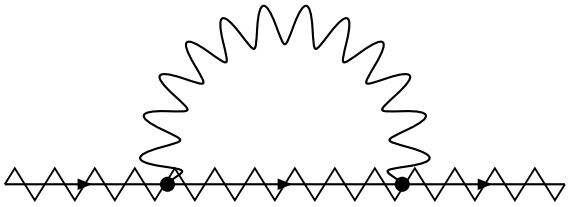

Figure 3.5: The mass operator of the electron in the laser.

For higher frequencies $\omega_b > \omega$ there will in general be destructive interference between the different pathways (level $n \to n'$, $n+1 \to n'+1$ etc.) so that the probability for Compton scattering will show an exponential falloff as a function of ω_b. This will be seen clearly from the numerical results in section 3.5. Compare also Fig. 3.3.

3.2.2 Decay width of Volkov states

The laser-dressed electron is not stable. The fact that an electron submitted to a laser field can spontaneously radiate makes it possible to speak about a lifetime τ of the laser-dressed electron. This lifetime is given by precisely the inverse of the total rate of Compton scattering, Eqs. (3.8), (3.10),

$$\tau = \frac{1}{W}. \tag{3.17}$$

As for other decaying states [141], this implies an imaginary contribution to the effective energy of the electron,

$$Q \to Q - iW, \tag{3.18}$$

so that the wave function actually decays over time:

$$\psi(x) \propto e^{-iQx^0 + i\boldsymbol{q}\cdot\boldsymbol{x}} \to e^{-iQx^0 - Wx^0 + i\boldsymbol{q}\cdot\boldsymbol{x}}. \tag{3.19}$$

An imaginary contribution to the energy implies, via the relation $q^2 = m_*^2$, an imaginary contribution to the electrons mass. If we let $m_* \to m_* - i\Gamma$, this means

$$(Q - iW)^2 - \boldsymbol{q}^2 = (m_* - i\Gamma)^2, \tag{3.20}$$

so that to first order in W (the imaginary mass contribution is expected to be a small contribution) we have

$$\Gamma = \frac{Q}{m} W. \tag{3.21}$$

The quantity Γ is shown in Fig. 3.2. Γ is related to the mass operator, or the self energy of the electron in the laser. The Feynman diagram for the self energy is shown in Fig. 3.5, and constitutes the first radiative correction to the Dirac-Volkov propagator (2.62). As in the usual QED [141], this diagram is the first correction to the mass in the denominator of the propagator,

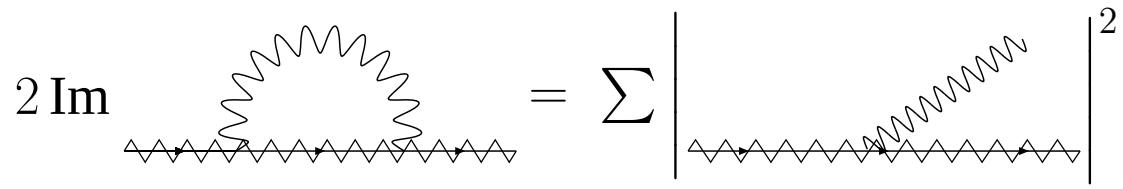

Figure 3.6: Equivalence of the mass operator and the total probability of laser-induced Compton scattering via the Cutkosky rules. The sum $\sum$ (integration) is over all final states of the electron and photon.

so that (using the notation of subsection 2.2.5)

$$\begin{aligned} G(x,x') =& \frac{1}{(2\pi)^4}\int \mathrm{d}^4p E(p,x)\frac{\hat{p}+m}{p^2-m^2}\bar{E}(p,x') \\ \rightarrow& \frac{1}{(2\pi)^4}\int \mathrm{d}^4p E(p,x)\frac{\hat{p}+m}{p^2-m^2+2im\Gamma}\bar{E}(p,x'). \end{aligned} \tag{3.22}$$

This modification is oversimplified, the true modification of the propagator is more complex [21], but the imaginary mass shift is, as we will see in section 3.4, enough to regularize the cross section when the propagator momentum reaches the mass shell $p^2 = m_*^2$. The diagram in Fig. 3.5 has in general one real part and one imaginary part. The real part gives a small real shift of the mass in the propagator, but we consider only the imaginary part, since this is enough to obtain finite cross sections. The complete mass operator is studied in [10, 21] with different methods.

The imaginary part of the mass operator and the total rate W for Compton scattering are related according to the Cutkosky rules, as discussed in section A.2. These rules, depicted graphically in Fig. 3.6, tell us that instead of calculating the imaginary part of the mass operator, we can instead calculate the total rate for Compton scattering, which turns out to be more manageable.

3.3 Bremsstrahlung matrix element and cross section

In this section we derive the matrix element and cross section for the process of laser-assisted bremsstrahlung. The Feynman diagrams, to be added together to obtain the total amplitude of the process, are shown in Fig. 3.7. To get a feeling what is meant by an "all-order" treatment, we show in Fig. 3.8 the perturbative expansion of one of the laser-dressed diagrams in Fig. 3.7, to first order in the electron-laser coupling.

3.3.1 Matrix element for linear polarization

Laser-assisted bremsstrahlung describes the interaction between an electron and three external fields: the laser field, the Coulomb field, and the field of the spontaneously emitted bremsstrahlung photon. Of these three fields, the interaction with the laser field is treated to all orders, non-perturbatively, by using Volkov states and the Dirac-Volkov propagator for the electron lines.

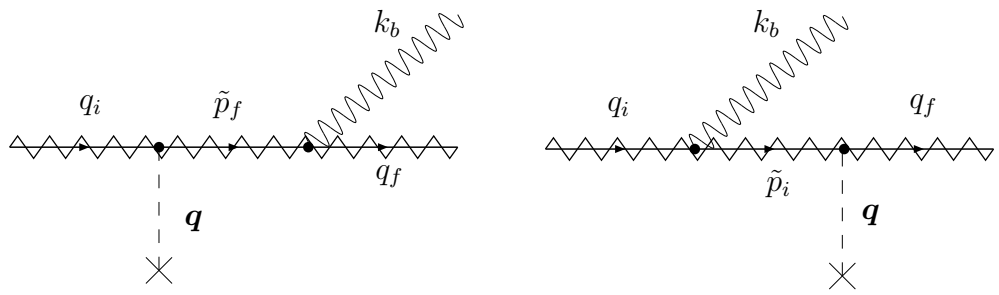

Figure 3.7: The Feynman diagrams for laser-assisted bremsstrahlung. External electron lines and propagators are denoted with a wiggling line superimposed on a straight line, to stress that the laser-electron interaction is treated nonperturbatively. The initial electron has effective four-momentum q_i, the final q_f and the intermediate electron propagator momentum is denoted by $\tilde{p}_{i,f}$ The emitted bremsstrahlung photon has four-momentum k_b, and the virtual Coulomb field photon, depicted with a dashed line, has three-momentum $\boldsymbol{q}$. Time flows from left to right.

The interaction with the Coulomb field and the emitted photon are treated as perturbations, they act only in one vertex each in the Feynman diagram Fig. 3.7. The linearly polarized laser is as in chapter 2 described by the four-vector potential

$$A^\mu(\phi) = a^\mu \cos\phi, \tag{3.23}$$

where $\phi = k \cdot x$ is the laser phase, and $k = (\omega, \boldsymbol{k})$ the laser wave four-vector. The polarization vector a satisfies $a \cdot k = 0$ in Lorenz gauge. In this section we only consider linear polarization of the laser. Note also that we do not enforce $a^0 = 0$, since we want to keep open the possibility of gauge-transforming $a^\mu \to a^\mu + \Lambda k^\mu$ later. The four-vector potential of the static screened Coulomb field in Coulomb gauge, with atomic number Z, reads [76]

$$A^\mu_C(x) = -Ze\frac{e^{-|\boldsymbol{x}|/\ell}}{4\pi|\boldsymbol{x}|}\delta^{0\mu} = -\frac{1}{(2\pi)^3}\int \mathrm{d}^4q \frac{Ze}{\boldsymbol{q}^2 + \ell^{-2}} e^{-iq\cdot x}\delta(q^0)\delta^{\mu 0}, \tag{3.24}$$

where the Fourier transform in the last step is introduced for practical reasons. Here we have introduced a parameter ℓ, the screening length. As will be obvious in the discussion in section 3.4, a finite screening length is needed to obtain finite cross sections for small momentum transfer $\boldsymbol{q}$. In the limit $\ell \to \infty$ we retrieve the usual Coulomb potential. Observe that the expression (3.24) is not relativistically invariant, by choosing this form of the potential we choose the frame of calculation to be the rest frame of the nucleus. For a nucleus at rest this frame coincides with the laboratory frame. We also need the four-vector potential of the emitted photon:

$$A^\mu_{b,\lambda}(x) = \frac{1}{\sqrt{2\omega_b V}}\epsilon^\mu_{b,\lambda} e^{ik_b\cdot x}, \tag{3.25}$$

the same as (3.3). Putting the two potentials Eqs. (3.25), (3.24), together with the initial and final Volkov wave functions $\psi_{q_{i,f},r_{i,f}}$, Eq. (2.32), with effective four-momentum $q_{i,f}$ and spin $r_{i,f}$ and the Dirac-Volkov propgator $G(x_2, x_1)$, Eq. (2.62), we can write the second order transition

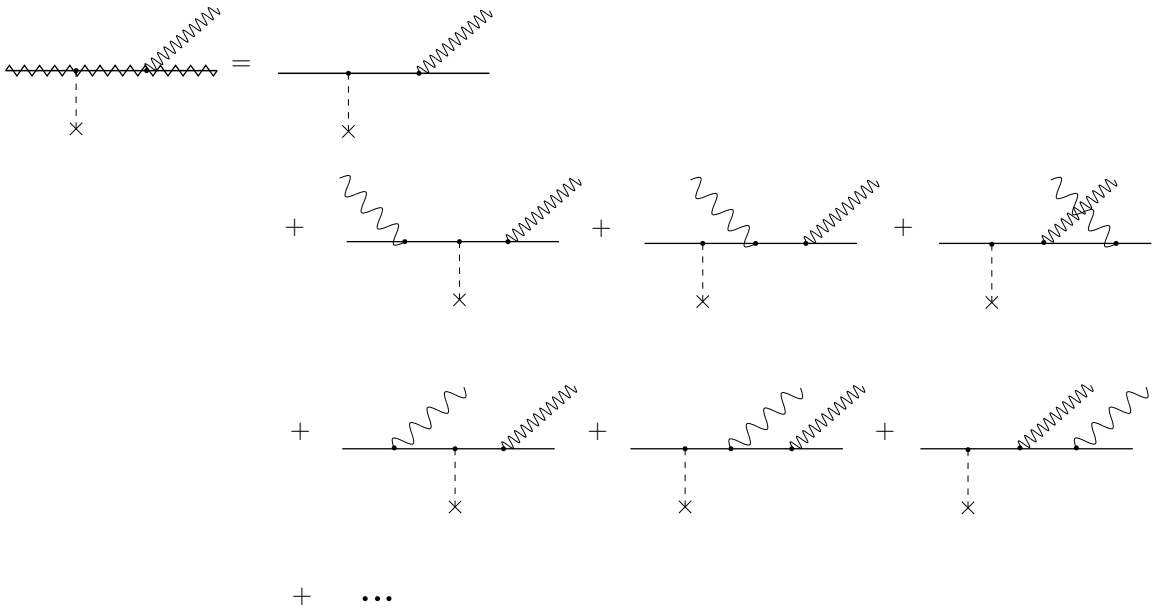

Figure 3.8: Laser-dressed Feynman diagrams in the perturbative picture. Here is shown the perturbative expansion of one of the diagrams in Fig. 3.7, to first order in the electron-laser coupling, that is, with one interaction with a laser photon. In the diagrams above, the laser photon is drawn as a wavy line with comparatively long wavelength, and the emitted bremsstrahlung photon as a wavy line with short wavelength. The Coulomb field photon is drawn with a dashed line. The first line shows the fully laser-dressed diagram to the left, and the field-free diagram to the right, the second line shows diagrams where one laser photon is absorbed, and the last line displays diagrams where one laser photon is emitted into the laser field. In the perturbative expansion, the number of diagrams to take into account grows extremely fast, already in second order (not shown in this figure) there are an additional 24 contributing diagrams. By employing the exact wave functions in the laser field, the Volkov states, all diagrams to all orders are accurately accounted for.

matrix element S_{fi} for laser-assisted bremsstrahlung corresponding to the coherent sum of the two Feynman diagrams in Fig. 3.7:

$$\begin{aligned} S_{fi} &= S_{fi}^{(1)} + S_{fi}^{(2)} \\ &= e^2 \int \mathrm{d}^4x_1 \int \mathrm{d}^4x_2 \overline{\psi}_{q_f,r_f}(x_2) \Big[i\hat{A}_{b,\lambda}(x_2) iG(x_2,x_1) i\hat{A}_C(x_1) \\ &\qquad + i\hat{A}_C(x_2) iG(x_2,x_1) i\hat{A}_{b,\lambda}(x_1) \Big] \psi_{q_i,r_i}(x_1) \\ &= 2\pi i \sum_{n,s=-\infty}^{\infty} \frac{Ze^3m}{\sqrt{2\omega_b Q_i Q_f V^3}} \frac{\delta(Q_f - Q_i + n\omega + \omega_b)}{\boldsymbol{q}^2 + \ell^{-2}} \bar{u}_{r_f}(p_f) \\ &\qquad \times \left[M_f^s \frac{\hat{\tilde{p}}_f + \frac{e^2a^2}{4k\cdot\tilde{p}_f}\hat{k} + m}{\tilde{p}_f^2 - m_*^2} F_i^{s-n} + F_f^{s+n} \frac{\hat{\tilde{p}}_i + \frac{e^2a^2}{4k\cdot\tilde{p}_i}\hat{k} + m}{\tilde{p}_i^2 - m_*^2} M_i^s \right] u_{r_i}(p_i). \end{aligned} \tag{3.26}$$

Here

$$\begin{aligned} M_f^s &= A_0(s, \alpha_f - \tilde{\alpha}_f, \beta_f - \tilde{\beta}_f) \hat{\epsilon}_{b,\lambda} \\ &\quad + A_1(s, \alpha_f - \tilde{\alpha}_f, \beta_f - \tilde{\beta}_f) \left(\hat{\epsilon}_{b,\lambda} \frac{e\hat{k}\hat{a}}{2k\cdot\tilde{p}_f} + \frac{e\hat{a}\hat{k}}{2k\cdot p_f} \hat{\epsilon}_{b,\lambda} \right) \\ &\quad + \frac{e\hat{a}\hat{k}}{2k\cdot p_f} \hat{\epsilon}_{b,\lambda} \frac{e\hat{k}\hat{a}}{2k\cdot\tilde{p}_f} A_2(s, \alpha_f - \tilde{\alpha}_f, \beta_f - \tilde{\beta}_f), \end{aligned} \tag{3.27}$$

$$\begin{aligned} F_i^{s-n} &= A_0(s-n, \alpha_i - \tilde{\alpha}_f, \beta_i - \tilde{\beta}_f) \gamma^0 \\ &\quad + A_1(s-n, \alpha_i - \tilde{\alpha}_f, \beta_i - \tilde{\beta}_f) \left(\gamma^0 \frac{e\hat{k}\hat{a}}{2k\cdot p_i} + \frac{e\hat{a}\hat{k}}{2k\cdot\tilde{p}_f} \gamma^0 \right) \\ &\quad + A_2(s-n, \alpha_i - \tilde{\alpha}_f, \beta_i - \tilde{\beta}_f) \frac{e\hat{a}\hat{k}}{2k\cdot\tilde{p}_f} \gamma^0 \frac{e\hat{k}\hat{a}}{2k\cdot p_i}, \end{aligned} \tag{3.28}$$

$$\begin{aligned} F_f^{s+n} &= A_0(s+n, \alpha_f - \tilde{\alpha}_i, \beta_f - \tilde{\beta}_i) \gamma^0 \\ &\quad + A_1(s+n, \alpha_f - \tilde{\alpha}_i, \beta_f - \tilde{\beta}_i) \left(\gamma^0 \frac{e\hat{k}\hat{a}}{2k\cdot\tilde{p}_i} + \frac{e\hat{a}\hat{k}}{2k\cdot p_f} \gamma^0 \right) \\ &\quad + \frac{e\hat{a}\hat{k}}{2k\cdot p_f} \gamma^0 \frac{e\hat{k}\hat{a}}{2k\cdot\tilde{p}_i} A_2(n+s, \alpha_f - \tilde{\alpha}_i, \beta_f - \tilde{\beta}_i), \end{aligned} \tag{3.29}$$

and

$$\begin{aligned} M_i^s &= A_0(s, \alpha_i - \tilde{\alpha}_i, \beta_i - \tilde{\beta}_i) \hat{\epsilon}_{b,\lambda} \\ &\quad + A_1(s, \alpha_i - \tilde{\alpha}_i, \beta_i - \tilde{\beta}_i) \left(\hat{\epsilon}_{b,\lambda} \frac{e\hat{k}\hat{a}}{2k\cdot p_i} + \frac{e\hat{a}\hat{k}}{2k\cdot\tilde{p}_i} \hat{\epsilon}_{b,\lambda} \right) \\ &\quad + A_2(s, \alpha_i - \tilde{\alpha}_i, \beta_i - \tilde{\beta}_i) \frac{e\hat{a}\hat{k}}{2k\cdot\tilde{p}_i} \hat{\epsilon}_{b,\lambda} \frac{e\hat{k}\hat{a}}{2k\cdot p_i}, \end{aligned} \tag{3.30}$$

with

$$\tilde{p}_f = q_f + sk + k_b, \qquad \tilde{p}_i = q_i + sk - k_b, \tag{3.31}$$

$$\boldsymbol{q} = \boldsymbol{q}_f - \boldsymbol{q}_i + n\boldsymbol{k} + \boldsymbol{k}_b, \tag{3.32}$$

$$\alpha_{i,f} = \frac{ea \cdot p_{i,f}}{k \cdot p_{i,f}}, \qquad \beta_{i,f} = \frac{e^2 a^2}{8 p_{i,f} \cdot k}, \tag{3.33}$$

and

$$\tilde{\alpha}_{i,f} = \frac{ea \cdot \tilde{p}_{i,f}}{k \cdot \tilde{p}_{i,f}}, \qquad \tilde{\beta}_{i,f} = \frac{e^2 a^2}{8 \tilde{p}_{i,f} \cdot k}. \tag{3.34}$$

The spinors $u_{r_{i,f}}$ describe the spin state of the in- and outgoing electron, respectively. Note that $k \cdot p_{i,f} = k \cdot q_{i,f}$, and that due to $k^2 = 0$, $\tilde{\alpha}_{i,f}$ and $\tilde{\beta}_{i,f}$ are independent of the summation index s. Equation (3.26) was first obtained in [156]. A few remarks regarding the derivation of Eq. (3.26) are in order. To be able to perform the space-time integration over the two interaction coordinates in the second row of Eq. (3.26), it was necessary to resort to the Fourier decomposition into infinite sums of plane waves of both the wave functions $\psi_{q_{i,f}}$, Eq. (2.47), and the Dirac-Volkov propagator, Eq. (2.64).

In general, one has to formulate an S-matrix scattering problem as transition from a collection of initial plane waves, defined at $t = -\infty$, to a collection of final plane waves, defined at $t = +\infty$. In other words, in the S-matrix formalism, only space-time integrations of the form

$$\int \mathrm{d}^4 x A(p) e^{-ip\cdot x} = (2\pi)^4 A(p) \delta^4(p) \tag{3.35}$$

are defined, with p being the sum of momenta flowing into the vertex and $A(p)$ being some space-time independent part of the amplitude. They give rise to energy-momentum conserving delta functions at the vertices of the Feynman diagram.

Inserting the Fourier decomposed expressions for the quantities $\psi_{q_{i,f}}$, G, A_C, and $A_{b,\lambda}$ in the second row of Eq. (3.26), all integrations can be taken, leaving one energy-conserving delta function. Since each of the wave functions involves one infinite sum, and the propagator two, the matrix element is a quadruple infinite sum. Two of these sums can fortunately be performed using the addition theorem [Eq. (5.21)], leaving the matrix element expressed as two infinite sums over n and s. We summarize the calculation procedure leading to the expression (3.26) by noting that this method of calculating transition amplitudes is very similar to Fourier's method of solving a differential equation: The solution for one mode of the initial wavefunction scattered into one final mode is known, and to obtain the total amplitude (to satisfy the boundary conditions) one has to sum over all modes.

From the delta function $\delta(Q_f - Q_i + n\omega + \omega_b)$ we gather two things: First, different from the field-free process, in the laser-dressed case it is the effective energy $Q_{i,f} = q^0_{i,f}$ that enters in the energy-conservation relation. The effective energy is related to the energy outside the laser in a nontrivial way, if we write $p = (E, \sqrt{E^2 - m^2}\boldsymbol{p}/|\boldsymbol{p}|)$ we have, according to the definition (2.33),

$$Q = E + \frac{e^2|a|^2}{4k \cdot p}\omega = E + \frac{e^2|a^2|}{E - \sqrt{E^2 - m^2}\frac{\boldsymbol{p}}{|\boldsymbol{p}|} \cdot \frac{\boldsymbol{k}}{|\boldsymbol{k}|}}, \tag{3.36}$$

which in general does not have a unique solution E even if Q and the direction $\boldsymbol{p}/|\boldsymbol{p}|$ is known. Note however that $Q \geq m_*$ implies $E \geq m$. Second, even though the laser field was introduced as a classical, external field, due to the periodicity of the laser, the matrix element is expressed

as an infinite sum over a discrete index n, the quantity appearing in the energy-conservation relation being $n\omega$. The interpretation is clear: we can speak of a net number of $|n|$ photon exchanged with the laser during the process. In our convention, negative n corresponds to absorption and positive n to emission of laser-mode photons. In the same way, the sum over s represents the propagation of the electron under the influence of the laser, the total amplitude for propagation from the first interaction coordinate to the second being given by a coherent sum over amplitudes in which s photons are exchanged. It is also intuitively clear that no further sum is needed; in general a laser-modified Feynman diagram with N number of vertices results in N infinite sums.

3.3.2 Gauge invariance

The matrix element (3.26) must be invariant under the gauge transformations

$$a^\mu \to a^\mu + \Lambda_1 k^\mu \tag{3.37}$$

and

$$\epsilon^\mu_{b,\lambda} \to \epsilon^\mu_{b,\lambda} + \Lambda_2 k^\mu_b, \tag{3.38}$$

where $\Lambda_{1,2}$ is an arbitrary constant (that may depend on k or k_b). In general, a gauge transformation in QED involves a shift

$$\mathcal{A}_\mu \to \mathcal{A}_\mu + \partial_\mu g(x), \tag{3.39}$$

where $\mathcal{A}_\mu$ is an arbitrary light field (laser or single photon) and $g(x)$ is an arbitrary function of the space-time coordinate x. However, by requiring the vector potential $\mathcal{A}_\mu$ to be a plane wave, $\mathcal{A}_\mu = \epsilon_\mu f(\varkappa \cdot x)$, with wave vector $\varkappa_\mu$ and polarization vector ϵ_μ, and that the gauge transformation (3.39) should not change the space-time dependence of $\mathcal{A}_\mu$ [24], then it follows that the most general transformation is $\mathcal{A}_\mu \to \mathcal{A}_\mu + \varkappa_\mu \Lambda f(\varkappa \cdot x)$, or $\epsilon_\mu \to \epsilon_\mu + \Lambda \varkappa_\mu$. Here Λ is an arbitrary constant that is independent on x. It is the gauge symmetry (3.39) that gives rise to current conservation: from the QED Lagrangian $\mathcal{L}_{\text{QED}}$ [141], by construction invariant under (3.39),

$$\mathcal{L}_{\text{QED}} = \overline{\psi}(i\hat{\partial} - m)\psi - \frac{1}{4}(\mathcal{F}_{\mu\nu})^2 - e\overline{\psi}\hat{\mathcal{A}}\psi, \tag{3.40}$$

with $\mathcal{F}_{\mu\nu} = \partial_\mu \mathcal{A}_\nu - \partial_\nu \mathcal{A}_\mu$, we obtain the Euler-Lagrange equation for the field tensor $\mathcal{F}_{\mu\nu}$, the inhomogeneous Maxwell equation,

$$\partial_\mu \mathcal{F}^{\mu\nu} = e\overline{\psi}\gamma^\nu\psi = ej^\nu. \tag{3.41}$$

Current conservation $\partial_\nu j^\nu = 0$ follows automatically from the antisymmetry of $\mathcal{F}_{\mu\nu}$.

To explicitly show invariance under the transformations (3.37), (3.38), it is easier to look at the expression for the matrix element before making any integrations and Bessel function expansions. To see invariance under the transformation (3.37), we note that because $a \cdot k = k \cdot k = 0$, terms like A^2 and $\hat{A}\hat{k}$ are invariant. Under the transformation (3.37), the conjugate wavefunction $\overline{\psi}_{q_f}(x_2)$ picks up an exponential $\exp(i\int_0^{k\cdot x_2} e\Lambda_1 \mathrm{d}\tilde{\phi})$, the wavefunction $\psi_{q_i}(x_1)$ picks up an exponential $\exp(-i\int_0^{k\cdot x_1} e\Lambda_1 \mathrm{d}\tilde{\phi})$ and the Green's function picks up the factor $\exp(-i\int_{k\cdot x_1}^{k\cdot x_2} e\Lambda_1 \mathrm{d}\tilde{\phi})$. These contributions cancel when forming the matrix element.

To see invariance under the transformation (3.38) is slightly more difficult. That the matrix element indeed is invariant is shown in section B.2.

3.3.3 Differential cross section

The differential cross section $\mathrm{d}\sigma$, or the rate divided by the incoming particle flux, is calculated from the matrix element in the usual way [76]

$$\mathrm{d}\sigma = \frac{1}{T|\boldsymbol{v}_i^{\text{eff}}|/V}\,|S_{fi}|^2\,\frac{V\mathrm{d}^3k_b}{(2\pi)^3}\frac{V\mathrm{d}^3q_f}{(2\pi)^3}. \tag{3.42}$$

Here T is the long observation time and the incoming particle flux $|\boldsymbol{v}_i^{\text{eff}}|/V$ is expressed through the effective velocity $\boldsymbol{v}_i^{\text{eff}}$, with which we understand the average velocity of the laser-dressed electron

$$\boldsymbol{v}_i^{\text{eff}} = \frac{\boldsymbol{q}_i}{Q_i}. \tag{3.43}$$

Since we are not interested in investigating polarization or spin properties, we average over the spin of the incoming electron, and sum over the spin of the final electron. This summation can be performed with the usual formulas, resulting in the cross section being expressed as a trace over a 4×4 matrix. Another way is to use an explicit representation of the spinors $u_{1,2}$ and to do the summation explicitly. For further discussion on the spin sums, see subsection 3.5.2. For the photon sums, gauge invariance (as shown in section B.2 on page 139) in principle allows to use the formula [76]

$$\sum_{\lambda=1,2}\epsilon_{b,\lambda}^{\mu}\epsilon_{b,\lambda}^{\nu} \to -g^{\mu\nu}. \tag{3.44}$$

However, here it is better to use an explicit basis of the polarization vectors $\epsilon_{b,1}$, $\epsilon_{b,2}$ and sum explicitly, when evaluating the cross section numerically.

Inserting the matrix element S_{fi} from Eq. (3.26) into Eq. (3.42), rewriting the phase space factors as

$$\mathrm{d}^3k_b = \omega_b^2\mathrm{d}\omega_b\mathrm{d}\Omega_b, \qquad \mathrm{d}^3q_f = |\boldsymbol{q}_f|Q_f\mathrm{d}Q_f\mathrm{d}\Omega_f, \tag{3.45}$$

where $\Omega_{b,f}$ is the solid angle of the corresponding particle, summing over spins and polarization, and making the standard substitution $\delta^2(x) = T\delta(x)/(2\pi)$ [76], we obtain the differential cross section $\mathrm{d}\sigma/(\mathrm{d}\omega_b\mathrm{d}\Omega_b\mathrm{d}\Omega_f)$ for laser-assisted bremsstrahlung,

$$\begin{aligned}\frac{\mathrm{d}\sigma}{\mathrm{d}\Omega_f\mathrm{d}\Omega_b\mathrm{d}\omega_b} = \frac{\alpha(\alpha Z)^2\omega_b}{8\pi^2}\sum_{\lambda,n}\frac{|\boldsymbol{q}_f|}{|\boldsymbol{q}_i|}\frac{1}{\left(\boldsymbol{q}^2+\ell^{-2}\right)^2}\delta(Q_f - Q_i + n\omega + \omega_b)\mathrm{d}Q_f \\ \times\,\mathrm{Tr}\left[(\hat{p}_f+m)\left(\sum_s\mathcal{H}_{s,n}\right)(\hat{p}_i+m)\left(\sum_{s'}\widetilde{\mathcal{H}}_{s',n}\right)\right],\end{aligned} \tag{3.46}$$

where

$$\mathcal{H}_{s,n} = \left[M_f^s\frac{\hat{\tilde{p}}_f + \frac{e^2a^2}{4k\cdot\tilde{p}_f}\hat{k}+m}{\tilde{p}_f^2-m_*^2}F_i^{s-n} + F_f^{s+n}\frac{\hat{\tilde{p}}_i + \frac{e^2a^2}{4k\cdot\tilde{p}_i}\hat{k}+m}{\tilde{p}_i^2-m_*^2}M_i^s\right] \tag{3.47}$$

and

$$\widetilde{\mathcal{H}}_{s',n} = \gamma^0 \mathcal{H}^\dagger_{s',n} \gamma^0. \tag{3.48}$$

The matrices $F_{i,f}$ and $M_{i,f}$ were given in Eqs. (3.27), (3.28), (3.29) and (3.30).

The cross section is thus expressed as an infinite sum over photon orders n, through one internal sum over intermediate photon orders s. After integration over $\mathrm{d}Q_f$, so that $Q_f = Q_i - n\omega - \omega_b$ everywhere, the sum over n in (3.46) is bounded by the condition $Q_f \geq m_*$, but the sum over s and s' goes from $-\infty$ to ∞. Note also that this integration makes the arguments $\alpha_{i,f} - \tilde{\alpha}_{i,f}$, $\beta_{i,f} - \tilde{\beta}_{i,f}$ implicitly dependent on n through q_f and Q_f. Another thing worth commenting is that the final phase space for the electron is expressed through the laser-dressed momentum $\boldsymbol{q}_f$. This is the most convenient way, since the energy conservation relation is expressed through the effective energies $Q_{i,f}$. An equally valid approach, pursued in [138, 139], is to express the final phase space through the momentum at infinity, $\mathrm{d}^3 p_f$. This will however create problems, since the correspondence between the effective energy Q_f and E_f is not one-to-one, as discussed after Eq. (3.36). The two approaches are equivalent if the final momentum of the electron is integrated out, and the normalization factor of the electron wave functions are changed accordingly, since we have $\mathrm{d}^3 q_f / Q_f = \mathrm{d}^3 p_f / E_f$ [24].

3.3.4 Limit of vanishing laser field

In the limit of vanishing laser field, $\xi \to 0$, we expect that the matrix element (3.26) goes to the field free case, the Bethe-Heitler matrix element. Indeed, when $\xi = 0$, the arguments of the generalized Bessel functions vanishes due to the property $A_0(n, 0, 0) = \delta_{n0}$, and the double sum in (3.26) collapses to a single term $n = s = 0$. Consequently, we end up with the Bethe-Heitler matrix element, found in many textbooks [76, 141],

$$\begin{aligned} M^{\text{Bethe-Heitler}} = 2\pi i \frac{Ze^3 m}{\sqrt{2\omega_b E_i E_f V^3}} \frac{\delta(E_f - E_i + \omega_b)}{\boldsymbol{q}^2 + \ell^{-2}} \\ \times \bar{u}_{r_f} \left(\hat{\epsilon}_{b,\lambda} \frac{\hat{p}_f + \hat{k}_b + m}{2p_f \cdot k_b} \gamma^0 - \gamma^0 \frac{\hat{p}_i - \hat{k}_b + m}{2p_i \cdot k_b} \epsilon_{b,\lambda} \right) u_{r_i}, \end{aligned} \tag{3.49}$$

using the same notation as in Eq. (3.26), in particular $\boldsymbol{q} = \boldsymbol{p}_f - \boldsymbol{p}_i + \boldsymbol{k}_b$. Constructing the spin and polarization-averaged cross section with formula (3.42), taking the trace (possible since there is at most products of 8 gamma matrices involved, see the discussion in subsection 3.5.2), we end up with the Bethe-Heitler cross section

$$\begin{aligned} \frac{\mathrm{d}\sigma}{\mathrm{d}\Omega_f \mathrm{d}\Omega_b \mathrm{d}\omega_b} = \frac{\alpha(Z\alpha)^2}{4\pi^2} \frac{|\boldsymbol{p}_f|}{|\boldsymbol{p}_i|} \frac{1}{(\boldsymbol{q}^2 + \ell^{-2})^2} \frac{\omega_b}{(k_b \cdot p_i)^2 (k_b \cdot p_f)^2} \\ \times \Big[2\boldsymbol{q}^2 k_b \cdot p_i k_b \cdot p_f (E_f^2 + E_i^2 - p_i \cdot p_f) \\ + \left((k_b \cdot p_i)^2 + (k_b \cdot p_f)^2 \right) (\boldsymbol{q}^2 m^2 - 2k_b \cdot p_i k_b \cdot p_f) \\ - 4m^2 (E_f k_b \cdot p_f - E_i k_b \cdot p_i)^2 \Big], \end{aligned} \tag{3.50}$$

where ω_b is bounded from above by the demand $E_f = E_i - \omega_b \geq m$. Eq. (3.50) is the preferred way to write the Bethe-Heitler cross section, expressed in relativistically invariant dot products of the different vectors involved. However, the original work [25], and most textbooks [24, 76] write the formula in a more explicit way, expressed in the angles between the vectors. To show the equivalence is a nice exercise in algebra.

3.3.5 Matrix element for circular polarization

Since we present results also for the case of circularly polarized laser light in section 3.5, we give the final result for the formula for the matrix element here for completeness, without any detailed discussion. See Eq. (2.38) for the expression of the Volkov wave function for circular polarization. For convenience, we repeat the expression for the vector potential of a circularly polarized laser,

$$A^\mu(\phi) = a_1^\mu \cos\phi + a_2^\mu \sin\phi, \tag{3.51}$$

with polarization vectors $a_{1,2}$ satisfying

$$a_1 \cdot a_2 = 0, \qquad a_1^2 = a_2^2 = -\tilde{a}^2. \tag{3.52}$$

The matrix element has the same form as Eq. (3.26), but with the terms $\frac{e^2a^2}{4k\cdot\tilde{p}_{i,f}}\hat{k}$ replaced by $-\frac{e^2\tilde{a}^2}{2k\cdot\tilde{p}_{i,f}}\hat{k}$, and M_f^s, F_i^{s-n}, F_f^{s+n} and M_i^s replaced by (see also [163])

$$\begin{aligned} M^s_{f,\text{circ}} = {} & B_0(s, \tilde{\alpha}_f^1 - \alpha_f^1, \tilde{\alpha}_f^2 - \alpha_f^2)\left(\hat{\epsilon}_{b,\lambda} + \frac{e^2\tilde{a}^2\hat{k}\hat{\epsilon}_{b,\lambda}\hat{k}}{4k\cdot q_f k\cdot\tilde{p}_f}\right) \\ & + B_1(s, \tilde{\alpha}_f^1 - \alpha_f^1, \tilde{\alpha}_f^2 - \alpha_f^2)\left(\frac{e\hat{\epsilon}_{b,\lambda}\hat{k}\hat{a}_1}{2k\cdot\tilde{p}_f} + \frac{e\hat{a}_1\hat{k}\hat{\epsilon}_{b,\lambda}}{2k\cdot q_f}\right) \\ & + B_2(s, \tilde{\alpha}_f^1 - \alpha_f^1, \tilde{\alpha}_f^2 - \alpha_f^2)\left(\frac{e\hat{\epsilon}_{b,\lambda}\hat{k}\hat{a}_2}{2k\cdot\tilde{p}_f} + \frac{e\hat{a}_2\hat{k}\hat{\epsilon}_{b,\lambda}}{2k\cdot q_f}\right), \end{aligned} \tag{3.53}$$

$$\begin{aligned} F^{s-n}_{i,\text{circ}} = {} & B_0^*(s-n, \tilde{\alpha}_f^1 - \alpha_i^1, \tilde{\alpha}_f^2 - \alpha_i^2)\left(\gamma^0 + \frac{e^2\tilde{a}^2\hat{k}\gamma^0\hat{k}}{4k\cdot q_i k\cdot\tilde{p}_f}\right) \\ & + B_1^*(s-n, \tilde{\alpha}_f^1 - \alpha_i^1, \tilde{\alpha}_f^2 - \alpha_i^2)\left(\frac{e\gamma^0\hat{k}\hat{a}_1}{2k\cdot q_i} + \frac{e\hat{a}_1\hat{k}\gamma^0}{2k\cdot\tilde{p}_f}\right) \\ & + B_2^*(s-n, \tilde{\alpha}_f^1 - \alpha_i^1, \tilde{\alpha}_f^2 - \alpha_i^2)\left(\frac{e\gamma^0\hat{k}\hat{a}_2}{2k\cdot q_i} + \frac{e\hat{a}_2\hat{k}\gamma^0}{2k\cdot\tilde{p}_f}\right), \end{aligned} \tag{3.54}$$

$$\begin{aligned} F^{s+n}_{f,\text{circ}} = {} & B_0(s+n, \tilde{\alpha}_i^1 - \alpha_f^1, \tilde{\alpha}_i^2 - \alpha_f^2)\left(\gamma^0 + \frac{e^2\tilde{a}^2\hat{k}\gamma^0\hat{k}}{4k\cdot q_f k\cdot\tilde{p}_i}\right) \\ & + B_1(s+n, \tilde{\alpha}_i^1 - \alpha_f^1, \tilde{\alpha}_i^2 - \alpha_f^2)\left(\frac{e\gamma^0\hat{k}\hat{a}_1}{2k\cdot\tilde{p}_i} + \frac{e\hat{a}_1\hat{k}\gamma^0}{2k\cdot q_f}\right) \\ & + B_2(s+n, \tilde{\alpha}_i^1 - \alpha_f^1, \tilde{\alpha}_i^2 - \alpha_f^2)\left(\frac{e\gamma^0\hat{k}\hat{a}_2}{2k\cdot\tilde{p}_i} + \frac{e\hat{a}_2\hat{k}\gamma^0}{2k\cdot q_f}\right), \end{aligned} \tag{3.55}$$

and

$$M^s_{i,\text{circ}} = B^*_0(s, \tilde{\alpha}^1_i - \alpha^1_i, \tilde{\alpha}^2_i - \alpha^2_i)\left(\hat{\epsilon}_{b,\lambda} + \frac{e^2\tilde{a}^2\hat{k}\hat{\epsilon}_{b,\lambda}\hat{k}}{4k\cdot q_i k\cdot \tilde{p}_i}\right) + B^*_1(s, \tilde{\alpha}^1_i - \alpha^1_i, \tilde{\alpha}^2_i - \alpha^2_i)\left(\frac{e\hat{\epsilon}_{b,\lambda}\hat{k}\hat{a}_1}{2k\cdot q_i} + \frac{e\hat{a}_1\hat{k}\hat{\epsilon}_{b,\lambda}}{2k\cdot \tilde{p}_i}\right) + B^*_2(s, \tilde{\alpha}^1_f - \alpha^1_f, \tilde{\alpha}^2_f - \alpha^2_f)\left(\frac{e\hat{\epsilon}_{b,\lambda}\hat{k}\hat{a}_2}{2k\cdot q_i} + \frac{e\hat{a}_2\hat{k}\hat{\epsilon}_{b,\lambda}}{2k\cdot \tilde{p}_i}\right), \tag{3.56}$$

with the obvious notation

$$\alpha^{1,2}_{i,f} = \frac{ea_{1,2}\cdot q_{i,f}}{k\cdot q_{i,f}}, \qquad \tilde{\alpha}^{1,2}_{i,f} = \frac{ea_{1,2}\cdot \tilde{p}_{i,f}}{k\cdot \tilde{p}_{i,f}}, \tag{3.57}$$

and the B_j's are defined through the usual Bessel function, if $x + iy = re^{i\varphi}$ and $x - iy = re^{i\tilde{\varphi}}$, with $\varphi, \tilde{\varphi} \in (-\pi, \pi]$, then

$$B_0(n, x, y) = J_n(r)e^{is(\varphi-\tilde{\varphi})}, \qquad B_j(n, x, y) = \frac{i^{1-j}}{2}\left[B_0(n-1, x, y) + B_0(n+1, x, y)\right], \tag{3.58}$$

with $j = 1, 2$. The main difference is thus that the matrix element is expressed in terms of the usual Bessel function $J_n(\alpha)$ instead of the generalized Bessel function $A_0(n, \alpha, \beta)$ as is the case for linear polarization. The reason is, as discussed in section 2.2 [page 25], that the amplitude of the vector potential (and consequently also the amplitude of the electric and magnetic field) for circular polarization is constant in time, $A^2(\phi) = -\tilde{a}^2$, and therefore the Volkov wave function contains no $\sin(2\phi)$ term, and can consequently be expanded into a Fourier series containing the usual Bessel function $J_n(\alpha)$ only. Since the usual Bessel function is considerably easier to handle from a numerical point of view (see chapter 5), this means that the evaluation of the cross section for circular polarization is less demanding, even though there are more terms to deal with (polarization vectors a^μ_1 and a^μ_2 instead of just a^μ).

3.4 Resonances in the laser-dressed propagator and unphysical infinities

The most obvious, and also most interesting, feature of the laser-dressed cross section (3.46) is the possibility for the momentum of the intermediate electron to satisfy the energy-momentum relation of a real Volkov particle,

$$\tilde{p}^2_f - m^2_* = 2(q_f\cdot k_b + sq_f\cdot k + sk\cdot k_b) = 0, \tag{3.59}$$

and

$$\tilde{p}^2_i - m^2_* = 2(-q_i\cdot k_b + sq_i\cdot k - sk\cdot k_b) = 0. \tag{3.60}$$

At values of the parameters satisfying either Eqs. (3.59), (3.60), the cross section is formally infinite. Physically, this divergence has the following reason: Since in a strong laser, both processes corresponding to the two vertices in the Feynman diagram for laser-assisted bremsstrahlung, laser-induced Compton scattering (see the discussion in section 3.2) and laser-assisted Coulomb scattering (see [139, 169]) can occur independently. Consequently, if the intermediate electron satisfies the conditions (3.59), (3.60), the matrix element (3.26) factorizes into the product of the matrix elements for the first-order processes Compton scattering and Coulomb scattering, with a divergent factor in between. One may check that the matrix M_i^s in Eq. (3.30) goes to a matrix element equivalent to the one for Compton scattering, Eq. (3.5), in the limit where (3.60) is satisfied. At the resonances, perturbation theory actually breaks down, and to obtain finite results, either all-order corrections have to be taken into account, or one has to introduce some kind of cutoff. We solve the problem, as discussed below in subsection 3.4.1, by including an imaginary part to the energy of the electron. In this section we also elaborate somewhat on other possible ways of regularizing the divergence. Mathematically, the divergence comes from the integration over an infinite volume in the second line of Eq. (3.26). Important is here that the sum over n in Eq. (3.26) is discrete. Were the sum over n replaced by an integral, we could use the Feynman prescription (the small imaginary term $i\varepsilon$ in the propagator $1/[\tilde{p}_{i,f}^2 - m_*^2 + i\varepsilon]$), and perform the integral. Compare the treatment of poles in the photon propagator in an external magnetic field in [13, page 167].

Solving Eqs. (3.59), (3.60) for the frequency ω_b we obtain

$$\begin{aligned} \omega_b^{\text{peak 1}} &= \frac{-sq_f \cdot k}{sk \cdot k_b^{\text{dir}} + q_f \cdot k_b^{\text{dir}}}, \\ \omega_b^{\text{peak 2}} &= \frac{sq_i \cdot k}{sk \cdot k_b^{\text{dir}} + q_i \cdot k_b^{\text{dir}}}, \end{aligned} \tag{3.61}$$

with $k_b^{\text{dir}} = (1, \boldsymbol{k}_b/|\boldsymbol{k}_b|)$, equivalent to the nonlinear Compton formula (3.9). Note that in general we have $\omega_b^{\text{peak 1}} \neq \omega_b^{\text{peak 2}}$. The spacing between the peaks depends both on ξ through $q_{i,f}$ and the direction of the emitted photon. One can also convince oneself that in the frame where the electron is on average at rest, $q_i = (m_*, \mathbf{0})$, the light will be emitted at integer multiples of the laser frequency, if the term $sk \cdot k_b^{\text{dir}}$ can be neglected, which is the case if $s\omega \ll Q_{i,f}$. Also when $k_b/\omega_b \approx k/\omega$ the resonance frequencies will be close to harmonics. In other cases, the intensity-dependent positions of the harmonics may be interpreted as a Doppler shift [92].

3.4.1 Regularization by imaginary energy

To obtain finite results at the resonances, we use the results from subsection 3.2.2, and add a small imaginary part to the energy of the initial and final Volkov state, and also shift the mass appearing in the propagator by an imaginary amount. This way of regularizing the Green's function divergences was used previously by several authors in [21, 36, 130, 131, 157]. This procedure is directly analogous to the inclusion of a small imaginary part in the energy of a discrete atomic state, to obtain finite results in resonance scattering [73]. The result after the

imaginary shift for the first propagator in Eq. (3.26) reads:

$$\begin{aligned}\tilde{p}_f^2 - m_*^2 &\to \left[q_f + sk + k_b - i\frac{m}{Q_f}\Gamma(k\cdot q_f)t\right]^2 - m_*^2 + 2im\Gamma(k\cdot\tilde{p}_f)\\ &= 2(q_f\cdot k_b + sq_f\cdot k + sk_b\cdot k) - 2i\frac{m}{Q_f}(s\omega+\omega_b)\Gamma(k\cdot q_f) + 2im\Gamma(k\cdot k_b)\\ &= 2(q_f\cdot k_b + sq_f\cdot k + sk_b\cdot k) + 2im\Gamma_C\left[k\cdot k_b - (s\omega+\omega_b)\frac{k\cdot q_f}{Q_f}\right],\end{aligned} \tag{3.62}$$

where $t^\mu = (1,0,0,0)$ is a timelike unit vector. We write $\Gamma(x)$ (which should not be confused with the mathematical Gamma function) to show the dependence on the variable $x = k\cdot p$. In the last line we have used that $\Gamma(x) = \Gamma_C x$, a linear function of x, which will be valid for our choice of parameters. The crucial thing to notice is that Γ for the final state depends on $k\cdot q_f$ but Γ in the imaginary mass in the propagator depends on the propagator intermediate momentum $\tilde{p}_f$ through $k\cdot\tilde{p}_f$. For the second propagator we have in the same way

$$\begin{aligned}\tilde{p}_i^2 - m_*^2 &\to \left[q_i + sk - k_b - i\frac{m}{Q_i}\Gamma(k\cdot q_i)t\right]^2 - m_*^2 + 2im\Gamma(k\cdot\tilde{p}_i)\\ &= 2sk\cdot q_i - 2q_i\cdot k_b - 2sk\cdot k_b - 2im\Gamma(k\cdot k_b) + 2i\frac{m}{Q_i}(\omega_b - s\omega)\Gamma(k\cdot q_i)\\ &= 2sk\cdot q_i - 2q_i\cdot k_b - 2sk\cdot k_b + 2im\Gamma_C\left[\frac{k\cdot q_i}{Q_i}(\omega_b - s\omega) - k\cdot k_b\right].\end{aligned} \tag{3.63}$$

It should be noted, that regularization by insertion of an imaginary mass *only*, that is, without also letting the energy acquire an imaginary part, which was the method proposed in earlier investigations of the problem [156, 157], overestimates the cross section (both for forward scattering angles, $\boldsymbol{q}_i/|\boldsymbol{q}_i| \approx \boldsymbol{q}_f/|\boldsymbol{q}_f|$ for the fully differential cross section, and for the cross section integrated over Ω_b) by up to 10 orders of magnitude. This is an example where a slight, but understandable, mistake makes a huge difference in the numerical result. The reason is that due to the Coulomb field factor $1/\boldsymbol{q}^4$ in the cross section (3.46), the major contribution to the integrated cross section comes from small values of $\boldsymbol{q}^2$, which occurs at forward scattering angles $\boldsymbol{q}_i/|\boldsymbol{q}_i| \approx \boldsymbol{q}_f/|\boldsymbol{q}_f|$ at small ω. However, for forward scattering (small $\boldsymbol{q}^2$) also the interference between the two amplitudes in Fig. 3.7 is large. Including only the imaginary mass shift destroys the interference, with a huge overestimation of the cross section as a result.

3.4.2 Validity of the imaginary energy method and other ways of regularization

Some remarks are in order regarding the inclusion of the finite widths of the intermediate states in the Dirac-Volkov propagator. First, we recall that our calculation is valid only if the electron spends enough time in the region where the laser field is present, as discussed in subsection 3.1.1. For our approach to be correct, this time period should be much larger than the period of the laser field and the spatial extent of the laser focus region should be much larger than the laser wavelength. In this case, it is permissible to use the employed approximation of a laser pulse of infinite duration (continuous-wave) and of infinite spatial extension, that is, to describe

the laser four-vector potential by $A^\mu(\phi) = a^\mu \cos\phi$. In the regime of short laser pulses, our approximation breaks down, and another approach is called for. A pulsed laser field can in principle be dealt with by the same theoretical framework as is used in this thesis, since Volkov wave functions [Eq. (2.27)] exist also for laser vector potentials of the form

$$A^\mu(\phi) = g(\phi)\left(a_1^\mu \cos\phi + \delta a_2^\mu \sin\phi\right), \tag{3.64}$$

where $g(\phi)$ is an envelope function and δ is a parameter controlling the polarization ($\delta = 1$ gives circular polarization, $\delta = 0$ linear). The only condition is that the laser field is a plane wave. Laser-induced Compton scattering in a pulsed laser field for the case when $g(\phi)$ is a slowly varying function was treated in [127].

Although we have not performed any concrete calculations, that a laser pulse of finite duration actually would provide a cutoff can be seen as follows. If the laser field is given by a vector potential of the form (3.64), the Volkov solution would not be periodic, and an expansion in discrete modes like Eq. (2.47) can not be made. Instead, the Volkov state would be an integral over the continuous spectrum of laser modes,

$$\psi(x) = \frac{1}{N}\int \mathrm{d}\varpi C(\varpi) e^{-ip\cdot x - i\varpi k\cdot x}, \tag{3.65}$$

where N is some normalization factor and $C(\varpi)$ is the continuous equivalent of the Bessel function factor multiplying the exponential in Eq. (2.47). When calculating the matrix element, we would instead of a sum end up with an integral [compare the expression (3.26)],

$$S_{fi} \propto \int \mathrm{d}\varpi \left[\frac{D_f(\varpi)}{(p_f + \varpi k + k_b)^2 - m^2 + i\varepsilon} + \frac{D_i(\varpi)}{(p_i + \varpi k - k_b)^2 - m^2 + i\varepsilon}\right], \tag{3.66}$$

with some non-diverging functions $D_{f,i}(\varpi)$. The point is now, that the integral over ϖ can be performed using the Feynman contour $i\varepsilon$, with finite results. This integration is however not trivial, and can probably only be done numerically even for simple pulse shapes $g(\phi)$.

For the radiative corrections, implemented by including Γ in the propagator denominator, to be the dominant regularization mechanism, it is crucial that the electron is allowed to travel in the laser field for a time span τ longer than $1/\Gamma$ before (or after) scattering at the Coulomb field. If this is not the case, the electron will not have enough time to radiate independently of the Coulomb interaction, and the peaks will necessarily disappear. As follows from Fig. 3.2, in the regime of parameters we are considering ($k\cdot q_i/m^2 \sim 10^{-5}$) we have $\Gamma \sim \omega$. The electron travels in the laser field over many wavelengths by assumption, and thus $\tau \gg 1/\Gamma$ as required. We also note that in an actual experiment, other external parameters like the frequency width of the laser $\Delta\omega$ and the width of the energy distribution of the incoming electron ΔE_i may additionally provide a cutoff for the resonances. For the radiative corrections to dominate as damping mechanism here, it is required that ΔE_i and $\Delta\omega$ are smaller than Γ. In our numerical examples in subsection 3.5.3, where $\Gamma \sim \omega$, $\omega = 1.17$ eV and $E_i = 5.11$ MeV, this condition may be difficult to realize for ΔE_i.

Another alternative is to separate out the non-divergent contribution in a parameter-independent way, as is done in [13, 153]. Here divergent integrals in the squared matrix element, coming

from the photon propagator, are regularized according to

$$\begin{aligned} M^2 \propto \int \mathrm{d}x \frac{f(x)}{|x+i\epsilon|^2} &= \int \mathrm{d}x f(x) \left[\frac{\mathcal{P}}{x} - i\pi\delta(x)\right]\left[\frac{\mathcal{P}}{x} + i\pi\delta(x)\right] \\ &= \mathcal{P}\mathcal{P}\int \mathrm{d}x \frac{f(x)}{x^2} + \pi^2 f(0)\delta(0), \end{aligned} \tag{3.67}$$

where $\mathcal{P}$ signifies the principal value. The factor containing $\delta(0)$ represents the diverging part of the probability, corresponding to the particle (in [13] the photon) going onto the mass shell, and thereby becoming real. The double principal value is evaluated according to [13]

$$\begin{aligned} \mathcal{P}\mathcal{P}\int \mathrm{d}x \frac{f(x)}{x^2} &= \mathcal{P}\mathcal{P}\lim_{h\to 0}\int \mathrm{d}x \frac{f(x)}{(x+h)x} = \mathcal{P}\mathcal{P}\lim_{h\to 0}\int \mathrm{d}x \frac{1}{h}\left[\frac{f(x)}{x} - \frac{f(x-h)}{x}\right] \\ &= \mathcal{P}\int \mathrm{d}x \frac{\frac{\mathrm{d}}{\mathrm{d}x}f(x)}{x} = \mathcal{P}\int \mathrm{d}x \frac{\frac{\mathrm{d}}{\mathrm{d}x}\left[f(x)-f(0)\right]}{x} = \mathcal{P}\int \mathrm{d}x \frac{f(x)-f(0)}{x^2}, \end{aligned} \tag{3.68}$$

which is now finite in the principal value sense. However, the integrand $T(x) = [f(x) - f(0)]/x^2$ is no longer positive definite, and we can no longer speak about this quantity as a differential cross section. To obtain positive definite values one has to perform the integral. Note also that in this way only the squared matrix element is made finite, not the matrix element itself. For the case of laser-assisted bremsstrahlung, we have the corresponding squared matrix element [see Eq. (3.26)]

$$\begin{aligned} \left|S_{fi}^{(2)}\right|^2 &\propto \sum_{s,s'} \frac{f(s,q_i,k_b,k)f^\dagger(s',q_i,k_b,k)}{\left[s(k\cdot q_i - k\cdot k_b) - k_b\cdot q_i + i\epsilon\right]\left[s'(k\cdot q_i - k\cdot k_b) - k_b\cdot q_i - i\epsilon\right]} \\ &\xrightarrow{\text{regularize}} \sum_{s,s'} \frac{f(s,q_i,k_b,k)f^\dagger(s',q_i,k_b,k) - f(s,\tilde{q}_i,\tilde{k}_b,\tilde{k})f^\dagger(s',\tilde{q}_i,\tilde{k}_b,\tilde{k})}{\left[s(k\cdot q_i - k\cdot k_b) - k_b\cdot q_i\right]\left[s'(k\cdot q_i - k\cdot k_b) - k_b\cdot q_i\right]}, \end{aligned} \tag{3.69}$$

where $\tilde{q}_i$, $\tilde{k}_b$ and $\tilde{k}$ are such that $s'(\tilde{k}\cdot\tilde{q}_i - \tilde{k}\cdot\tilde{k}_b) - \tilde{k}_b\cdot\tilde{q}_i = 0$ and $s(\tilde{k}\cdot\tilde{q}_i - \tilde{k}\cdot\tilde{k}_b) - \tilde{k}_b\cdot\tilde{q}_i = 0$. We wrote down only one of the four terms resulting from the squared matrix element $|S_{fi}|^2 = |S_{fi}^{(1)} + S_{fi}^{(2)}|^2$, and we have not written out the dependence on the summation index n, since the cross section should be finite separately for every n. However, if we regularize the squared matrix element in this way, retaining only the virtual contribution to laser-assisted bremsstrahlung, we must perform at least one additional integration (which is finite in the principal value sense) to obtain a positive definite differential cross section. This integration could be over the frequency ω_b, averaging over the initial energy Q_i or momentum $\boldsymbol{q}_i$, or the laser frequency ω. Integrating over Q_i, $\boldsymbol{q}_i$ or ω requires the introduction of an additional distribution function, describing the initial momentum or frequency distribution.

3.4.3 Divergence due to the infinite range of the Coulomb field

Related to the Green's function divergence discussed previously in this section, is the fact that the Coulomb field will introduce a divergence of its own. The Coulomb divergence is well

known from quantum mechanical scattering theory [73], and is a divergence of the scattering matrix element at zero momentum transfer from the Coulomb field, which occurs at forward scattering. When the initial momentum of the projectile $\boldsymbol{p}_i$ equals the final momentum $\boldsymbol{p}_f$, the factor $1/\boldsymbol{q}^2 = 1/(\boldsymbol{p}_i - \boldsymbol{p}_f)^2$ in the matrix element diverges. The physical origin of this divergence is the slow decay of the Coulomb field at large distances. Due to this long-range behavior, it is impossible for the initial particle to avoid scattering, and imposing such a demand consequently results in an unphysical divergence. For the laser-free bremsstrahlung [25] there is no such problem, since here we can have $\boldsymbol{p}_i = \boldsymbol{p}_f$ only if the energy ω_b of the emitted photon vanishes, and then the matrix element diverges anyway, due to the infrared divergence [141]. See formulas (3.49), (3.50). To see that the Coulomb factor $1/\boldsymbol{q}^2$ poses a problem in laser-assisted bremsstrahlung we note that the condition

$$\boldsymbol{q}^2 = -q^2 = -(q_f - q_i + nk + k_b)^2 = 0, \tag{3.70}$$

vanishing momentum transfer, is equivalent to the on-shell conditions (3.59), (3.60), with s changed to n. Thus, whenever we have a frequency ω_b such that either of the conditions in Eq. (3.61) is satisfied, there exists a vector $\boldsymbol{q}_f$ and an integer n such that $\boldsymbol{q}^2 = 0$, with an infinite cross section as a result. In particular the integral over the final electron solid angle $\mathrm{d}\Omega_f$ diverges whenever ω_b satisfies Eq. (3.61). The usual solution to the Coulomb infinity is to include screening, that is to cut the Coulomb potential in a smooth way at a certain distance from the nuclear core. Physically, this choice can be motivated by other electrons being around, shielding the nucleus, other particles being around, or in the extreme case the walls of the laboratory provide a cutoff for the Coulomb field. As we have seen, we have implemented this screening in our formulas by employing the Yukawa potential $e^{-|\boldsymbol{x}|/\ell}/|\boldsymbol{x}|$ [Eq. (3.24)] instead of the bare Coulomb potential. For large values of $|\boldsymbol{x}| > \ell$, the exponential provides damping so that no interaction occurs, and for small $|\boldsymbol{x}| < \ell$ the exponential factor is close to unity, so that the bare Coulomb potential is recovered.

3.5 Numerical results for different laser intensities and photon emission angles

In this section, we present our main results on laser-assisted bremsstrahlung. The results are presented as a series of graphs for different values of the parameters involved, resulting from numerical evaluation of the formula (3.46). We mention that the status of the problem of laser-assisted bremsstrahlung and in fact of second-order laser-assisted QED processes involving the Dirac-Volkov propagator in general before our contributions [104, 164] was that some analytical results had been published [131, 157], but numerical results were lacking completely. On the nonrelativistic side some numerical studies were performed [60, 68], which however lacked the feature of the resonant behavior discussed in section 3.4. In [68], where the laser-assisted bremsstrahlung problem was treated beyond the first Born approximation, resonances were found as higher order terms in ξ, but it was argued that they should be discarded in the low-field, nonrelativistic approximation. By our concrete evaluation of the cross section for laser-assisted bremsstrahlung, the complex analytical expressions resulting from the theory has

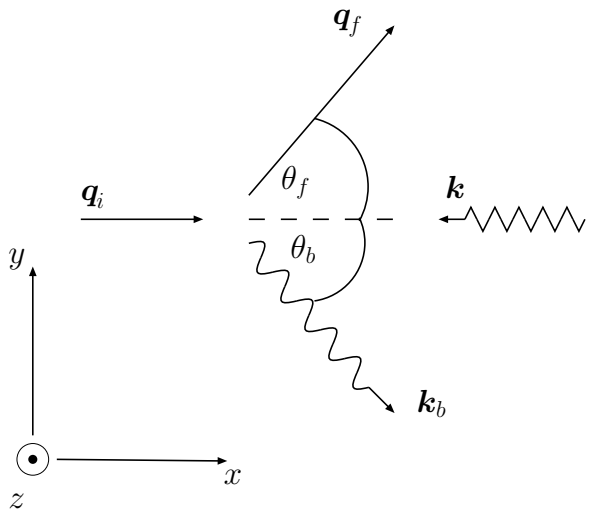

Figure 3.9: The scattering geometry considered. The initial electron with effective four-momentum $q_i = (Q_i, \boldsymbol{q}_i)$ counterpropagates with the laser with wave four-vector $k = (\omega, \boldsymbol{k})$. The direction of the effective momentum $q_f = (Q_f, \boldsymbol{q}_f)$ of the final electron is described by θ_f, and the direction of the emitted bremsstrahlung photon with four-momentum $k_b = (\omega_b, \boldsymbol{k}_b)$ is described by the angle θ_b. All the vectors are in the same plane (the x-y plane, or the plane of the paper). The nucleus with atomic number $Z = 1$ is situated in the origin.

for the first time been expressed in real numbers, so that one knows what to expect from a future experiment.

3.5.1 Parameters used for evaluation

Here we discuss the parameters used for the evaluation. For the laser, we always consider an infrared laser of angular frequency $\omega = 1.1698$ eV, which corresponds to the typical wavelength $\lambda = 1.06$ μm of a neodymium-yttrium-aluminum-garnet (NdYAG) laser. Typical values of ξ we consider are $5 < \xi < 20$, which correspond to intensities 3.0×10^{19} W/cm^2 $< I < 4.9 \times 10^{20}$ W/cm^2, well in the range of what modern lasers can produce nowadays. The geometrical setup of our scattering problem is shown in Fig. 3.9.

We always consider, if not otherwise stated, an initial electron with $E_i = 10m = 5.11$ MeV, counterpropagating with the laser beam, that is $\boldsymbol{q}_i/|\boldsymbol{q}_i| = -\boldsymbol{k}/\omega$. Recall that E_i is the energy of the electron beam outside the laser, given the energy E_i, the effective energy Q_i follows as $Q_i = E_i + m^2\xi^2\omega/(4p_i \cdot k)$. The angle θ_f describes the angle between the incoming electron and the outgoing electron, and θ_b the angle between the emitted bremsstrahlung photon and the initial electron. Both θ_f and θ_b are only considered in the x-y plane. In the case of linear polarization this plane corresponds to the plane spanned by the laser propagation direction $\boldsymbol{k}/\omega$ and polarization direction $\boldsymbol{a}/|\boldsymbol{a}|$.

For the screening length ℓ, we have performed calculations for two rather large values of ℓ, $\ell = 10^6 r_0 \approx 2.7 \times 10^8$ MeV^{-1} for the graphs where only linear polarization is shown (Figs. 3.10,

3.12 and 3.16), and $\ell = 2 \times 10^9 r_0 \approx 5 \times 10^{11}$ MeV^{-1} for the graphs where linear and circular polarization are compared (Figs. 3.11, 3.13 and 3.14). Here $r_0 \approx 270$ MeV$^{-1} \approx 5.3 \times 10^{-11}$ m is the Bohr radius. As a physical motivation for the two choices, we have that the distance $\ell = 10^6 r_0$ corresponds to the average distance between the particles in a gas at ultrahigh vacuum (a pressure of 3×10^{-8} Pa at room temperature), and $\ell = 2 \times 10^9 r_0$ corresponds to the mean free path in a medium vacuum. The choice of ℓ is arbitrary, all that is needed is a finite value to regularize the Coulomb infinities, as discussed in subsection 3.4.3. When performing an actual experiment, the value of ℓ will depend on the experimental conditions.

All calculations are without exception made for atomic number $Z = 1$, corresponding to protons. Since the interaction with the Coulomb field is taken into account in first Born approximation, the cross section (3.46) of the process scales as Z^2. We note that to learn something about the Z-dependence of bremsstrahlung, one has to go to higher order interactions in Z, that is to include several Coulomb vertices.

3.5.2 Comments on the numerical evaluation

In this subsection we discuss a number of issues connected with the numerical evaluation of the cross section (3.46). To make this evaluation feasible, a number of approximations have to be made. We also discuss some nonstandard methods to evaluate spin sums.

Sums over electron spin and photon polarization

As already mentioned in section 3.3.3, gauge invariance makes it in principle possible to use the formula (3.44) to calculate sums over photon polarization states. However, since the identity (3.44) involves cancellation of equally sized terms, it is numerically advantageous to choose an explicit base for the polarization vectors $\epsilon_{b,\lambda=1,2}$ and do the sum over these two vectors. For linear polarization, we make the choice

$$\epsilon_{b,1} = (0, \sin\theta_b, -\cos\theta_b, 0), \qquad \epsilon_{b,2} = (0, 0, 0, 1), \tag{3.71}$$

if k_b is given by $k_b = \omega_b(0, \cos\theta_b, \sin\theta_b, 0)$, as in Fig. 3.9. For the electron spin sums, they can, according to the theorem [141]

$$\sum_{r_f, r_i = 1,2} \left| \bar{u}_{r_f}(p_f) M u_{r_i}(p_i) \right|^2 = \mathrm{Tr}\left(M \frac{\hat{p}_i + m}{2m} \overline{M} \frac{\hat{p}_f + m}{2m} \right), \tag{3.72}$$

valid for any matrix M, be converted into a trace over gamma matrices. The usual approach is now to use the properties of the gamma matrices, in particular the identity [141]

$$\mathrm{Tr}(\hat{b}_1 \hat{b}_2 \cdots \hat{b}_n) = b_1 \cdot b_2 \mathrm{Tr}(\hat{b}_3 \cdots \hat{b}_n) - b_1 \cdot b_3 \mathrm{Tr}(\hat{b}_2 \hat{b}_4 \cdots \hat{b}_n) + \ldots + b_1 \cdot b_n \mathrm{Tr}(\hat{b}_2 \cdots \hat{b}_{n-1}), \tag{3.73}$$

valid for an even number n four-vectors $b_{1..n}$, to perform the trace in an analytic way, either by hand, or by using a computer program capable of symbolic manipulations (for example [82]). However, to remove n number of four-vectors from the trace, the identity (3.73) must be used repeatedly $n/2$ times, yielding $(n-1)!! = (n-1)(n-3)\cdots 3 \cdot 1$ terms, each containing $n/2$ dot

products of four-vectors. Since in our matrix element (3.26) we have up to 7 matrices in between the spinors, it means that the spin-summed cross section (3.46) contains traces of up to 16 hatted four-vectors. Evaluating such a formula, resulting in $15!! \approx 2 \times 10^6$ terms (or actually slightly less, since some terms vanish due to $a \cdot k = k^2 = 0$), is clearly not manageable. Printed out, the formula obtained in this way would fill several printed pages. Different from usual field-theoretic calculations, where cancellations between different terms resulting from a gamma matrix trace occur almost without exception and thereby reduce the number of terms, such cancellations do not seem to occur in laser-dressed problems as the one at hand. Our approach is instead to use an explicit representation of the Dirac algebra, the Dirac representation (see subsection 1.1.2 on page 17) and perform the trace numerically. Alternatively, one can use an explicit representation of the spinors [76]

$$u_r(p) = \sqrt{\frac{E+m}{2m}} \begin{pmatrix} \zeta_r \\ \boldsymbol{\sigma} \cdot \boldsymbol{p}\, \zeta_r/(E+m) \end{pmatrix}, \qquad \zeta_r = \begin{pmatrix} \delta_{r1} \\ \delta_{r2} \end{pmatrix}, \tag{3.74}$$

$$\boldsymbol{\sigma} = \left(\begin{bmatrix} 0 & 1 \\ 1 & 0 \end{bmatrix}, \begin{bmatrix} 0 & -i \\ i & 0 \end{bmatrix}, \begin{bmatrix} 1 & 0 \\ 0 & -1 \end{bmatrix} \right), \tag{3.75}$$

and do the spin sum explicitly over $r_{f,i} = 1, 2$. We also mention, that although the spin sum is not the bottleneck of the numerical calculation, evaluating a trace like (3.73) numerically is much faster than to first do the trace analytically, and then evaluating the resulting expression. Multiplying n number of 4×4 matrices takes $N_n^{\text{num.}} = 64(n-1)$ multiplications, while tracing out and performing the dot products takes $N_n^{\text{anal.}} = 4(n/2-1)(n-1)!!$ multiplications. The number of multiplications (which is the numerically most time-consuming operation, compared to additions) are thus greater in the analytical case even for $n > 3$, $N_{n>3}^{\text{anal.}} > N_{n>3}^{\text{num.}}$.

Approximations for the sum over n and s

As is seen in 3.5.3, the bremsstrahlung spectra consist of resonance peaks, generated by Compton scattering, superimposed on a smooth background curve generated by bremsstrahlung from Coulomb scattering. In the region where the peaks still are visible, due to the factors $1/\boldsymbol{q}^4$ and $1/(\tilde{p}_{f,i}^2 - m_*^2)$ in the cross section, the indices s, n closest to the (not necessarily integer) numbers

$$n_{\max} = s_{\max,i} = \frac{q_i \cdot k_b}{k \cdot q_i - k \cdot k_b}, \qquad s_{\max,f} = \frac{-q_f \cdot k_b}{k \cdot k_b + k \cdot q_i} \tag{3.76}$$

will contribute the most to the cross section. In practice, this makes it possible to approximate the sums over n and s with say 20-30 terms each around the resonant indices (3.76).

Integration over $\mathrm{d}\Omega_f$

Most of the spectra we present in section 3.5.3 are integrated over the directions of the final electron, that is, we show

$$\frac{\mathrm{d}\sigma}{\mathrm{d}\Omega_b \mathrm{d}\omega_b} = \int \frac{\mathrm{d}\sigma}{\mathrm{d}\Omega_b \mathrm{d}\omega_b \mathrm{d}\Omega_f} \mathrm{d}\Omega_f. \tag{3.77}$$

As expected, most of the contribution to the integrand in Eq. (3.77) comes from a small cone where $\boldsymbol{q}^2$ is small. For small $\omega, \omega_b < Q_{f,i}$, this cone will point roughly in the forward direction $\boldsymbol{q}_i/|\boldsymbol{q}_i|$. However, at values of q_f such that $\boldsymbol{q}^2$ is small, we also have that the interference between the two diagrams for laser assisted bremsstrahlung (see the Feynman diagrams Fig. 3.7 on page 45) is the largest. This means that evaluation of the cross section (3.46) involves subtraction of equally sized terms, which is prone to cancellation error. In other words, close to the resonant frequencies with small $\boldsymbol{q}^2$, the modulus of the total sum $|S_{fi}|$ [see Eq. (3.26)] is many orders of magnitude smaller than the absolute values of the individual diagrams $|S_{fi}^{(1)}|$ and $|S_{fi}^{(2)}|$. Consequently, the calculation has to be done in quadruple precision, something that slows down the numerical integration considerably. By splitting up the task of evaluating a spectrum over an interval $0 \leq \omega_b \leq \omega_b^{\max}$ into several subintervals $\omega_b^N \leq \omega_b \leq \omega_b^{N+1}$, $N = 1, \ldots, N_{\max}$, and calculating these subintervals simultaneously on different processors in a computer cluster, computing time could be reduced to a reasonable amount. Each spectrum (integrated over $\mathrm{d}\Omega_f$) shown in subsection 3.5.3 demands about 1 week of cluster time, using about 10-30 different processors. We employ a Romberg integration routine [144], with in general a relative precision of 10^{-3}.

Furthermore, in the case $\theta_b = 179^\circ$, a further speed-up of the calculation comes from the observation that if we write q_f as

$$q_f = (Q_f, \sqrt{Q_f^2 - m_*^2}\,[\cos\theta_f \sin\phi_f, \sin\theta_f \sin\phi_f, \cos\phi_f]), \tag{3.78}$$

where the plane of the vectors in Fig. 3.9 corresponds to $\phi_f = \pi/2$, then since effectively only a small cone around $\phi_f = \pi/2$, $\theta_f = 0$ contributes to the integral, we can in the integration over $\mathrm{d}\phi_f$ approximate $\sin\phi_f \approx 1$, $\cos\phi_f \approx 0$ in the arguments $\alpha_{i,f} - \tilde{\alpha}_{i,f}$, $\beta_{i,f} - \tilde{\beta}_{i,f}$ of the generalized Bessel functions. This means that the generalized Bessel functions do not depend of ϕ_f, and that we only need to calculate the required arrays $A_0(s_{\min} \leq s \leq s_{\max}, \alpha_{i,f} - \tilde{\alpha}_{i,f}, \beta_{i,f} - \tilde{\beta}_{i,f})$ once for every new value of θ_f in the integration over $\mathrm{d}\Omega_f = \sin\phi_f \mathrm{d}\phi_f \mathrm{d}\theta_f$.

Numerical tests of validity

We have performed the following tests of validity for the computer program used for the evaluation of the cross section (3.46).

Gauge invariance of the cross section (3.46) under the transformations $\epsilon_{b,\lambda} \to \epsilon_{b,\lambda} + \Lambda_1 k_b$ and $a \to a + \Lambda_2 k$, for arbitrary constants $\Lambda_{1,2}$, has been numerically tested. Sometimes quadruple precision has to be used to do this test, due to cancellation errors. Gauge invariance actually provides the most sensible test of correctness, since this symmetry is broken by any incorrect plus or minus sign, or inexact value of the generalized Bessel functions. For the analytic proof of gauge invariance, we refer to section B.2.

Correct non-relativistic limit. In region of parameters where the nonrelativistic formula (3.102) applies (see the discussion in section 3.6), the two expressions (3.102) and (3.46) were found to agree numerically, as expected from the analytical considerations in section 3.6.

Correct limit of vanishing laser field. In the limit $|a| \to 0$, we should recover the Bethe-Heitler cross section (3.50), as discussed in subsection 3.3.4. This has been tested numerically, both for

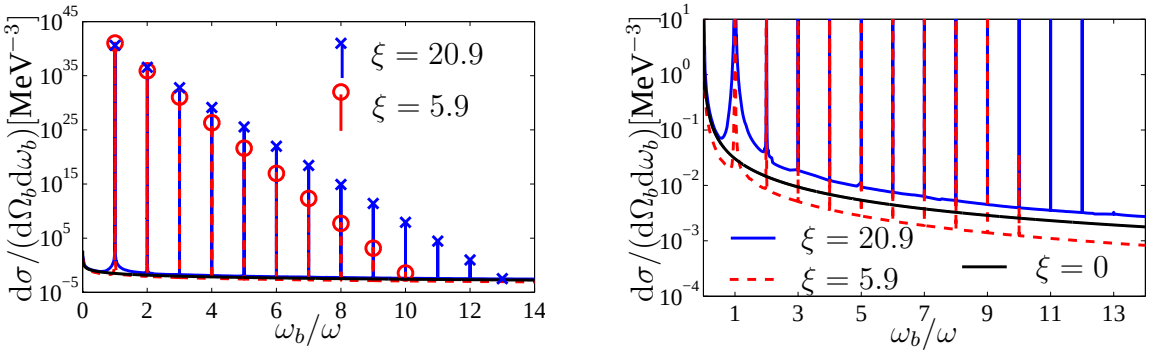

Figure 3.10: The cross section for $\theta_b = 179°$, differential in solid angle Ω_b and energy ω_b of the emitted bremsstrahlung photon, for linear polarization of the laser. The values on the peaks are shown with crosses ($\xi = 20.9$) and circles ($\xi = 5.9$) for clarity. The values of ξ used correspond to laser intensities $I = 5.2 \times 10^{20}$ W/cm^2 for $\xi = 20.9$ (solid blue curve) and $I = 4.3 \times 10^{19}$ W/cm^2 for $\xi = 5.9$ (dashed red curve). The screening length is here $\ell = 10^6 r_0$. A magnification of the left graph for small values of the cross section is shown to the right. Here it is interesting to note that for $\xi = 5.9$ the background curve is below the Bethe-Heitler curve (solid black line), but for $\xi = 20.9$ it is above. The transition occurs at approximately $\xi = 12$. We comment that in the nonrelativistic case [90], the curve always goes below the laser-free curve.

the fully differential cross section and for the cross section integrated over $\mathrm{d}\Omega_b$.

3.5.3 Numerically evaluated spectra

In this subsection we present the results of the numerically evaluated cross sections, both integrated over $\mathrm{d}\Omega_f$ and fully differential ones. In most graphs, the cross section for the laser-free case, calculated with the formulas in [25, 72], is included for comparison. Departure of the parameters used from the ones discussed in subsection 3.5.1 will be stated explicitly.

Spectra integrated over $\mathrm{d}\Omega_f$

Figure 3.10 shows the spectrum, integrated over the direction Ω_f of the final electron, for photon emission angle $\theta_b = 179°$, which corresponds to almost the same direction as the laser propagation direction. As expected, the spectrum is composed of a number of very high peaks, with positions $\omega_b^{\mathrm{peak}\,2}$ given by the resonance condition (3.61), and a background of magnitude comparable to the laser-free curve. For this value of θ_b, the peaks appear very close to integer multiples of the laser frequency. Here the magnitude of the peaks drops exponentially very fast, and only up to 13 peaks can be seen. In Fig. 3.11, the spectra for linear and circular polarization are compared, for $\theta_b = 179°$. More interesting is the case with $\theta_b = 1°$, which corresponds to bremsstrahlung emission in a direction close to the direction of the initial electron, or in the backward direction of laser propagation. This corresponds to so-called backscattering with respect to the laser. The spectra are displayed in Fig. 3.12 for two different values of ξ and linear polarization, and in Fig. 3.13 for a comparison between linear and circular polarization. Clearly, in this geometry much a larger number of Compton peaks are generated, and the background

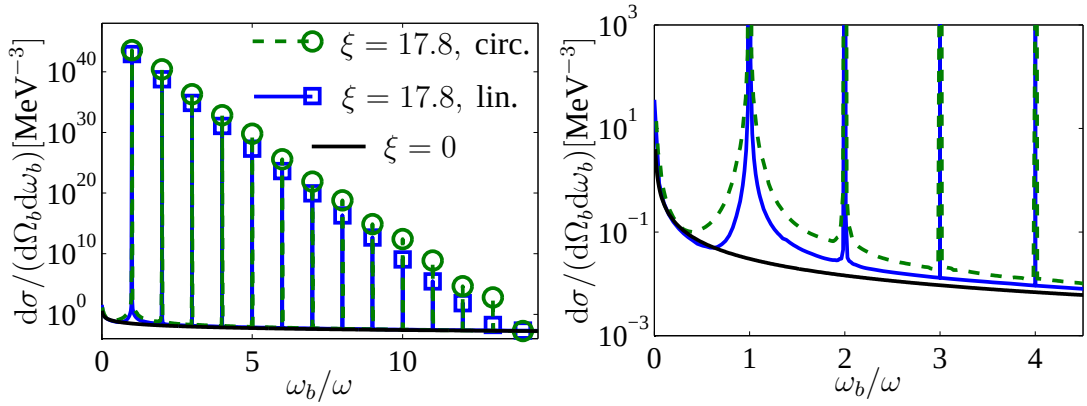

Figure 3.11: The differential cross section for $\theta_b = 179°$, comparing circular (green dashed curve) and linear polarization (solid blue curve) at the same value of $\xi = 17.8$. In the left graph, the values of $\mathrm{d}\sigma/(\mathrm{d}\Omega_b \mathrm{d}\omega_b)$ on the peaks are plotted with green circles (circular polarization) and blue squares (linear polarization) for clarity. Note that for the same value of ξ, the intensity for linear polarization is smaller than the the one corresponding to circular polarization by a factor of two. The right graph shows a magnification of the left one for small values of the cross section. In this graph, $\ell = 2 \times 10^9 r_0$ is used. We see that the behavior for linear and circular polarization for this photon emission angle is very similar.

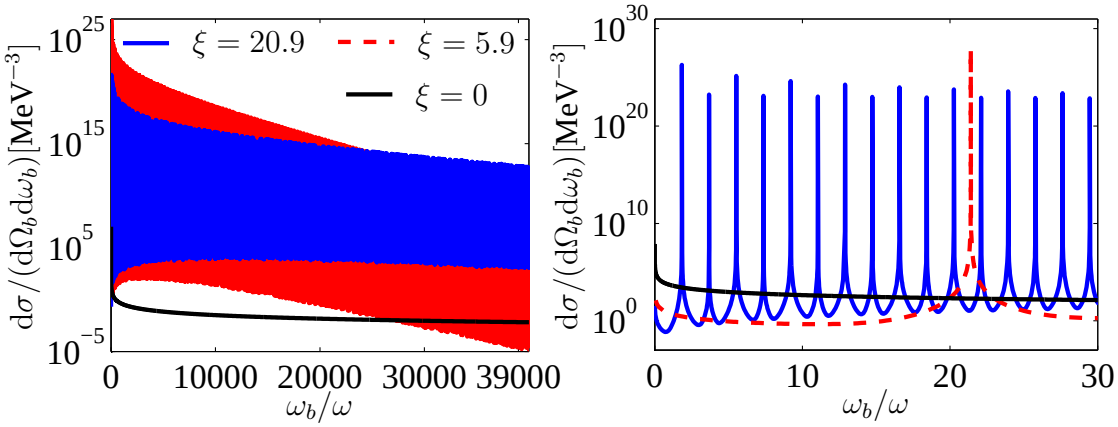

Figure 3.12: The differential cross section for $\theta_b = 1°$, integrated over $\mathrm{d}\Omega_f$. Except for θ_b, the parameters used are the same as in Fig. 3.10, with $\xi = 20.9$ for the solid blue curve, $\xi = 5.9$ for the dashed red curve and $\xi = 0$ for the solid black curve. As the zoom-in graph to the right shows, a peculiar feature is that the background is here lower than the Bethe-Heitler cross section for small order harmonics, but overtakes it for large values of ω_b.

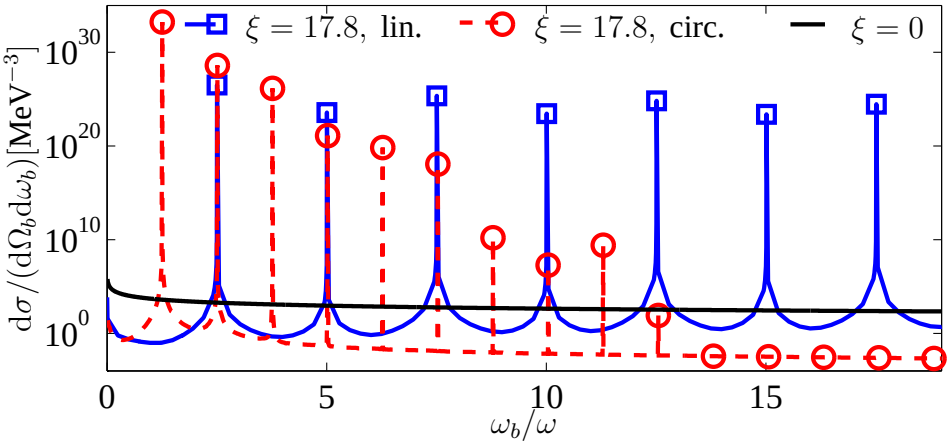

Figure 3.13: The differential cross section for $\theta_b = 1°$, comparing linear (solid blue curve, peak values shown with squares) and circular (dashed red curve, peak values shown with circles) polarization for the same value of $\xi = 17.8$, and $\ell = 2 \times 10^9 r_0$. Here there is a clear difference between the circular and linear case. The circular curve is here similar to the one for $\theta_b = 179°$ (see Fig. 3.11), with rapidly decaying peaks, while the linear curve features peaks up to large values of ω_b, compare Fig. 3.12. The background for the linear case is dominated by contributions from around the Compton/Coulomb peaks, which provides the reason for the background being so large.

is much larger that the laser-free case, at least for large frequency values $\omega_b \gg \omega$ for linear polarization. Also observe that the position of the peaks are now no longer harmonics of the laser frequency, but depend on the value of ξ according to Eq. (3.61). In the case of $\theta_b = 1°$ this results in $\omega_b^{\text{peak 2, lin.}} \approx 2\omega_b^{\text{peak 2, circ.}}$, as is seen in Fig. 3.13.

Peculiar behavior of the fully differential cross section

Assuming a fixed energy, $E_i = 10m$, (as for the all of the graphs Fig. 3.10, Fig. 3.11, Fig. 3.12, Fig. 3.13, Fig. 3.16), and fixed direction $\boldsymbol{p}_i/|\boldsymbol{p}_i|$ for the initial electron outside the laser, the initial effective energy Q_i and effective three-momentum $\boldsymbol{q}_i$ depend on the intensity parameter ξ. In fact, assuming the direction $\boldsymbol{p}_i/|\boldsymbol{p}_i| = -\boldsymbol{k}/\omega$ of the electron outside the laser field, the electron counter propagates with the laser field, that is $\boldsymbol{q}_i \cdot \boldsymbol{k} = -\omega|\boldsymbol{q}_i|$, for small values of ξ. However, at some value ξ_0 of ξ, the electron is at average at rest in the laser field, $Q_i = m_*$, and for larger values of $\xi > \xi_0$ the electron moves in the same direction as the laser wave, $\boldsymbol{q}_i \cdot \boldsymbol{k} = \omega|\boldsymbol{q}_i|$. The numerical value of ξ_0 can be solved for, by demanding that the x-component of the effective momentum vanishes:

$$q_i^x = 0 = \sqrt{E_i - m^2} + \frac{\xi_0^2 m^2}{4(E_i + \sqrt{E_i - m^2})}, \tag{3.79}$$

which gives $\xi_0 = 28.2$ for linear polarization and $E_i = 10m = 5.11$ MeV. For circular polarization one gets instead, due to a factor of $1/2$ instead of $1/4$ in the effective momentum,

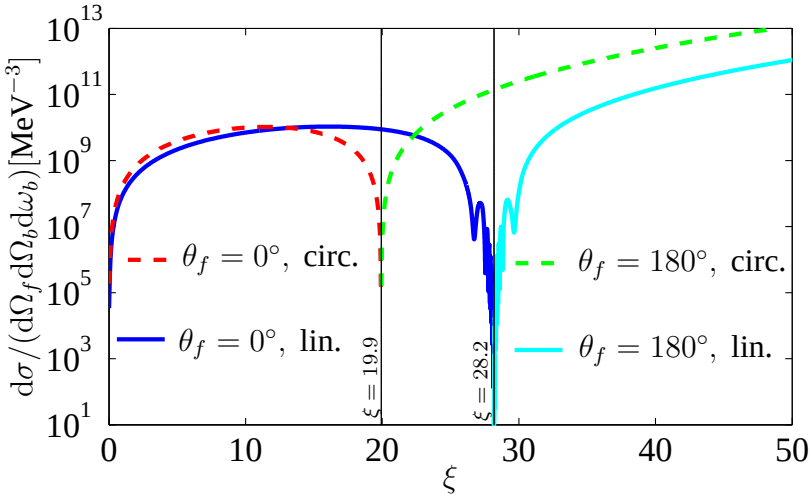

Figure 3.14: The fully differential cross section, differential in the solid angle Ω_f of the final electron, frequency ω_b and solid angle Ω_b of the emitted photon, for two different values of θ_f. In this graph, $\theta_b = 179°$, and ω_b is taken to be exactly half way between the first peak and the second peak. That is, we have from Eq. (3.61) that $\omega_b = \left(\omega_b^{\mathrm{peak}\,2}(s=1) + \omega_b^{\mathrm{peak}\,2}(s=2)\right)/2$. Note that since θ_b is close to $180°$, ω_b defined in this way is only weakly dependent on ξ. The graph illustrates the dramatic decrease in the differential cross section as a function of ξ, for circular and linear polarization. The thin black line indicates the value of ξ_0, when $Q_i = m_*$.

$\xi_0 = 19.9$. The result is that, as a function of ξ, the differential cross section with observation direction $\theta_f = 0$ or $\theta_f = 180°$ (see Fig. 3.9) shows a steep step-like decay at the value ξ_0. Fig. 3.14 illustrates this behavior for both linear and circular polarization. The physical reason is that the cross section for forward scattering, when $\boldsymbol{q}_i/|\boldsymbol{q}_i| \approx \boldsymbol{q}_f/|\boldsymbol{q}_f|$, is very large compared to that of backward scattering, $\boldsymbol{q}_i/|\boldsymbol{q}_i| \approx -\boldsymbol{q}_f/|\boldsymbol{q}_f|$, due to the Coulomb factor $1/\boldsymbol{q}^4$ in the cross section (3.46). The value ξ_0 from Eq. (3.79) signifies the transition from forward scattering to backward scattering for an initial electron with three-momentum antiparallel to the laser, outside the laser, $\boldsymbol{p}_i \cdot \boldsymbol{k} = -\omega|\boldsymbol{p}_i|$, and the final electron observed in the forward direction $\theta_f = 0$. If the final electron is instead observed in the direction $\theta_f = 180°$, values of $\xi < \xi_0$ correspond to backward scattering with small cross section, and $\xi > \xi_0$ corresponds to forward scattering with large cross section.

3.5.4 Comparison with the free propagator

One motivation for the present project, evaluation of the cross section for laser-assisted bremsstrahlung, was to investigate if the matrix element of this process could be well approximated by the matrix element obtained by removing the dressing of the laser in the propagator. The Feynman diagrams corresponding to this situation are shown in Fig. 3.15. In other words, would it be a good approximation to use, instead of the full Dirac-Volkov propagator $G(x, x')$ [see Eq. (2.62)], the free electron propagator $G_{\mathrm{free}}(x, x')$ [see Eq. (2.63)]? A handwaving argument

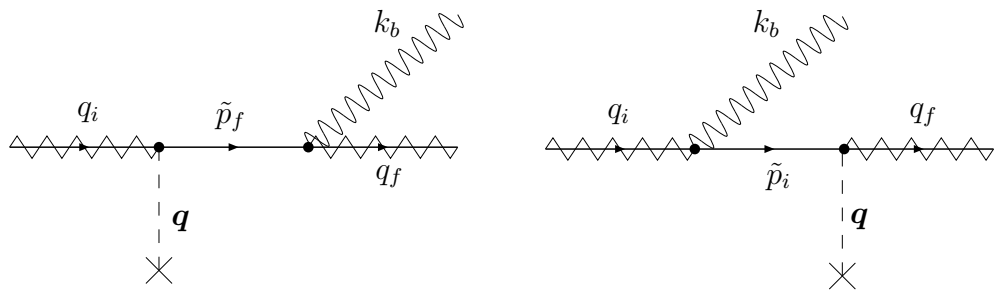

Figure 3.15: The Feynman diagrams for laser-assisted bremsstrahlung, using the free propagator approximation. Here external electron lines are Volkov states, and therefore denoted with a wiggling line superimposed on a straight line, while the intermediate line is the free propagator in absence of the laser. As before, the initial electron has effective four-momentum q_i, the final q_f and the intermediate electron propagator momentum is denoted by $\tilde{p}_{i,f}$ The emitted bremsstrahlung photon has four-momentum k_b, and the virtual Coulomb field photon, depicted with a dashed line, has three-momentum $\boldsymbol{q}$. Time flows from left to right.

shows that it is at least reasonable to assume so for large frequencies ω_b: If the frequency ω_b of the emitted photon is large, it means that the time between the Coulomb interaction and the emission of the photon ω_b is short, then the comparatively slow oscillations of the laser can be neglected, since there is simply not enough time to interact with the laser. We will see that this is indeed the case, but that the condition for when the approximation is good is not $\omega_b \gg \omega$, but rather $\omega_b \gg E_i$. The matrix element in this approximation (for linear polarization, the circular case is similar) is exactly as the laser-dressed matrix element $S_{f,i}$ from Eq. (3.26) on page 47, but with the factor between the large brackets $\Big[\cdots\Big]$ replaced by

$$\mathcal{M}^{s}_{\text{free}}\hat{\epsilon}_{b,\lambda}\frac{\hat{\tilde{p}}_f + m}{\tilde{p}_f^2 - m^2}\gamma^0\mathcal{F}^{s-n}_{\text{free}} + \mathcal{M}^{s+n}_{\text{free}}\gamma^0\frac{\hat{\tilde{p}}_i + m}{\tilde{p}_i^2 - m^2}\hat{\epsilon}_{b,\lambda}\mathcal{F}^{s}_{\text{free}}, \tag{3.80}$$

with

$$\mathcal{M}^{N}_{\text{free}} = \left[A_0(N,\alpha_f,\beta_f) + \frac{e\hat{a}\hat{k}}{2k\cdot q_f}A_1(N,\alpha_f,\beta_f)\right], \tag{3.81}$$

$$\mathcal{F}^{N}_{\text{free}} = \left[A_0(N,\alpha_i,\beta_i) + \frac{e\hat{k}\hat{a}}{2k\cdot q_i}A_1(N,\alpha_i,\beta_i)\right], \tag{3.82}$$

and the same definitions as in Eqs. (3.33), (3.31) of the vector $\tilde{p}_{i,f}$ and the Bessel function arguments $\alpha_{i,f}$, $\beta_{i,f}$. However, from the denominators $1/(\tilde{p}_{i,f}^2 - m^2)$ in Eq. (3.80), we see that using this approximation will give Green's function resonances at different positions than in the laser-dressed matrix element (3.26). Thus, a better approximation is to take m_* instead of m in the propagator denominator. We note that a similar approximation has been tried before [33]. The result of a calculation comparing the approximation of employing the free electron propagator, but with the effective mass m_* instead of m in the propagator denominator, with the fully laser-dressed cross section is displayed in Fig. 3.16. From the lower graph of Fig. 3.16 it is

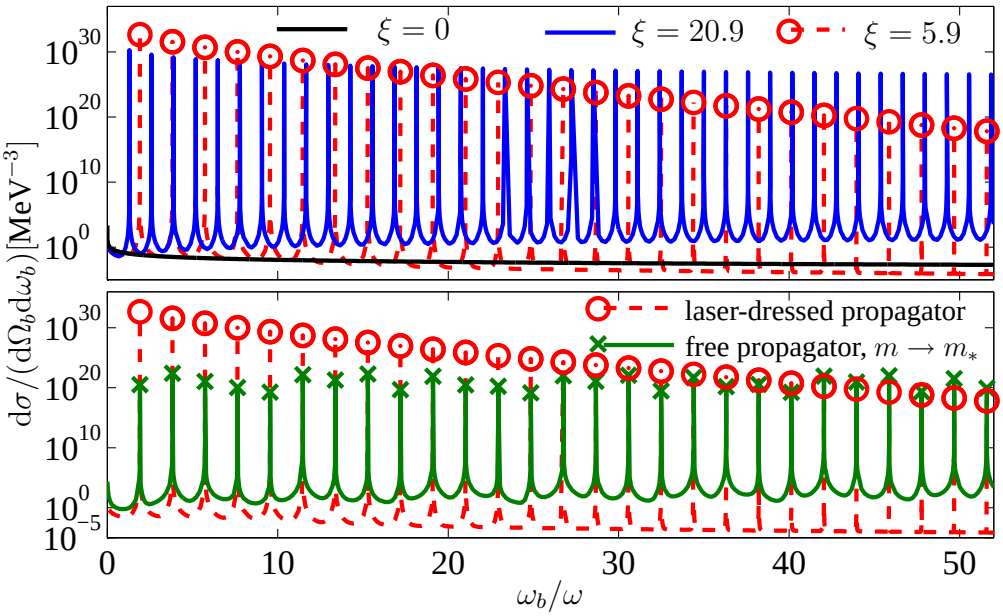

Figure 3.16: The differential cross section for $\theta_b = 90°$. In the upper graph the cross section using the full, laser-dressed propagator for the description of the virtual states in Fig. 3.15 is shown for $\xi = 20.9$ (solid blue curve) and $\xi = 5.9$ (dashed red curve, with peak values shown with circles), and the solid black curve represents the laser-free case. In the lower graph we compare calculations performed using the full, laser-dressed propagator (dashed red curve, circled peak values) with the cross section obtained using the free electron propagator with effective mass m_* (solid green curve, peak values shown with green crosses), both for $\xi = 5.9$. The screening length is $\ell = 10^6 r_0$ in both graphs.

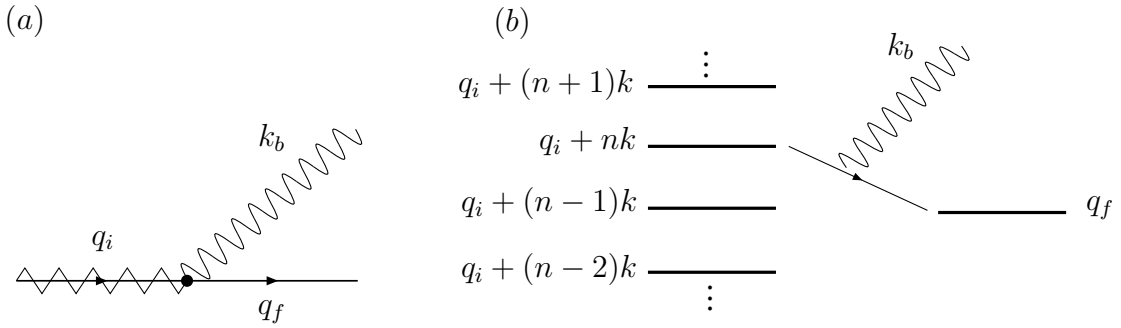

Figure 3.17: Illustration of the intuitive explanation of the failure of the free propagator approximation. The left diagram (a) shows the Feynman diagram for photon emission (Compton scattering) of a photon k_b from a Volkov state with effective momentum q_i into a free electron state with momentum q_f. The right diagram (b) shows the corresponding level picture.

clear that the free electron propagator-approximation is not a good one, even for large $\omega_b \gg \omega$. In this regime of parameters, where Compton peaks are clearly visible, the shortcoming of the free electron propagator can be explained intuitively. In fact, since here the contribution to the integral over $\mathrm{d}\Omega_f$ comes from a small region where $\boldsymbol{q}^2$ is small, it means that the interaction with the Coulomb field is very small. To get the intuitive picture it is therefore sufficient to just consider photon emission by Compton scattering, discussed in section 3.2, Feynman diagram in Fig. 3.1. To remove the laser-dressing of the propagator is now roughly the same thing as requiring that the final state of the Compton scattering process is not dressed at all by the laser, but simply a free electron with momentum q_f. An illustration is given in Fig. 3.17, the Feynman diagram in graph (a). Another way of viewing the free electron approximation is provided by the level picture, shown in graph (b), Fig. 3.17. Here the final level is constrained to only one. The amplitude of this process is therefore approximately, by the same arguments as the ones leading to Eq. (3.15),

$$M_{\text{free}} = \sum_{\Delta n} A_0(\Delta n, \alpha_i, \beta_i) A_0(0, \alpha_f, \beta_f) \delta(q_i - q_f - k_b + \Delta n k), \tag{3.83}$$

where we note that there is only one sum, as opposed to Eq. (3.15). The amplitude M_{free} for one transition with level difference Δn in this case is proportional to $A_0(\Delta n, \alpha_i, \beta_i) A_0(0, \alpha_f, \beta_f)$, and not to $A_0(\Delta n, \alpha_i - \alpha_f, \beta_i - \beta_f)$ as in the fully laser-dressed case. The reason is that the restriction of the final level removes the destructive interference between the different pathways with the same level difference Δn. It is this destructive interference that gives rise to the exponential decay of the peak amplitude seen in the upper graph of Fig. 3.16 (and also in Figs. 3.10, 3.12). Mathematically speaking, we see, by using the delta function in Eq. (3.83), that since here $\omega_b \ll Q_{i,f}$ the arguments α_f, β_f are almost independent of ω_b, so that the peak amplitude is almost constant as a function of ω_b (see lower graph of Fig. 3.16), but that the difference $\alpha_f - \alpha_i \approx -ea \cdot k_b/(k \cdot q_i)$ depend linearly on ω_b. For the second argument of the generalized Bessel function we have $\beta_f - \beta_i \approx 0$.

On the other hand, if we consider the case when $\omega_b \gg E_{i,f}$, and also choose the gauge so that $a \cdot k_b = 0$ (this can be done by gauge transforming $a \to a - \frac{a \cdot k_b}{k \cdot k_b} k$), then it follows that for the

arguments of the generalized Bessel functions in Eq. (3.26)

$$\begin{aligned}\alpha_f - \tilde{\alpha}_f &= \frac{ea\cdot p_f}{k\cdot p_f} - \frac{ea\cdot p_f + ea\cdot k_b}{k\cdot p_f + k\cdot k_b} \\ &= \frac{ea\cdot p_f k\cdot p_f + ea\cdot p_f k\cdot k_b - ek\cdot p_f a\cdot p_f - ea\cdot k_b k\cdot p_f}{k\cdot p_f(k\cdot k_b + k\cdot p_f)} \approx \frac{ea\cdot p_f}{k\cdot p_f} = \alpha_f,\end{aligned} \tag{3.84}$$

and also

$$\beta_f - \tilde{\beta}_f = \frac{e^2\tilde{a}^2}{8}\left(\frac{1}{k\cdot p_f} - \frac{1}{k\cdot p_f + k\cdot k_b}\right) \approx \frac{e^2\tilde{a}^2}{8k\cdot p_f} = \beta_f. \tag{3.85}$$

Similarly $\alpha_i - \tilde{\alpha}_{f,i} \approx \alpha_i$ and $\beta_i - \tilde{\beta}_{f,i} \approx \beta_i$. In addition, $\omega_b \gg E_{i,f}$ means that we can ignore terms proportional to $\frac{1}{k\cdot\tilde{p}_{i,f}}$ compared to terms proportional to $\frac{1}{k\cdot p_{i,f}}$. Using all these approximations in the matrix element (3.26), we have that

$$S_{fi} \approx S_{fi}^{\text{free prop, } m\to m_*}, \qquad \omega_b \gg E_{i,f}. \tag{3.86}$$

However, to have $\omega_b \gg E_{i,f}$ we have from the energy conservation relation that

$$\omega = Q_i - Q_f - n\omega \approx -n\omega \gg E_{i,f}, \tag{3.87}$$

if we in addition consider $Q_{i,f} \sim E_{i,f}$, which holds for the laser intensities and electron energies we have considered in section 3.5.3. But for the arguments of the generalized Bessel functions we now have

$$|\alpha_{i,f}| + 2|\beta_{i,f}| \sim \frac{E_{i,f}}{\omega} \ll |n|, \tag{3.88}$$

from Eq. (3.87). It follows from the cutoff rules (2.49) (see page 27) that the generalized Bessel functions $A_0(n, \alpha_{i,f}, \beta_{i,f})$ are vanishingly small. We thus conclude that when the condition $E_{i,f} \sim Q_{i,f}$ is satisfied, the free electron propagator will only be a good approximation in the region where the cross section is very small, and therefore uninteresting.

3.6 Comparison with the nonrelativistic laser-assisted bremsstrahlung cross section

In the nonrelativistic limit and for small fields, the cross section should go to the one found by Karapetyan and Fedorov in [90]. We show in this section that this really is the case, following the lines in [157].

3.6.1 Derivation of the first Born matrix element for laser-assisted bremsstrahlung in the dipole approximation

In this subsection, we derive the result found in [90], for linear polarization of the laser. To make the dipole approximation for the laser field (and also the radiation field) means that the

dependence on space in the vector potential is dropped,

$$\boldsymbol{A}(x) = \boldsymbol{a}\cos\phi \approx \boldsymbol{a}\cos\omega t. \tag{3.89}$$

To calculate the matrix element, we need the nonrelativistic Volkov state,

$$\psi_{\boldsymbol{p}}^{\text{nonrel}}(x,t) = \exp\left(-iEt + i\boldsymbol{p}\cdot\boldsymbol{x} - \alpha_{\boldsymbol{p}}\sin\omega t\right), \tag{3.90}$$

with the nonrelativistic energy $E = \boldsymbol{p}^2/(2m)$ and where

$$\alpha_{\boldsymbol{p}} = \frac{e\boldsymbol{a}\cdot\boldsymbol{p}}{\omega m}. \tag{3.91}$$

Note in particular that we have dropped the A^2-term in the argument of the exponential in Eq. (3.90) already at this stage, since we assume $\xi \ll 1$ here [see Eq. (3.105)]. The Volkov solution solves as it should the Schrödinger equation with an external plane wave laser with linear polarization,

$$\left(i\frac{\partial}{\partial t} + \frac{1}{2m}\boldsymbol{\nabla}^2 - i\frac{e\boldsymbol{a}\cdot\nabla\cos(\omega t)}{m}\right)\psi_{\boldsymbol{p}}^{\text{nonrel}}(x,t) = 0. \tag{3.92}$$

The nonrelativistic Volkov-Schrödinger propagator reads [24]

$$\begin{aligned} G^{\text{nonrel}}(x,x') = \frac{i}{(2\pi)^4}\int \mathrm{d}^3\boldsymbol{p}_G \mathrm{d}E_G \\ \times \frac{\exp\left[-iE_G(t-t') + i\boldsymbol{p}_G\cdot(\boldsymbol{x}-\boldsymbol{x}') - \alpha_G(\sin(\omega t) - \sin(\omega t'))\right]}{E_G - \frac{\boldsymbol{p}_G^2}{2m} + i\epsilon}, \end{aligned} \tag{3.93}$$

where $\alpha_G = e\boldsymbol{a}\cdot\boldsymbol{p}_G/(\omega m)$. The potentials of the Coulomb field $V(x)$ and the emitted photon $\boldsymbol{A}_b(x)$ are

$$V(x) = -\frac{1}{(2\pi)^3}\int \mathrm{d}^3\boldsymbol{q}\frac{Ze}{\boldsymbol{q}^2}e^{-i\boldsymbol{q}\cdot\boldsymbol{x}}, \qquad \boldsymbol{A}_b(x) = \frac{1}{\sqrt{2\omega_b}}\boldsymbol{\epsilon}_{b,\lambda}e^{i\omega_b t}, \tag{3.94}$$

where the important thing to note is that in the vector potential $\boldsymbol{A}_b(x)$ for the bremsstrahlung photon, the dipole approximation is made. This will be crucial in the understanding of why Green's function resonances do not appear in the nonrelativistic matrix element. The matrix element is now given by the standard formula, the nonrelativistic equivalent to the two Feynman diagrams in Fig. 3.7 on page 45 (see also [99]):

$$\begin{aligned} S_{fi}^{\text{nonrel}} =& S_{fi}^{\text{nonrel}(1)} + S_{fi}^{\text{nonrel}(2)} \\ =& ie^2\int \mathrm{d}^3\boldsymbol{x}\,\mathrm{d}^3\boldsymbol{x}'\mathrm{d}t\,\mathrm{d}t'\psi_{\boldsymbol{p}_f}^{\text{nonrel}\,*}(x)\Big[V(x)G^{\text{nonrel}}(x,x')W(x') \\ &+ W(x)G^{\text{nonrel}}(x,x')V(x')\Big]\psi_{\boldsymbol{p}_i}^{\text{nonrel}}(x'), \end{aligned} \tag{3.95}$$

with the nonrelativistic interaction energy

$$W(x) = -i\frac{\boldsymbol{\nabla}\cdot\boldsymbol{A}_b(x)}{m} - \frac{e\boldsymbol{a}\cdot\boldsymbol{A}_b(x)\cos(\omega t)}{m}. \tag{3.96}$$

Before we write down the result for S_{fi}^{nonrel}, a couple of comments are appropriate. We know [90] that no propagator resonances occur in the nonrelativistic expression for the matrix element, as presented below in Eq. (3.101). What is the reason for this? Below we restrict the discussion to the first matrix element $S_{fi}^{\text{nonrel}(1)}$, with completely analogous arguments for $S_{fi}^{\text{nonrel}(2)}$. First, due to the dipole approximation in $\boldsymbol{A}_b(x) = \boldsymbol{\epsilon}_{b,\lambda} \exp(i\omega_b t)/\sqrt{2\omega_b}$, momentum conservation yields

$$\boldsymbol{p}_G = \boldsymbol{p}_i, \qquad \boldsymbol{q} = \boldsymbol{p}_f - \boldsymbol{p}_i. \tag{3.97}$$

Second, energy conservation gives

$$E_f - E_i - n\omega + \omega_b = 0, \qquad E_G = E_f - n\omega, \tag{3.98}$$

where n is the index used in the Bessel function expansion, it represents the number of photons absorbed during the process. Observe that due to property (3.97), we have $\alpha_G = \alpha_{\boldsymbol{p}_i}$, so at the time t_1 in Eq. (3.95), the $\sin$-term in the exponential cancel:

$$\exp\left[i\alpha_G \sin(\omega t_1) - i\alpha_{\boldsymbol{p}_i} \sin(\omega t_1)\right] = 1, \tag{3.99}$$

so that no Bessel function expansion is needed at time t_1. We conclude that the intermediate sum over s [see the relativistic expression (3.26), page 47] is absent in the nonrelativistic case. Moreover, by combining (3.97) and (3.98) we obtain for the propagator denominator

$$E_G - \frac{\boldsymbol{p}_G^2}{2m} = E_f - n\omega - E_i = -\omega_b, \tag{3.100}$$

which is clearly different from zero, except at $\omega_b = 0$. This demonstrates that there will be no propagator denominator resonances in the nonrelativistic case. The matrix element resulting from Eq. (3.95) is

$$S_{fi}^{\text{nonrel}} = \frac{Ze^3\pi\sqrt{2}}{m\omega_b^{3/2}} \sum_n \frac{\boldsymbol{\epsilon}_{b,\lambda} \cdot (\boldsymbol{p}_f - \boldsymbol{p}_i)}{(\boldsymbol{p}_f - \boldsymbol{p}_i)^2} J_n(\alpha) \delta\left(\frac{\boldsymbol{p}_f^2 - \boldsymbol{p}_i^2}{2m} + \omega_b - n\omega\right), \tag{3.101}$$

where we have dropped the terms proportional to $\boldsymbol{a}\cdot\boldsymbol{\epsilon}_{b,\lambda}$, since after summation over polarization λ they give contributions proportional to $\boldsymbol{a}^2$, which should be dropped for consistency. In Eq. (3.101), $J_n(\alpha)$ is the usual Bessel function, and $\alpha = \frac{e}{m\omega}\boldsymbol{a} \cdot (\boldsymbol{p}_f - \boldsymbol{p}_i)$. Multiplying with the appropriate phase factors [like in Eq. (3.42)] and dividing with the incoming electron flux (velocity) $|\boldsymbol{p}_i|/m$ (throughout this section we have let the quantization volume $V = 1$ for simplicity) gives the differential cross section (see also the discussion in [60], to which formula (3.102) is in agreement):

$$\begin{aligned}
\frac{\mathrm{d}\sigma^{KF}}{\mathrm{d}\Omega_b \mathrm{d}|\boldsymbol{p}_f|\mathrm{d}\Omega_f \mathrm{d}\omega_b} &= \frac{Z^2\alpha^3}{\omega_b \pi^2} \sum_\lambda \sum_n \frac{|\boldsymbol{p}_f|^2}{m|\boldsymbol{p}_i|} \frac{\left[\boldsymbol{\epsilon}_{b,\lambda} \cdot (\boldsymbol{p}_f - \boldsymbol{p}_i)\right]^2}{(\boldsymbol{p}_f - \boldsymbol{p}_i)^4} J_n^2(\alpha) \delta\left(\frac{\boldsymbol{p}_f^2 - \boldsymbol{p}_i^2}{2m} + \omega_b - n\omega\right) \\
&= \frac{Z^2\alpha^3}{\omega_b \pi^2} \sum_n \frac{|\boldsymbol{p}_f|^2}{m|\boldsymbol{p}_i|} \frac{(\boldsymbol{p}_f - \boldsymbol{p}_i)^2 - \left[\boldsymbol{k}_b^{\text{dir}} \cdot (\boldsymbol{p}_f - \boldsymbol{p}_i)\right]^2}{(\boldsymbol{p}_f - \boldsymbol{p}_i)^4} J_n^2(\alpha) \\
&\qquad \times \delta\left(\frac{\boldsymbol{p}_f^2 - \boldsymbol{p}_i^2}{2m} + \omega_b - n\omega\right),
\end{aligned} \tag{3.102}$$

where we have summed over polarizations of the bremsstrahlung photon to obtain the last line. Here $\boldsymbol{k}_b^{\text{dir}} = \boldsymbol{k}_b/|\boldsymbol{k}_b|$. Energy conservation gives

$$\boldsymbol{p}_f^2 = \boldsymbol{p}_i^2 + 2m(n\omega - \omega_b) \tag{3.103}$$

and the sum over n is limited by the condition $\boldsymbol{p}_f^2 \geq 0$. Thus, we have shown that since Karapetyan and Fedorov [90] use the dipole approximation for the laser, the singularities where the virtual electron goes on shell disappear. Thus, it will only be possible to compare the cross section (3.46) with the nonrelativistic formula (3.102) in regions where there are no resonances, that is, at frequencies ω_b far from where $\tilde{p}_{i,f}^2 - m_*^2 = 0$ [see Eq. (3.61)].

3.6.2 Demonstration of the correct nonrelativistic limit of the relativistic cross section

For nonrelativistic formulas to apply, we must have the ingoing and outgoing translational velocities much smaller that one:

$$|\boldsymbol{v}_{i,f}| = \frac{\sqrt{E_{i,f}^2 - m^2}}{E_{i,f}} \ll 1. \tag{3.104}$$

Also the peak velocity ξ of the electron's motion in the laser field must be small,

$$1 \gg \xi = \frac{|e\boldsymbol{a}|}{m}. \tag{3.105}$$

In addition, it is assumed that the kinetic energy of the translational motion of the electron (the kinetic energy outside the field) is much larger than the angular frequency of the laser,

$$\frac{m|\boldsymbol{v}_{i,f}|^2}{2} \gg \omega, \tag{3.106}$$

from which $\omega \ll m$ obviously follows. Now look at the energy conservation relation, from the delta function in Eq. (3.46)

$$q^0 = E_f + \frac{e^2|\boldsymbol{a}|^2}{4p_f \cdot k^{\text{dir}}} - E_i - \frac{e^2|\boldsymbol{a}|^2\omega}{4p_i \cdot k^{\text{dir}}} + n\omega + \omega_b = 0, \tag{3.107}$$

where $k^{\text{dir}} = k/\omega$ is a four-vector independent on ω. For nonrelativistic E_i, E_f this relation is approximated by

$$q^0_{\text{nonrel}} = \frac{\boldsymbol{p}_f^2 - \boldsymbol{p}_i^2}{m} + \frac{e^2|\boldsymbol{a}|^2}{4p_f \cdot k^{\text{dir}}} - \frac{e^2|\boldsymbol{a}|^2}{4p_i \cdot k^{\text{dir}}} + n\omega + \omega_b = 0. \tag{3.108}$$

We will now argue that for nonrelativistic $E_{i,f} \approx m$, the bremsstrahlung frequency must be smaller than the momentum of the electron $|\boldsymbol{p}_{i,f}|$, that is $\omega_b \ll |\boldsymbol{p}_{i,f}|$, just as the nonrelativistic case without the laser field [24]. For nonrelativistic energies $E_i \approx E_f \approx m$, by the energy conservation relation we must have $|n| \approx \omega_b/\omega$. To have nonvanishing generalized Bessel

functions, the (absolute value of the) arguments α and β of the generalized Bessel functions must satisfy $|\alpha| + 2|\beta| \gtrapprox |n|$. In the factor F_i^s [see Eq. (3.28)] we have the arguments $\alpha = \alpha_i - \tilde{\alpha}_f$ and $\beta = \beta_i - \tilde{\beta}_f$. Moreover, β is proportional to $|\boldsymbol{a}|^2$, and therefore small. Now

$$\alpha_i - \tilde{\alpha}_f = \frac{ea \cdot p_i}{k \cdot p_i} - \frac{ea \cdot p_f + ea \cdot k_b}{k \cdot p_f + k \cdot k_b}. \tag{3.109}$$

However, if $\omega_b \sim |\boldsymbol{p}_{i,f}|$ we have $|\alpha_i - \tilde{\alpha}_f| \approx |e\boldsymbol{a}||\boldsymbol{p}_{i,f}|/(m\omega)$ which is much smaller than $|n| = |\boldsymbol{p}_{i,f}|/\omega$, since we have $|e\boldsymbol{a}|/m \ll 1$, and the generalized Bessel functions vanish. Thus, we must have $\omega_b \ll |\boldsymbol{p}_{i,f}|$ to have non-vanishing non-relativistic matrix elements. It follows that the arguments $\alpha_f - \tilde{\alpha}_f$, $\alpha_i - \tilde{\alpha}_i$ are small, and that the sum over s can be approximated by only one term $s = 0$, if we also ignore terms proportional to $|e\boldsymbol{a}|$, since from Eq. (3.105) we have $|e\boldsymbol{a}| \ll m$. Observe that even if we use the expansion (5.28), this gives terms in powers of $|\boldsymbol{a}|/\omega$ for which we have $\frac{|\boldsymbol{a}|}{\omega} \gg \frac{|\boldsymbol{a}|}{E_{i,f}}$. We thus get for the matrix element

$$\begin{aligned} S_{fi}^{\text{approx}} &= 2\pi i \sum_n \frac{Ze^3 m}{\sqrt{2\omega_b E_i E_f}} \frac{\delta(q^0_{\text{nonrel}})}{(\boldsymbol{p}_f - \boldsymbol{p}_i)^2} \bar{u}_{r_f}(p_f) \\ &\qquad \times \left[A_0(n, \tilde{\alpha}_f - \alpha_i, \tilde{\beta}_f - \beta_i) \hat{\epsilon}_{b,\lambda} \frac{\hat{p}_f + \hat{k}_b + m}{(p_f + k_b)^2 - m^2} \gamma^0 \right. \\ &\qquad \left. + A_0(n, \alpha_f - \tilde{\alpha}_i, \beta_f - \tilde{\beta}_i) \gamma^0 \frac{\hat{p}_i - \hat{k}_b + m}{(p_i - k_b)^2 - m^2} \hat{\epsilon}_{b,\lambda} \right] u_{r_i}(p_i) \\ &= \sum_n M^{BH} \delta(q^0_{\text{nonrel}}) J_n \left(\frac{ea \cdot (p_f - p_i)}{\omega m} \right), \end{aligned} \tag{3.110}$$

where we in the last step, according to the above discussion, approximated $\boldsymbol{q} = \boldsymbol{q}_f - \boldsymbol{q}_i + n\boldsymbol{k} + \boldsymbol{k}_b \approx \boldsymbol{p}_f - \boldsymbol{p}_i$, $k \cdot p_f \approx k \cdot p_i \approx \omega m$, $\tilde{\beta}_f - \beta_i \approx \beta_f - \tilde{\beta}_i \approx 0$, $\tilde{\alpha}_{i,f} \approx \alpha_{i,f}$, and used $A_0(n, \alpha, 0) = J_n(\alpha)$. The factor M^{BH} is the Bethe-Heitler matrix element [24] without the delta function,

$$\begin{aligned} M^{BH} &= 2\pi i \frac{Ze^3 m_e}{\sqrt{2\omega_b E_i E_f}} \frac{1}{(\boldsymbol{p}_f - \boldsymbol{p}_i)^2} \bar{u}_{r_f}(p_f) \\ &\qquad \times \left[\hat{\epsilon}_{b,\lambda} \frac{\hat{p}_f + \hat{k}_b + m}{(p_f + k_b)^2 - m^2} \gamma^0 + \gamma^0 \frac{\hat{p}_i - \hat{k}_b + m}{(p_i - k_b)^2 - m^2} \hat{\epsilon}_{b,\lambda} \right] u_{r_i}(p_i). \end{aligned} \tag{3.111}$$

When treating the energy conservation relation, we have to be a little careful. Rewriting the nonrelativistic energy conservation relation (3.108) as

$$q^0_{\text{nonrel}} = \frac{\boldsymbol{p}_f^2 - \boldsymbol{p}_i^2}{2m} + \frac{e^2|\boldsymbol{a}|^2(\boldsymbol{k}^{dir} \cdot \boldsymbol{p}_f - \boldsymbol{k}^{dir} \cdot \boldsymbol{p}_i)}{4m^2} + n\omega + \omega_b = 0, \tag{3.112}$$

we see that to recover the Karapetyan-Fedorov result for the energy conservation relation

$$q^0_{\text{nonrel}} = \frac{\boldsymbol{p}_f^2 - \boldsymbol{p}_i^2}{2m} + n\omega + \omega_b = 0, \tag{3.113}$$

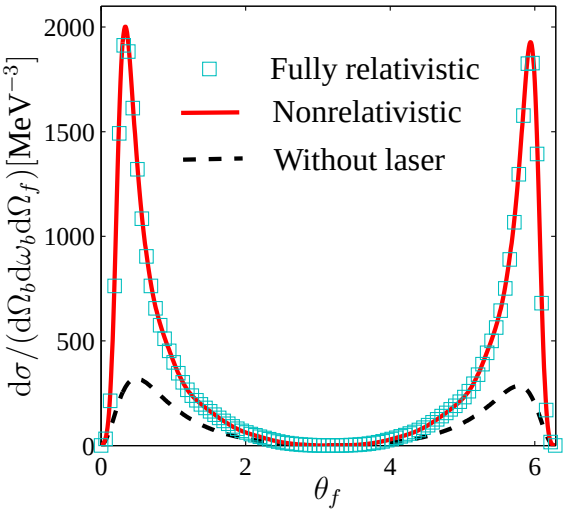

Figure 3.18: Illustration of the validity of the relativistic formula for the cross section of laser-assisted bremsstrahlung. The light blue squares show the differential cross section $\mathrm{d}\sigma/(\mathrm{d}\Omega_b \mathrm{d}\omega_b \mathrm{d}\Omega_f)$ evaluated with the fully relativistic formula (3.46), and the solid red line was calculated by the nonrelativistic expression (3.102), which makes the dipole approximation for the laser field. For comparison, we also display the field-free case [the Bethe-Heitler cross section (3.50)], the black dashed line. The angle θ_f refers to the angle relative to the direction of the initial electron (see Fig. 3.9), so that $\boldsymbol{p}_f = |\boldsymbol{p}_f|(\cos\theta_f, \sin\theta_f, 0)$. The other parameters used in the calculation are $\xi = 6 \times 10^{-3}$, $\omega = 1.17$ eV (corresponding to a laser intensity $I = 4.4 \times 10^{13}$ W/cm^2), $E_i = m + 10$ eV, $\omega_b = 5.5\omega$, $\theta_b = 179°$. Note that at this low value of ξ, the asymptotic momentum p_f in practice equals the effective momentum $q_f = p_f + m^2\xi^2 k/(k \cdot p_f)$, since ξ^2 is very small.

we have to demand

$$\frac{e^2|\boldsymbol{a}|^2}{m} \ll |\boldsymbol{p}_{i,f}| = |\boldsymbol{v}_{i,f}|m, \tag{3.114}$$

or

$$\xi^2 \ll |\boldsymbol{v}_{i,f}|. \tag{3.115}$$

Constructing the cross section from the matrix element (3.110), summing over photon polarizations and taking the nonrelativistic limit [24] of the Bethe-Heitler cross section, we end up with precisely the Karapetyan-Fedorov formula (3.102).

That the cross sections (3.46) and (3.102) actually coincide for parameters satisfying Eqs. (3.104) and (3.105) have been checked numerically for the employed computer program used for the numerical evaluation of the relativistic cross section in section 3.5. One example for the fully differential cross section is shown in Fig. 3.18.

Chapter 4

Laser-assisted pair creation

4.1 Introduction

The creation of an electron-positron pair by an external electromagnetic field is a striking manifestation of the equivalence of matter and energy, and intrinsically very interesting. Intuitively, the possibility to create matter from electromagnetic energy is clear from Einsteins relation

$$E = m, \tag{4.1}$$

for an electron at rest, its energy E is equal to its rest mass m. The usual way to think of pair production is by two energetic gamma photons, where the sum of the two frequencies must overcome the threshold of twice the electron mass, $\omega_1 + \omega_2 \geq 2m$. That pair production by only one photon, no matter how high frequency, is impossible, can be seen from the energy-momentum conservation relation. Let p_- be the four-momentum of the created electron, p_+ that of the created positron, and k_γ the wave four-vector of the gamma photon. We must then have

$$p_- + p_+ = k_\gamma, \tag{4.2}$$

which is however impossible to satisfy; in the center-of-mass frame we have $\boldsymbol{p}_- + \boldsymbol{p}_+ = \boldsymbol{0}$, which is not compatible with the requirement $k_\gamma^2 = 0$. The second standard way of producing pairs in the laboratory is by one gamma photon and the Coulomb field of a heavy nucleus. Theoretically, this process was treated by Bethe and Heitler in their bremsstrahlung paper [25]. Here the threshold is $\omega_\gamma \geq 2m$ for the gamma photon, since no energy is absorbed from the Coulomb field.

That not only energetic photon fields, but also strong, macroscopic electric fields can produce pairs was first predicted by Sauter [162] and later considered by Schwinger [165]. The basic prediction is that pairs are spontaneously created, but the rate is exponentially damped unless the electric field strength is of the order of the so-called critical field $E_c = m^2/|e|$, that is, the parameter $\chi = E_{\text{peak}}/E_c$, where E_{peak} is the peak electric field, must be at least of the order of unity. For the generalization to oscillating electric fields, the nature of the pair production process is governed by the parameter ξ. For $\xi \ll 1$, the process is a multiphoton process (for purely electric fields, the photons are virtual) with the probabilities scaling as ξ^{2n}, where n is

the minimum number of photons required to create one pair at rest. This is the normal case of pair production by gamma photon absorption. In the opposite case of $\xi \gg 1$, pair production takes place as tunneling, where the positron from the Dirac sea tunnels through the $2m$-barrier to produce one free electron and one Dirac-sea hole, or positron. We note that this is in direct analogy with field-ionization of an atom, which is governed by the Keldysh parameter [91]

$$\gamma_K = \frac{1}{\xi}\sqrt{\frac{2I_p}{m}}\,, \tag{4.3}$$

where I_p is the ionization potential, and in which case we have the multiphoton regime for $\gamma_K \gg 1$ and the tunneling regime for $\gamma_K \ll 1$. We see that γ_K corresponds to ξ^{-1} in the case of pair creation, where $I_p = 2m$.

The transition from the nonperturbative, tunneling regime for pair production to high-frequency perturbative pair production was studied by Brezin and Itzykson [37] and also by Popov [142, 143]. The strongest electromagnetic fields available in the laboratory are not purely electric, but laser fields with a magnetic component. However, a plane laser wave cannot alone produce any pairs from the vacuum due to the impossibility of satisfying energy-momentum conservation, just like a single photon. Like in the case with a static magnetic field [9, 12], a probing particle is needed in order to break the symmetry and obtain nonvanishing pair production rates. If the laser wave is not a plane wave but a focused pulse [40], or a standing laser wave [5, 29, 54, 171], pair production is possible without a second agent.

This brings us to the subject of laser-induced pair production. Pair production in a laser field with an additional source of momentum was first investigated theoretically in the context of pair production by simultaneous absorption of one non-laser mode photon and a number of laser-mode photons [129, 147]; quite recently, this process was also observed experimentally [16, 41]. Another possibility which is currently discussed in the literature is laser-induced pair creation in the vicinity of a nucleus. Unfortunately, for a nucleus at rest, the pair production rates are very low for presently available low-frequency high-power lasers [96, 112, 114, 176]. Recently, this process has been reexamined, with the idea of introducing a moving nucleus [89, 121–124, 167]. By letting the nucleus collide head on with the laser beam at high Lorentz factor γ, in the rest frame of the nucleus the frequency of the laser beam is blue-shifted or enhanced with a factor of approximately 2γ. In this way, the peak electric field seen by the nucleus in its rest frame approaches the critical field E_c, and the rates are calculated to reach observable values. See also the recent experiment [70], where the laser is used to accelerate the electrons, before they are converted into positrons using lead. Very interesting is the theoretical proposal to use a powerful laser to symmetrically accelerate the electron and positron in a positronium atom, so that they collide at high velocity and small impact parameter, to produce a muon-antimuon pair [120]. Here however the muon-antimuon pair is not created by the field itself, but by the collision of the electron with the positron.

In this section, we investigate the possibility to create pairs from vacuum in the presence of three external fields: a laser field, a Coulomb field and a single photon, whose frequency ω_γ is of the order $2m$. The Feynman diagrams are shown in Fig. 4.1. The matrix element for this process was first calculated by Roshchupkin [155], and also by Borisov *et. al.* in [31, 32, 34], however without performing any concrete numerical evaluations. The matrix element has a crossing symmetry (see the discussion in section A.3) with the one for laser-assisted bremsstrahlung,

which permits to write down the matrix element immediately. The dynamics of the process will however be rather different.

In our case, pair production is possible in the absence of the laser field through the Bethe-Heitler process [25, 62, 118, 178], if we assume the angular frequency ω_γ of the single non-laser mode photon to be larger than the threshold $2m$. The presence of the laser then modifies the process, so that we can speak about laser-assisted pair production. By contrast, if $\omega_\gamma < 2m$, the laser field would not really assist; it would be even necessary to produce any pairs at all, and we would call the process laser-induced rather than just laser-assisted. In particular the transition between these two regimes is interesting, by tuning the gamma photon frequency from $\omega_\gamma < 2m$ to $\omega_\gamma > 2m$, we can study the transition from a laser-induced to a laser-assisted process.

We note the general observation [22] that for the laser field to participate in producing an appreciable number of pairs, the laser electric field in the rest frame of the nucleus has to exceed the critical field. Alternatively we can obtain a large value of χ with respect to the photon four-momentum $k_\gamma^\nu = (\omega_\gamma, \boldsymbol{k}_\gamma)$,

$$\chi_\gamma = \frac{-e\sqrt{\left|(F_{\mu\nu}k_\gamma^\nu)^2\right|}}{m^3} = 2\frac{\omega}{m}\frac{\omega_\gamma}{m}\xi, \tag{4.4}$$

if the gamma photon and laser photons are counter propagating, $k \cdot k_\gamma = 2\omega\omega_\gamma$. In this section we however consider only moderate gamma photon energies of order $\sim m$, so that $\chi_\gamma \sim \omega\xi/m$. We thus expect that for a subcritical field, the *total* cross section of laser-assisted pair production is essentially unaffected by the laser field. However, the *differential* cross section, that is, the dependence of the cross section on the directions and energy of the produced particles, can change drastically, since a strong laser is able to accelerate the produced particles after the creation. For the same reasons, we expect the rate to be very small for a subcritical field and $\omega_\gamma < 2m$, where the Bethe-Heitler cross section vanishes identically. All of the assertions above will be demonstrated in section 4.3 by explicit numerical evaluation. As the total number of pairs produced even by low energy energy photons $\omega_\gamma \sim 2m$, is large enough to be experimentally measurable [51, 62], the addition of a strong laser makes it possible to experimentally measure nonlinear laser effects on a pair production process, for nuclei at rest. Other proposals [95, 121] require a beam of charged ions, moving with relativistic velocities.

In the following, after deriving the laser-modified cross section for pair creation, we present results for two different scenarios: In the first (section 4.3), we let the gamma photon counter propagate with the laser beam. This represents the theoretically most interesting setup, and also the most numerically demanding. A considerable simplification occurs if the gamma photon with four-momentum k_γ and the laser with wave four-vector k propagate in the same direction, a condition that implies $k \cdot k_\gamma = 0$. Numerical results and discussion on this configuration are found in section 4.4.

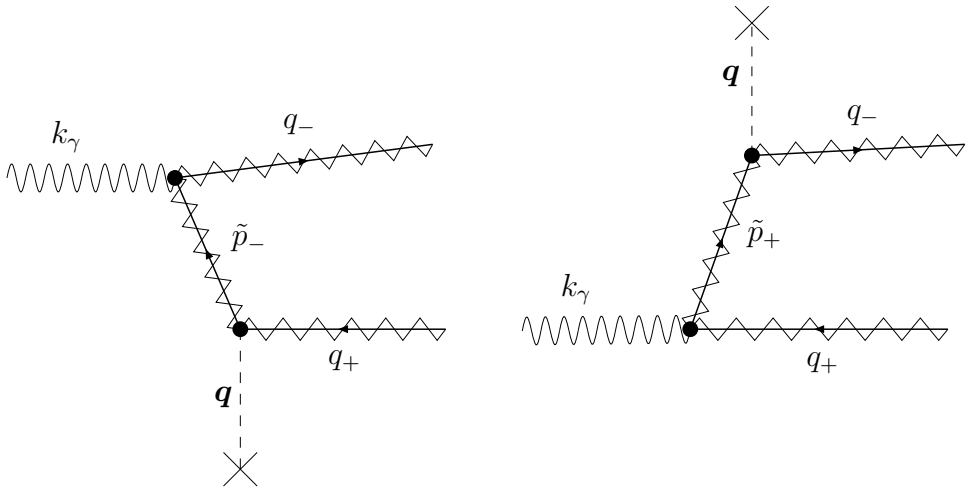

Figure 4.1: The Feynman diagrams for laser-assisted pair creation. External electron and positron lines and propagators are denoted with a wiggling line superimposed on a straight line, to stress that the laser-lepton interaction is treated nonperturbatively. The electron is created with effective four-momentum q_-, the positron is created with effective four-momentum q_+ and the intermediate electron propagator momentum is denoted by $\tilde{p}_\pm$. The absorbed non-laser mode photon has four-momentum k_γ, and the virtual Coulomb field photon, depicted with a dashed line, has three-momentum $\boldsymbol{q}$. Time flows from left to right.

4.2 Matrix element and cross section for laser-assisted pair creation in a linearly polarized laser field

In this section we derive the matrix element and the expression for the cross section of the considered process, pair production in the combined field of a gamma photon, Coulomb field and a laser. Here, we will treat linear polarization of the laser only, but circular polarization can be handled in the same way as for bremsstrahlung, see subsection 3.3.5.

4.2.1 Matrix element

By the crossing symmetry of QED processes, also applicable to laser-assisted processes as discussed in section A.3, the matrix element for pair production is precisely given by the corresponding bremsstrahlung matrix element (3.26), with the replacements $k_b \to -k_\gamma$, $p_i \to -p_+$, $p_f \to p_-$ and $u_{r_i}(p_i) \to v_{r_+}(p_+)$. Of course, it is also possible to derive the matrix element using the usual Feynman rules from appendix A, which constitutes an independent check of validity. In any case, the matrix element $S_\pm^{\text{pair}}$ for the process of pair creation in the combined field of a gamma photon, Coulomb field and a linearly polarized laser is the sum of the two

diagrams in Fig. 4.1:

$$
\begin{aligned}
S_{\pm}^{\text{pair}} = 2\pi i \sum_{s,n} & \frac{Ze^3 m}{\sqrt{2\omega_\gamma Q_+ Q_- V^3}} \frac{\delta(Q_+ + Q_- + n\omega - \omega_\gamma)}{\boldsymbol{q}^2} \\
& \times \bar{u}_{r_-}(p_-) \Bigg(M_-^s \frac{\hat{\tilde{p}}_- + \hat{k} e^2 a^2/(4k\cdot\tilde{p}_-) + m}{\tilde{p}_-^2 - m_*^2 + iK_-} F_+^{s-n} \\
& \qquad + F_-^{s+n} \frac{\hat{\tilde{p}}_+ + \hat{k} e^2 a^2/(4k\cdot\tilde{p}_+) + m}{\tilde{p}_+^2 - m_*^2 + iK_+} M_+^s \Bigg) v_{r_+}(p_+),
\end{aligned}
\tag{4.5}
$$

where

$$
\begin{aligned}
M_{\pm}^s = {} & A_0(s, \alpha_\pm - \tilde{\alpha}_\pm, \mp\beta_\pm - \tilde{\beta}_\pm) \hat{\epsilon}_{\gamma,\lambda} \\
& + A_1(s, \alpha_\pm - \tilde{\alpha}_\pm, \mp\beta_\pm - \tilde{\beta}_\pm) \left(\hat{\epsilon}_{\gamma,\lambda} \frac{e\hat{k}\hat{a}}{2k\cdot\binom{-p_+}{\tilde{p}_-}} + \frac{e\hat{a}\hat{k}}{2k\cdot\binom{\tilde{p}_+}{p_-}} \hat{\epsilon}_{\gamma,\lambda} \right) \\
& + A_2(s, \alpha_\pm - \tilde{\alpha}_\pm, \mp\beta_\pm - \tilde{\beta}_\pm) \frac{e\hat{a}\hat{k}}{(\mp 2k\cdot p_\pm)} \hat{\epsilon}_{\gamma,\lambda} \frac{e\hat{k}\hat{a}}{2k\cdot\tilde{p}_\pm},
\end{aligned}
\tag{4.6}
$$

$$
\begin{aligned}
F_{\pm}^s = {} & A_0(s, \alpha_\pm - \tilde{\alpha}_\mp, \mp\beta_\pm - \tilde{\beta}_\mp) \gamma^0 \\
& + A_1(s, \alpha_\pm - \tilde{\alpha}_\mp, \mp\beta_\pm - \tilde{\beta}_\mp) \left(\gamma^0 \frac{e\hat{k}\hat{a}}{2k\cdot\binom{-p_+}{\tilde{p}_+}} + \frac{e\hat{a}\hat{k}}{2k\cdot\binom{\tilde{p}_-}{p_-}} \gamma^0 \right) \\
& + A_2(s, \alpha_\pm - \tilde{\alpha}_\mp, \mp\beta_\pm - \tilde{\beta}_\mp) \frac{e\hat{a}\hat{k}}{2k\cdot\tilde{p}_\mp} \gamma^0 \frac{e\hat{k}\hat{a}}{(\mp 2k\cdot p_\pm)},
\end{aligned}
\tag{4.7}
$$

and $\tilde{p}_+ = -q_+ + sk + k_\gamma$ and $\tilde{p}_- = q_- + sk - k_\gamma$ is the intermediate momentum of the propagators, $k_\gamma = (\omega_\gamma, \boldsymbol{k}_\gamma)$ and $\epsilon_{\gamma,\lambda}$ is the wave four-vector and the polarization (labeled with $\lambda = 1, 2$) four-vector of the absorbed non-laser mode photon. The arguments of the Bessel functions are similar to the bremsstrahlung case,

$$
\alpha_\pm = ea\cdot p_\pm/(k\cdot p_\pm), \qquad \beta_\pm = e^2a^2/(8k\cdot p_\pm), \tag{4.8}
$$

$$
\tilde{\alpha}_\pm = ea\cdot \tilde{p}_\pm/(k\cdot \tilde{p}_\pm), \qquad \tilde{\beta}_\pm = e^2a^2/(8k\cdot \tilde{p}_\pm), \tag{4.9}
$$

The $+$ and $-$ signs refer to the charge of the involved particles, that is, p_+ refers to the positron momentum and p_- to the electron momentum. If needed, the denominators of the propagators are regularized by the term $iK_\pm$, which is explained in detail in subsection 4.2.2.

4.2.2 Regularization of the propagators

For a proper regularization of the propagators [104,164] it is, as for the bremsstrahlung case (see subsection 3.4.1), crucial to include both the imaginary mass shift in the propagator according to $m_*^2 \to m_*^2 - 2im\Gamma(k\cdot\tilde{p}_\pm)$ and the imaginary energy shift in the positron and electron four-momentum $q_\pm$ as $Q_\pm \to Q_\pm - i\frac{m}{Q_\pm}\Gamma(k\cdot q_\pm)$. The corrected denominators of the propagators

look like

$$\begin{aligned}\tilde{p}_-^2 - m_*^2 \to \tilde{p}_-^2 - m_*^2 + 2im\Gamma(k\cdot\tilde{p}_-) - 2i\frac{m}{Q_-}(Q_- + s\omega - \omega_\gamma)\Gamma(k\cdot q_-)\\ = \tilde{p}_-^2 - m_*^2 - 2im\Gamma(k\cdot k_\gamma) - 2i\frac{m}{Q_-}(s\omega - \omega_\gamma)\Gamma(k\cdot q_-),\end{aligned} \tag{4.10}$$

and

$$\begin{aligned}\tilde{p}_+^2 - m_*^2 \to \tilde{p}_+^2 - m_*^2 + 2im\Gamma(k\cdot\tilde{p}_+) + 2i\frac{m}{Q_+}(Q_+ - s\omega - \omega_\gamma)\Gamma(k\cdot q_+)\\ = \tilde{p}_+^2 - m_*^2 + 2im\Gamma(k\cdot k_b) - 2i\frac{m}{Q_+}(s\omega + \omega_\gamma)\Gamma(k\cdot q_+),\end{aligned} \tag{4.11}$$

where the last line in both equations holds if $\Gamma(x)$ (again, not to mix up with the mathematical Gamma function) is linear in the argument x. We have seen in Fig. 3.2 that this holds for small values of $x/m^2 < 10^{-4}$, but if the pairs are produced at very high energies, or if the frequency ω of the laser is large, the behavior of $\Gamma(x)$ must be investigated in the considered parameter range. Equations (4.10) and (4.11) define the $K_\pm$ used in the expression for the matrix element (4.5).

The above discussion makes clear how to, in principle, regularize the propagators so finite results are obtained even if the on-shell condition is satisfied. However, as is discussed in subsection 4.3.2, we only discuss the subcritical case $\chi \ll 1$, and therefore our results are independent of the actual regularization method.

4.2.3 Cross section

From the matrix element we obtain by the usual methods [76] the differential cross section $\mathrm{d}\sigma$, averaged over the polarization of the gamma photon and summed over the spins of the electron and positron,

$$\begin{aligned}\mathrm{d}\sigma =& \frac{1}{2}\sum_{\text{spin, pol.}} \frac{\mathrm{d}^3q_+}{(2\pi)^3}\frac{\mathrm{d}^3q_-}{(2\pi)^3}\left|S_\pm^{\text{pair}}\right|^2\frac{1}{T}\\ =& \frac{1}{2}\sum_{\substack{\text{spin, pol.}\\ n}} \frac{\mathrm{d}^3q_+}{(2\pi)^3}\frac{\mathrm{d}^3q_-}{(2\pi)^3}|S_n|^2\delta(Q_+ + Q_- + n\omega - \omega_\gamma),\end{aligned} \tag{4.12}$$

where the last line defines the partial squared amplitude S_n. Numerically, the spin and polarization sums are performed in the same way as for the bremsstrahlung matrix element, see subsection 3.5.2.

4.3 Numerical results and discussion on laser-assisted pair creation: gamma photon and laser wave counter propagating

In this section, we present results of a concrete numerical evaluation of the differential cross section. If not stated otherwise, we take the atomic number $Z = 1$, but we remark that since the amplitude is calculated in first Born approximation, the cross section scales as Z^2. Close to the threshold $\omega_\gamma \approx 2m$, Coulomb corrections to the first Born approximation are expected to make significant contributions [136], at the level of a few percent for $Z = 1$. In particular, the differential cross section will no longer be symmetric with respect to electron-positron exchange, since the positron is repelled by the nucleus. However, since our aim here is to compare the laser-modified cross section with the Bethe-Heitler cross section, and we can assume that the magnitude of the Coulomb corrections to the laser-dressed cross section is of the same size as for the laser-free case, we restrict ourselves to the first-order Born approximation here. The frequency of the laser is taken to be $\omega = 1$ keV, and the amplitude a is chosen such that the classical nonlinearity parameter $\xi = -ea/m$ is of order unity. Experimentally, this choice of parameters can be realized in either of the two following scenarios. For a high-power laser, operating at a photon energy of 1 eV and intensity of 9×10^{17} W/cm^2, head-on collision with a relativistic nucleus with a Lorentz boost factor $\gamma \approx 500$ will give $\xi = 1$ and $\omega = 1$ keV in the rest frame of the nucleus. In an alternative scenario, a focused x-ray free electron laser [151] applied to a nucleus at rest may also give access to the parameters above. Here $\xi = 1$ and $\omega = 1$ keV in the laboratory frame requires an intensity of 9×10^{23} W/cm^2 at the focus of the laser. In this regime, the peak electric field of the laser is still much smaller than the critical field, $E_{\text{peak}}/E_c = -\xi e\omega/m \ll 1$. We also expect that the qualitative behavior of the cross sections is independent of ω, as long as $\chi \ll 1$. We consider the case where the laser counter propagates with the gamma photon, and describe the directions of the produced electron and positron by the angles θ_- and θ_+, as depicted in Fig. 4.2.

4.3.1 Energy cutoff

In principle, since the sum over n in Eq. (4.5) extends from $-\infty$ to $+\infty$, the created positron and electron can acquire arbitrarily high effective energies Q_+, Q_-. This should be compared to the field-free case, given by the Bethe-Heitler formula [25], where the cross section vanishes identically for positron (or electron) energies $E_\pm > \omega_\gamma - m$. In practice, however, an apparent cutoff occurs in the energy spectrum, and thereby limits the available energy for the produced pair. In the following, we assume the directions $\boldsymbol{q}_-/|\boldsymbol{q}_-|$, $\boldsymbol{q}_+/|\boldsymbol{q}_+|$ of the electron and positron given, and consider the differential cross section (4.12) as a function of the effective energy Q_+ of the positron. The effective energy Q_- of the electron is fixed by energy conservation for each n. It follows from the expression (4.5) that to find the energy cutoff, we should consider the behavior of the function

$$H_n = \sum_{s=-\infty}^{\infty} \frac{A_0(s, \alpha_- - \tilde{\alpha}, \beta_- - \tilde{\beta}) A_0(s-n, \alpha_+ - \tilde{\alpha}, \beta_+ - \tilde{\beta})}{s + C} \tag{4.13}$$

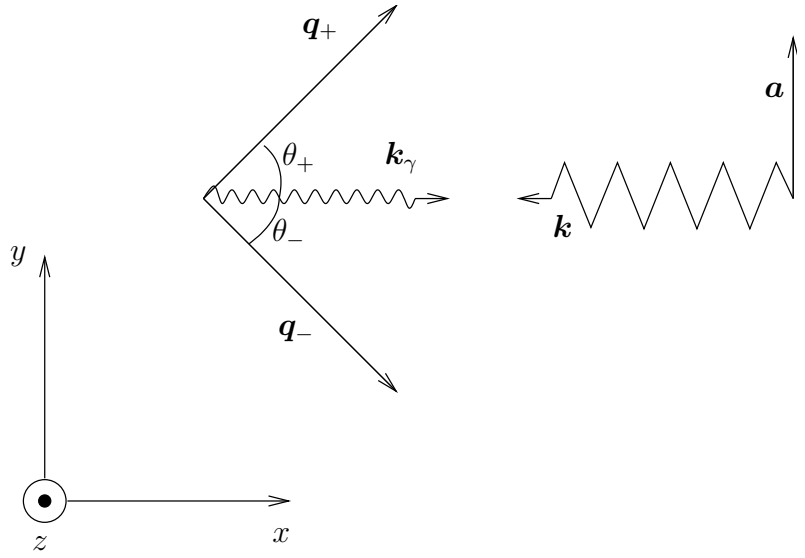

Figure 4.2: Illustration of the geometrical setup of the considered problem of laser-assisted pair creation.

as a function of n. As follows from the discussion in section 4.3.2, we can assume that C is non-integer. As shown in subsection 5.3.5, the function (4.13) has the same cutoff properties as the generalized Bessel function

$$A_0(n, \alpha_- - \alpha_+, \beta_- - \beta_+), \tag{4.14}$$

provided C is larger than the cutoff index of both of the A_0's in the numerator in Eq. (4.13). As $\beta_- - \beta_+ = [(k \cdot q_-)^{-1} + (k \cdot q_+)^{-1}]\, e^2 a^2/8 < 0$, and high values of Q_+ are obtained by absorbing photons, that is, for negative n, it follows that Q_+^{cutoff} is the largest positron energy for which the inequality

$$n_{\text{pos. cutoff}} > |n|, \tag{4.15}$$

is still satisfied. For the integer $n_{\text{pos. cutoff}}$, see Eq. (2.49). Since the quantities $k \cdot q_-$ and $k \cdot q_+$ involve direction cosines, it becomes clear that the energy cutoff is direction dependent. In particular, this implies that the maximal energy Q_+^{cutoff} will depend not only on the direction of the positron, but also on the direction of the electron. In order to determine the direction-dependent energy cutoff, one therefore proceeds as follows. In the first step, one fixes the directions of the electron and positron, which defines $n_{\text{pos. cutoff}}$ as a function of n and Q_+. In the second step, one varies Q_+ and in this way finds the largest positron effective energy Q_+ satisfying Eq. (4.15).

As a concrete example, we let the positron and electron be ejected at equal angles $\theta_+ = \theta_- \equiv \theta$, and show in Fig. 4.3 the cutoff as a function of θ for different values of the intensity parameter ξ. The frequency of the single photon is $\omega_\gamma = \sqrt{6}\, m$, which corresponds exactly to the threshold value $2m_*$ for $\xi = 1$. In Fig. 4.4, we also show a concrete evaluation of the differential cross section for the corresponding parameters, compared to the laser-free case. The magnitude of the differential cross section is here significantly larger that the case without the laser, and also displays a complex oscillatory behavior.

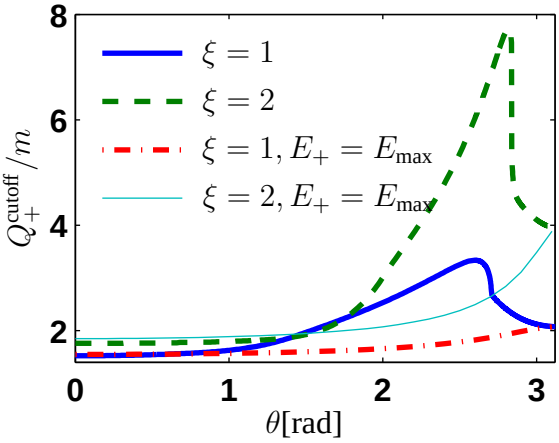

Figure 4.3: Effective energy cutoff as a function of the angle $\theta = \theta_+ = \theta_-$, resulting from the solution of Eq. (4.15). For comparison, we also show the effective energy that would result if the positron were created with the largest available energy in absence of the laser, $E_+ = E_{\max} = m - \omega_\gamma$, and then placed in the laser field with fixed direction of $\boldsymbol{q}_+$ (all curves are labeled accordingly). The difference of the latter two curves to the laser-dressed solution is because of the correlation between the electron and positron induced by the laser. This kind of correlation was also observed in [121].

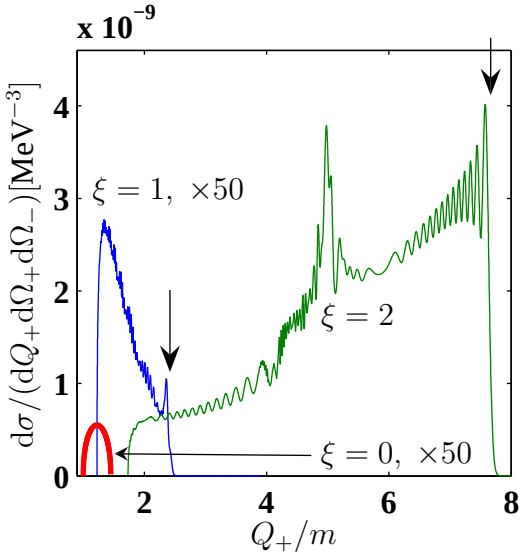

Figure 4.4: Here we show a concrete example of the cross section, for $\theta = 2.8$ rad, chosen to maximize the cutoff energy Q_+^{cutoff} for $\xi = 2$. We have $\xi = 0$ for the red curve, $\xi = 1$ for the blue curve, and $\xi = 2$ for the green curve. The "laser-assisted" curves show a complex oscillatory behavior, with a peak just before the cutoff. The cutoff positions predicted by Eq. (4.15) are indicated by vertical arrows. Note that the curves for $\xi = 1$ and $\xi = 0$ were multiplied by a factor 50; the ordinate axis is kept on a linear scale.

4.3.2 Resonances and competing processes

In principle, the matrix element (4.5) diverges if one of the intermediate momenta $\tilde{p}_-$, $\tilde{p}_+$ satisfies the on-shell condition

$$\tilde{p}_-^2 = (q_- + sk - k_\gamma)^2 = m_*^2, \qquad \tilde{p}_+^2 = (k_\gamma - q_+ + sk)^2 = m_*^2 \tag{4.16}$$

for some s. Physically, this means that the considered second-order process splits up into two consecutive first-order processes, laser-induced pair creation by a gamma photon followed by Coulomb scattering of the electron or the positron. As discussed in subsection 4.2.2, the usual way to regularize the matrix element, so that it remains finite also at the condition (4.16), is to add a small imaginary part to the energy of the electron (positron) [21], related to the total probability for the intermediate state to decay by Compton scattering. Finite values will results also if the finite extent of the laser field or the frequency width of the laser or photon beam is taken into account, like for the bremsstrahlung case. In the current thesis, however, we consider a regime of parameters where the resonances are strongly suppressed. Mathematically, this means that the value of s needed to satisfy the resonance condition (4.16) is larger than the corresponding cutoff index for the generalized Bessel function, and that the contribution from this index in the sum over s is negligible, once properly regularized. Physically speaking, we are dealing with laser parameters such that purely laser-induced processes, that cannot occur in the absence of the laser, have vanishingly small probability to occur. The basic requirement for laser-induced processes like pair creation by a photon [129] (at photon frequency $\omega_\gamma \approx 2m_* \sim 2m$) or pair creation by a nucleus [176] to have substantial probability is that the peak electric field $E_{\text{peak}} = a\omega$ should be comparable to the critical field, $E_{\text{peak}}/E_c \approx 1$, and, as mentioned before, we consider only laser parameters a, ω such that $E_{\text{peak}} \ll E_c$. This also means that at the field strengths considered, there will be no competing processes, so that our process will indeed be the dominating one.

4.3.3 Apparent singularity

For some specific values of the parameters involved, we may have that

$$k \cdot \tilde{p}_- = k \cdot q_- - k \cdot k_\gamma = 0, \tag{4.17}$$

or

$$k \cdot \tilde{p}_+ = k \cdot k_\gamma - k \cdot q_+ = 0. \tag{4.18}$$

Due to the numerous factors of $1/(k \cdot \tilde{p}_+)$ and $1/(k \cdot \tilde{p}_-)$ in the matrix element (4.5), it looks as if the matrix element diverges. For definiteness, in the following discussion, we assume parameters such that condition (4.18) holds, or is close to hold. Solving Eq. (4.18) explicitly, with $k \cdot k_\gamma = 2\omega\omega_\gamma$, and assuming $q_+ = (Q_+, \sqrt{Q_+^2 - m_*^2}, 0, 0)$ for simplicity, we obtain

$$Q_+ = \omega_\gamma + \frac{m_*^2}{4\omega_\gamma}, \tag{4.19}$$

which makes it clear that the conditions (4.17), (4.18) can actually be satisfied for $\omega_\gamma \sim m_*$. If Q_+ is fixed by (4.19), Q_- becomes fixed by the energy conservation relation $Q_- = \omega_\gamma - n\omega -$

Q_+. Another difficulty is that the arguments of the generalized Bessel functions tend to infinity,

$$|\alpha_\pm - \tilde{\alpha}_+| \to \infty, \qquad \left|\beta_\pm - \tilde{\beta}_+\right| \to \infty, \tag{4.20}$$

as $k\cdot\tilde{p}_+ \to 0$, since both $\tilde{\alpha}_+$ and $\tilde{\beta}_+$ include a factor $1/(k\cdot\tilde{p}_+)$. For the propagator denominator, we have

$$\tilde{p}_+^2 - m_*^2 = 2\left[sk\cdot(k_\gamma - q_+) - k_\gamma\cdot q_+\right], \tag{4.21}$$

which becomes s-independent as $k\cdot\tilde{p}_+ \to 0$. Therefore, one might think that the sum over s in the matrix element (4.5) can be performed using the summation theorem (5.22) (see page 105). However, in general we have, in the limit $x \to 0$,

$$\sum_s \frac{A_0(s, a_1 - c/x, b_1 - d/x)A_0(s-n, a_2 - c/x, b_2 - d/x)}{xs + F} \neq \frac{A_0(n, a_1 - a_2, b_1 - b_2)}{F}, \tag{4.22}$$

for constant $a_{1,2}$, $b_{1,2}$, c, d, and F, even though it is tempting to assume equality. We should say that the limit $x \to 0$ gives a finite result for the left hand side of Eq. (4.22).

As it turns out, the matrix element is finite, even in the limit $k\cdot\tilde{p}_\pm \to 0$. We have not been able to show this analytically, but accurate numerical evaluation of the cross section (4.12) proves that it is true. There is also no physical argument why the cross section should be resonant at $k\cdot\tilde{p}_\pm = 0$. In fact, the requirement that the cross section should be finite at conditions (4.17), (4.18) can be used as a sensible numerical check of the computer code used to evaluate the cross section, since finiteness requires a proper evaluation of the s-sum of products of generalized Bessel functions, and is furthermore sensible to sign errors among the different terms constituting the cross section.

4.3.4 Angular distribution

For the field-free case, the pairs prefer to emerge at an angle $\theta \sim m/\omega_\gamma$ with the vector $\boldsymbol{k}_\gamma$ [25]. When the laser field is turned on, we expect to find more pairs in the direction of the laser wave vector $\boldsymbol{k}$. This tendency is expected to increase as the intensity parameter ξ grows, since with rising intensity the Lorentz force of the laser field pushes the pairs increasingly in the propagation direction. In Fig. 4.5, we display the differential cross section integrated over $\mathrm{d}Q_+$ and $\mathrm{d}Q_-$, for $\xi = 1, 2$. The peak is seen to shift from the direction of the gamma photon to the direction of the laser wave.

4.3.5 Total cross section

The total cross section is obtained by integrating the differential cross section (4.12) over the energies Q_+, Q_- and solid angles Ω_+, Ω_- of the produced positron and electron:

$$\sigma_{\text{tot}} = \int \frac{1}{2}\sum_{\substack{\text{spin, pol.}\\ n}} \frac{Q_+|\boldsymbol{q}_+|\mathrm{d}Q_+\mathrm{d}\Omega_+}{(2\pi)^3}\frac{Q_-|\boldsymbol{q}_-|\mathrm{d}Q_-\mathrm{d}\Omega_-}{(2\pi)^3}|S_n|^2\delta(Q_+ + Q_- + n\omega - \omega_\gamma). \tag{4.23}$$

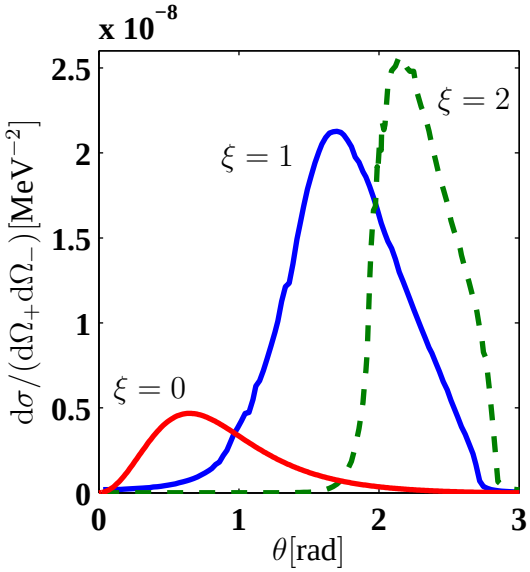

Figure 4.5: The differential cross section integrated over the effective energies $Q_{\pm}$, for $\xi = 0$ (solid red line), $\xi = 1$ (solid blue line) and for $\xi = 2$ (dashed green line). As in Fig. 4.3, $\omega_\gamma = \sqrt{6}\, m$. The pair is emitted at equal angles $\theta_+ = \theta_- = \theta$ (see Fig. 4.2), in the plane spanned by $\boldsymbol{k}$ and $\boldsymbol{a}$. We note that the area under these curves are notably different, which implies that the presence of the laser enhances the number of pairs produced at $\theta_+ = \theta_-$. The differential cross section integrated over all angles will however, as we will see later (see Fig. 4.6), be almost unchanged as compared to the laser free case.

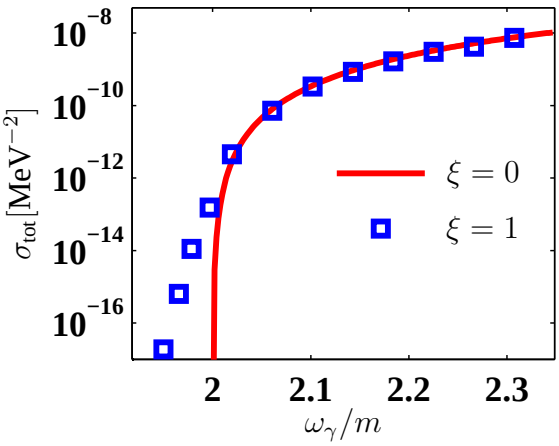

Figure 4.6: The total cross section as a function of the frequency ω_γ of the non-laser mode photon, compared with the case without the laser field. The laser frequency used is $\omega = 1$ keV. Due to the laser, there remains a finite probability of pair creation below the field-free threshold $\omega_\gamma = 2m$. However, the magnitude drops exponentially, as expected.

Here, it is convenient to replace the sum over the number of exchanged photons n by an integral, and to evaluate this integral with the delta function so that n equals the integer closest to n_0, with

$$n_0 = (\omega_\gamma - Q_+ - Q_-)/\omega. \tag{4.24}$$

This is a good approximation if $\omega \ll Q_\pm, \omega_\gamma$, and if $n_0 \gg 1$, which is the case for the parameters used. The remaining six-fold integral,

$$\sigma_{\rm tot} = \frac{1}{2} \sum_{\text{spin, pol.}} \int_{m_*}^{\infty} \mathrm{d}Q_+ \int_{m_*}^{\infty} \mathrm{d}Q_- \int \mathrm{d}\Omega_+ \int \mathrm{d}\Omega_- \frac{Q_+ |\boldsymbol{q}_+|}{(2\pi)^3} \frac{Q_- |\boldsymbol{q}_-|}{(2\pi)^3} |S_{n_0}|^2, \tag{4.25}$$

has to be performed numerically, we employ a Monte Carlo method [144]. We note that this method has been used before to obtain total rates for the production of pairs from a colliding laser beam and a nucleus [89, 167]. In general, Monte Carlo integration is the method of choice for integrals of high dimensionality where the accuracy demand is modest. In fact, for such high dimensionality as 6, and with the evaluation of the integrand being numerically expensive (mainly due to the generalized Bessel functions with large values of both arguments and index), we have not found any other integration method than the Monte Carlo integration method that can deliver modestly accurate numerical results within reasonable computer time. The result of one such calculation is shown in Fig. 4.6, where we present the total cross section as a function of the frequency ω_γ of the perturbative photon. As expected, in the region where pair production is possible without the laser, the rates are almost indistinguishable.

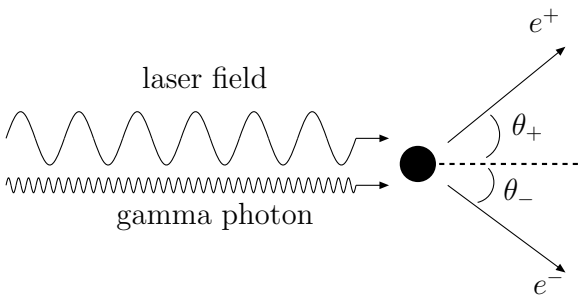

Figure 4.7: Schematic picture of the considered pair creation process. A low-frequency, high-intensity laser beam of linear polarization and a high-frequency gamma photon, propagating in the same direction, impinge on a stationary nucleus, depicted as a filled black circle, to produce an electron and a positron. The angle $\theta_\pm$ denotes the ejection angle in the plane spanned by the propagation direction and the polarization direction of the laser. Note that the wavelengths of the two waves are not drawn to scale, in reality we consider the case where the laser wavelength is many orders of magnitude larger than the wavelength of the gamma photon.

4.4 Numerical results and discussion on laser-assisted pair creation: collinear gamma photon and laser wave

In this section, we present results on the setup, where the photon beam and the laser beam propagate in the same direction, schematically pictured in 4.7. This configuration is actually nothing else than pair creation by a Coulomb field and a plane wave, with one weak, high-frequency component, and has been studied before: see [30, 32]. However, no numerical work was performed, and we are the first to actually evaluate the cross section. The idea behind considering the configuration shown in Fig. 4.7 is the following: It is known from the field-free case [25, 118] that the pairs prefer to come out roughly in the same direction as the propagation direction of the creating photon. However, for low photon energies $\omega_\gamma \sim m$, the angular distribution is quite broad. If a high-power laser is added, the Lorentz force of this laser pushes the pairs in the forward direction, and therefore focuses the produced pairs to mainly appear in the forward direction. The total number of pairs produced, or the total cross section, is not changed for subcritical lasers, as argued in the introduction of this chapter.

4.4.1 Simplification of the matrix element in the collinear geometry

That the laser, with wave four-vector $k^\mu = (\omega, \boldsymbol{k})$, and the gamma photon, with four-momentum $k_\gamma^\mu = (\omega_\gamma, \boldsymbol{k}_\gamma)$ propagate in the same direction means that

$$k_\gamma \cdot k = 0. \tag{4.26}$$

This fact provides for a considerable simplification of the matrix element, under the condition (4.26) the expression (4.5) can be written as

$$\begin{aligned} S_{p_+p_-} =& 2\pi i \sum_{n=-\infty}^{\infty} \frac{Ze^3\, m}{\sqrt{2\omega_\gamma E_+ E_-}} \frac{\delta(Q_+ + Q_- - n\omega - \omega_\gamma)}{(\boldsymbol{q}_- + \boldsymbol{q}_+ - n\,\boldsymbol{k} - \boldsymbol{k}_\gamma)^2} \\ & \times \bar{u}^-_{p_-} \left(\hat{\epsilon}_\gamma \frac{\hat{k}_\gamma - \hat{p}_- - m}{2p_- \cdot k_\gamma} F_n + F_n \frac{\hat{p}_+ - \hat{k}_\gamma - m}{2p_+ \cdot k_\gamma} \hat{\epsilon}_\gamma \right) u^+_{p_+}, \end{aligned} \tag{4.27}$$

where now

$$\begin{aligned} F_n =& A_0(n, \alpha_+ - \alpha_-, -\beta_+ - \beta_-)\gamma^0 \\ & + A_1(n, \alpha_+ - \alpha_-, -\beta_+ - \beta_-) \left(\frac{\gamma^0 e\, \hat{a}\hat{k}}{2k \cdot p_+} + \frac{e\, \hat{a}\hat{k}\gamma^0}{2k \cdot p_-} \right) \\ & + A_2(n, \alpha_+ - \alpha_-, -\beta_+ - \beta_-) \frac{e^2\, a^2 \omega \hat{k}}{2k \cdot p_- k \cdot p_+}, \end{aligned} \tag{4.28}$$

and

$$\alpha_\pm = \frac{e\, a \cdot p_\pm}{k \cdot p_\pm}, \qquad \beta_\pm = \frac{e^2\, a^2}{8\, k \cdot p_\pm}. \tag{4.29}$$

Note that if we choose the propagation direction of the laser as $\boldsymbol{k}/\omega = (1,0,0) = \boldsymbol{k}_\gamma/\omega_\gamma$, then $n\boldsymbol{k} + \boldsymbol{k}_\gamma = (Q_+ + Q_-, 0, 0)$ by energy conservation, so that the Coulomb momentum $\boldsymbol{q} = \boldsymbol{q}_- + \boldsymbol{q}_+ - n\boldsymbol{k} - \boldsymbol{k}_\gamma$ is independent of n. From the expression (4.27) we gather several differences compared to the general matrix element (4.5). In (4.27), there is only one sum over n, the intermediate propagator sum over s is absent. This means that the possibility of the intermediate particle to go on-shell has vanished. In the collinear geometry there are no resonances. The reason is simple: As already mentioned, the total field gamma photon + laser wave is a plane wave, and is as such unable to produce pairs of its own. Pair production by a plane wave together with a Coulomb field is indeed possible [112, 121, 176], but absorption of a photon from a plane wave by a free electron is not, so that the sequence process pair creation by Coulomb field and plane wave followed by photon absorption is impossible. We conclude that the split-up of a second order laser-dressed process into two first-order processes does not take place here.

4.4.2 Angular distribution: focusing of the produced pairs

Here we present the evaluation of the angular distribution of the pairs, the differential cross section. We note that due to symmetry reasons, the differential cross section is symmetric under the exchange of electron and positron, and we show, in all following figures, the positron spectra, $\mathrm{d}\sigma/\mathrm{d}\Omega_+$. The differential cross section is formed from the matrix element according to formula (4.12), just as the case with counter propagating gamma photon and laser wave. The laser frequency is chosen as $\omega = 10$ eV. However, we expect that the qualitative behavior of the cross section is independent of ω, as long as $\chi \ll 1$. Again, instead of performing the sum over photon orders n in Eq. (4.27), it is convenient to replace the sum with an integral,

	θ_0[rad]	c_1	c_2	b [MeV^{-2}]
$\xi = 6$	0.15	130	15	0.95×10^{-4}
$\xi = 10$	0.11	150	25	1.1×10^{-3}

Table 4.1: Table showing the numerical values used in Eq. (4.30) to produce the solid lines in Fig. 4.8.

and to utilize the delta function to integrate over n, so that $n = n_0 = (Q_+ + Q_- - \omega_\gamma)/\omega$. The remaining fourfold integral in the differential cross section is evaluated by employing a Monte-Carlo integration routine [144]. To better guide the eye, we furthermore perform a fit of the pointwise obtained Monte-Carlo differential cross section, which is necessarily plagued by numerical sampling error, to a function of the form

$$\frac{\mathrm{d}\sigma_{\text{fit}}}{\mathrm{d}\Omega_+} = \frac{b}{e^{-c_1(\theta_+ - \theta_0)} + e^{c_2(\theta_+ - \theta_0)}}, \tag{4.30}$$

where b, $c_{1,2}$ and θ_0 are positive constants. We found this functional form to be numerically adequate, and this is probably the form of the true expression for the differential cross section. At least the exponential decay for angles θ_+ larger than the peak angle θ_0 has been numerically confirmed.

In Fig. 4.8, we show the cross section $\mathrm{d}\sigma/\mathrm{d}\Omega_+$, which remains differential only in the solid angle Ω_+ of the created positron. Observe that here the solid angle refers to the direction $\boldsymbol{p}_+/|\boldsymbol{p}_+|$ of the positron outside the laser, to allow explicit comparison with the laser-free case. The gamma photon energy ω_γ is $\omega_\gamma = 1.25$ MeV $> 2m$, so that pair production is possible without the laser. However, as is clearly seen in Fig. 4.8, the angular distribution in the field-free case [25] is broad, indistinguishable from an isotropic distribution within the parameter range plotted in Fig. 4.8. Quite to the contrary, the laser-dressed curves show sharp peaks, with the peak height increasing with increasing laser intensity, and the peak position given roughly by $\theta_{\text{peak}} = 1/\xi$. Also observe that the laser introduces a "splitting" of the angular distribution, so that very few positrons appear in the laser propagation direction $\theta_+ = 0$. The numerical values of the constants used to produce the dashed and solid lines for $\xi = 6$ and $\xi = 10$ are displayed in table 4.4.2.

Actually, the peak angle $\theta_{\text{peak}} = 1/\xi$ can be intuitively explained by the classical equations of motion. A similar way of reasoning can be applied to ionization induced by a laser, and is called "simple man's theory" [18]. If we assume that the positron is created during a time much shorter that the laser field period, at the laser phase ϕ_0, with initial momentum p_{+i} (with momentum distribution according to the Bethe-Heitler cross section), the kinetic momentum $\mathfrak{p}_+$ evolve according to Eq. (2.11):

$$\begin{aligned}\mathfrak{p}_+^\mu(\phi) =& p_{+i}^\mu + e\,[A^\mu(\phi_0) - A^\mu(\phi)] \\ &+ \frac{k^\mu}{2p_{+i}\cdot k}\Big(2e[A_\nu(\phi) - A_\nu(\phi_0)]p_{+i}^\nu - e^2[A^\nu(\phi)A_\nu(\phi) - A^\nu(\phi_0)A_\nu(\phi_0)]\Big),\end{aligned} \tag{4.31}$$

depending on the initial phase ϕ_0 at the moment of creation, and the initial momentum p_{+i}. Now, what is actually measured is the asymptotic momentum $p_+ = \mathfrak{p}(\phi = \infty)$, that is, when

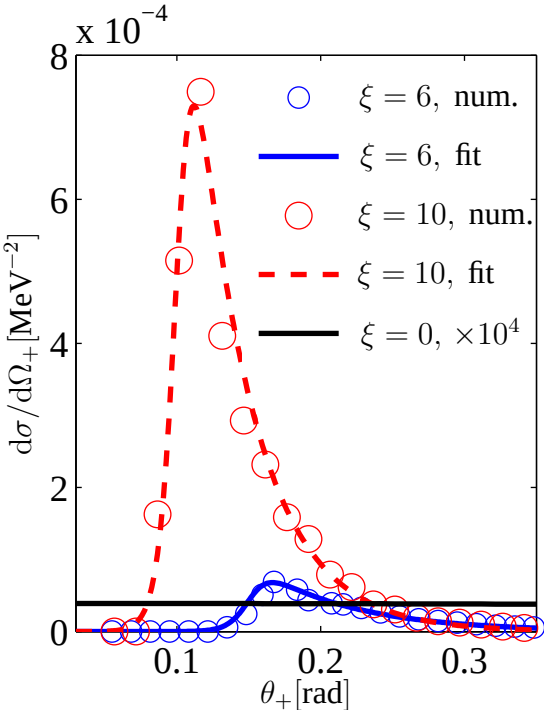

Figure 4.8: The differential cross section $\mathrm{d}\sigma/\mathrm{d}\Omega_+$ as a function of the angle of ejection θ_+ (see Fig. 4.7), in the plane spanned by the propagation direction $\boldsymbol{k}/\omega$ and the polarization direction $\boldsymbol{a}/|\boldsymbol{a}|$. The laser frequency is $\omega = 10$ eV and the gamma photon energy is $\omega_\gamma = 1.25$ MeV. Here, the parameter values $\xi = 6$ and $\xi = 10$ correspond to laser intensities $I = 3.2 \times 10^{21}$ W/cm^2 and $I = 8.9 \times 10^{21}$ W/cm^2, respectively. The nuclear atomic number is $Z = 1$, and we remark that as the cross section is evaluated in the first Born approximation, it scales as Z^2. In the graph, circles represent numerical estimates of the differential cross section obtained by fourfold Monte-Carlo integration, and the red dashed and blue solid lines are analytical fits [see Eq. (4.30), numerical values in table 4.4.2] to the numerical values. For comparison, the solid black line shows the laser-free case, multiplied by a factor of 10^4 (the laser-free differential cross section would otherwise not be visually distinguishable from zero). For the conversion to other frequently used units for the cross section, one uses $1\ \mathrm{MeV}^{-2} \approx 4 \times 10^2$ barn $= 4 \times 10^{-22}$ cm^2.

the laser pulse has passed. Since it is assumed that the vector potential is adiabatically turned off, and satisfies $A^\mu(\infty) = 0$, we have

$$\begin{aligned} p_+^\mu =& p_{+i}^\mu + eA^\mu(\phi_0) \\ &+ \frac{k^\mu}{2p_{+i}\cdot k}\Big(- 2eA_\nu(\phi_0)p_{+i}^\nu + e^2A^\nu(\phi_0)A_\nu(\phi_0)\Big), \end{aligned} \tag{4.32}$$

so that the angle θ_+ is given by

$$\begin{aligned} \theta_+ = \arctan\frac{|p_+^y|}{|p_+^x|} =& \arctan\frac{\left|p_{+i}^y + eA^y(\phi_0)\right|}{\left|p_{+i}^x + \frac{\omega}{2p_{+i}\cdot k}\left(e^2A^2(\phi_0) - 2ep_{+i}\cdot A(\phi_0)\right)\right|} \\ \approx& \frac{2k\cdot p_{+i}}{\omega|e\boldsymbol{a}\cos\phi_0|}, \end{aligned} \tag{4.33}$$

where we have assumed $\boldsymbol{k} = (\omega, 0, 0)$, $A^\mu(\phi) = (0, \boldsymbol{a}\cos\phi) = (0, 0, |\boldsymbol{a}|\cos\phi, 0)$ and the last approximation is valid for small angles $\theta_+ \ll 1$ and for small initial energies E_{+i} so that the term e^2A^2 is the dominating one in the denominator of the first line of (4.33). Typically, for $\omega_\gamma \approx 2m$, according to the Bethe-Heitler distribution [25], the energy is shared between the positron and electron so that $E_{+i} = \omega_\gamma/2$. Now, using the Bethe-Heitler distribution of positron momenta (assuming the energy to be $E_{+i} = \omega_\gamma/2$), so that positrons initially emitted with momentum p_{+i}^μ end up at angle θ_+ after interaction with the laser field, and summing the contributions from all laser phases $-\pi/2 \le \phi_0 \le \pi/2$, we obtain a modified momentum distribution, as shown in Fig. 4.9.

4.4.3 Total cross section

We show in Fig. 4.10 the total cross section σ_{tot}, obtained in the same way as for the counter propagating case, see Eq. (4.23). Note that the parameters are different compared to those used to produce Fig. 4.6. Here we have $\omega = 10$ eV and $\xi = 10$. This is a more realistic choice of parameters, which however makes it more demanding to make the integration algorithm converge. As a result, we could only do the calculation for small values of $\omega_\gamma \sim 2m$ close to the threshold.

4.4.4 Experimental realization

In this subsection we elaborate on the possible experimental verication of the results found in section 4.4, focusing of the created positrons in the collinear setup of gamma photon beam and laser beam. A good way of obtaining photon beams of moderately high energy is by Compton backscattering of photons from a laser (for example an XFEL [53]) on high-energy electrons. If we look at the formula (3.9) for the emitted frequency, for $n = 1$ (since the laser is assumed to be weak ($\xi \ll 1$), only one photon is absorbed, which also means that $q_i \approx p_i$), we retrieve the usual Compton formula [141] for the frequency ω_γ of the scattered photon in the lab frame,

$$\omega_\gamma = \frac{k\cdot p_i}{p_i\cdot k_\gamma/\omega_\gamma + k\cdot k_\gamma/\omega_\gamma} \approx \frac{4E_i^2\omega}{m^2}, \tag{4.34}$$

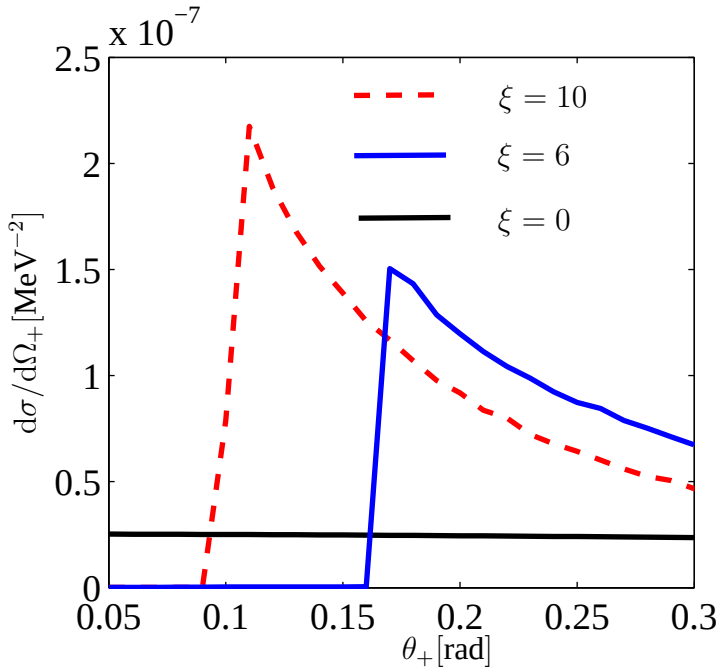

Figure 4.9: Illustration of the modification of the differential cross section with inclusion of the laser. The dashed red curve and blue solid curve are obtained by summing over all laser phases, assuming that the positron is created with the momentum given by the Bethe-Heitler distribution. The laser-modified cross sections are normalized so that the number of created positrons is the same as for the field-free case. From this graph, we see by comparing with the quantum treatment, Fig. 4.8, that the position $\theta_{\text{peak}} \approx 1/\xi$ is correctly predicted, but that the peaks are much narrower in Fig. 4.8. This implies that a full, quantum treatment is necessary to obtain the detailed features of the spectrum.

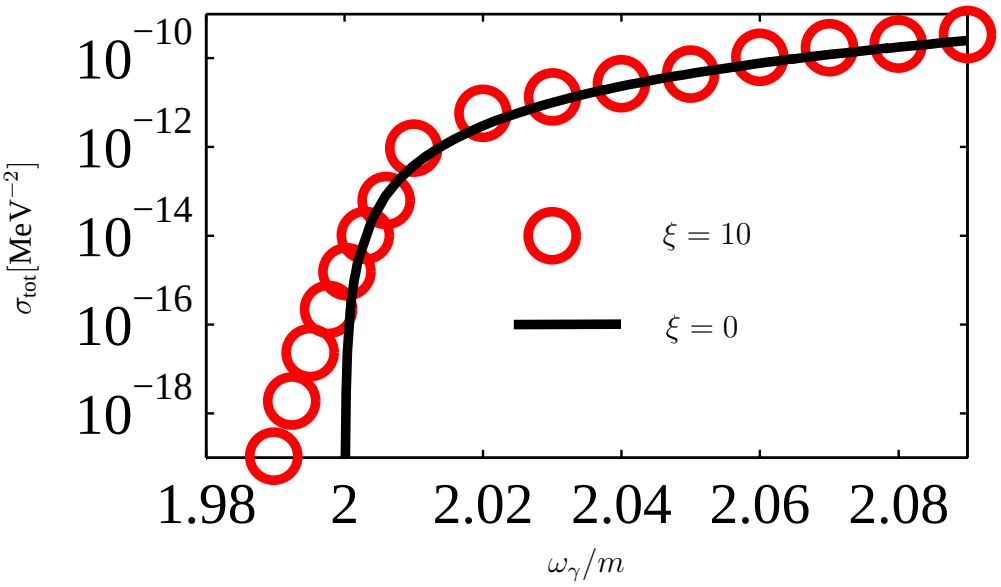

Figure 4.10: The total cross section for electron-positron pair creation close to the threshold, displayed in logarithmic scale as a function of the perturbative photon energy ω_γ. The solid black line shows the field-free case, given by the Bethe-Heitler formula [25]. The cross section is in this case identically zero below the pair production threshold $\omega_\gamma/m = 2$. Below threshold, the laser-induced (rather than laser-assisted) pair creation cross section exhibits an exponential decrease. Parameters in the calculation are the same as in Fig. 4.8: $\omega_\gamma = 10$ eV, $\xi = 10$, $Z = 1$. Note that in this graph the gamma photon is propagating in the same direction as the laser, as opposed to Fig. 4.6, where the gamma photon and laser are taken to counter propagate. Although this makes a considerable difference in the analytic formula for the matrix element [compare Eq. (4.27) with the more complex expression Eq. (4.5)], the behavior of the two curves is very similar. One quantitative difference is that the decay of the laser-induced cross section below the threshold $\omega_\gamma = 2m$ is here even faster than the corresponding curve in Fig. 4.6, which can be explained by the lower value of χ: In Fig. 4.6, we have $\chi = \xi\omega/m = 2 \times 10^{-3}$, as compared to $\chi = 2 \times 10^{-4}$ in this figure.

where $E_i \gg m$ is the energy of the incoming electron, and the last approximation assumes $\omega \ll m$, that the initial electron and the laser collide head on at a small angle, $\boldsymbol{p}_i \cdot \boldsymbol{k} + |\boldsymbol{p}_i||\boldsymbol{k}| \ll 1$, and that the photon is scattered in the same direction as the incoming electron, $\boldsymbol{p}_i \cdot \boldsymbol{k}_\gamma = |\boldsymbol{p}_i||\boldsymbol{k}_\gamma|$, which represents the geometry where the largest photon energy ω_γ is achieved. From Eq. (4.34) we gather that high energy photons can be obtained by scattering laser light at high-energy electrons in for example a storage ring. As an example, to obtain backscattered photon energy $\omega_\gamma = 2m$ (pair creation threshold) at $\omega = 10$ eV, one needs electrons with energy $E_i \approx 80$ MeV. Now for the experimental realization, we propose to synchronize photon pulses produced from Compton backscattering with a laser pulse from a strong laser. According to [81, 134], pulse duration of the gamma photon pulse is determined by the electrons in the storage ring. We can therefore assume gamma photon pulse length 1 ps, with repetition rate 1 Hz (much higher repetition rates can be obtained, but as will be clear below, the limitation of the repetition rate comes form the strong laser), and $N_\gamma = 10^7$ photons per pulse [81, 134]. For the photon energy, we assume $\omega_\gamma = 1.25$ MeV, to comply with the parameter values assumed in Fig. 4.8. We note that much higher photon energies are available, the limitation being the energy of the electron beam [16, 81]. As the atomic target, we assume a 1 mm thick foil of lead ($Z = 82$). Lead has average atomic mass $m_u = 207.22$ g/mole, density 11.34 g/mole, so that the number area density in the 1-mm-foil is $N_d = 3.3 \times 10^{21}$ atoms/cm^2 (Avogadro's number $N_A = 6.022 \times 10^{23}$). From the numerical evaluation and theoretical arguments, we know that the total number of pairs is determined by the gamma photons, for which $\omega_\gamma = 1.25$ MeV and $Z = 82$ yields $\sigma_{\text{tot}} = 1.3 \times 10^{-4}$ MeV^{-2} $= 5.4 \times 10^{-26}$ cm^2, in accordance with the Bethe-Heitler cross section. The number of pairs $N_{e^+e^-}$ produced during one pulse is therefore $N_{e^+e^-} = \sigma_{\text{tot}} N_\gamma N_d = 1.8 \times 10^3$. If now a long laser pulse of duration 1 ps (same duration as the gamma photon pulse) is synchronized with the gamma photon pulse, it follows from the preceding discussion and results in this section that the laser focuses the produced particles to emerge at a typical angle $\theta \approx 1/\xi$. To obtain the tight focusing shown in Fig. 4.8 at $\xi = 10$, the pulse energy required is 1.4 J, if a laser wavelength $\lambda = 1054$ nm and focusing of the pulse down to one wavelength is assumed. This kind of long, strong laser pulses are available at for example the Vulcan laser facility in the UK [173]. If, in addition, the same repetition rate is assumed, it follows that essentially all pairs (1.8×10^3 per pulse) emerge with the angle $\theta = 6^\circ \pm 2^\circ$ (see Fig. 4.7). The uncertainty out of the plane spanned by the laser polarization direction and the propagation direction is approximately $\pm 0.3^\circ$.

Chapter 5

An essential ingredient of laser-modified QED processes: generalized Bessel functions

5.1 On special functions in general

Special functions like the Bessel function have always been important to theoretical physics. What makes a special function special? Most often, a special function is defined through its differential equation. However, just by stating that one particular function solves a differential equation contributes nothing to the understanding of the solution. A function is only promoted to be "special" once its properties are well understood. Several representations should be known, asymptotic expansions in different regimes of the parameters together with analytic properties should be there so that a feeling for the function in question can be developed. The definitive source of information about special functions is of course the classical reference [1]. Finally, one should not only be able to make a graph of the function in reasonable time, but also be able to use the function as a building block in more complicated formulas, for making actual calculations of physical processes. This last demand is not to be underestimated, since it implies that there is an efficient numerical algorithm for evaluation available. If one is to sum or integrate over complicated functions depending on the special function, fast evaluation is called for. For many special functions this is the case, the common ones included in commercial software such as MATLAB® or Mathematica®.

In theoretical physics one sometimes reads the word "exact" or "analytical" for an expression describing some physical quantity. Usually this means that the expression is free from integration or indefinite summations. Expressions containing special functions are however often considered to be analytical, even when this means nothing else than replacing the integration over one function with another symbol. To obtain real numbers out of the formulas, numerical algorithms for evaluation are necessary. A complex formula containing a large number of special functions is useless unless definite numbers can be produced out of it.

In this chapter we present an overview of two special functions important to the theoretical

description of laser-modified QED, the usual Bessel function and the generalized Bessel function. In the description of relativistic laser-matter interaction, the generalized Bessel function is extremely important in the case of a linearly polarized laser. The reason is that the nonperturbative, exact solution, to the basic problem "electron in a strong laser field" can be expressed through generalized Bessel functions [see chapter 2], and with this solution as a basis we can include the interaction with other fields in a perturbative way.

In this chapter, being more mathematical in character, the letter m does not stand for the electron mass, but is used as an integer index, and α is used as a real variable and does not have the meaning of the fine-structure constant.

5.2 Usual Bessel functions

First introduced by Bernoulli, and systematically studied by Bessel, the usual Bessel function $J_n(\alpha)$, for integer index n, is one of the most widely used special functions in theoretical physics. The standard reference on Bessel functions is [174]. In the context of laser-matter interaction, Bessel functions appear as coefficients in the Fourier series expansion of the wave function of an electron in a plane wave electromagnetic field. As we have seen in chapter 2, for electrons dressed by a circularly polarized laser field, we get the normal Bessel function $J_n(\alpha)$ directly. In the case of a laser of linear polarization, we instead have the generalized Bessel function $A_0(n, \alpha, \beta)$, which however can be defined as a sum over ordinary Bessel functions. The Bessel function and the generalized Bessel function are very similar, and share several properties. A thorough understanding of the generalized Bessel function thus necessitates a knowledge of the properties of the usual Bessel function. In the following, we discuss some properties of $J_n(\alpha)$, and most important, we describe a numerical algorithm, originally due to Miller [26], for efficient calculation of large arrays of Bessel function.

5.2.1 Basic properties of the usual Bessel function

Our viewpoint of the Bessel function is that it is the coefficient in the Fourier series expansion of the periodic function $\exp(i\alpha \sin\theta)$:

$$e^{i\alpha \sin\theta} = \sum_{n=-\infty}^{\infty} J_n(\alpha) e^{in\theta}. \tag{5.1}$$

By performing "Fourier's trick", that is we multiply with $\exp(-im\theta)$ on both sides of Eq. (5.1) and integrate over one period $\frac{1}{2\pi}\int_{-\pi}^{\pi} \mathrm{d}\theta$, we find the integral representation

$$J_m(\alpha) = \frac{1}{2\pi}\int_{-\pi}^{\pi} e^{i(\sin\theta - m\theta)}\mathrm{d}\theta = \frac{1}{\pi}\int_0^{\pi} \cos(\alpha \sin\theta - m\theta)\mathrm{d}\theta, \tag{5.2}$$

where the last equality follows from symmetry arguments. Eq. (5.2) can be taken as a definition of $J_n(\alpha)$ for real values of α and integer n (which are the only cases we deal with). The equation (5.2) gives immediately two symmetries:

$$J_n(\alpha) = J_{-n}(-\alpha) = (-1)^n J_n(-\alpha). \tag{5.3}$$

Another property that follows from the definition is

$$J_n(0) = \delta_{0n}, \tag{5.4}$$

where δ_{0n} is Kronecker's delta, $\delta_{0n} = 1$ if $n = 0$, and vanishes otherwise. The relation (5.2) may also be used to check that the Bessel function satisfies the following recursion relation:

$$2nJ_n(\alpha) = \alpha \left[J_{n+1}(\alpha) + J_{n-1}(\alpha) \right]. \tag{5.5}$$

The recursion relation (5.5) is an important tool in the numerical evaluation, described in subsection 5.2.3. For sums of products of Bessel functions we have

$$\begin{aligned} \sum_{n=-\infty}^{\infty} J_{n+m}(\alpha) J_{n+m'}(\beta) =& \sum_{n=-\infty}^{\infty} \frac{1}{4\pi^2} \int_{-\pi}^{\pi} e^{i[-n(\theta+\theta')-m\theta-m'\theta'+\alpha\sin\theta+\beta\sin\theta']} \mathrm{d}\theta \mathrm{d}\theta' \\ =& \frac{1}{2\pi} \int_{-\pi}^{\pi} e^{i[\theta(m'-m)+(\alpha-\beta)\sin\theta]} \mathrm{d}\theta \\ =& J_{m-m'}(\alpha-\beta), \end{aligned} \tag{5.6}$$

where we have used the identity

$$\frac{1}{2\pi} \sum_n e^{-inx} = \sum_k \delta(2\pi k + x) = \delta(x), \tag{5.7}$$

since we have in this case $|x| < 2\pi$. Eq. (5.6) yields as a particular case

$$\sum_{n=-\infty}^{\infty} \left[J_n(x) \right]^2 = 1. \tag{5.8}$$

Another expression for the Bessel function is through an infinite sum [174],

$$J_n(\alpha) = \left(\frac{\alpha}{2} \right) \sum_{j=0}^{\infty} \frac{(-1)^j \left(\frac{\alpha}{2} \right)^{2j}}{j!(n+j)!}. \tag{5.9}$$

The two representations (5.2) and (5.9) are the only ones we will use, there exists however many more ways [174].

5.2.2 Saddle point approximation and cutoff properties

The integral representation (5.2) can also be used to calculate asymptotic expansions of $J_n(\alpha)$, for large values of n and α, by the saddle point method. In short, the saddle point method works as follows: By Cauchy's integration theorem [145], we can deform the integration path in Eq. (5.2) into the complex plane, without changing the value of the integral. If the path is taken to go through the saddle points (also called stationary points) of the integrand, that is, where the argument of the exponential has vanishing derivative, most of the contribution to the integral will come from an area close to the saddle point. To obtain a first order approximation,

we expand the integrand around the saddle point, and extend the integration limits to infinity, so that the integral can be taken analytically. In general, functions expressed like $F = \int e^{if(x)}\mathrm{d}x$, with large $|f(x)|$, have a sizeable value if there are real stationary points, and are at least exponentially small if the stationary points are imaginary [133]. To find the asymptotics for the Bessel function $J_n(\alpha)$, we first find the stationary point θ_s of the exponential, which satisfies

$$\cos\theta_s = \frac{n}{\alpha}. \tag{5.10}$$

Based on Eq. (5.10), we thus expect that for $|n/\alpha| > 1$, the Bessel function $J_n(\alpha)$ is exponentially small. Written out, the saddle point approximation amounts to, with $f(\theta) = -n\theta + \alpha\sin\theta$,

$$\begin{aligned} J_n(\alpha) &= \mathrm{Re}\,\frac{1}{\pi}\int_0^\pi e^{if(\theta)}\mathrm{d}\theta \approx \mathrm{Re}\,\frac{1}{\pi}\int_C e^{f(\theta_s)+f''(\theta_s)(\theta-\theta_s)^2}\mathrm{d}\theta \\ &\approx \mathrm{Re}\,e^{if(\theta_s)-i\frac{\pi}{4}}\sqrt{\frac{2}{\pi|f''(\theta_s)|}}, \end{aligned} \tag{5.11}$$

where the curve C is a straight line with constant imaginary part passing through the saddle point, and we used $\int_0^\infty \cos t^2\mathrm{d}t = \int_0^\infty \sin t^2\mathrm{d}t = \sqrt{2\pi}/4$. We use formula (5.11) to compute two asymptotics:
$\alpha \gg n$. We assume positive n and α. Here the saddle point is real and tend to $\cos\theta_s = 0$, or $\theta_s = \pi/2$ in the limit $n/\alpha \to 0$. If we take the saddle point with $\sin\theta_s = 1$, we get $f(\theta_s) = -n\pi/2$ and $f''(\theta_s) = -\alpha$, which inserted into Eq. (5.11) gives

$$J_n(\alpha) \approx \sqrt{\frac{2}{\pi\alpha}}\cos\left(\alpha - \frac{n\pi}{2} - \frac{\pi}{4}\right), \qquad \alpha \gg n. \tag{5.12}$$

$n \gg \alpha$. Here $\cos\theta_s = n/\alpha \gg 1$, which means that θ_s is purely imaginary. This time we have to take the saddle point with negative imaginary part, so that $\sin\theta_s = -in/\alpha$, and $\theta_s = -i(\ln 2n - \ln\alpha)$, which together with Eq. (5.11) produces

$$J_n(\alpha) \approx \frac{1}{\sqrt{2\pi n}}\left(\frac{e\alpha}{2n}\right)^n, \qquad n \gg \alpha. \tag{5.13}$$

Thus, we can speak of a "cutoff" at $n = \alpha$, beyond which the amplitude of $J_n(\alpha)$ drops sharply. This cutoff is depicted in Fig. 5.1.

5.2.3 Miller's algorithm for numerical evaluation

As mentioned in the introduction, to be able to use the Bessel functions in actual numerical evaluation, a fast, stable numerical algorithm is necessary. The most widely used algorithm is originally due to Miller [26], and has later been extended and refined by various authors [1, 71, 115, 144]. Another good method of numerical evaluation is direct integration through a path of steepest descent [108]. In this work we use Miller's algorithm, since it is suitable for producing many Bessel functions of the same argument, but of different indices, needed to

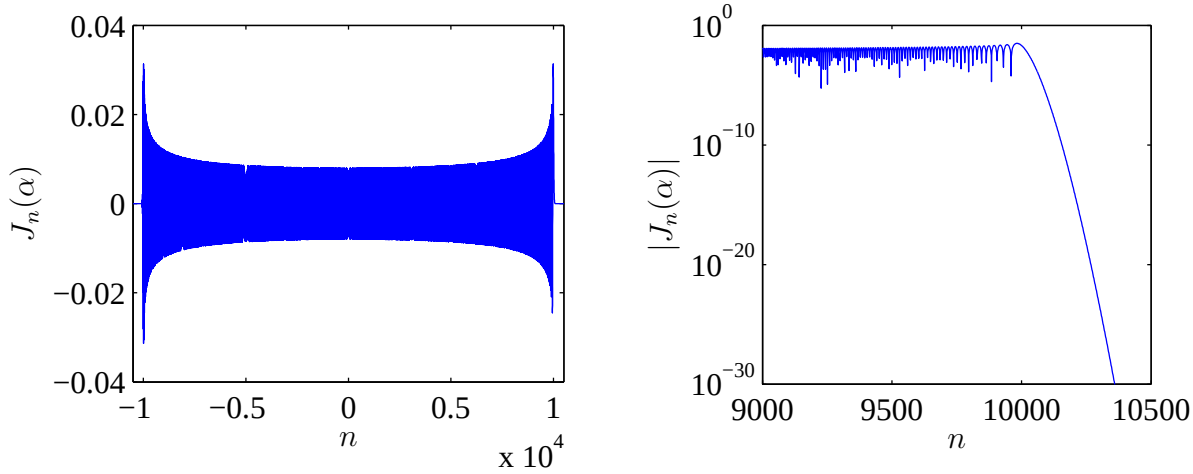

Figure 5.1: The graph to the left shows the Bessel function $J_n(\alpha)$ as a function of n, with $\alpha = 10^4$, the right graph shows the absolute value $|J_n(\alpha)|$ on a logarithmic scale. The cutoff at $n = \alpha$ is clearly visible. In both graphs, the points are connected with blue lines. The rapid oscillations then causes the left plot to look "filled".

calculate the generalized Bessel function. Miller's algorithm is based on the recursion relation Eq. (5.5) and Eq. (5.1), which with $\theta = 0$ can be rewritten as

$$J_0(\alpha) + 2\sum_{n=1}^{\infty} J_n(\alpha) = 1, \tag{5.14}$$

where we used $J_{-n}(\alpha) = (-1)^n J_n(\alpha)$. We consider the case for positive α and n. First we note that we cannot use the recursion relation (5.5) directly in the case of growing n, since besides $J_n(\alpha)$ there is also a second function $Y_n(\alpha)$ satisfying the same recursion relation [174]. This function however, goes as [174]

$$Y_n(\alpha) \approx -\sqrt{\frac{2}{\pi n}} \left(\frac{2n}{e\alpha}\right)^n \tag{5.15}$$

as $n \gg \alpha$, a factorial growth. Thus, when trying to apply the recursion relation (5.5) in the direction of growing n, any round-off error that introduces a little bit of $Y_n(\alpha)$ besides the desired solution $J_n(\alpha)$ will soon dominate completely over the factorially small $J_n(\alpha)$. The solution is now to begin the recursion at some large $n_{\text{start}} > \alpha$, and apply Eq. (5.5) in the direction of decreasing n. In this direction, any erroneous $Y_n(\alpha)$ will disappear exponentially fast. In addition, Miller's observation was that it is possible to start the recursion with arbitrary initial values, say $J_{n_{\text{start}}}(\alpha) = 0$ and $J_{n_{\text{start}}+1}(\alpha) = 1$, compute the array $J_{0,1,\ldots,n_{\text{start}}+1}(\alpha)$ and then normalize the values with the sum $J_0(\alpha) + 2\sum_n J_n(\alpha)$ from Eq. (5.14). Miller's algorithm gives roughly N number of significant figures of accuracy for $J_m(\alpha)$, provided the downward recursion relation is started at an n_{start} satisfying at least $n_{\text{start}} > m + N\sqrt{m}$, with $n_{\text{start}}, m > \alpha$ [144]. For $m < \alpha$, the recursion should be started at $n_{\text{start}} > \alpha + N\sqrt{\alpha}$ to obtain N significant figures (roughly) for $J_m(\alpha)$.

Miller's recursive algorithm is a very efficient algorithm for the numerical calculation of Bessel functions, especially if large arrays $J_{-N,-N+1,\ldots,N-1,N}(\alpha)$ are needed. This is indeed the case when we want to calculate generalized Bessel functions from the definition (5.18), see section 5.3. It should also be mentioned that Miller's algorithm can be coded in a superior way [71], [86, appendix C], to circumvent the problem of overflow on the computer. When starting the backward recursion from a large index n_{start} at arbitrary initial conditions, subsequent values of $J_n(\alpha)$ tend to grow very fast, due to the extremely rapid increase in the region $n > \alpha$, for decreasing n [see Eq. (5.13)].

5.3 Generalized Bessel functions

As can be understood from the name, the generalized Bessel function $A_0(n, \alpha, \beta)$ is a generalization of the usual Bessel function $J_n(\alpha)$, and is a function of one integer index n and two real variables α and β. It was first introduced by Reiss [147] in the context of pair creation by a photon and a laser beam (later for field-induced ionization [148, 150]), and has subsequently been studied by many authors [46–48, 50, 129]. Although the main application area so far has been laser-matter interaction, use of generalized Bessel functions is also made in other fields such as crystallography [137]. The generalized Bessel function has been even further generalized to several indices and more than two variables [45, 49, 94]. On the numerical side, there has been comparatively little work. Apart from the important work of Leubner [101–103], no publications on numerical algorithms for generalized Bessel functions exist. There is so far nothing like the Miller algorithm for $A_0(n, \alpha, \beta)$. In the work leading to this thesis, we have accomplished exactly this: a generalization of Miller's algorithm so that it works also for the generalized Bessel function. This algorithm is presented in subsection 5.3.3.

5.3.1 Basic properties

The generalized Bessel function share many of the properties of the usual Bessel function. Since the generalized Bessel function depends on two variables instead of only one, things are however more complicated. Similarly to the usual Bessel function, we view the generalized Bessel function $A_0(n, \alpha, \beta)$ as the coefficient in the Fourier series expansion of the periodic function $\exp[i\alpha \sin\theta - i\beta \sin(2\theta)]$:

$$e^{i[\alpha \sin\theta - \beta \sin(2\theta)]} = \sum_{n=-\infty}^{\infty} A_0(n, \alpha, \beta) e^{in\theta}, \tag{5.16}$$

which by virtue of Fourier's trick yields the integral representation

$$\begin{aligned} A_0(n, \alpha, \beta) =& \frac{1}{2\pi} \int_{-\pi}^{\pi} e^{-in\phi + i\alpha \sin(\phi) - i\beta \sin(2\phi)} \mathrm{d}\phi \\ =& \frac{1}{\pi} \int_{0}^{\pi} \cos\left[-n\phi + \alpha \sin(\phi) - \beta \sin(2\phi)\right] \mathrm{d}\phi. \end{aligned} \tag{5.17}$$

If we now insert the Fourier expansion (5.1) for each of the exponentials $\exp(i\alpha\sin\theta)$ and $\exp(-i\beta\sin 2\theta)$, the integral over θ collapses the double sum to a single one, so that the generalized Bessel function can be expressed as an infinite sum over products of the usual Bessel function:

$$A_0(n,\alpha,\beta) = \sum_{m=-\infty}^{\infty} J_{n+2m}(\alpha)J_m(\beta). \tag{5.18}$$

Either of Eqs. (5.17) or (5.18) can be taken as the definition of $A_0(n,\alpha,\beta)$. The subscript 0 in $A_0(n,\alpha,\beta)$ has the following meaning: We define

$$\cos^L\theta e^{i[\alpha\sin\theta-\beta\sin(2\theta)]} = \sum_{n=-\infty}^{\infty} A_L(n,\alpha,\beta)e^{in\theta}, \tag{5.19}$$

with $L = 0, 1, 2, \ldots$. From definition (5.19) follows that

$$A_L(n,\alpha,\beta) = \frac{1}{2}\left[A_{L-1}(n-1,\alpha,\beta) + A_{L-1}(n+1,\alpha,\beta)\right], \tag{5.20}$$

with positive integer L. The A_L's are needed in the applications in chapters 3 and 4. Using the sum rule (5.6), we derive the sum rule for $A_0(n,\alpha,\beta)$:

$$\sum_{m=-\infty}^{\infty} A_0(N+m,\alpha_1,\beta_1)A_0(M+m,\alpha_2,\beta_2) = A_0(N-M,\alpha_1-\alpha_2,\beta_1-\beta_2), \tag{5.21}$$

or more generally for $A_L(n,\alpha,\beta)$

$$\sum_{m=-\infty}^{\infty} A_i(m+N,\alpha_1,\beta_1)A_j(m+M,\alpha_2,\beta_2) = A_{i+j}(N-M,\alpha_1-\alpha_2,\beta_1-\beta_2), \tag{5.22}$$

for integer N and M. From partial derivation of the integral representation (5.17) follows the recursion relation

$$\begin{aligned} 2nA_0(n,\alpha,\beta) =& \alpha\left[A_0(n-1,\alpha,\beta) + A_0(n+1,\alpha,\beta)\right] \\ &- 2\beta\left[A_0(n-2,\alpha,\beta) + A_0(n+2,\alpha,\beta)\right], \end{aligned} \tag{5.23}$$

which we found by physical means in section 2.2.4. Note that the relation (5.23) is more complex than that for $J_n(\alpha)$, here every index depends on the four neighboring ones. In general, since the recurrence relation (5.23) is of order four, there are four linearly independent solutions, see Fig. 5.6. Of the four solutions, only the true $A_0(n,\alpha,\beta)$ is normalizable. Still, Eq. (5.23) can be used in a meaningful way for the numerical evaluation of $A_0(n,\alpha,\beta)$, as we will see in subsection 5.3.3.

Evident from the definitions (5.17) and (5.18), the generalized Bessel functions have the following symmetries:

$$\begin{aligned} A_0(n,\alpha,-\beta) &= (-1)^n A_0(-n,\alpha,\beta), \\ A_0(n,-\alpha,\beta) &= (-1)^n A_0(n,\alpha,\beta), \end{aligned} \tag{5.24}$$

from which follows

$$A_0(-n,\alpha,\beta) = A_0(n,-\alpha,-\beta). \tag{5.25}$$

When either of the arguments α or β is zero, the generalized Bessel function $A_0(n,\alpha,\beta)$ simplifies to the usual Bessel function:

$$A_0(n,\alpha,0) = J_n(\alpha), \tag{5.26}$$

and

$$A_0(n,0,\beta) = \begin{cases} J_{\frac{-n}{2}} & n \text{ even}, \\ 0 & n \text{ odd}. \end{cases} \tag{5.27}$$

We conclude this subsection with the Taylor expansion for small arguments and $N \geq 0$, correct to second order:

$$\begin{aligned} A_0(N,\alpha,\beta) =& \delta_{N0} + \frac{\alpha}{2}\delta_{N1} - \frac{\beta}{2}\delta_{N2} + \left(\frac{\alpha}{2}\right)^2\left(\frac{1}{2}\delta_{N2} - \delta_{N0}\right) + \left(\frac{\beta}{2}\right)^2\left(\frac{1}{2}\delta_{N4} - \delta_{N0}\right) \\ &+ \frac{\alpha\beta}{4}\left(\delta_{N1} - \delta_{N3}\right) + \mathcal{O}(\alpha^3,\beta^3,\alpha^2\beta,\beta^2\alpha), \end{aligned} \tag{5.28}$$

which is derived using Eqs. (5.9) and (5.18). Here δ_{ij} is Kronecker's delta function. For negative N we use the symmetry relation (5.25). This means also that

$$\begin{aligned} A_1(N,\alpha,\beta) =& \frac{1}{2}\left(A_0(N-1,\alpha,\beta) + A_0(N+1,\alpha,\beta)\right) \\ =& \frac{1}{2}\Bigg[\delta_{N1} + \frac{\alpha}{2}\delta_{N2} + \frac{\beta}{2}\left(-\delta_{N1} - \delta_{N3}\right) + \left(\frac{\alpha}{2}\right)^2\left(-\frac{1}{2}\delta_{N1} + \frac{1}{2}\delta_{N3}\right) \\ &+ \left(\frac{\beta}{2}\right)^2\left(\frac{1}{2}\delta_{N3} + \frac{1}{2}\delta_{N5} - \delta_{N1}\right) - \frac{\alpha\beta}{4}\delta_{N4}\Bigg] + \mathcal{O}(\alpha^3,\beta^3,\alpha^2\beta,\beta^2\alpha), \end{aligned} \tag{5.29}$$

for $N > 0$. For the case $N = 0$ we have

$$A_1(0,\alpha,\beta) = \frac{\alpha\beta}{4} + \mathcal{O}(\alpha^3,\beta^3). \tag{5.30}$$

Finally, the case with A_2 gives

$$\begin{aligned} A_2(N,\alpha,\beta) =& \frac{1}{2}\left(A_1(N-1,\alpha,\beta) + A_1(N+1,\alpha,\beta)\right) \\ =& \frac{1}{4}\Bigg[\delta_{N2} + \frac{\alpha}{2}\left(2\delta_{N1} + \delta_{N3}\right) + \frac{\beta}{2}\left(-2\delta_{N2} - \delta_{N4}\right) + \left(\frac{\alpha}{2}\right)^2\frac{1}{2}\delta_{N4} \\ &+ \left(\frac{\beta}{2}\right)^2\left(\delta_{N4} + \frac{1}{2}\delta_{N6}\right) - \frac{\alpha\beta}{4}\left(\delta_{N5} + \delta_{N3}\right)\Bigg] + \mathcal{O}(\alpha^3,\beta^3,\alpha^2\beta,\beta^2\alpha), \end{aligned} \tag{5.31}$$

$N > 0$, and

$$A_2(0,\alpha,\beta) = \frac{1}{2} - \frac{\alpha^2}{8} - \frac{\beta^2}{4} + \mathcal{O}(\alpha^3,\beta^3,\alpha^2\beta,\beta^2\alpha). \tag{5.32}$$

5.3.2 Saddle point approximation and cutoff properties

As already mentioned in section 2.2.3, understanding of the cutoff properties of $A_0(n, \alpha, \beta)$ is important for the understanding of physical processes written in terms of generalized Bessel functions, and has also practical significance. A rule is needed for how many terms that should be included in sums for the matrix elements, Eq. (3.26) and Eq. (4.5). In this subsection, without loss of generality, we restrict the discussion to positive arguments α and β in $A_0(n, \alpha, \beta)$. This will cover the general case, by virtue of the symmetries (5.24), and by treating both positive and negative values of n. If either α or β equals 0, the generalized Bessel function $A_0(n, \alpha, \beta)$ can be expressed as the usual Bessel function, see Eqs. (5.26) and (5.27).

For the usual Bessel function $J_n(\alpha)$ we have the well known cutoff at $|n| > |\alpha|$, but for the generalized Bessel function (5.18) the cutoff behavior is more complex. A naïve guess for the cutoff of $A_0(n, \alpha, \beta)$ is $|n| > 2|\alpha| + |\beta|$, since according to the cutoff rule for normal Bessel functions we must have

$$-|\alpha| < 2s + n < |\alpha|, \quad -|\beta| < s < |\beta|, \tag{5.33}$$

to have nonvanishing $J_{2s+n}(\alpha)$ and $J_s(\beta)$, so that

$$A_0(n, \alpha, \beta) \approx \sum_{s=s_{\min}}^{s_{\max}} J_{2s+n}(\alpha) J_s(\beta), \tag{5.34}$$

with

$$s_{\min} = \max\left(-|\beta|, \frac{-|\alpha| - n}{2}\right), \quad s_{\max} = \min\left(|\beta|, \frac{|\alpha| - n}{2}\right). \tag{5.35}$$

For $|n| > 2|\beta| + |\alpha|$ we obtain $s_{\min} > s_{\max}$, and therefore $A_0(n, x, y) \approx 0$. This rule correctly gives an upper limit for the cutoff, and is correct for negative n, but for positive n the cutoff will occur sooner, due to cancellation among the terms in the sum. As a comparison, if we apply the above reasoning to the function

$$B_0(n, x, y) = \sum_s J_{s+n}(x) J_s(y), \tag{5.36}$$

we obtain the cutoff $|n| > |x| + |y|$. However, we know from the addition theorem of Bessel functions [Eq. (5.6)] that $B_0(n, x, y) = J_n(y - x)$, and therefore the correct cutoff law is $|n| > |y - x|$, which is smaller than (or equal to) $|x| + |y|$.

Saddle point treatment

As we have seen in chapter 2.2.3, the correct cutoff law for the generalized Bessel function can be derived from the maximal and minimal classical energies of a laser-dressed electron. Here we derive them from the position of the saddle points in the complex plane of the integrand in Eq. (5.17). As follows from the general treatment of saddle point expansions [133], saddle points found on the real axis give substantial contribution to the integral (5.17), imaginary saddle points give exponentially small contributions. The saddle points θ_s are found from the

requirement that the first derivative with respect to θ of the argument of the exponential in Eq. (5.17) should vanish, θ_s therefore satisfies

$$-n + \alpha \cos\theta_s - 2\beta \cos(2\theta_s) = 0, \tag{5.37}$$

with solutions

$$\cos\theta_s = \frac{\alpha}{8\beta} \pm \sqrt{\frac{\alpha^2}{64\beta^2} + \frac{1}{2} - \frac{n}{4\beta}}\,. \tag{5.38}$$

Inspection of Eq. (5.38) gives two different cases (recall that we assume positive α and β but arbitrary n):

Case 1. $8\beta \geq \alpha$. Here there are four regimes. When $n < -\alpha - 2\beta$, both saddle points are imaginary, and $A_0(n, \alpha, \beta)$ is exponentially small. For $-\alpha - 2\beta < n < -2\beta + \alpha$, one saddle point is imaginary, and one is on the real axis. Here the generalized Bessel function exhibits an oscillatory behavior. In the regime $-2\beta + \alpha < n < 2\beta + \alpha^2/(16\beta)$ there are two real saddle points. Here $A_0(n, \alpha, \beta)$ oscillates, but with larger amplitude than for the previous regime with only one real saddle point since there are two real saddle points contributing. Finally, for $n > 2\beta + \alpha^2/(16\beta)$ both saddle points are again imaginary, and $A_0(n, \alpha, \beta)$ is exponentially small.

Case 2. $8\beta \leq \alpha$. In this case, there are three regimes. As for case 1, when $n < -\alpha - 2\beta$, both saddle points are imaginary. For $-2\beta - \alpha < n < -2\beta + \alpha$ there is one real saddle point contributing, and for $n > -2\beta + \alpha$ both saddle points are imaginary.

When $\alpha = 8\beta$, case 1 and case 2 coincide. The two cases are illustrated by an explicit example in Fig. 5.2. Further numerical examples are shown in Figs. 5.3, 5.4 and 5.5, to get a feeling for the behavior of the generalized Bessel function as a function of the index n and of the arguments α and β. We conclude that a mathematical treatment confirms the physical cutoff law, Eq. (2.49).

Asymptotic formulas

As for the Bessel function $J_n(\alpha)$ in section 5.2.1, we can use the saddle point approximation to obtain asymptotic formulas for the generalized Bessel function, corresponding to the asymptotic limits (5.12) and (5.13) of the usual Bessel function. These formulas are valid far from the turning points, that is, where the saddle point configuration changes character, and are exact in the limit where either of $\alpha, \beta, |n| \to \infty$. In the following formulas [102] we set

$$F(z) = i\left(-nz + \alpha \sin z - \beta \sin(2z)\right), \tag{5.39}$$

and

$$z_\pm = \pm \arccos\left(\frac{\alpha}{8\beta} \pm \sqrt{\frac{\alpha^2}{64\beta^2} + \frac{1}{2} - \frac{n}{4\beta}}\right). \tag{5.40}$$

We have the for the two different cases, using the labeling from Fig. 5.2 (the following asymptotic formulas were first found in [102]):

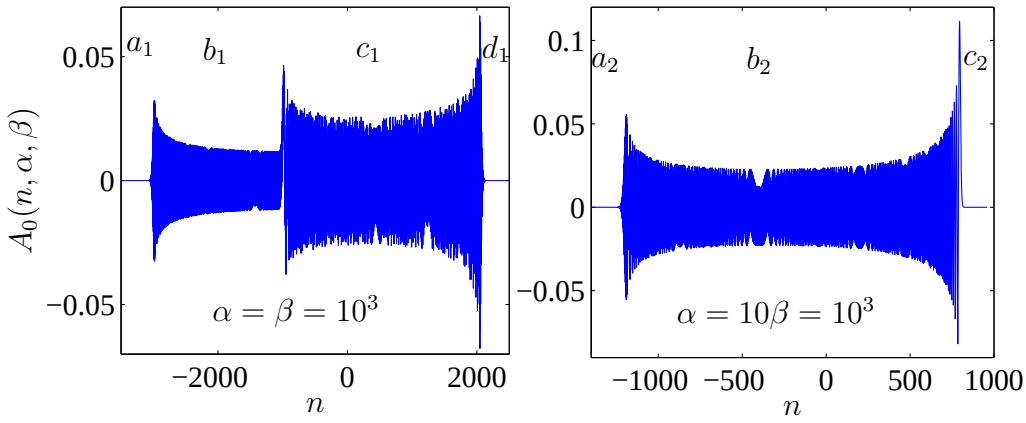

Figure 5.2: Different saddle point contributions to $A_0(n,\alpha,\beta)$. In the left graph, we have $8\beta > \alpha$, with four regions labeled a_1–d_1. We have $n < -2\beta - \alpha = -3 \times 10^3$ in region a_1, $-2\beta - \alpha < n < -2\beta + \alpha = -10^3$ in region b_1, $-2\beta + \alpha < n < 2\beta + \frac{\alpha^2}{16\beta} = 2062.5$ in region c_1, and $n > 2\beta + \frac{\alpha^2}{16\beta}$ in region d_1. In the right graph we have $n < -2\beta - \alpha = -1.2 \times 10^3$ in region a_2, $-2\beta - \alpha < n < -2\beta + \alpha = 800$ in region b_2, and $-2\beta + \alpha < n$ in region c_2. The transition between the different regions are clearly visible, and makes it possible to speak about a "plateau" and "cutoff" of the generalized Bessel function.

Case 1. $8\beta \geq \alpha$.
For $n < -\alpha - 2\beta$, region a_1,

$$\begin{aligned} A_0(n,\alpha,\beta) &\approx \frac{1}{4\sqrt{\pi\beta\sqrt{\frac{\alpha^2}{64\beta^2}+\frac{1}{2}-\frac{n}{4\beta}}}}\left(\frac{\exp\left[\mathrm{Re}F(z_-)\right]}{\sqrt{-\sinh \mathrm{Im}z_-}}+\frac{\exp\left[\mathrm{Re}F(z_+)\right]}{\sqrt{-\sinh \mathrm{Im}z_+}}\right) \\ &\overset{n\ll -2\beta-\alpha}{\approx} \frac{1}{\sqrt{-\pi n}}\left(\frac{\beta e}{-n}\right)^{-\frac{n}{2}} e^{-\frac{\alpha^2}{16\beta}}\cosh\left(\frac{\alpha}{2}\sqrt{\frac{-n}{\beta}}\right), \end{aligned} \tag{5.41}$$

for $-\alpha - 2\beta < n < -2\beta + \alpha$, region b_1,

$$\begin{aligned} A_0(n,\alpha,\beta) &\approx \frac{1}{2\sqrt{\pi\beta\sqrt{\frac{\alpha^2}{64\beta^2}+\frac{1}{2}-\frac{n}{4\beta}}}}\frac{\cos\left[\mathrm{Im}F(z_-)-\frac{\pi}{4}\right]}{\sqrt{\sin z_-}} \\ &\overset{-2\beta-\alpha\ll n\ll -2\beta+\alpha}{\approx} \sqrt{\frac{2}{\pi\alpha}}\cos\left(\alpha-\frac{n\pi}{2}-\frac{\pi}{4}\right), \end{aligned} \tag{5.42}$$

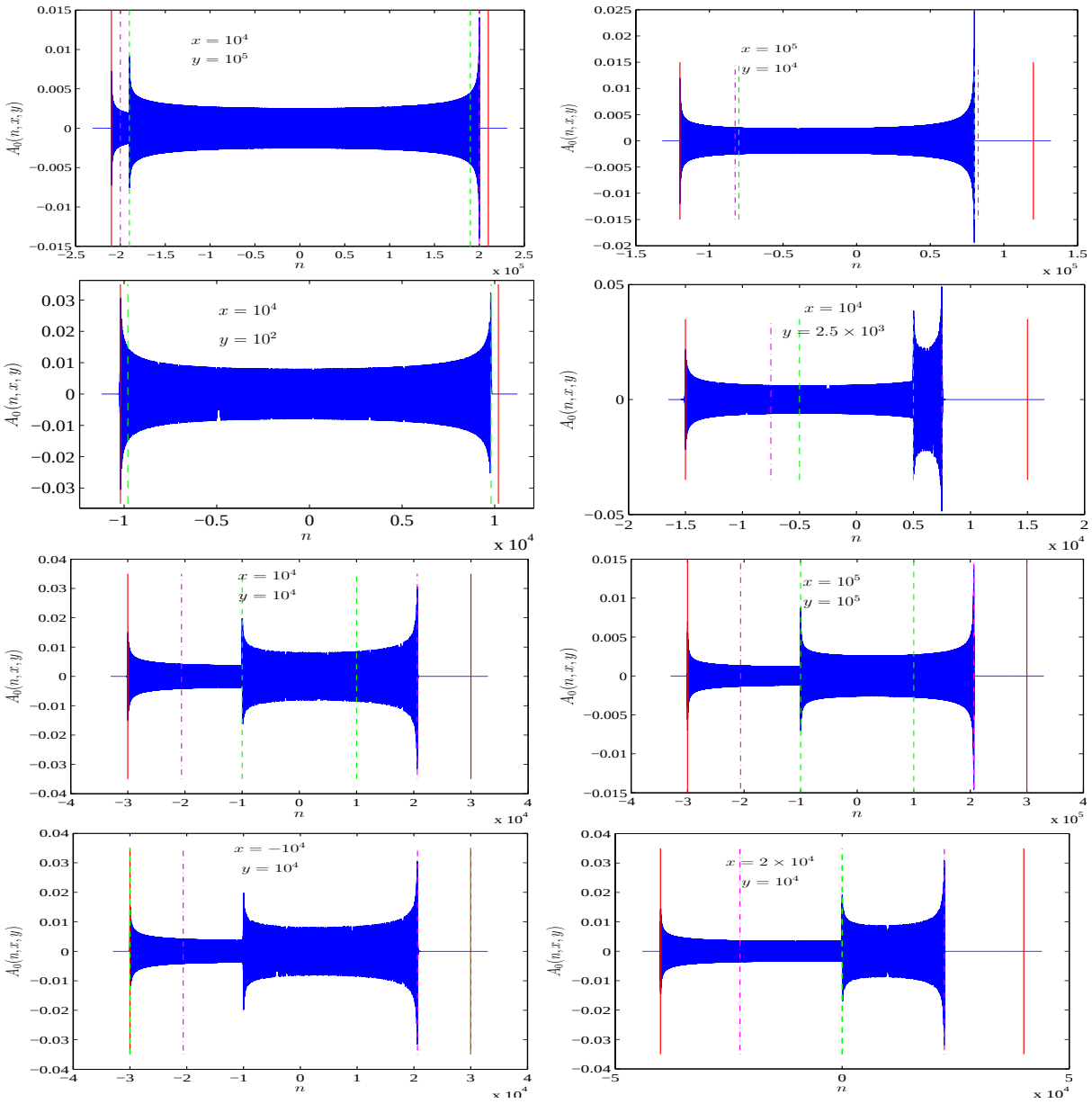

Figure 5.3: Plots of the generalized Bessel function $A_0(n, x, y)$ to illustrate the cutoff rules. In all graphs the solid red line is $n_{\text{red}} = |x| + 2|y|$, the green dashed line is $n_{\text{green}} = |x - 2y|$ and the pink dash-dotted line is $n_{\text{pink}} = (32y^2 + x^2)/(16y)$. The lower left and below middle left are related by the symmetry $A_0(n, -x, y) = (-1)^n A_0(n, x, y)$, and this is also the reason why the first plateau cutoff is not correctly predicted by the green dashed line.

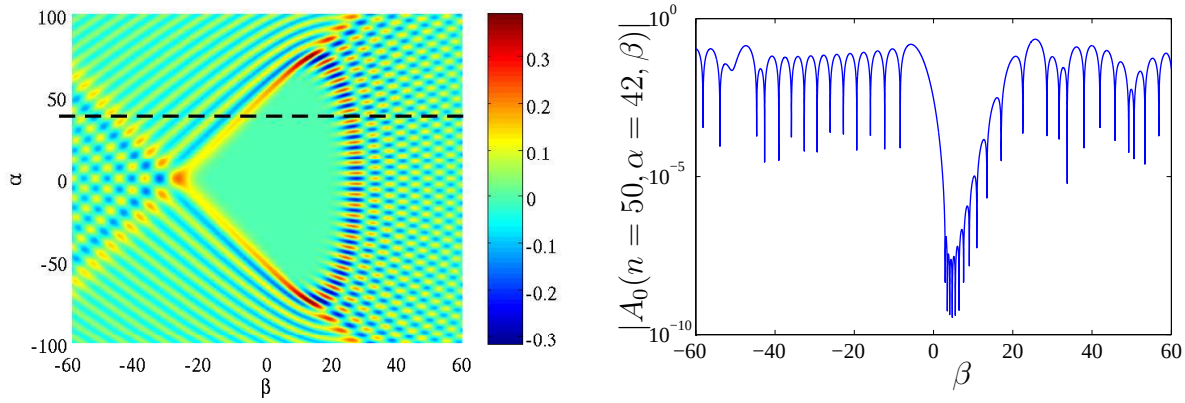

Figure 5.4: Demonstration of the complex behavior of $A_0(n, \alpha, \beta)$ as a function of α and β, for a moderately large value of the index $n = 50$. The left graph shows a two-dimensional graph of the generalized Bessel function $A_0(n = 50, \alpha, \beta)$, with the value indicated by the color coding of the adjacent color bar. Recognizable is the central area where $A_0(n, \alpha, \beta)$ is exponentially small, according to Eqs. (5.41) and (5.44). The right graph shows the cut at $\alpha = 42$, along the dashed line in the left graph. In the right graph, the absolute value $|A_0(n = 50, \alpha = 42, \beta)|$ is displayed as a function of β in logarithmic scale, to display in detail the hole in the center.

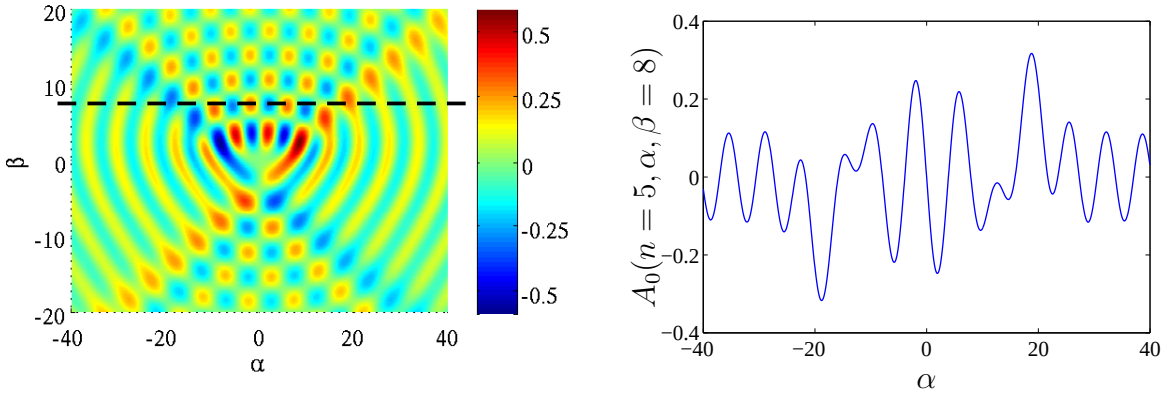

Figure 5.5: Another demonstration of the rich behavior of $A_0(n, \alpha, \beta)$ as a function of α and β, for small index $n = 5$. The left graph pictures a two-dimensional plot of $A_0(n = 5, \alpha, \beta)$, with the function value indicated by the color. To the right is shown $A_0(n = 5, \alpha, \beta = 8)$ as a function of α, as obtained by cutting the left graph along the dashed line ($\beta = 8$).

the same asymptotics as for the usual Bessel function, Eq. (5.12). For $-2\beta+\alpha<n<2\beta+\alpha^2/(16\beta)$, region c_1,

$$\begin{aligned} A_0(n,\alpha,\beta) &\approx \frac{1}{2\sqrt{\pi\beta\sqrt{\frac{\alpha^2}{64\beta^2}+\frac{1}{2}-\frac{n}{4\beta}}}}\left(\frac{\cos\left[\mathrm{Im}F(z_-)-\frac{\pi}{4}\right]}{\sqrt{\sin z_-}}+\frac{\cos\left[\mathrm{Im}F(z_+)+\frac{\pi}{4}\right]}{\sqrt{\sin z_+}}\right) \\ &\overset{-2\beta+\alpha\ll n\ll 2\beta+\frac{\alpha^2}{16\beta}}{\approx} \sqrt{\frac{2}{\pi\beta}}\cos\left(\frac{\alpha}{\sqrt{2}}-\frac{n\pi}{2}\right)\cos\left(\beta-\frac{\pi}{4}-\frac{n\pi}{4}\right), \end{aligned} \tag{5.43}$$

and for $n>2\beta+\alpha^2/(16\beta)$, region d_1,

$$\begin{aligned} A_0(n,\alpha,\beta) &\approx \frac{\exp\left[\mathrm{Re}F(z_-)\right]\cos\left[\mathrm{Im}F(z_-)+\phi_-\right]}{2\sqrt{\pi n\beta\sqrt{\frac{n}{4\beta}-\frac{\alpha^2}{64\beta^2}-\frac{1}{2}}\left[\left(1+\frac{n}{4\beta}-\frac{1}{2}\right)^2-\frac{\alpha^2}{16\beta^2}\right]^{\frac{1}{8}}}} \\ &\overset{n\gg 2\beta+\frac{\alpha^2}{16\beta}}{\approx} \frac{1}{\sqrt{\pi n}}\left(\frac{\beta e}{n}\right)^{\frac{n}{2}} e^{\frac{\alpha^2}{16\beta}}\cos\left(\frac{\pi n}{2}-\frac{\alpha}{2}\sqrt{\frac{n}{\beta}}\right), \end{aligned} \tag{5.44}$$

with

$$\phi_-=\frac{1}{2}\arctan\left(\frac{-\cos(\mathrm{Re}z_-)\sinh(\mathrm{Im}z_-)}{\sin(\mathrm{Re}z_-)\cosh(\mathrm{Im}z_-)}\right). \tag{5.45}$$

Note that the asymptotic formulas (5.41) and (5.44) coincide with the asymptotics (5.13) of the usual Bessel function if $\alpha=0$, and Eq. (5.27) is used. The asymptotics (5.43) coincide with (5.12), with $\alpha=0$ and Eq. (5.27).

Case 2. $8\beta\leq\alpha$.
For $n<-\alpha-2\beta$, region a_2, and $-2\beta-\alpha<n<-2\beta+\alpha$, region b_2, the asymptotic formula is the same as in case 1, region a_1 and b_1. However, in region a_2 we may have very small β, for which formula (5.41) is correct only for very large $|n|>\alpha^2/(16\beta)$. To see that the limit $\beta\to 0$ leads to the asymptotics (5.13) for the normal Bessel function, we note that in region a_2,

$$\cos z_- \overset{\beta\to 0}{\longrightarrow} \frac{n}{\alpha}, \tag{5.46}$$

which together with the first line in Eq. (5.41) leads to the asymptotics (5.13). For $n>-2\beta+\alpha$, region c_2, we have the same asymptotic formula (5.44) as in case 1, region d_1. The first line in Eq. (5.44) has the correct limit for $\beta\to 0$.

We conclude this subsection by remarking that for numerical purposes, it is better to use the full expressions [the first lines of Eqs. (5.41)–(5.44)], since the asymptotic expressions [the second lines of Eqs. (5.41)–(5.44)] are valid only for large values of the parameters, within the specified regions. If α and β are large, the asymptotic expressions are not valid for n close to the turning indices n_t (with turning index is meant the index separating two regions of different saddle point configuration), even though the actual distance $|n_t-n|$ may be large, $|n_t-n|\gg 1$. The full expressions are in general good approximations, provided $|n_t-n|\gg 1$.

5.3.3 Generalized recursive Miller's algorithm for generalized Bessel functions

For many applications in laser-modified QED, in particular for calculation of the cross section (4.12) for laser-assisted pair creation, a large number of generalized Bessel functions $A_0(s,\alpha,\beta)$ of the same arguments α, β but of different indices s, has to be numerically evaluated. The fastest way to do this is to observe that the generalized Bessel functions satisfy the recurrence relation [a rewritten form of Eq. (5.23)]

$$\begin{aligned} 2\beta A_0(s+1,\alpha,\beta) - \alpha A_0(s,\alpha,\beta) + 2(s-1)A_0(s-1,\alpha,\beta) \\ - \alpha A_0(s-2,\alpha,\beta) + 2\beta A_0(s-3,\alpha,\beta) = 0, \end{aligned} \tag{5.47}$$

a five-term (fourth order) recurrence relation, with four linearly independent solutions, of which $A_0(s,\alpha,\beta)$ constitutes only one. This should be compared with the simpler recurrence relation for the usual Bessel function $J_s(\alpha)$:

$$-\alpha J_{s+1}(\alpha) + 2sJ_s(\alpha) - \alpha J_{s-1}(\alpha) = 0, \tag{5.48}$$

which is obtained if you set $\beta = 0$ in equation (5.47). However, contrary to the case with $J_s(\alpha)$, the recurrence relation (5.47) can not be used directly for numerical evaluation, since it is numerically unstable in both directions of s. We illustrate this statement by showing in Fig. 5.6 the character of the four different solutions to the recurrence relation (5.47).

The trick is now to define a new three-term recursion relation which is numerically stable. The price for reducing the five-term recurrence relation is that now also the coefficients have to satisfy another recursion relation. The idea here comes from [135], where a similar technique is used in connection with calculations on gravitational waves. We make a transformation so that the following recursion relation holds:

$$2\beta A_0(s-1,\alpha,\beta) + C_1(s)A_0(s,\alpha,\beta) + C_2(s)A_0(s+1,\alpha,\beta) = 0, \tag{5.49}$$

with

$$\begin{aligned} B_1(s) =& -\alpha - \frac{4\beta^2}{B_3(s+1)}, \\ B_2(s) =& 2(s+1) - \frac{2\beta B_1(s+1)}{B_3(s+1)}, \\ B_3(s) =& -\alpha - \frac{2\beta B_2(s+1)}{B_3(s+1)}, \end{aligned} \tag{5.50}$$

and

$$\begin{aligned} C_1(s) =& B_1(s) - \frac{2\beta B_3(s)}{C_2(s+1)}, \\ C_2(s) =& B_2(s) - \frac{C_1(s+1)B_3(s)}{C_2(s+1)}. \end{aligned} \tag{5.51}$$

These recursion relations are now stable, if the recursion (5.50), (5.51) for the coefficients is performed in the direction of decreasing s, and the recursion (5.49) for the generalized Bessel

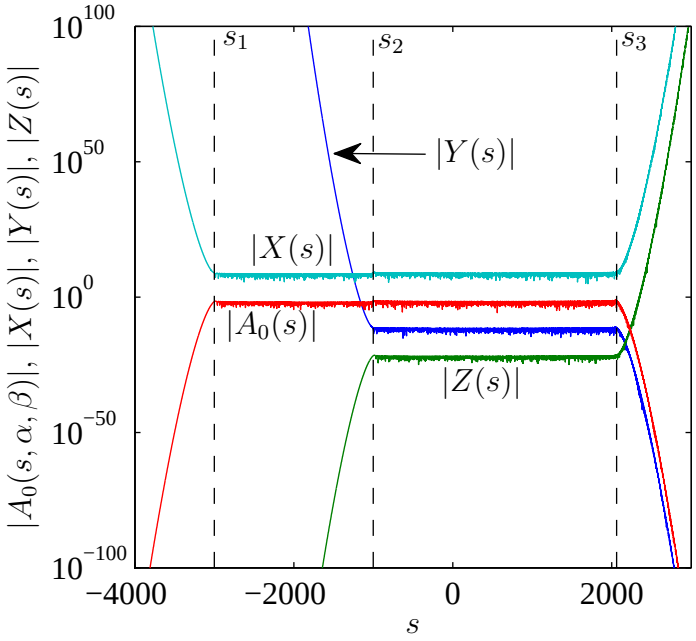

Figure 5.6: The four linearly independent solutions to the recurrence equation (5.47), here called $A_0(s)$ (the true generalized Bessel function $A_0(s,\alpha,\beta)$, the red line), $X(s)$ (light blue line), $Y(s)$ (blue line), and $Z(s)$ (green line). The values $\alpha = \beta = 1000$ were used for the calculation. The dashed lines indicate the turning points $s_1 = -3000$, $s_2 = -1000$, and $s_3 = 2062.5$. Note that the constant prefactors of the solutions $X(s)$, $Y(s)$, and $Z(s)$ are chosen so that the different curves are easily visible on the scale used for this graph, to illustrate the different qualitative behavior. Out of the four solutions, only $A_0(s,\alpha,\beta)$ is normalizable (finite sum $\sum_s |A_0(s,\alpha,\beta)|$). The graph clearly shows why the recurrence equation (5.47) cannot be used directly for numerical evaluation. For example, in the region $s_1 \leq s \leq s_2$, the sought solution $A_0(s)$ neither dominates nor is dominated by the other solutions, we have here $|Y(s)| > |A_0(s)| > |Z(s)|$. This means that recursion in both directions is numerically unstable, since either $Y(s)$ or $Z(s)$ will swamp the calculated solution. The algorithm described in this subsection effectively filters away two solutions, $X(s)$ and $Y(s)$, or $X(s)$ and $Z(s)$ depending on the recurrence direction, so that only two solutions remain. With only two solutions remaining, a variant of Miller's algorithm (see subsection 5.2.3) can be formulated, and allows for fast evaluation of the generalized Bessel function $A_0(s,\alpha,\beta)$.

functions $A_0(s,\alpha,\beta)$ themselves in the other direction, that is, increasing s. In the other direction, we have correspondingly

$$2\beta A_0(s+1,\alpha,\beta)+\tilde{C}_1(s)A_0(s,\alpha,\beta)+\tilde{C}_2(s)A_0(s-1,\alpha,\beta)=0, \tag{5.52}$$

with

$$\begin{aligned}\tilde{B}_1(s) =& -\alpha-\frac{4\beta^2}{\tilde{B}_3(s-1)},\\ \tilde{B}_2(s) =& 2(s-1)-\frac{2\beta\tilde{B}_1(s-1)}{\tilde{B}_3(s-1)},\\ \tilde{B}_3(s) =& -\alpha-\frac{2\beta\tilde{B}_2(s-1)}{\tilde{B}_3(s-1)},\end{aligned} \tag{5.53}$$

and

$$\begin{aligned}\tilde{C}_1(s) =& \tilde{B}_1(s)-\frac{2\beta\tilde{B}_3(s)}{\tilde{C}_2(s-1)},\\ \tilde{C}_2(s) =& \tilde{B}_2(s)-\frac{\tilde{C}_1(s-1)\tilde{B}_3(s)}{\tilde{C}_2(s-1)},\end{aligned} \tag{5.54}$$

where the recurrence (5.53), (5.54) for the coefficients are stable for increasing s and recurrence (5.52) for decreasing s. In addition, numerical experiments show that the both the downward [upward] recursion (5.50), (5.51) [(5.53), (5.54)] for the coefficients and the upward [downward] recursion (5.49) [(5.52)] is exponentially stable, which means that *any* non-vanishing initial condition will do, provided the recursion is started at enough large index s_0. The reason for this remarkable stability can be traced back to the rapid growth of the complementary solution $Z(s)$ (or $Y(s)$, depending on the direction of recurrence) beyond the cutoff index. See Fig. 5.6. There are now two ways of utilizing the stable recurrence formulas for calculation of large arrays of $A_0(s,\alpha,\beta)$, described below.

Calculation of $A_0(s,\alpha,\beta)$ with the recurrence relation and the normalization condition

Together with the normalization condition

$$\sum_{s=-\infty}^{\infty} A_0(s,\alpha,\beta)=1, \tag{5.55}$$

obtained by setting $\theta=0$ in Eq. (5.16), the recurrence relations described above can be used to compute the complete array $A_0(s_{0-}\le s\le s_{0+},\alpha,\beta)$ with s_{0-} (s_{0+}) smaller (bigger) than the corresponding cutoff index [see Eq. (2.49)] by using nothing but the recurrence relations. Remarkably, no initial conditions are needed. In practice, the algorithm proceeds as follows:

Step 1. Fix the starting indices $s_{0+} > s_{\text{pos. cutoff}}$ and $s_{0-} < s_{\text{neg. cutoff}}$. Calculate the four arrays $C_{1,2}(s_{0-} < s < s_{0+})$ [using recurrence relations (5.50), (5.51), starting from $s = s_{0+}$ with arbitrary initial conditions and recurring towards smaller s] and $\tilde{C}_{1,2}(s_{0-} < s < s_{0+})$ [using recurrence relations (5.53), (5.54), starting from $s = s_{0-}$ with arbitrary initial conditions and recurring towards larger s].

Step 2. Calculate the two arrays $K(s_{0-} < s < s_{0+})$ [using recurrence relation (5.49), starting from $s = s_{0-}$ with arbitrary starting values, for example $K(s_{0-}) = 1$, $K(s_{0-} + 1) = 0$, and recurring upwards] and $\tilde{K}(s_{0-} < s < s_{0+})$ [using recurrence relation (5.52), starting from $s = s_{0+}$ with arbitrary starting values, and recurring downwards]. In this step one must be careful against computer overflow and underflow.

Step 3. The arrays K and $\tilde{K}$ are now approximately proportional to the true $A_0(s, \alpha, \beta)$, in the region where they are converged:

$$\begin{aligned} K(s_{\text{neg. cutoff}} \le s \le s_{0+}) &\propto A_0(s_{\text{neg. cutoff}} \le s \le s_{0+}, \alpha, \beta), \\ \tilde{K}(s_{0-} \le s \le s_{\text{pos. cutoff}}) &\propto A_0(s_{0-} \le s \le s_{\text{pos. cutoff}}, \alpha, \beta). \end{aligned} \tag{5.56}$$

We now normalize K and $\tilde{K}$ with respect to each other at $s = 0$ (or any other suitable index, if $\tilde{K}(0)$ happens to be very small):

$$L(s_{0-} < s < s_{0+}) = \tilde{K}(s_{0-} < s < s_{0+}) K(0)/\tilde{K}(0). \tag{5.57}$$

Then merge the two arrays K and L into one array M,

$$M(s_{0-} < s < s_{0+}) = \begin{cases} L(s) & \text{if } s_{0-} \le s \le 0, \\ K(s) & \text{if } 1 \le s \le s_{0+}. \end{cases} \tag{5.58}$$

Step 4. Finally, the approximation to the true generalized Bessel function is given by normalizing M with the condition (5.55):

$$A_0(s_{0-} \le s \le s_{0+}, \alpha, \beta) \approx \frac{M(s_{0-} \le s \le s_{0+})}{\sum_{s=s_{0-}}^{s_{0+}} M(s)}. \tag{5.59}$$

Figure 5.7 illustrates the accuracy that is obtained by employing the algorithm described above. For this purpose, we let $\tilde{A}_0(s_{\text{neg. cutoff}} \le s \le s_{\text{pos. cutoff}}, \alpha, \beta)$ be the values obtained by the generalized recursive Miller's algorithm, starting at indices

$$s_{0+} = s_{\text{pos. cutoff}} + \Delta s, \qquad s_{0-} = s_{\text{neg. cutoff}} - \Delta s, \tag{5.60}$$

(see **Step 1.** above), and $A_0(s_{\text{neg. cutoff}} \le s \le s_{\text{pos. cutoff}}, \alpha, \beta)$ be the true value of the generalized Bessel function. We then define the average relative error $\overline{\varepsilon}_{\text{rel}}$ as

$$\overline{\varepsilon}_{\text{rel}} = \frac{\sum_{s=s_{\text{neg. cutoff}}}^{s_{\text{pos. cutoff}}} \left| \frac{\tilde{A}_0(s,\alpha,\beta) - A_0(s,\alpha,\beta)}{A_0(s,\alpha,\beta)} \right|}{s_{\text{pos. cutoff}} - s_{\text{neg. cutoff}}}. \tag{5.61}$$

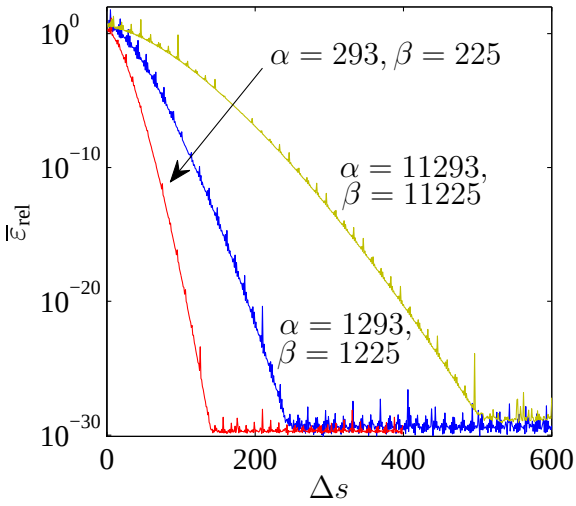

Figure 5.7: This graph displays the average relative error $\overline{\varepsilon}_{\text{rel}}$, defined in Eq. (5.61), of the calculated generalized Bessel function $\tilde{A}_0(s, \alpha, \beta)$, as a function of the starting index difference Δs, defined in Eq. (5.60). We see that up to 25 significant figures can easily be obtained. At a certain value $\approx 10^{-30}$, the obtainable accuracy is limited by the machine precision, in this case quadruple precision arithmetic was used (roughly 32 decimals accuracy).

The reference value, the "true" value $A_0(s, \alpha, \beta)$, is calculated by the same algorithm, but with a sufficiently large Δs so that highest obtainable precision is reached.

Calculation of $A_0(s, \alpha, \beta)$ with the recurrence relation and initial values

An alternative way to utilize the stable recurrence relations requires two initial values, say $A_0(0, \alpha, \beta)$ and $A_0(1, \alpha, \beta)$. These values have to be calculated in some independent way, either by the definition (5.18) and Miller's algorithm for the usual Bessel function as described in 5.2.3, or by a suitable asymptotic expansion, see section 5.3.2 and [102]. Below, we describe the algorithm for positive indices s, the case for negative s is completely analogous.

Step 1. Fix the starting index $s_{0+} > s_{\text{pos. cutoff}}$. Calculate the two arrays $C_{1,2}(1 < s < s_{0+})$ [using recurrence relations (5.50), (5.51), starting from $s = s_{0+}$ with arbitrary initial conditions and recurring towards smaller s].

Step 2. Use the recurrence relation (5.49) in the direction of growing s, starting from the initial values $A_0(0, \alpha, \beta)$, $A_0(1, \alpha, \beta)$ and calculate in a stable way the whole array $A_0(0 \leq s \leq s_{0+}, \alpha, \beta)$.

This way of using the recurrence relation demands fewer recurrence runs, to the price of having to calculate the initial conditions by some independent way. We have numerically tested that essentially no significant figures get lost in the recursion step, so the accuracy of this method is limited by the precision of the initial values $A_0(0,\alpha,\beta)$ and $A_0(1,\alpha,\beta)$. We estimated numerically the minimum value of $N_{\text{min}} = s_0 - s_{\text{pos. cutoff}}$, the difference between the cutoff index and the starting index, that is required to reach the same precision for all values $A_0(2 \leq s \leq s_{0+},\alpha,\beta)$ as the initial values $A_0(0,\alpha,\beta)$, $A_0(1,\alpha,\beta)$, and found $N_{\text{min}} \approx \Xi\,(s_{\text{pos. cutoff}})^{0.3}$. Here Ξ is a constant depending on α and β of order $\mathcal{O}(10)$. As a numerical example, take $\alpha = 10^3 = \beta$, so that $s_{\text{pos. cutoff}} \approx 2.06 \times 10^3$. Then $N_{\text{min}} \approx 100$, which is one order of magnitude smaller than the cutoff index $s_{\text{pos. cutoff}}$. The fast convergence is due to the rapid falloff of the generalized Bessel function (and rapid growth of the complementary solution) beyond the cutoff index.

5.3.4 Explanation of the stability of the generalized recursive Miller's algorithm

Why the algorithm described in subsection 5.3.3 works is explained by the theory in [132,175]. The key observation is that solving the recurrence system (5.47) for $A_{a+2<s\leq b-2}$, with a, b being some integers, and with the boundary values $A_{a+1}, A_{a+2}, A_{b-1}, A_b$ assumed to be known (in the rest of this discussion we suppress the dependence on α and β and write A_s for $A_0(s,\alpha,\beta)$ for increased readability), is equivalent to solving the matrix equation

$$\boldsymbol{P}\boldsymbol{Y} = \boldsymbol{\rho}, \tag{5.62}$$

where

$$\boldsymbol{P} = \begin{pmatrix} 2(a+3) & -\alpha & 2\beta & 0 & \dots & & & \\ -\alpha & 2(a+4) & -\alpha & 2\beta & 0 & \dots & & \\ 2\beta & -\alpha & 2(a+5) & -\alpha & 2\beta & 0 & \dots & \\ 0 & 2\beta & -\alpha & 2(a+6) & -\alpha & 2\beta & 0 & \dots \\ 0 & 0 & \ddots & \ddots & \ddots & \ddots & \ddots & 0 \\ \dots & 0 & 2\beta & -\alpha & 2(b-5) & -\alpha & 2\beta & 0 \\ & \dots & 0 & 2\beta & -\alpha & 2(b-4) & -\alpha & 2\beta \\ & & \dots & 0 & 2\beta & -\alpha & 2(b-3) & -\alpha \\ & & & \dots & 0 & 2\beta & -\alpha & 2(b-2) \end{pmatrix}, \tag{5.63}$$

$$\boldsymbol{Y} = \begin{pmatrix} A_{a+3} \\ A_{a+4} \\ \vdots \\ A_{b-3} \\ A_{b-2} \end{pmatrix}, \tag{5.64}$$

and

$$\boldsymbol{\rho} = -\begin{pmatrix} 2\beta A_{a+1} - \alpha A_{a+2} \\ 2\beta A_{a+2} \\ 0 \\ \vdots \\ 0 \\ 2\beta A_{b-1} \\ 2\beta A_b - \alpha A_{b-1} \end{pmatrix}. \tag{5.65}$$

We see that the vector $\boldsymbol{\rho}$ carries the boundary condition information. Now, one can show [132] that the generalized Miller's algorithm described in section 5.3.3 is equivalent to solving the matrix equation (5.62) by factorizing the matrix $\boldsymbol{P}$ into $\boldsymbol{P} = \boldsymbol{LU}$, with

$$\boldsymbol{L} = \begin{pmatrix} L^2_{a+1} & 0 & \dots & & & & \\ L^3_{a+2} & L^2_{a+2} & 0 & \dots & & & \\ L^4_{a+3} & L^3_{a+3} & L^2_{a+3} & 0 & \dots & & \\ 0 & L^4_{a+4} & L^3_{a+4} & L^2_{a+4} & 0 & \dots & \\ 0 & 0 & \ddots & \ddots & \ddots & 0 & \dots \\ & \dots & 0 & L^4_{b-5} & L^3_{b-5} & L^2_{b-5} & 0 \\ & & \dots & 0 & L^4_{b-4} & L^3_{b-4} & L^2_{b-4} \end{pmatrix}, \tag{5.66}$$

and

$$\boldsymbol{U} = \begin{pmatrix} U^2_{a+1} & U^1_{a+1} & U^0_{a+1} & 0 & \dots & & \\ 0 & U^2_{a+1} & U^1_{a+1} & U^0_{a+1} & 0 & \dots & \\ 0 & 0 & \ddots & \ddots & \ddots & 0 & \dots \\ & \dots & 0 & U^2_{b-7} & U^1_{b-7} & U^0_{b-7} & 0 \\ & & \dots & 0 & U^2_{b-6} & U^1_{b-6} & U^0_{b-6} \\ & & & \dots & 0 & U^2_{b-5} & U^1_{b-5} \\ & & & & \dots & 0 & U^2_{b-4} \end{pmatrix}, \tag{5.67}$$

and back-substituting using the intermediate vector

$$\boldsymbol{\zeta} = \begin{pmatrix} \zeta_{a+3} \\ \vdots \\ \zeta_{b-2} \end{pmatrix}, \tag{5.68}$$

satisfying

$$\boldsymbol{L\zeta} = \boldsymbol{\rho}, \tag{5.69}$$

$$\boldsymbol{UY} = \boldsymbol{\zeta}, \tag{5.70}$$

so that $\boldsymbol{PY} = \boldsymbol{LUY} = \boldsymbol{\rho}$. Solving the matrix equation (5.70) is in turn equivalent to solving the recurrence relation

$$U^2_s A_{s+2} + U^1_s A_{s+3} + U^0_s A_{s+4} = 0, \qquad s \geq a+1, \tag{5.71}$$

with boundary conditions contained in $\boldsymbol{\zeta}$. The recursion relation (5.71) is now of second order. Thus, instead of solving the fourth-order recurrence relation (5.47), it is sufficient to solve the

second-order system (5.71). It can be shown [132] that the two solutions to the second-order recurrence relation (5.71) [corresponding to Eqs. (5.49) and (5.52)] are precisely the sought $A_0(s,\alpha,\beta)$ and another function $y(s,\alpha,\beta)$ which falls off much faster as a function of s compared to $A_0(s,\alpha,\beta)$ [for example, for forward recursion $A_0(s,\alpha,\beta)/y(s,\alpha,\beta) \overset{s\to\infty}{\longrightarrow} 0$], so that a variant of Miller's algorithm, without initial values, can be used. Our algorithm can be said to separate the recursion relation, so that the exponentially growing solutions are factorized out, leaving the generalized Bessel function $A_0(s,\alpha,\beta)$ as the dominant solution.

5.3.5 The function S_n

Important for the applications of the generalized Bessel functions, in particular in chapter 4, is the function S_n, a function of 5 variables and one integer index, defined through a sum over products of generalized Bessel functions,

$$S_n(C,\alpha,\beta,\tilde{\alpha},\tilde{\beta}) \equiv \sum_{s=-\infty}^{\infty} \frac{A_0(s,\alpha,\beta)A_0(s-n,\tilde{\alpha},\tilde{\beta})}{s+C}, \tag{5.72}$$

where C is non-integer. Convergence of the sum (5.72) is guaranteed by the fast asymptotic falloff beyond the cutoff index of the generalized Bessel functions. It is this function that is responsible for the intermediate propagator sum in the matrix element (4.5).

Expansion for large C

If $|C| > |\alpha|, |\beta|$, then by using the expansion

$$\frac{1}{s+C} = \frac{1}{C} - \frac{s}{C^2} + \frac{s^2}{C^3} + \ldots, \tag{5.73}$$

we can obtain an expansion of the function S_n around the simpler generalized Bessel function $A_0(n,\delta,\gamma)$, where $\delta = \alpha - \tilde{\alpha}$ and $\gamma = \beta - \tilde{\beta}$. We have

$$S_n = \frac{A_0(n,\delta,\gamma)}{C} + \frac{W_2(n,\delta,\gamma)}{C^2} + \frac{W_3(n,\delta,\gamma)}{C^3} + \frac{W_4(n,\delta,\gamma)}{C^4} + \ldots, \tag{5.74}$$

where

$$W_2(n,\delta,\gamma) = -\frac{\alpha}{2}\left[A_0(n-1,\delta,\gamma) + A_0(n+1,\delta,\gamma)\right] + \beta\left[A_0(n-2,\delta,\gamma) + A_0(n+2,\delta,\gamma)\right], \tag{5.75}$$

and the more involved third and fourth order corrections read

$$\begin{aligned} W_3(n,\delta,\gamma) =& \frac{\alpha^2}{4}\big(2A_0(n,\delta,\gamma) + A_0(n+2,\delta,\gamma) + A_0(n-2,\delta,\gamma)\big) \\ &- \beta\alpha\big(A_0(n-1,\delta,\gamma) + A_0(n+1,\delta,\gamma) + A_0(n+3,\delta,\gamma) + A_0(n-3,\delta,\gamma)\big) \\ &+ \beta^2\big(2A_0(n,\delta,\gamma) + A_0(n+4,\delta,\gamma) + A_0(n-4,\delta,\gamma)\big), \end{aligned} \tag{5.76}$$

and

$$\begin{aligned}W_4(n,\delta,\gamma) = &-\frac{\alpha^3}{8}\big(3A_0(n+1,\delta,\gamma)+3A_0(n-1,\delta,\gamma)+A_0(n+3,\delta,\gamma)+A_0(n-3,\delta,\gamma)\big)\\ &+\frac{3\alpha^2\beta}{4}\big(3A_0(n,\delta,\gamma)+3A_0(n+2,\delta,\gamma)+3A_0(n-2,\delta,\gamma)\\ &\qquad +A_0(n+4,\delta,\gamma)+A_0(n-4,\delta,\gamma)\big)\\ &-\frac{3\alpha\beta^2}{2}\big(3A_0(n+1,\delta,\gamma)+3A_0(n-1,\delta,\gamma)+A_0(n-3,\delta,\gamma)\\ &\qquad +A_0(n+3,\delta,\gamma)+A_0(n-5,\delta,\gamma)+A_0(n+5,\delta,\gamma)\big)\\ &+\beta^3\big(3A_0(n-2,\delta,\gamma)+3A_0(n+2,\delta,\gamma)+A_0(n+6,\delta,\gamma)+A_0(n-6,\delta,\gamma)\big).\end{aligned} \tag{5.77}$$

From the expansion (5.74), it is clear that if C is larger than both of the cutoff indices for $A_0(s,\alpha,\beta)$ and $A_0(s-n,\tilde{\alpha},\tilde{\beta})$, the cutoff behavior of the function $S_n(C,\alpha,\beta,\tilde{\alpha},\tilde{\beta})$ is equivalent to that of the generalized Bessel function $A_0(n,\alpha-\tilde{\alpha},\beta-\tilde{\beta})$, which is easy to analyze. The transition from C smaller than the cutoff index to C larger than the cutoff index is shown in Fig. 5.8.

Relation between different indices

We also state some useful relations between S_n and sums of products of generalized Bessel functions $A_K(n,\alpha,\beta)$ of different indices K. First, recall the definition

$$A_K(s,\alpha,\beta) = \frac{1}{2}\big(A_{K-1}(s-1,\alpha,\beta)+A_{K-1}(s+1,\alpha,\beta)\big), \tag{5.78}$$

where K is a positive integer. We have (supressing the dependence on $\alpha,\beta,\tilde{\alpha},\tilde{\beta}$)

$$\sum_s \frac{A_0(s,\alpha,\beta)A_1(s-n,\tilde{\alpha},\tilde{\beta})}{s+C} = \frac{1}{2}\big[S_{n+1}(C)+S_{n-1}(C)\big], \tag{5.79}$$

$$\sum_s \frac{A_1(s,\alpha,\beta)A_0(s-n,\tilde{\alpha},\tilde{\beta})}{s+C} = \frac{1}{2}\big[S_{n+1}(C-1)+S_{n-1}(C+1)\big], \tag{5.80}$$

$$\begin{aligned}\sum_s \frac{A_1(s,\alpha,\beta)A_1(s-n,\tilde{\alpha},\tilde{\beta})}{s+C} = \frac{1}{4}\big[&S_n(C+1)+S_{n-2}(C+1)\\ &+S_{n+2}(C-1)+S_n(C-1)\big],\end{aligned} \tag{5.81}$$

$$\sum_s \frac{A_0(s,\alpha,\beta)A_2(s-n,\tilde{\alpha},\tilde{\beta})}{s+C} = \frac{1}{4}\big[2S_n(C)+S_{n-2}(C)+S_{n+2}(C)\big], \tag{5.82}$$

$$\begin{aligned}\sum_s \frac{A_2(s,\alpha,\beta)A_0(s-n,\tilde{\alpha},\tilde{\beta})}{s+C} = \frac{1}{4}\big[&S_n(C-1)+S_{n+2}(C-1)\\ &+S_{n-2}(C+1)+S_n(C+1)\big],\end{aligned} \tag{5.83}$$

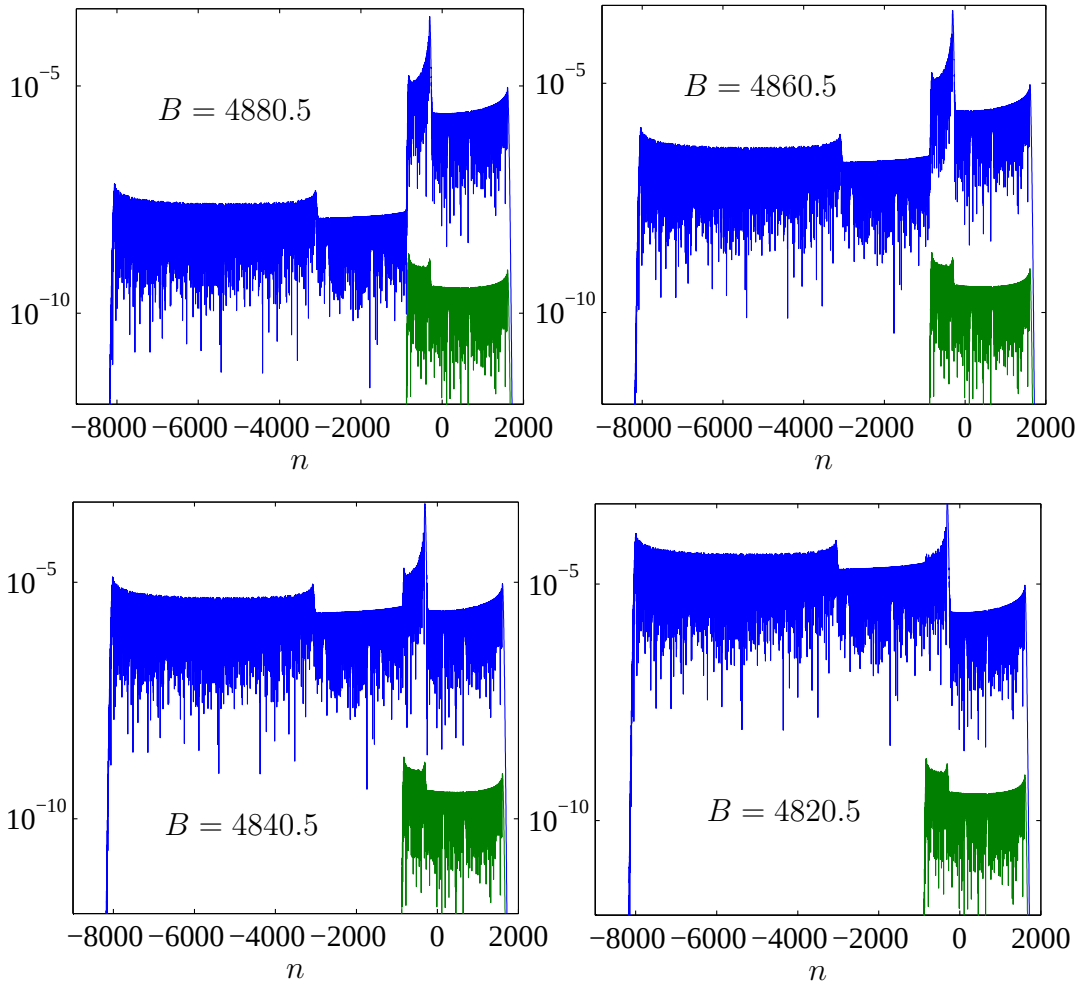

Figure 5.8: Cut-off properties of the function $S_n(B, \alpha, \beta, \tilde{\alpha}, \tilde{\beta})$ [for definition, see Eq. (5.72)], for different values of B. In all graphs $\alpha = 2300$, $\beta = 1230$, $\tilde{\alpha} = 1340$ and $\tilde{\beta} = 1560$. The blue line shows the function $S_n(B, \alpha, \beta, \tilde{\alpha}, \tilde{\beta})$, the green line shows for comparison the function $\frac{A_0(n,\alpha-\tilde{\alpha},\beta-\tilde{\beta})}{B}$, multiplied with a factor 10^{-4} for clarity. Visible is the multiple plateau structure of the function $S_n(B, \alpha, \beta, \tilde{\alpha}, \tilde{\beta})$. For values of $B \gtrsim 4860$ the cutoff occurs in practice at the same value for n as for $A_0(n, \alpha - \tilde{\alpha}, \beta - \tilde{\beta})$, which has the cut-off values [see equation (2.49) on page 27] $n = |\alpha - \tilde{\alpha}| + 2|\beta - \tilde{\beta}| = 1620$ and $n = \frac{|\alpha-\tilde{\alpha}|^2+32|\beta-\tilde{\beta}|^2}{16(\beta-\tilde{\beta})} \approx -835$.

$$\sum_s \frac{A_1(s,\alpha,\beta)A_2(s-n,\tilde{\alpha},\tilde{\beta})}{s+C} = \frac{1}{8}\big[S_{n+1}(C+1)+2S_{n-1}(C+1)+S_{n-3}(C+1) + S_{n-1}(C-1)+2S_{n+1}(C-1)+S_{n+3}(C-1)\big], \tag{5.84}$$

$$\sum_s \frac{A_2(s,\alpha,\beta)A_1(s-n,\tilde{\alpha},\tilde{\beta})}{s+C} = \frac{1}{8}\big[S_{n-1}(C+2)+S_{n-3}(C+2)+2S_{n+1}(C) + 2S_{n-1}(C)+S_{n+3}(C-2)+S_{n+1}(C-2)\big], \tag{5.85}$$

and finally

$$\sum_s \frac{A_2(s,\alpha,\beta)A_2(s-n,\tilde{\alpha},\tilde{\beta})}{s+C} = \frac{1}{16}\big[4S_n(C)+2S_{n-2}(C)+2S_{n+2}(C)+2S_{n+2}(C-2) + S_n(C-2)+S_{n+4}(C-2)+2S_{n-2}(C+2) + S_n(C+2)+S_{n-4}(C+2)\big]. \tag{5.86}$$

Also needed is

$$\sum_s \frac{sA_0(s,\alpha,\beta)A_0(s-n,\tilde{\alpha},\tilde{\beta})}{s+C} = \frac{\alpha}{2}\big[S_{n-1}(C+1)+S_{n+1}(C-1)\big] - \beta\big[S_{n-2}(C+2)+S_{n+2}(C+2)\big], \tag{5.87}$$

$$\sum_s \frac{sA_0(s,\alpha,\beta)A_1(s-n,\tilde{\alpha},\tilde{\beta})}{s+C} = \frac{\alpha}{4}\big[S_n(C+1)+S_{n+2}(C-1)+S_{n-2}(C+1) + S_n(C-1)\big] - \frac{\beta}{2}\big[S_{n-1}(C+2)+S_{n+3}(C-2) + S_{n-3}(C+2)+S_{n+1}(C-2)\big], \tag{5.88}$$

obtained using the recursion relations (5.23). Another useful symmetry is

$$S_n(C-n,\alpha,\beta,\tilde{\alpha},\tilde{\beta}) = S_{-n}(C,\tilde{\alpha},\tilde{\beta},\alpha,\beta). \tag{5.89}$$

Chapter 6

Conclusions and outlook

6.1 General conclusions and summary of obtained results

The aim of this thesis was to advance the understanding of second-order laser-modified QED processes. This goal has been achieved, resulting in particular in a thorough investigation of the following processes: laser-assisted bremsstrahlung and laser-assisted/laser-induced pair creation. Apart from theoretical results, special emphasis was put on the actual numerical evaluation of the formulas involved. The main results of this thesis are the numerical values produced from the formulas of laser-modified QED, presented in a number of plots in chapters 3 and 4.

After an introduction to the subject of QED in strong laser fields in chapter 1, in chapter 2, we reviewed the solution of the problem of the motion of an electron in an electromagnetic plane wave in two ways, both classically and quantum mechanically. By integrating the relativistic, classical equations of motion and the Dirac equation, we saw that this system allows for an analytic solution. Moreover, we recognized the strong quantum-classical correspondence of the classical solution and the quantum Volkov solution. In particular, the probability for a quantum electron in a laser wave to occupy instantaneous energy levels with energies larger (or smaller) than the classically allowed values is exponentially small. This correspondence also provided an intuitive, physical explanation for the cutoff behavior of the generalized Bessel functions, the special functions that appear as coefficients in the plane wave Fourier expansion of the Volkov wave function.

An expression for the Dirac-Volkov propagator was also presented, suitable for application to calculation of differential cross sections for higher-order laser-dressed QED processes. In the appendix section B.1, we demonstrated the completeness property of Volkov states.

In chapter 3 we described in detail the evaluation of the cross section for laser-assisted bremsstrahlung. While the analytic expression for the cross section was known previously, no concrete numerical evaluation had been performed. This step is achieved in this thesis. Furthermore, we showed how to properly regularize the Green's function singularities by adding an imaginary part to the laser-dressed electron's mass and energy. These singularities arise due to the possibility of the second-order bremsstrahlung process to split up into two first order processes, laser-induced Compton scattering and laser-assisted Coulomb scattering. There are other ways

of regularizing these singularities, but the discussion in section 3.4.2 showed that the method employed in this thesis gives the dominant contribution in the limit of long laser pulses. Analogous to the lifetime of a discrete energy state, the lowest order imaginary correction to the electron's mass can be calculated as the total rate of one-photon decay of a Volkov state. Employing the mentioned way of regularizing the Green's function singularities, we performed a number of calculations of the laser-assisted bremsstrahlung cross section for different values of the intensity parameter ξ and directions of the emitted bremsstrahlung photon. Considering a head-on collision of an electron and a laser beam, a large number of resonant peaks was found, mainly when the photon is emitted in almost the same direction as the incoming electron. In section 3.5.4 we showed that quite surprisingly, the full, laser-dressed Dirac-Volkov propagator cannot be well approximated by the free electron propagator, even if the bremsstrahlung photon energy ω_b is much larger than the laser energy ω. Both direct numerical calculations were performed and an intuitive picture was found to support this claim.

As a second project, we have applied the formalism described in chapter 2 to the process of laser-modified pair creation by a gamma photon and a nuclear Coulomb field, with the results presented in chapter 4. The formal expression for the matrix element is related to that of laser-assisted bremsstrahlung by a crossing symmetry, however, the characteristics and qualitative behavior as well as the numerical evaluation of this process are rather different compared to the laser-assisted bremsstrahlung case. Here we investigated the influence of a subcritical (with respect to Schwinger's critical field) laser field on the process of pair creation. That the field is subcritical means that the laser itself cannot create any pairs, so that the total cross section stays almost unchanged. This assertion was shown both by theoretical arguments and by explicit numerical evaluation of the laser-dressed cross section, which required sixfold numerical integration. Differential cross sections were calculated for two configurations of laser field and gamma photon: the collinear case, where the photon and the laser beam propagate in the same direction, and the counter propagating case where the gamma photon and the laser beam are set up to collide head on. The latter case with counter propagating gamma photon and laser field is the most interesting from a theoretical point of view, while the first case with collinear gamma photon and laser may be most useful for applications. In particular, we found that in the collinear case, both the gamma photon and the laser work together to strongly focus the created pairs. The pairs are created by the highly energetic gamma photon and then accelerated by the laser field to emerge outside the laser field at a characteristic angle $\theta \approx 1/\xi$. This setup may thus provide a realizable way of measuring nonlinear laser effects related to electron-positron pair production.

A necessary ingredient in our approach to laser-modified QED by Fourier expansion of the wave functions and propagators was the generalized Bessel function $A_0(n, \alpha, \beta)$, a special function occurring naturally in problems where the laser is linearly polarized. In chapter 5 we gave a thorough review of the properties of generalized Bessel functions, together with references to literature perhaps not so widely read by physicists. We also found an important new result: a stable recursive algorithm for evaluation of generalized Bessel functions. This kind of algorithm, usually referred to as Miller's algorithm, is the standard way of evaluating the usual Bessel function $J_n(\alpha)$ based on the second-order recurrence relation satisfied by $J_n(\alpha)$. However, for $A_0(n, \alpha, \beta)$ such an algorithm was not previously known, due to the more complex behavior of the fourth-order recurrence relation satisfied by the generalized Bessel function.

This algorithm was crucial for the evaluation of the cross section for laser-dressed pair creation in the counter propagating configuration in section 4.3.

In conclusion, we have shown that it is possible to numerically evaluate second-order laser-assisted QED cross sections in the relativistic domain, using the Dirac-Volkov propagator.

6.2 Outlook

In chapter 3 we described the calculation of the cross section for laser-assisted bremsstrahlung in the resonance region. We employed the imaginary energy regularization, although other ways of regularization are possible, for example by limiting the pulse length of the laser field. One important future project is therefore to do the calculation in another regularization scheme, and compare the results. One open question is how the bremsstrahlung cross section compares to the corresponding rate of laser-induced Compton scattering, if a finite laser pulse length is assumed. For an infinite laser field, as was assumed in this thesis, the rate for laser-induced Compton scattering as a function of the emitted photon frequency, with fixed direction of the emitted photon, is a series of delta function peaks and cannot be compared directly to the bremsstrahlung cross section. However, by introducing a finite pulse length, the delta function peaks acquire a width, and the rate can then be compared to the corresponding bremsstrahlung rate.

Regarding the pair creation process, it would be interesting to investigate the behavior of the total cross section more in detail. For the collinear case, this should be possible, at least in some limiting cases, since the polarization operator in a laser field is known for arbitrary laser polarization and frequency [14], and the collinear system of one laser wave + one energetic photon is nothing else than a plane wave with one strong, low-frequency, and one weak, high-frequency component. The total probability for pair production can then be calculated as the imaginary part of the polarization operator contracted with the Coulomb field photon, much like it is done in [112]. Presumably, the correction to the Bethe-Heitler cross section, for $\omega_\gamma \gtrapprox 2m$, is proportional to $\chi^2 = \xi^2\omega^2/m^2$, where ω is the frequency of the laser field in the rest frame of the nucleus.

Other laser-modified QED processes may be treated with the same theoretical framework presented in this thesis, with fast numerical evaluation provided by the novel recursive evaluation algorithm for the generalized Bessel functions. One interesting process is field-induced pair production by an electron, which has not been treated in a laser field before (calculations for the case of an external magnetic field exist, see [9], and for the crossed field configuration [117, 153]). The Feynman diagram is shown in Fig. 6.1. Here the electron emits a virtual photon that decays into a laser-dressed electron-positron pair. In this process, the virtual photon can become real, and this Green's function pole has to be treated correctly.

Finally, a theoretically challenging question is how to include the Coulomb-field interaction in laser-dressed problems on a nonperturbative level, in particular in connection with electron-positron pair production. By employing the Dirac-Volkov propagator one can calculate second-order, and maybe third-order, corrections to the rate of pairs produced by a laser field and a Coulomb field. However, if an all-order treatment for the Coulomb field becomes necessary (for $Z \approx 100$, say), then something beyond the perturbative approach is needed. The first

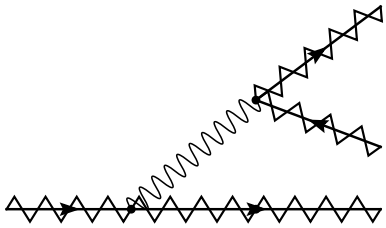

Figure 6.1: Feynman diagram for electron-positron pair production by a laser-dressed electron. The diagram where the two final electrons are exchanged should also be added.

step should be to find an approximate form of the electron (and positron) wave function in the combined system of a strong laser and a strong Coulomb field.

Appendix A

Basics of strong-field QED

A.1 The Furry picture in the presence of a strong laser field

In this section we establish the Feynman rules for intense laser-modified QED, used for the calculations in chapters 3 and 4. This way of treating one field nonperturbatively, and the interaction with all the other fields perturbatively is originally due to Furry [69], who used it to treat electrons bound in a Coulomb field. We follow a simplified way, the propagator approach, similar to the one in [28, 66, 67]. To this end, we start with the Dirac equation, coupled to an electromagnetic field

$$\left(i\hat{\partial} - m - e\hat{A}_{\text{total}}\right)\Psi(x) = \left(D_{\text{free}} - e\hat{A}_{\text{total}}\right)\Psi(x) \equiv D_{\text{total}}\Psi(x) = 0, \tag{A.1}$$

where $A_{\text{total}} = A_{\text{laser}} + A_{\text{inter.}}$ is the total interaction potential, the sum of the laser vector potential and of the rest of the interactions (perturbative photons, Coulomb fields). The goal is now to solve Eq. (A.1) in a perturbative way, and for the moment we assume that the laser is weak as well. We note that the exact solution to Eq. (A.1) can be written as

$$\Psi(x) = \psi(x) + \int \mathrm{d}^4x' G_{\text{free}}(x,x') e\hat{A}_{\text{total}}(x')\Psi(x'), \tag{A.2}$$

provided $G_{\text{free}}(x,x')$, the free Green's function, satisfies

$$D_{\text{free}}G_{\text{free}}(x,x') = \delta(x,x'), \tag{A.3}$$

and where $\psi(x)$, satisfying $D_{\text{free}}\psi(x) = 0$, is a function inserted to satisfy the boundary conditions when the potential is turned off. The Green's function, or propagator, of the free Dirac equation is known [141],

$$\begin{aligned} G_{\text{free}}(x,x') &= \frac{1}{(2\pi)^4}\int \mathrm{d}^4p \frac{\hat{p}+m}{p^2-m^2+i\varepsilon} e^{-ip(x-x')} \\ &= \frac{-i}{(2\pi)^3}\int \mathrm{d}^3p \frac{\frac{x'^0-x^0}{|x'^0-x^0|}E_{\boldsymbol{p}}\gamma^0 - \boldsymbol{p}\cdot\boldsymbol{\gamma} + m}{2E_{\boldsymbol{p}}} e^{i\boldsymbol{p}\cdot\boldsymbol{x} - iE_{\boldsymbol{p}}|x'^0-x^0|}, \end{aligned} \tag{A.4}$$

where $E_{\boldsymbol{p}} = \sqrt{\boldsymbol{p}^2 - m^2}$. This free Green's function realizes the Feynman boundary conditions [28, 66, 67], which ensure that frequency components with negative frequency are propagated backwards in time, while positive frequencies are propagated forward in time. The Feynman boundary conditions make it possible to treat pair creation problems as scattering problems, by taking the initial state at $x^0 = -\infty$ to be a negative-energy state which scatters into a positive energy state, with the interpretation that one positron and one electron have been created. Equation (A.2) is an implicit solution, that is, the wave function $\Psi(x)$ is expressed in terms of itself. However, Eq. (A.2) provides a way to obtain a perturbative solution, valid if the interaction is weak. To see this, replace $\Psi(x')$ under the integral in Eq. (A.2) with the same expression,

$$\begin{aligned}\Psi(x) = &\psi(x) + \int \mathrm{d}^4x' G_{\text{free}}(x,x') e\hat{A}_{\text{total}}(x')\psi(x') \\ &+ \int \mathrm{d}^4x'\mathrm{d}^4x'' G_{\text{free}}(x,x') e\hat{A}_{\text{total}}(x') G_{\text{free}}(x',x'') e\hat{A}_{\text{total}}(x'')\Psi(x''),\end{aligned} \tag{A.5}$$

a double integral, with terms up to second order in the interaction A_{total}. This procedure can be iterated up to arbitrary orders, and it is assumed that the expansion converges, even if a strict proof of convergence is difficult [28]. To obtain the approximate wavefunction, we take $\Psi(x'') = \psi(x'')$ (with the free wave function satisfying $D_{\text{free}}\psi = 0$) under the integration in Eq. (A.5), so that

$$\begin{aligned}\Psi(x) \approx &\psi(x) + \int \mathrm{d}^4x' G_{\text{free}}(x,x') e\hat{A}_{\text{total}}(x')\psi(x') \\ &+ \int \mathrm{d}^4x'\mathrm{d}^4x'' G_{\text{free}}(x,x') e\hat{A}_{\text{total}}(x') G_{\text{free}}(x',x'') e\hat{A}_{\text{total}}(x'')\psi(x''),\end{aligned} \tag{A.6}$$

a second-order approximation to the true wave function. If the interaction potential is a sum of two different terms,

$$A_{\text{total}}(x) = A_1(x) + A_2(x), \tag{A.7}$$

and we want to account for first-order interaction in both potentials, the second-order term [the last term in Eq. (A.5)] has two terms,

$$\begin{aligned}\Psi(x) = \int \mathrm{d}^4x'\mathrm{d}^4x'' G_{\text{free}}(x,x') \Big[&e\hat{A}_1(x') G_{\text{free}}(x',x'') e\hat{A}_2(x'') \\ &+ e\hat{A}_2(x') G_{\text{free}}(x',x'') e\hat{A}_1(x'') \Big] \Psi(x'').\end{aligned} \tag{A.8}$$

To obtain a second-order transition amplitudes S, we assume an initial free wave function $\psi_i(x)$ and a final $\Psi_f(x)$ and calculate the overlap integral (considering only second-order terms), using the approximation (A.6) for $\Psi_f(x)$:

$$\begin{aligned}S &= \int \mathrm{d}^4x \overline{\Psi}_f(x)\Psi_i(x) \\ &= \int \mathrm{d}^4x\mathrm{d}^4x'\mathrm{d}^4x'' \overline{\psi}_{\text{free},f}(x'') e\hat{A}_{\text{total}}(x'') G_{\text{free}}(x'',x') e\hat{A}_{\text{total}}(x') G_{\text{free}}(x,x')\psi_i(x) \\ &= \int \mathrm{d}^4x'\mathrm{d}^4x'' \overline{\psi}_{\text{free},f}(x'') e\hat{A}_{\text{total}}(x'') G_{\text{free}}(x'',x') e\hat{A}_{\text{total}}(x')\psi_i(x').\end{aligned} \tag{A.9}$$

If we now let the interaction consist of a Coulomb potential A_C and the vector potential A_b of an emitted photon, that is we let $A_{\text{total}} = A_C + A_b$ in (A.9), we recover the matrix element for bremsstrahlung (without a laser), leading to the Bethe-Heitler cross section [see Eqs. (3.49) and (3.50) on page 51].

The trick that makes it possible to treat the strong laser potential nonperturbatively is now to include the laser interaction potential in the operator D_{free}, that is, we let

$$D_{\text{laser}} = i\hat{\partial} - m - e\hat{A}_{\text{laser}} \tag{A.10}$$

replace the free operator D_{free} in Eq. (A.1). All the steps following Eq. (A.1) now go through unchanged, provided we identify D_{free} with the laser-modified operator D_{laser}, and the free wave function $\psi(x)$ with the Volkov states, exact solutions to

$$D_{\text{laser}}\psi_{\text{Volkov}}(x) = 0, \tag{A.11}$$

and the free Green's function G_{free} with the Dirac-Volkov Green's function $G_{\text{Dirac-Volkov}}$, satisfying

$$D_{\text{laser}}G_{\text{Dirac-Volkov}}(x, x') = \delta(x - x'). \tag{A.12}$$

Thus, to calculate a laser-modified QED amplitude, we draw the usual Feynman diagram in coordinate space, but replace the external electron lines with Volkov states ψ_{Volkov}, and the internal propagator lines with Volkov propagators $G_{\text{Dirac-Volkov}}$. The ensuing integration over the interaction space-time coordinates gives the amplitude. The method relies on the assumption that the laser is a plane wave, $A_{\text{laser}}(x) = A_{\text{laser}}(k \cdot x)$. The functions $G_{\text{Dirac-Volkov}}$ and ψ_{Volkov} are described in detail in chapter 2. Transition amplitudes are now calculated between different Volkov states, with the transition caused by a perturbation from a non-laser mode photon or another external field, or both. That this works relies on the fact that a Volkov state can be uniquely labeled by its asymptotic momentum p, or equivalently its effective momentum q [see Eq. (2.33)]. The asymptotic momentum does not change inside a plane laser wave, which is crucial for pair creation processes: Since a plane laser wave cannot create pairs, the sign of the zeroth component p^0 does not change unless the Volkov state is perturbed.

A.2 Cutkosky's rules and the optical theorem

The Cutkosky rules, originally derived in [43], basically relates the imaginary part of a forward scattering amplitude with the total probability, or the same amplitude squared. This is also called the optical theorem, and has a classical counterpart [84]. For Feynman diagrams, we have that for the amplitude of any loop diagram, twice the imaginary part of that diagram can be calculated by cutting through all loops in all such ways that the propagators can simultaneously be put on shell, that is real particles, and summing (integrating) over all possible final states [141]. This also works for the strong-field Feynman rules we have derived in section A.1. Further discussion and application to various forward scattering amplitudes can be found in [152, 153]. Recently, the optical theorem has been used to calculate the total probability of pair creation by a laser field and a Coulomb field [112], using the known expression for the

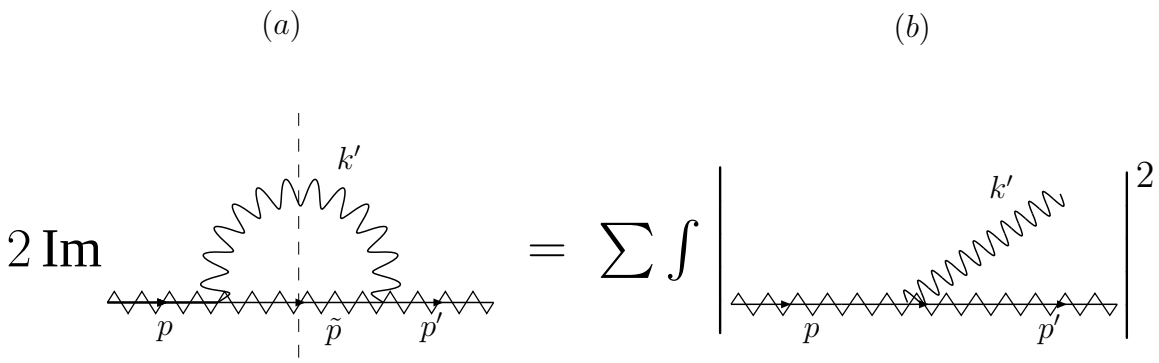

Figure A.1: Illustration of the optical theorem, providing a way to calculate the imaginary part of the self energy of the laser-dressed electron (a) by instead cutting along the dashed line and calculating the total probability of Compton scattering (b). In both graphs, the initial electron has four-momentum p, the final electron four-momentum p' and the intermediate electron $\tilde{p}$. The initial and final momenta refers to the momenta outside the laser. The emitted photon [which is absorbed again in (a)] has four-momentum k'. The sum and integration in (b) are over all possible final states, that is spin, direction and energy of the final electron and polarization, direction and energy of the final photon.

forward scattering amplitude of an arbitrary field quantum, also called the photon polarization operator [14, 20].

Here we do not prove the general strong-field Cutkosky rules, but we are satisfied with proving the identity shown in Fig. 3.6 on page 44. We display the same drawing again in Fig. A.1, but this time with labels attached to facilitate the discussion. To prove the identity in Fig. A.1, we start with the expression for the amplitude $M^{(a)}$ for the graph (a) in Fig. A.1, with the photon propagator given by

$$G^{\mu\nu}_{\text{photon}}(x,x') = \frac{-i}{(2\pi)^4}\int \mathrm{d}^4k' \frac{g^{\mu\nu}}{k'^2+i\varepsilon} e^{-ik'\cdot(x-x')}. \tag{A.13}$$

Defining the phase

$$f(p) = \frac{ep\cdot A(\tilde{\phi})}{k\cdot p} - \frac{e^2A^2(\tilde{\phi})}{2k\cdot p}, \tag{A.14}$$

we have

$$\begin{aligned}
M^{(a)} =& -e^2 \int \mathrm{d}^4x\mathrm{d}^4x' \overline{\psi}_p(x)\gamma_\mu G^{\mu\nu}_{\text{photon}}(x,x')G(x,x')\gamma_\nu\psi_{p'}(x') \\
=& \frac{-ie^2}{(2\pi)^8}\frac{m}{\sqrt{EE'}}\int \mathrm{d}^4x\mathrm{d}^4x'\mathrm{d}^4\tilde{p}\mathrm{d}^4k'\overline{u}_p\left[1+\frac{e\hat{A}(\phi)\hat{k}}{2k\cdot p}\right]\gamma^\mu\frac{1}{k'^2+i\varepsilon}\left[1+\frac{\hat{k}e\hat{A}(\phi)}{2k\cdot\tilde{p}}\right] \\
&\times\frac{\hat{\tilde{p}}+m}{\tilde{p}^2-m^2+i\varepsilon}\left[1+\frac{e\hat{A}(\phi)\hat{k}}{2k\cdot\tilde{p}}\right]\gamma_\mu\left[1+\frac{\hat{k}e\hat{A}(\phi)\hat{k}}{2k\cdot p}\right]u_{p'} \\
&\times\exp\Big[i(p-k'-\tilde{p})\cdot x+i(\tilde{p}+k'-p')\cdot x' \\
&\qquad +i\int^{\phi}\mathrm{d}\tilde{\phi}\,[f(p)-f(\tilde{p})]+i\int^{\phi'}\mathrm{d}\tilde{\phi}\,[f(\tilde{p})-f(p')]\Big].
\end{aligned} \tag{A.15}$$

If we now use the mathematical identity (the Dirac prescription) [141]

$$\int \mathrm{d}x\frac{g(x)}{x+i\varepsilon} = -i\pi g(0)+\mathcal{P}\int\mathrm{d}x\frac{g(x)}{x}, \tag{A.16}$$

or

$$\frac{g(x)}{x+i\varepsilon} = -i\pi\delta(x)g(x)+\mathcal{P}\frac{g(x)}{x}, \tag{A.17}$$

where $\mathcal{P}$ stands for the Cauchy principal value, for the integration over $\mathrm{d}k'^0$, we see that the imaginary contribution to $M^{(a)}$ comes from the double delta function contribution when replacing the propagators according to Eq. (A.17) [the double principal value $\mathcal{PP}$ does not contribute to the imaginary value of the amplitude]. However, only two of the four poles contribute, so that to obtain the imaginary value one should replace [141]

$$\frac{1}{\tilde{p}^2-m^2+i\varepsilon}\to -2i\pi\delta\left(\tilde{p}^2-m^2\right)\Theta(\tilde{p}^0), \qquad \frac{1}{k'^2+i\varepsilon}\to -2i\pi\delta(k'^2)\Theta(k'^0), \tag{A.18}$$

where $\Theta(x)$ is the step function. In addition, for forward scattering we require $p=p'$, the electron momentum should not change, and we also assumed a spin-averaged initial electron. This requirement together with remembering the formula for photon polarization and electron spin sums

$$\sum_{\text{pol.}}\epsilon_\mu\epsilon_\nu\to -g^{\mu\nu}, \qquad \sum_{\text{spin}}u(p)\bar{u}(p)=\frac{\hat{p}+m}{2m}, \tag{A.19}$$

and the identities

$$\begin{aligned}
\int \mathrm{d}^4\tilde{p}\delta(\tilde{p}^2-m^2)\Theta(\tilde{p}^0)g(\tilde{p}) &= \int\mathrm{d}^3\tilde{p}\frac{g(\tilde{p}^0=\sqrt{\tilde{\boldsymbol{p}}^2+m^2})}{2\tilde{p}^0}, \\
\int \mathrm{d}^4k'\delta(k'^2)\Theta(k'^0)h(k') &= \int\mathrm{d}^3k'\frac{h(k'^0=\sqrt{\boldsymbol{k}'^2})}{2k'^0},
\end{aligned} \tag{A.20}$$

for some functions $g(\tilde{p})$ and $h(k')$, we see that making the replacement (A.18) in Eq. (A.15), we get exactly the squared amplitude for Compton scattering, integrated and summed over final states. This proves the identity in Fig. A.1.

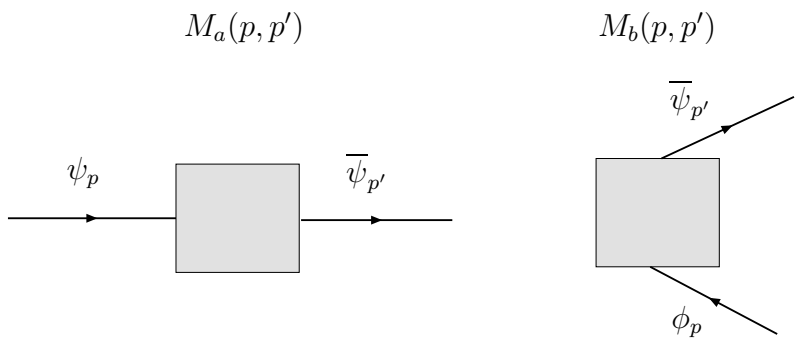

Figure A.2: Illustration of the crossing symmetry of QED. The left diagram pictures the scattering amplitude $M_a(p,p')$, the amplitude for the incoming particle with wavefunction ψ_p and momentum p to scatter by some process (indicated by the grey box) and come out with momentum p'. The right diagram, amplitude $M_b(p,p')$, describes pair production of one particle with wavefunction $\psi_{p'}$ momentum p' and one antiparticle with wavefunction ϕ_p and momentum p by the same process (the grey box). The amplitudes M_a and M_b are related by the crossing symmetry (A.21).

A.3 Crossing symmetries

A crossing symmetry of a QED process means that the matrix element of some scattering process can be transformed into the matrix element of a corresponding antiparticle creation process [141]. There is a close connection between the crossing symmetry and Feynman's interpretation [67] of negative energy solutions of the Dirac equation as positive energy particles travelling backwards in time. A general pair creation amplitude like $M_b(p,p')$ in Fig. A.2, can be obtained from the corresponding scattering amplitude $M_a(p,p')$ by letting $p' \rightarrow p'$, and $p \rightarrow -p$ in M_a so that we have

$$M_b(p,p') = M_a(-p,p'). \tag{A.21}$$

In addition, when summing over the spin degrees of freedom, there appears an extra minus sign [141]. In the spin-summed squared matrix element [like the one for bremsstrahlung (3.46) or for pair creation (4.12)] there appear sums like

$$\sum_{\text{spin}} u(p)\overline{u}(p) = \frac{\hat{p}+m}{2m}, \tag{A.22}$$

where $u(p)$ is a positive energy spinor satisfying $(\hat{p}-m)u(p)=0$. If now we change $p \rightarrow -p$ in Eq. (A.22), then we get

$$\frac{-\hat{p}+m}{2m} = -\sum_{\text{spin}} v(p)\overline{v}(p), \tag{A.23}$$

where now $v(p)$ is a negative energy spinor, $(\hat{p}+m)v(p)=0$. We see that we get an overall minus sign in the squared amplitude, which has to be corrected by hand. The final crossing

symmetry formula thus reads

$$\sum_{\text{spin}} |M_b(p,p')|^2 = -\frac{1}{4m^2}\text{Tr}\left[(m+\hat{p}')H_a(-p,p')(m-\hat{p})\overline{H}_a(-p,p')\right], \tag{A.24}$$

with $M_a(p,p') = \bar{u}(p')H_a(p,p')u(p)$, and where M_a and M_b refer to the scattering and pair creation amplitudes in Fig. A.2. That the crossing symmetry exists also for laser-modified Feynman diagrams follows directly from the positive energy Volkov solution ψ_p [see Eq. (2.27)], from which the negative energy Volkov solution (corresponding to the antiparticle, the laser-dressed positron) can be obtained by letting $p \to -p$.

Appendix B

Completeness and gauge invariance

B.1 Demonstration of the completeness property of the function $E(x,p)$

The task is to show the equality

$$\frac{1}{(2\pi)^4}\int \mathrm{d}^4 p E(p,x)\bar{E}(p,x') = \delta(x-x'), \tag{B.1}$$

where $E(p,x)$ and $\bar{E}(p,x)$ are defined in Eqs. (2.55) and (2.56). First, write the integral out as

$$\begin{aligned}
&\frac{1}{(2\pi)^4}\int \mathrm{d}^4 p E(p,x)\bar{E}(p,x') \\
=&\frac{1}{(2\pi)^4}\int \mathrm{d}^4 p \left[1+\frac{e\hat{k}\left(\hat{A}(\phi)-\hat{A}(\phi')\right)}{2k\cdot p}\right] \\
&\times \exp\left(-ip\cdot(x-x') - i\int_{\phi'}^{\phi}\left[\frac{ep\cdot A(\tilde{\phi})}{k\cdot p} - \frac{e^2A^2(\tilde{\phi})}{2k\cdot p}\right]\mathrm{d}\tilde{\phi}\right).
\end{aligned} \tag{B.2}$$

We see that if $x = x'$, then equation (B.1) holds. For definiteness, we now take the case of linear polarization, and choose our coordinate system so that $A^\mu = (0,0,\tilde{a},0)\cos(\phi)$ and $k^\mu = (\omega,\omega,0,0)$. The integral becomes

$$\begin{aligned}
&\frac{1}{(2\pi)^4}\int \mathrm{d}^4 p E(p,x)\bar{E}(p,x') \\
=&\frac{1}{(2\pi)^4}\int \mathrm{d}^4 p \left[1+\frac{e\hat{k}\left(\hat{A}(\phi)-\hat{A}(\phi')\right)}{2\omega(p_0-p_1)}\right] \\
&\times \exp\left(-ip_0(x_0-x_0') + ip_1(x_1-x_1') + ip_2(x_2-x_2') + ip_3(x_3-x_3')\right) \\
&\times \exp\left(i\int_{\phi'}^{\phi}\left[\frac{ep_2\tilde{a}\cos(\tilde{\phi})}{\omega(p_0-p_1)} + \frac{e^2A^2(\tilde{\phi})}{2\omega(p_0-p_1)}\right]\mathrm{d}\tilde{\phi}\right).
\end{aligned} \tag{B.3}$$

Here we see that the p_3-integral always gives a delta function. How about the other p_0, p_1 and p_2-dimensions? It is easy to see that if $x_0 = x_0'$ and $x_1 = x_1'$, then Eq. (2.60) holds. The two difficult cases are the following.
Case 1. $x_0 \neq x_0'$, $x_{i\neq 0} = x_i'$.(The treatment of the case $x_1 \neq x_1'$, $x_{i\neq 1} = x_i'$ is done analogously) We have

$$\begin{aligned}
&\frac{1}{(2\pi)^4}\int \mathrm{d}^4 p E(p,x)\bar{E}(p,x') \\
=&\frac{1}{(2\pi)^4}\int \mathrm{d}^4 p \left[1+\frac{e\hat{k}\left(\hat{A}(\phi)-\hat{A}(\phi')\right)}{2\omega(p_0-p_1)}\right] \\
&\times \exp\left(-ip_0(x_0-x_0')+i\int_{\phi'}^{\phi}\left[\frac{ep_2\tilde{a}\cos(\tilde{\phi})}{\omega(p_0-p_1)}+\frac{e^2A^2(\tilde{\phi})}{2\omega(p_0-p_1)}\right]\mathrm{d}\tilde{\phi}\right).
\end{aligned} \tag{B.4}$$

Integration over p_2 now gives

$$\begin{aligned}
&\frac{1}{(2\pi)^4}\int \mathrm{d}^4 p E(p,x)\bar{E}(p,x') \\
=&\frac{1}{(2\pi)^3}\int \mathrm{d}p_0\mathrm{d}p_1\mathrm{d}p_3 \left[1+\frac{e\hat{k}\left(\hat{A}(\phi)-\hat{A}(\phi')\right)}{2\omega(p_0-p_1)}\right] \\
&\times \exp\left(-ip_0(x_0-x_0')+i\int_{\phi'}^{\phi}\frac{e^2A^2(\tilde{\phi})}{2\omega(p_0-p_1)}\mathrm{d}\tilde{\phi}\right)\delta\left(\frac{e\tilde{a}\int_{\phi'}^{\phi}\cos(\tilde{\phi})\mathrm{d}\tilde{\phi}}{\omega(p_0-p_1)}\right).
\end{aligned} \tag{B.5}$$

This expression equals zero, since the argument of the delta function has no roots. (The delta function satisfies $\int_{-\infty}^{\infty}\delta(\frac{1}{x})\mathrm{d}x = 0$.)
Case 2. $x_0 \neq x_0'$, $x_2 \neq x_2'$, $x_1 = x_1'$ and $x_3 = x_3'$. Again the case $x_1 \neq x_1'$, $x_2 \neq x_2'$, $x_0 = x_0'$ and $x_3 = x_3'$ is analogous.
This time the integral reads

$$\begin{aligned}
&\frac{1}{(2\pi)^4}\int \mathrm{d}^4 p E(p,x)\bar{E}(p,x') \\
=&\frac{1}{(2\pi)^4}\int \mathrm{d}^4 p \left[1+\frac{e\hat{k}\left(\hat{A}(\phi)-\hat{A}(\phi')\right)}{2\omega(p_0-p_1)}\right] \\
&\times \exp\left(-ip_0(x_0-x_0')+ip_2(x_2-x_2')+i\int_{\phi'}^{\phi}\left[\frac{ep_2\tilde{a}\cos(\tilde{\phi})}{\omega(p_0-p_1)}+\frac{e^2A^2(\tilde{\phi})}{2\omega(p_0-p_1)}\right]\mathrm{d}\tilde{\phi}\right).
\end{aligned} \tag{B.6}$$

After p_2-integration we get

$$\begin{aligned}
&\frac{1}{(2\pi)^4}\int \mathrm{d}^4 p E(p,x)\bar{E}(p,x') \\
=&\frac{1}{(2\pi)^3}\int \mathrm{d}p_0\mathrm{d}p_1\mathrm{d}p_3 \left[1+\frac{e\hat{k}\left(\hat{A}(\phi)-\hat{A}(\phi')\right)}{2\omega(p_0-p_1)}\right] \\
&\times\exp\left(-ip_0(x_0-x_0')+i\int_{\phi'}^{\phi}\frac{e^2A^2(\tilde{\phi})}{2\omega(p_0-p_1)}\mathrm{d}\tilde{\phi}\right)\delta\left(x_2-x_2'+\frac{e\tilde{a}\int_{\phi'}^{\phi}\cos(\tilde{\phi})\mathrm{d}\tilde{\phi}}{\omega(p_0-p_1)}\right).
\end{aligned} \tag{B.7}$$

Now, the equation

$$x_2-x_2'+\frac{e\tilde{a}\int_{\phi'}^{\phi}\cos(\tilde{\phi})\mathrm{d}\tilde{\phi}}{\omega(p_0-p_1)}=0 \tag{B.8}$$

has the root

$$p_1^{\mathrm{root}}=\frac{e\tilde{a}\int_{\phi'}^{\phi}\cos(\tilde{\phi})\mathrm{d}\tilde{\phi}}{\omega(x_2-x_2')}+p_0, \tag{B.9}$$

so that

$$\delta\left(x_2-x_2'+\frac{e\tilde{a}\int_{\phi'}^{\phi}\cos(\tilde{\phi})\mathrm{d}\tilde{\phi}}{\omega(p_0-p_1)}\right)=\frac{\delta(p_1-p_1^{\mathrm{root}})}{\left|\frac{e\tilde{a}\int_{\phi'}^{\phi}\cos(\tilde{\phi})\mathrm{d}\tilde{\phi}}{\omega(p_0-p_1)^2}\right|}. \tag{B.10}$$

Integrating also over p_1 using the delta function (note that the singularity at $p_1=p_0$ is no problem, since the delta function gives zero at this point) yields

$$\begin{aligned}
&\frac{1}{(2\pi)^4}\int \mathrm{d}^4 p E(p,x)\bar{E}(p,x') \\
=&\frac{1}{(2\pi)^3}\int \mathrm{d}p_0\mathrm{d}p_3 \left[1+\frac{e\hat{k}(x_2-x_2')\left(\hat{A}(\phi)-\hat{A}(\phi')\right)}{2e\tilde{a}\int_{\phi'}^{\phi}\cos(\tilde{\phi})\mathrm{d}\tilde{\phi}}\right] \\
&\times\exp\left(-ip_0(x_0-x_0')+i\int_{\phi'}^{\phi}\frac{e^2A^2(\tilde{\phi})(x_2-x_2')}{2e\tilde{a}\int_{\phi'}^{\phi}\cos(\tilde{\phi})\mathrm{d}\tilde{\phi}}\mathrm{d}\tilde{\phi}\right)\frac{\omega\,(x_2-x_2')}{e\tilde{a}\int_{\phi'}^{\phi}\cos(\tilde{\phi})\mathrm{d}\tilde{\phi}}.
\end{aligned} \tag{B.11}$$

This integral however gives zero after integrating over p_0, since we assumed $x_0\neq x_0'$. In summary, we have shown that $\int \mathrm{d}^4 p E(p,x)\bar{E}(p,x')$ is different from zero only when $x=x'$, and at that point equals $(2\pi)^4\delta(x-x')$.

B.2 Demonstration of gauge invariance

In this section we demonstrate that the laser-assisted bremsstrahlung matrix element (3.26) is gauge invariant. Gauge invariance of the pair creation matrix element (4.5) can be shown in

the same manner. We here use the E-notation of Mitter [113] (originally of Ritus [154]), see equation (2.55) and (2.56). Following Mitter [113], we first show that

$$\begin{aligned}&\int \mathrm{d}^4x\bar{E}(x,p_1)\hat{k}_bE(x,p_2)e^{ik_b\cdot x}\\ =&(\hat{p}_1-m)\int \mathrm{d}^4x\bar{E}(x,p_1)E(x,p_2)e^{ik_b\cdot x}-\int \mathrm{d}^4x\bar{E}(x,p_1)E(x,p_2)e^{ik_b\cdot x}(\hat{p}_2-m).\end{aligned} \tag{B.12}$$

This is seen by partial integration:

$$\begin{aligned}&\int \mathrm{d}^4x\bar{E}(x,p_1)\hat{k}_bE(x,p_2)e^{ik_b\cdot x}=\int \mathrm{d}^4x\bar{E}(x,p_1)\left[-i\hat{\partial}e^{ik_b\cdot x}\right]E(x,p_2)\\ =&-i\int \mathrm{d}^4x\partial_\mu\left[\bar{E}(x,p_1)\gamma^\mu e^{ik_b\cdot x}E(x,p_2)\right]+i\int \mathrm{d}^4x\left[\partial_\mu\bar{E}(x,p_1)\right]\gamma^\mu e^{ik_b\cdot x}E(x,p_2)\\ &+i\int \mathrm{d}^4x\bar{E}(x,p_1)\gamma^\mu e^{ik_b\cdot x}\left[\partial_\mu E(x,p_2)\right]\\ =&-i\int_{S_\infty}\mathrm{d}S_\mu\bar{E}(x,p_1)\gamma^\mu e^{ik_b\cdot x}E(x,p_2)+\int \mathrm{d}^4x\left[\hat{p}_1\bar{E}(x,p_1)+e\bar{E}(x,p_1)\hat{A}\right]e^{ik_b\cdot x}E(x,p_2)\\ &+\int \mathrm{d}^4x\bar{E}(x,p_1)e^{ik_b\cdot x}\left[-E(x,p_2)\hat{p}_2-e\hat{A}E(x,p_1)\right]\\ =&(\hat{p}_1-m)\int \mathrm{d}^4x\bar{E}(x,p_1)E(x,p_2)e^{ik_b\cdot x}-\int \mathrm{d}^4x\bar{E}(x,p_1)E(x,p_2)e^{ik_b\cdot x}(\hat{p}_2-m),\end{aligned} \tag{B.13}$$

where the surface integral is zero due to the rapid oscillations at infinity of the exponentials in $\bar{E}E$. Now we show that replacing $\epsilon_{b\lambda}$ with k_b in the matrix element will give zero, and that the matrix element therefore is invariant under the transformation $\epsilon_{b\lambda}\rightarrow\epsilon_{b\lambda}+\Lambda k_b$, with arbitrary constant Λ. Writing the matrix element with $\epsilon_{b\lambda}\rightarrow k_b$ as (omitting constant prefactors)

$$\begin{aligned}M_{\epsilon_{b\lambda}\rightarrow k_b}=\int \mathrm{d}^4x_2\mathrm{d}^4x_1\mathrm{d}^4p\Big[&\bar{\Psi}_{p_2}(x_2)\hat{k}_be^{ik_b\cdot x_2}G(x_2,x_1)\hat{A}_C\Psi_{p_1}(x_1)\\ &+\bar{\Psi}_{p_2}(x_2)\hat{A}_CG(x_2,x_1)\hat{k}_be^{ik_b\cdot x_1}\Psi_{p_1}(x_1)\Big],\end{aligned} \tag{B.14}$$

where A_C is the Coulomb potential, we use the rule (B.12) to show

$$\begin{aligned}&\int \mathrm{d}^4x_2\mathrm{d}^4p\bar{\Psi}_{p_2}(x_2)\hat{k}_be^{ik_b\cdot x_2}G(x_2,x_1)\hat{A}_C\Psi_{p_1}(x_1)\\ =&\int \mathrm{d}^4x_2\mathrm{d}^4p\bar{u}_{r_2}(p_2)\bar{E}(x_2,p_2)\hat{k}_be^{ik_b\cdot x_2}E(x_2,p)\frac{1}{\hat{p}-m}\bar{E}(x_1,p)\hat{A}_C\Psi_{p_1}(x_1)\\ =&-\int \mathrm{d}^4x_2\mathrm{d}^4p\bar{u}_{r_2}(p_2)\bar{E}(x_2,p_2)e^{ik_b\cdot x_2}E(x_2,p)\frac{\hat{p}-m}{\hat{p}-m}\bar{E}(x_1,p)\hat{A}_C\Psi_{p_1}(x_1)\\ =&-\int \mathrm{d}^4x_2\mathrm{d}^4p\bar{\Psi}_{p_2}(x_2)e^{ik_b\cdot x_2}E(x_2,p)\bar{E}(x_1,p)\hat{A}_C\Psi_{p_1}(x_1),\end{aligned} \tag{B.15}$$

and in the same fashion

$$\begin{aligned}
&\int \mathrm{d}^4x_1\mathrm{d}^4p\bar{\Psi}_{p_2}(x_2)\hat{A}_C G(x_2,x_1)\hat{k}_b e^{ik_b\cdot x_1}\Psi_{p_1}(x_1)\\
=&\int \mathrm{d}^4x_1\mathrm{d}^4p\bar{\Psi}_{p_2}(x_2)\hat{A}_C E(x_2,p)\frac{1}{\hat{p}-m}\bar{E}(x_1,p)\hat{k}_b e^{ik_b\cdot x_1}E(x_1,p_1)u_{r_1}(p_1) \qquad \text{(B.16)}\\
=&\int \mathrm{d}^4x_1\mathrm{d}^4p\bar{\Psi}_{p_2}(x_2)\hat{A}_C E(x_2,p)\bar{E}(x_1,p)e^{ik_b\cdot x_1}\Psi_{p_1}(x_1).
\end{aligned}$$

Here we made use of the relation $(\hat{p}-m)u(p)=0=\bar{u}(p)(\hat{p}-m)$. From the equation

$$\int \mathrm{d}^4pE(x_1,p)\bar{E}(x_2,p)=(2\pi)^4\delta(x_1-x_2) \qquad \text{(B.17)}$$

we finally conclude that

$$M_{\epsilon_{b\lambda}\to k_b}=0. \qquad \text{(B.18)}$$

Thus it becomes possible to use the sum rule for photon polarization sums

$$\sum_{\lambda=1,2}\epsilon^{\mu}_{b\lambda}M_\mu\epsilon^{\nu}_{b\lambda}M_\nu=-M_\mu M^\mu. \qquad \text{(B.19)}$$

However, since this relation involves exact cancellation between equally sized terms, numerically it is better to do the photon polarization sum by actual summation over two suitable polarization vectors. Gauge invariance is also useful as a numerical check of the correctness of the computer code used for evaluation of the different cross sections.

Appendix C

Appended preprints of completed / submitted papers

C.1 Laser channeling of Bethe-Heitler pairs

Laser Channeling of Bethe-Heitler Pairs

Erik Lötstedt,* Ulrich D. Jentschura, and Christoph H. Keitel
Max-Planck-Institut für Kernphysik, Postfach 103980, 69029 Heidelberg, Germany
(Dated: February 1, 2008)

Electron-positron pair creation is analyzed for an arrangement involving three external fields: a high-frequency gamma photon, the Coulomb field of a nucleus and a strong laser wave. The frequency of the incoming gamma photon is assumed to be larger than the threshold for pair production in the absence of a laser, and the peak electric field of the laser is assumed to be much weaker than Schwinger's critical field. The total number of pairs produced is found to be essentially unchanged by the laser field, while the differential cross section is drastically modified. We show that the laser can channel the angular distribution of electron-positron pairs into a narrow angular region, which also facilitates experimental observation.

PACS numbers: 12.20.Ds, 25.75.Dw, 32.80.Wr

The creation of an electron-positron pair by an external electromagnetic field—the conversion of field energy into matter—remains an intriguing phenomenon, and its exploration continues to enhance our understanding of the foundations of field theory. Usually, pair creation is accomplished by weak, high frequency fields, gamma photons, with the standard examples being the merging of two high-energy photons into an electron-positron pair or the conversion of a photon into a pair in the vicinity of a nucleus (the Bethe–Heitler process, see Ref. [1]). Strong, static macroscopic fields can also create pairs, as first predicted by Sauter [2] and later by Schwinger [3] for the case of a static electric field. In the sense of QED perturbation theory, pair creation by a static field is a nonperturbative phenomenon, and its magnitude is controlled by a parameter χ, defined as

$$\chi = \frac{E}{E_{\text{crit}}} = -\frac{e\hbar}{m^2c^3}E, \tag{1}$$

where E is the peak value of the electric field, $e = -|e|$ and m are the electron charge and mass, respectively, and $E_{\text{crit}} \approx 1.3 \times 10^{16}$ V/cm is the so-called critical field. The basic result, which holds for any strong static electromagnetic field, is that the probability for pair creation is exponentially suppressed unless χ is at least of the order of unity. If the field is allowed to oscillate, another parameter ξ, related to the angular frequency ω of the oscillation, becomes relevant:

$$\xi = -\frac{eE}{mc\omega}. \tag{2}$$

The value of ξ governs the nature of pair production. Specifically, the regime $\xi \ll 1$ is called the multiphoton regime, while for $\xi \gg 1$ the pairs are created by tunneling through the tilted potential gap of magnitude $2mc^2$, and one may call ξ the Keldysh parameter of vacuum ionization. The transition between the two regimes for an oscillating electric field was treated by Brézin and Itzykson [4] and also by Popov [5, 6]. Nowadays, strong lasers offer the best possibility to experimentally test nonlinear strong-field pair production. Modern lasers achieve $\xi \gg 1$ for infrared frequencies, but even for the strongest lasers available we have $\chi \ll 1$. As is well known, a plane laser wave cannot create pairs by itself, due to energy-momentum conservation. Just like in a pure magnetic field [7], a second particle is necessary to provide the required momentum. In a focused laser pulse [8] or a standing wave [9–11], pair creation is possible, since the field configuration is different from a plane wave. Indeed, pair creation in a strong laser field induced by an additional high-energy gamma photon has been studied both theoretically [12–14] and experimentally [15, 16]. If the probing particle is replaced by a nuclear field [17–21], it was shown that the pair production rate is exponentially suppressed for nuclei at rest, and that acceleration of the nucleus to highly relativistic velocities is necessary to obtain observable rates.

In this Letter, we study the creation of an electron-positron pair by three fields: a high-energy gamma photon (possibly produced by Compton backscattering), the Coulomb field of a nucleus and an intense, low-frequency laser field, as schematically shown in Fig. 1. Numerical estimates of the cross section for pair production in this field configuration are absent in the literature, to the best of our knowledge. Previous studies of related processes [22, 23] obtained approximate analytical formulas for weak ($\xi \ll 1$) fields or ultrarelativistic gamma

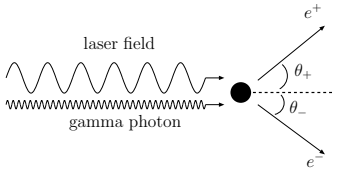

FIG. 1: Schematic picture of the considered pair creation process. A low-frequency, high-intensity laser beam of linear polarization and a high-frequency gamma photon, propagating in the same direction, impinge on a stationary nucleus, depicted as a filled black circle, to produce an electron and a positron. The angle $\theta_\pm$ denotes the ejection angle in the plane spanned by the propagation direction and the polarization direction of the laser. Note that the wavelengths of the two waves are not drawn to scale, in reality we consider the case where the laser wavelength is many order of magnitudes larger than the wavelength of the gamma photon.

photon energies [24]. Here we find that an interesting laser-channeling phenomenon requires the opposite limit $\xi > 1$, and we have accessed this region by a full numerical treatment.

We assume the laser beam and gamma photon beam to propagate in the same direction. For the laser field, we employ a low-frequency ($\hbar\omega \sim 10$ eV), high-power laser beam with typically $\xi \sim 10$, corresponding to an intensity $I_l = 9 \times 10^{21}$ W/cm^2. Since we still have $\chi \ll 1$, and we consider a nucleus at rest, the laser field will affect the total probability of the pair creation only marginally. This can be justified by the following heuristic argument: The electron-positron pair is expected to be created over a distance of the order of the Compton wavelength $\lambda_C = \hbar/(mc)$. Over this distance, the peak electric field of the laser accomplishes an amount of work $W = \xi\hbar\omega$, which is much smaller than the threshold $2mc^2$ to create a pair, since we assume $\hbar\omega \ll mc^2$. We thus expect that the total number of pairs, or the total cross section for pair production, is not changed even for a strong laser. However, the differential cross section, that is the dependence on the directions and energies of the produced pairs, is expected to differ drastically from the laser-free case, due to the interaction with the laser field after the actual creation. In particular, we find that the laser field strongly focuses the pairs to form a narrow beam. In this way, laser-assisted signatures of the created pairs become experimentally observable, since we do not suffer from the exponential smallness of the creation rate as other proposals do.

From here on, we use natural units with $\hbar = c = \epsilon_0 = 1$. Furthermore, we denote four-vector dot products with a dot, so that $a_\mu b^\mu = a \cdot b = a_0\, b_0 - \boldsymbol{a} \cdot \boldsymbol{b}$ for two four-vectors a^μ and b^μ. Contraction with the Dirac gamma matrices γ^μ is written with a hat, $\gamma^\mu b_\mu = \hat{b}$. Quantum electrodynamics in the presence of a strong laser can be treated with a theoretical framework [25] analogous to the Furry picture, that is otherwise used to describe electrons bound in strong Coulomb fields. Since the laser is strong, $\xi \geq 1$, the lepton-laser interaction needs to be treated nonperturbatively to all orders, while we include the interaction with the Coulomb field and the gamma photon in first-order perturbation theory. We consider linear polarization of the laser field, described by the vector potential $A^\mu(\phi) = a^\mu \cos\phi$, where $a^\mu = (0, \boldsymbol{a})$ is the polarization vector, and $\phi = k \cdot x$ is the Lorentz invariant laser phase, expressed through the wave vector $k^\mu = (\omega, \boldsymbol{k})$. The amplitude of the vector potential is related to the parameter ξ as $\xi = -e|\boldsymbol{a}|/m$.

The basis states for the electron and positron are the Volkov states $\psi_p^\mp(x)$ [26], which are exact solutions of the Dirac equation coupled to an external laser field:

$$\left(i\hat{\partial} - m - e\hat{A}(\phi)\right)\psi_{p_\mp}^\mp(x) = 0. \tag{3}$$

Here $p_\mp$ is the asymptotic momentum of the electron or positron outside the laser, and we define $q_\mp^\mu = (Q_\mp, \boldsymbol{q}_\mp) = p_\mp^\mu + k^\mu e^2|\boldsymbol{a}|^2/(4k \cdot p_\mp)$, the effective momentum of the electron or positron inside the laser. From the Volkov solutions, it is relatively easy [25, 27] to construct the Dirac-Volkov propagator $G(x, x')$, the Green's function of Eq. (3). We also need the potential $A_C^\mu(x) = -Ze\delta^{\mu 0}/(4\pi|\boldsymbol{x}|)$ of the nucleus with atomic charge number Z and the vector potential $A_\gamma^\mu(x) = \epsilon_\gamma^\mu e^{-ik_\gamma \cdot x}/\sqrt{2\omega_\gamma}$ of the high-energy photon with wave vector $k_\gamma^\mu = (\omega_\gamma, \boldsymbol{k}_\gamma)$ and polarization vector $\epsilon_\gamma^\mu = (0, \boldsymbol{\epsilon}_\gamma)$.

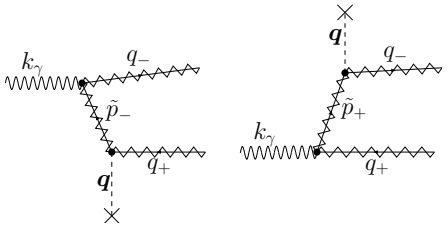

FIG. 2: The Feynman diagrams for laser-assisted pair creation. External electron and positron lines, as well as propagators are denoted by a wiggly line superimposed on a straight line, to stress that the laser-lepton interaction is treated nonperturbatively. The electron is created with an effective four-momentum q_-, and the four-momentum of the positron is q_+. The intermediate electron propagator momentum is denoted by $\tilde{p}_\pm$. The absorbed non-laser mode photon has four-momentum k_γ, and the virtual Coulomb field photon, depicted with a dashed line, has three-momentum $\boldsymbol{q}$. Time flows from left to right.

The amplitude $S_{p_+p_-}$ for laser-dressed creation of one electron with asymptotic momentum p_- and one positron with asymptotic momentum p_+ can be calculated by adding the contributions from the two Feynman diagrams in Fig. 2. We consider a collinear arrangement of the gamma photon and the laser beam, which in particular implies $k \cdot k_\gamma = 0$, and provides for a considerable simplification of the matrix element. We have

$$\begin{aligned} S_{p_+p_-} &= ie^2 \int \mathrm{d}^4x\, \mathrm{d}^4x'\, \bar{\psi}_{p_-}^-(x)\big[\hat{A}_\gamma(x)G(x,x')\hat{A}_C(x') \\ &\qquad + \hat{A}_C(x)G(x,x')\hat{A}_\gamma(x')\big]\psi_{p_+}^+(x') \\ &= 2\pi i \sum_{n=-\infty}^{\infty} \frac{Ze^3\, m}{\sqrt{2\omega_\gamma E_+ E_-}} \frac{\delta(Q_+ + Q_- - n\omega - \omega_\gamma)}{(\boldsymbol{q}_- + \boldsymbol{q}_+ - n\,\boldsymbol{k} - \boldsymbol{k}_\gamma)^2} u_{p_-}^{-\dagger}\gamma^0 \\ &\quad \times \left(\hat{\epsilon}_\gamma \frac{\hat{k}_\gamma - \hat{p}_- - m}{2p_- \cdot k_\gamma} F_n + F_n \frac{\hat{p}_+ - \hat{k}_\gamma - m}{2p_+ \cdot k_\gamma}\hat{\epsilon}_\gamma\right) u_{p_+}^+, \end{aligned} \tag{4}$$

where

$$\begin{aligned} F_n =& A_0(n, \alpha_+ - \alpha_-, -\beta_+ - \beta_-)\gamma^0 \\ &+ A_1(n, \alpha_+ - \alpha_-, -\beta_+ - \beta_-)\left(\frac{\gamma^0 e\,\hat{a}\hat{k}}{2k \cdot p_+} + \frac{e\,\hat{a}\hat{k}\gamma^0}{2k \cdot p_-}\right) \\ &+ A_2(n, \alpha_+ - \alpha_-, -\beta_+ - \beta_-)\frac{e^2\, a^2\omega\hat{k}}{2k \cdot p_- k \cdot p_+}, \end{aligned} \tag{5}$$

$\alpha_\pm = ea \cdot p_\pm/(k \cdot p_\pm)$, $\beta_\pm = e^2a^2/(8k \cdot p_\pm)$, and $u_{p_\mp}^\mp$ are constant spinors satisfying $(\hat{p}_\mp \mp m)u_{p_\mp}^\mp = 0$. The generalized

Bessel function $A_K(n,\alpha,\beta)$ is defined as [12, 13]

$$A_K(n,\alpha,\beta) = \frac{1}{2\pi}\int_{-\pi}^{\pi} \cos^K\varphi\, e^{-in\varphi+i\alpha\sin\varphi-i\beta\sin(2\varphi)}\mathrm{d}\varphi. \tag{6}$$

The expression (4) was first obtained in Ref. [23]. We note that the matrix element (4) is related to that of laser-assisted bremsstrahlung [28, 29] by a crossing symmetry. Energy conservation is enforced by the delta function $\delta(Q_+ + Q_- - n\,\omega - \omega_\gamma)$, which clarifies the meaning of the integer n: It signifies the net number of photons absorbed during the process. To obtain the total amplitude, one should sum over all photon orders n. Note, however, that energy conservation is expressed through the effective energies $Q_\mp$, and that photon number n is bounded from below by the laser-dressed pair-production threshold condition $n\,\omega \geq 2m_* - \omega_\gamma$.

The laser-modified differential cross section $\mathrm{d}\sigma$ is given by the standard formula

$$\begin{aligned}\mathrm{d}\sigma =& \frac{1}{T}\left|S_{p_+p_-}\right|^2 \frac{\mathrm{d}^3p_-}{(2\pi)^3}\frac{\mathrm{d}^3p_+}{(2\pi)^3} \\ =& \sum_n s_n\,\delta(Q_+ + Q_- - n\omega - \omega_\gamma)\,\mathrm{d}^3p_-\,\mathrm{d}^3p_+, \end{aligned} \tag{7}$$

where the large observation time T is cancelled by the relation $\delta^2(x) = T\delta(x)/(2\pi)$. Note that the final-state phase space is expressed in terms of the momenta $p_\pm$ outside the laser.

We have evaluated the differential cross section (7) for different values of the parameter ξ. In all cases, we have averaged over the polarization of the initial gamma photon and summed over the spins of the final electron and positron. Due to symmetry reasons, the differential cross section is symmetric under the exchange of electron and positron, and we show the positron spectrum. The laser frequency is chosen as $\omega = 10$ eV. However, we expect that the qualitative behavior of the cross sections is independent of ω, as long as $\chi \ll 1$.

In Fig. 3, we show the cross section $\mathrm{d}\sigma/\mathrm{d}\Omega_+$, resulting from fourfold Monte Carlo integration, which remains differential only in the solid angle $\mathrm{d}\Omega_+ = \mathrm{d}\theta_+\mathrm{d}\varphi_+\sin\varphi_+$ of the created positron. Here φ_+ is the corresponding polar angle. Observe that the solid angle refers to the direction $\boldsymbol{p}_+/|\boldsymbol{p}_+|$ of the positron outside the laser, to allow comparison with the laser-free case. The gamma photon energy is $\omega_\gamma = 1.25\ \mathrm{MeV} > 2m$, so that pair production is possible without the laser. However, as is clearly seen in Fig. 3, the angular distribution in the field-free case [1] is broad. Quite to the contrary, the laser-dressed curves show sharp peaks, with the peak height increasing with increasing laser intensity, and the peak position given roughly by $\theta_{\text{peak}} = 1/\xi$. This value can be understood intuitively by classical arguments: If we assume that the positron is created from the photon energy $\omega_\gamma = 1.25\ \mathrm{MeV}$ by the Bethe-Heitler process, with resulting momentum p^μ_{i+}, then from the classical equations of motion for p^μ_+ we have, outside the laser field for small angles ($\theta_+ \ll 1$),

$$\theta_+(\phi_0) \approx \frac{p^x_+}{p^y_+} \approx \frac{2k\cdot p_{i+}}{\omega|e\boldsymbol{A}(\phi_0)|}. \tag{8}$$

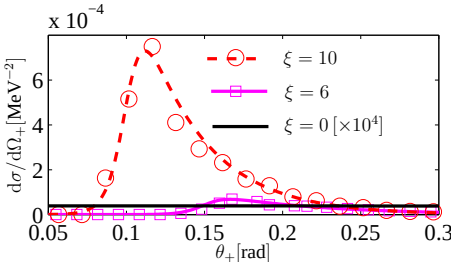

FIG. 3: (Color online) The differential cross section $\mathrm{d}\sigma/\mathrm{d}\Omega_+$ as a function of the angle of ejection θ_+ (see Fig. 1), in the plane spanned by the propagation direction $\boldsymbol{k}/\omega$ and the polarization direction $\boldsymbol{a}/|\boldsymbol{a}|$ (polar angle $\varphi_+ = \pi/2$). Note that $\mathrm{d}\sigma/\mathrm{d}\Omega_+$ is symmetric around $\theta_+ = 0$, we show only positive θ_+. The laser frequency is $\omega = 10$ eV and the gamma photon energy is $\omega_\gamma = 1.25$ MeV. Here, the parameter values $\xi = 6$ and $\xi = 10$ correspond to laser intensities $I_l = 3.2{\times}10^{21}$ W/cm^2 and $I_l = 8.9{\times}10^{21}$ W/cm^2, respectively. The nuclear atomic number is $Z = 1$, and we remark that as the cross section is evaluated in the first Born approximation, it scales as Z^2. In the graph, circles and squares represent numerical estimates of the differential cross section obtained by fourfold Monte-Carlo integration, and the red dashed and pink solid lines are analytical fits to the numerical values. For comparison, the solid black line shows the laser-free case, multiplied by a factor of 10^4 (the laser-free differential cross section would otherwise not be visually distinguishable from zero). For the conversion to other frequently used units for the cross section, one uses $1\,\mathrm{MeV}^{-2} \approx 4\times10^2\,\mathrm{barn} = 4\times10^{-22}\,\mathrm{cm}^2$.

Here $|\boldsymbol{A}(\phi_0)|$ is the amplitude of the vector potential at the moment of creation. Taking into account the initial momentum distribution given by the Bethe-Heitler formula, one finds that the angular distribution after the laser pulse, integrated over all phases of the laser, has a peak close to $\theta_+(\phi_0 = 0)$, so that $\theta_{\text{peak}} = \theta_+(0) \approx 1/\xi$. Note that the angle θ_{peak} is independent of ω. The differential cross section $\mathrm{d}\sigma/\mathrm{d}\Omega_+$ as a function of the polar angle φ_+, is peaked sharply around $\varphi_+ = \pi/2$ for fixed $\theta+ \approx \theta_{\text{peak}}$, with a peak width of approximately 0.01 rad for the case $\xi = 10$. The Lorentz force of the laser field, with rising intensity, transfers an increasingly larger amount of momentum to the positron in the propagation direction, compared to the amount transferred in the polarization direction, which consequently leads to the described laser channeling of the pairs into a narrow angular region.

To demonstrate the assertion that the total cross section, or the total number of produced pairs is unchanged even by a laser field as strong as $\xi = 10$, we show in Fig. 4 the total cross section $\sigma_{\text{tot}} = \int \mathrm{d}\sigma$, resulting from sixfold numerical integration over the created electron and positron momenta. Due to energy conservation, the laser-free cross section has a sharp cutoff at $\omega_\gamma = 2m$, below which it vanishes. When the laser is included, absorption of a sufficient number of laser photons to overcome the laser-modified threshold $2m_*$ results in a finite, but small, total cross section. Since we may speak of a

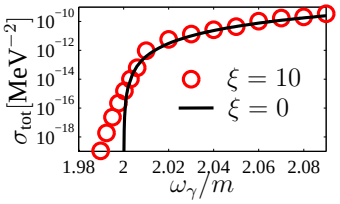

FIG. 4: (Color online) The total cross section for electron-positron pair creation close to the threshold, displayed in logarithmic scale as a function of the perturbative photon energy ω_γ. The solid black line shows the field-free case [1], which vanishes below the pair production threshold $\omega_\gamma/m = 2$. Below threshold, the laser-induced (rather than laser-assisted) pair creation cross section exhibits an exponential decrease. Parameters in the calculation are the same as in Fig. 3: $\omega_\gamma = 10$ eV, $\xi = 10$, $Z = 1$.

laser-assisted pair creation process for $\omega_\gamma > 2m$, but laser-induced for $\omega_\gamma < 2m$, the considered process enables us to study the transition between laser-assisted and laser-induced by varying the frequency ω_γ. By "laser-assisted" we mean a process that occurs without the laser, but is modified by its presence and by "laser-induced" we mean a process where the presence of the laser is a necessary requirement.

A few remarks on possible background processes is appropriate. In principle, pairs can also be created by the laser wave together with the Coulomb field only [17]. However, in the regime of subcritical laser fields $\chi \ll 1$ that we are considering here (the parameters used in fig. 4 give $\chi = \xi\omega/m = 2 \times 10^{-4}$), the rate is exponentially small $\sim \exp(-\chi^{-1})$ [18, 20] and can safely be neglected. The photon together with the laser wave only is unable to create pairs in our geometry since $k \cdot k_\gamma = 0$ [13]. As for the experimental verification of our results, we note that Bethe-Heitler pair creation for small photon energies $\omega_\gamma \gtrsim 2m$ has been successfully measured [30], using germanium detectors. A strong laser field however, is likely to destroy its target, and it may be preferred to instead use a thin metal foil when measuring the laser-dressed cross section. If an incoming gamma photon flux of 10^7 photons/bunch, in bunches of duration 1 ps, repetition rate 1 Hz, with hard x-ray energy $\omega_\gamma = 1.25$ MeV, obtainable by Compton backscattering of a free electron laser on storage ring electrons [31, 32], together with a lead ($Z = 82$) target of 1 mm thickness is assumed, the total number of pairs $N_{\rm tot}$ produced in one second can be estimated as $N_{\rm tot} \approx 2 \times 10^3$, in accordance with the Bethe-Heitler cross section. If now the gamma photon beam is synchronized with a strong laser field with $\xi = 10$, corresponding to pulse energy 1.4 J, 1 ps pulse duration, wavelength 1054 nm focused to one wavelength (available at the Vulcan laser facility [33], at repetition rate 1 Hz), all produced pairs will emerge in the angular cone $\theta_+ \approx 6^\circ \pm 2^\circ$, $\varphi_+ = 90^\circ \pm 0.3^\circ$ relative to the laser propagation direction, in the plane spanned by the propagation direction and the polarization direction. Placing a detector in this direction will therefore detect essentially all of the created pairs. We conclude that the proposed scheme of pair creation by a gamma photon together with channeling of the pairs with a strong laser is a realistic way to observe nonlinear laser effects, accessible to current laser facilities, without resorting to ultrahigh-energy photon or proton beams.

We thank A. Di Piazza for useful discussions. One of us (U.D.J.) acknowledges support by the Deutsche Forschungsgemeinschaft (Heisenberg program).

* Electronic address: Erik.Loetstedt@mpi-hd.mpg.de

[1] H. A. Bethe and W. Heitler, Proc. Roy. Soc. A **146**, 83 (1934).
[2] F. Sauter, Z. Phys **69**, 742 (1931).
[3] J. Schwinger, Phys. Rev. **82**, 664 (1951).
[4] E. Brézin and C. Itzykson, Phys. Rev. D **2**, 1191 (1970).
[5] V. S. Popov, Pis'ma v. Zh. Éksp. Teor. Fiz. **13**, 261 (1971) [JETP Lett. **13**, 185 (1971)].
[6] V. S. Popov, Pis'ma v. Zh. Éksp. Teor. Fiz. **74**, 151 (2001) [JETP Lett. **74**, 133 (2001)].
[7] V. N. Baĭer, V. M. Katkov, and V. M. Strakhovenko, Yad. Fiz. **53**, 1021 (1991) [Sov. J. Nucl. Phys **53**, 632 (1991)].
[8] S. S. Bulanov *et al.*, Zh. Éksp. Teor. Fiz. **129** 14 (2006) [JETP **102**, 9 (2006)].
[9] A. Ringwald, Phys. Lett. B **510**, 107 (2001).
[10] A. Di Piazza, Phys. Rev. D **70**, 053013 (2004).
[11] D. B. Blaschke *et al.*, Phys. Rev. Lett. **96**, 140402 (2006).
[12] H. R. Reiss, J. Math. Phys. **3**, 59 (1962).
[13] A. I. Nikishov and V. I. Ritus, Zh. Éksp. Teor. Fiz. **46** 776 (1964) [Sov. Phys. JETP **19**, 529 (1964)].
[14] N. B. Narozhnyi and M. S. Fofanov, Laser Phys. **7**, 141 (1996).
[15] D. L. Burke *et al.*, Phys. Rev. Lett. **79**, 1626 (1997).
[16] C. Bamber *et al.*, Phys. Rev. D **60**, 092004 (1999).
[17] C. Müller, A. B. Voitkiv, and N. Grün, Phys. Rev. A **67**, 063407 (2003).
[18] A. I. Milstein *et al.*, Phys. Rev. A **73**, 062106 (2006).
[19] P. Sieczka *et al.*, Phys. Rev. A **73**, 053409 (2006).
[20] M. Y. Kuchiev and D. J. Robinson, Phys. Rev. A **76**, 012107 (2007).
[21] M. Y. Kuchiev, Phys. Rev. Lett. **99**, 130404 (2007).
[22] A. V. Borisov, O. G. Goryaga, and V. C. Zhukovskii, Izv. Vyssh. Uchebn. Zaved., Fiz. **20**, 15 (1977) [Rus. Phys. J. **20**, 569 (1977)].
[23] S. P. Roshchupkin, Izv. Vyssh. Uchebn. Zaved., Fiz. **26**, 12 (1983) [Rus. Phys. J. **26**, 683 (1983)].
[24] A. V. Borisov *et al.*, Izv. Vyssh. Uchebn. Zaved., Fiz. **21**, 33 (1978) [Rus. Phys. J. **21**, 1136 (1978)].
[25] H. Mitter, Acta Phys. Austriaca Suppl. **14**, 397 (1975).
[26] D. M. Volkov, Z. Phys. **94**, 250 (1935).
[27] H. R. Reiss and J. H. Eberly, Phys. Rev. **151**, 1058 (1966).
[28] S. P. Roshchupkin, Yad. Fiz. **41**, 1244 (1985) [Sov. J. Nucl. Phys. **41**, 796 (1985)].
[29] S. Schnez *et al.*, Phys. Rev. A **75**, 053412 (2007).
[30] L. De Braeckeleer, E. G. Adelberger, and A. García, Phys. Rev. A **46**, R5324 (1992).
[31] M. Hosaka *et al.*, Nucl. Instrum. Methods **A 393**, 525 (1997).
[32] T. Omori *et al.*, Phys. Rev. Lett. **96**, 114801 (2006).
[33] http://www.clf.rl.ac.uk/Facilities/vulcan/laser.htm

C.2 Bethe-Heitler pair creation assisted by a subcritical laser field

Bethe–Heitler pair creation assisted by a subcritical laser field

Erik Lötstedt,* Ulrich D. Jentschura, and Christoph H. Keitel
Max-Planck-Institut für Kernphysik, Postfach 103980, 69029 Heidelberg, Germany
(Dated: January 15, 2008)

We investigate the cross section for the production of electron-positron pairs in the field of a laser wave and a nucleus. Specifically, we consider pair production by the fusion of a non-laser mode photon, whose energy exceeds the pair production threshold, with an arbitrary number of laser photons. The peak electric field of the laser is assumed to be much smaller than the critical field. The total cross section is estimated to be almost unchanged with respect to the Bethe–Heitler formula by the presence of the laser, whereas the differential cross section is found to be drastically modified.

PACS numbers: 12.20.Ds, 25.75.Dw, 32.80.Wr

I. INTRODUCTION

The creation of an electron-positron pair by an external electromagnetic field is a striking manifestation of the equivalence of matter and energy. That not only energetic photon fields, but also strong, macroscopic electric fields can produce pairs was first predicted by Sauter [1] and later considered by Schwinger [2]. The basic prediction is that pairs are spontaneously created, but the rate is exponentially damped unless the electric field strength exceeds the so-called critical field $E_c = m^2/|e|$, where m is the electron mass, $e = -|e|$ the electron charge, and we use natural units such that $c = \hbar = 1$. The transition from the nonperturbative, tunneling regime for pair production to high-frequency perturbative pair production was studied by Brezin and Itzykson [3] and also by Popov [4, 5]. At present, the strongest electromagnetic fields available in the laboratory are laser fields. However, a plane laser wave cannot alone produce any pairs from the vacuum due to the impossibility of satisfying energy-momentum conservation. Just like in a static magnetic field [6, 7], a probing particle is needed in order to obtain a nonvanishing pair production rate. If the laser wave is not plane but a focused pulse [8], or a standing laser wave [9–11], pair production is possible without a second agent.

Laser induced pair production with an additional source of momentum was first investigated theoretically in the context of pair production by simultaneous absorption of one non-laser-mode photon and a number of laser-mode photons [12, 13]; quite recently, this process was also observed experimentally [14, 15]. Another possibility discussed in the literature is laser-induced pair creation in the vicinity of a nucleus. Unfortunately, for a nucleus at rest, the pair production rates are very low [16–20]. Recently, this process has been reexamined, with the idea of introducing a moving nucleus [21–26]. By letting the nucleus collide head on with the laser beam at high Lorentz factor γ, in the rest frame of the nucleus the frequency of the laser beam will be blue-shifted or enhanced with a factor of approximately 2γ. In this way, the peak electric field seen by the nucleus in its rest frame approaches the critical field, and the rates are calculated to reach observable values.

In this paper, we investigate the possibility to create pairs from vacuum in the presence of three external fields: a laser field, a Coulomb field and a single photon, whose frequency exceeds the pair production threshold. The Feynman diagrams are shown in Fig. 1. The matrix element for this process was first calculated by Roshchupkin [27], and also by Borisov *et. al.* in [28, 29], however without performing any concrete numerical evaluations. The matrix element has a crossing symmetry with the one for laser-assisted bremsstrahlung, which was studied previously in many papers, including Ref. [30], and by us recently in [31, 32].

In our case, pair production is possible in the absence of the laser field through the Bethe-Heitler process [33], because we assume the angular frequency ω^γ of the single photon to be larger than the threshold $2m$ (we denote the frequency of the single photon by a superscript rather than a subscript in view of a rather large number of Lorentz subscripts that we will need to introduce in the analysis later). The presence of the laser will then modify the process, so that we can speak about laser-assisted pair production. By contrast, if $\omega^\gamma < 2m$, the laser field would not really assist; it would be even necessary to produce any pairs at all, and we would call the process laser-induced rather than just laser-assisted.

We note the general observation [34] that to produce an appreciable number of pairs, the electric field in the rest frame of the nucleus has to exceed the critical field. We thus expect that for a subcritical field, the *total* rate of laser-assisted pair production will be essentially unaffected by the laser field. However, the *differential* rates, that is, the dependence of the production rate on the directions and energy of the produced particles, can change drastically. For the same reasons, we expect the rate to be very small for a subcritical field and $\omega^\gamma < 2m$, where the Bethe-Heitler rate vanishes identically. All of the assertions above will be demonstrated in the paper by explicit numerical evaluation.

The paper is organized as follows. In Sec. II, we introduce the theory necessary to describe the laser-assisted process, including Volkov states and the Dirac-Volkov propagator, leading to the expression for the S-matrix elements. Next, we present numerical results together with a detailed discussion in Sec. III. An Appendix is dedicated to an efficient algorithm for the numerical evaluation of generalized Bessel functions, which occur quite naturally in the treatment of the problem.

*Electronic address: Erik.Loetstedt@mpi-hd.mpg.de

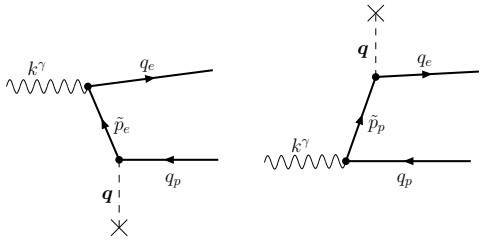

FIG. 1: Feynman diagrams describing the process of laser-assisted pair creation. Laser-dressed fermions are denoted by thick lines. The electron effective four-momentum in the laser field is q_e, and the laser-dressed positron has an effective momentum q_p. The momentum of the virtual state in the laser-dressed propagator is $\tilde{p}_{e,p}$. The virtual Coulomb photon with spatial momentum $\boldsymbol{q}$ is drawn as a dashed line, and the absorbed high-energy photon with momentum k^γ as a wavy line. The direction of time is from left to right.

II. THEORY

In this section, we review the theory used to describe laser-matter interaction. The interaction of the electron and positron with the laser field will be treated non-perturbatively, whereas the interaction with the high-frequency photon field and the Coulomb field is taken into account by first-order perturbation theory.

A. Volkov wave functions and propagator

We start from the Dirac equation coupled to an external plane electromagnetic wave $A_\mu(\phi)$:

$$(i\hat{\partial} - e\hat{A}(\phi) - m)\psi(x) = 0, \tag{1}$$

where $\phi = k^\mu x_\mu$ is the phase of the wave, and k^μ is the wave vector. Scalar products will be written with a dot as $a \cdot b = a_\mu b^\mu = a_0 b^0 - \boldsymbol{a}\cdot\boldsymbol{b}$, and a hat denotes the contraction with the Dirac gamma matrices: $\hat{A} = \gamma^\mu A_\mu$. The solution to Eq. (1) is the well known Volkov solution [35] and reads

$$\psi_\mp(x) = \sqrt{\frac{m}{Q}}\left(1 \mp \frac{e\hat{A}\,\hat{k}}{2k\cdot p}\right) u_p^\mp \exp\left[iS_\mp(x,p)\right], \tag{2}$$

where

$$S_\mp(x,p) = \mp p\cdot x \mp \int_{\phi_0}^{\phi}\left(\frac{e\,p\cdot A(\phi')}{k\cdot p} \mp \frac{e^2A^2(\phi')}{2k\cdot p}\right)d\phi'. \tag{3}$$

Here, $\psi_-(x)$ denotes the electron wave function, and $\psi_+(x)$ is the corresponding positron wave function. Note that e always denotes the charge of the electron. The spinor $u_p^\mp$ satisfies $(\hat{p} \mp m)u_p^\mp = 0$. In the following, we specialize to a monochromatic laser wave of linear polarization,

$$A_\mu(\phi) = a\,\epsilon_\mu\cos(\phi), \tag{4}$$

where $\epsilon_\mu = (0,\boldsymbol{\epsilon})$ is the polarization vector satisfying $\epsilon^2 = -1$, $k\cdot\epsilon = 0$, and a is the amplitude of the vector potential. The integral in Eq. (3) can then be performed analytically and reads

$$\begin{aligned} S_\mp(x,p) &= \mp p\cdot x \mp \frac{e^2a^2}{4k\cdot p}\phi - \frac{eap\cdot\epsilon}{k\cdot p}\sin\phi \\ &\quad \mp \frac{e^2a^2}{8k\cdot p}\sin(2\phi) \\ &= \mp q\cdot x - \alpha\sin\phi \pm \beta\sin(2\phi), \end{aligned} \tag{5}$$

where in the last line we have defined the effective momentum $q_\mu = p_\mu + e^2a^2k_\mu/(4k\cdot p)$, with corresponding effective mass $m_*^2 = q^2 = m^2 + e^2a^2/2$, effective energy $Q = q_0$, and the other parameters are $\alpha = e\,a\,(p\cdot\epsilon)/(k\cdot p)$ and $\beta = -e^2\,a^2/(8k\cdot p)$. Later, when we write down the matrix element we will use the following Fourier decomposition of the wave function (2):

$$\begin{aligned} \psi_\mp(x) =& \sqrt{\frac{m}{Q}}\sum_{s=-\infty}^{\infty}\exp\left(\mp iq\cdot x - ik\cdot x\right) \\ &\times\left(A_0(s,\alpha,\pm\beta) \pm \frac{ea\hat{k}\hat{\epsilon}}{2k\cdot p}A_1(s,\alpha,\pm\beta)\right)u_\mp(p), \end{aligned} \tag{6}$$

where the generalized Bessel function $A_0(s,\alpha,\beta)$ is defined as an infinite sum over products of ordinary Bessel functions,

$$A_0(s,\alpha,\beta) = \sum_{n=-\infty}^{\infty} J_{2n+s}(\alpha)J_n(\beta), \tag{7}$$

and for positive integer i

$$A_i(s,\alpha,\beta) = \frac{1}{2}\left(A_{i-1}(s-1,\alpha,\beta) + A_{i-1}(s+1,\alpha,\beta)\right). \tag{8}$$

The generalized Bessel function was first introduced by Reiss [12], and was later studied by several authors [13, 36–39]. In the Appendix, we discuss some of the properties of $A_0(s,\alpha,\beta)$ and also present an efficient algorithm for their numerical evaluation.

To write down a second-order matrix element we also need the Dirac-Volkov propagator $G(x,x')$, which can be expressed in a number of different ways [40]. We use the repre-

sentation [41, 42]

$$
\begin{aligned}
G(x,x') &= \int \frac{d^4p}{(2\pi)^4}\left(1+\frac{e\hat{k}\hat{A}(\phi)}{2k\cdot p}\right)\frac{\hat{p}+m}{p^2-m^2+i0}\\
&\times\left(1+\frac{e\hat{A}(\phi)\hat{k}}{2k\cdot p}\right)\exp\left[iS_-(x,p)-iS_-(x',p)\right]\\
&=\int\frac{d^4p}{(2\pi)^4}\sum_{s,s'=-\infty}^{\infty}\left(A_0(s,\alpha,\beta)+\frac{ea\hat{k}\hat{\epsilon}}{2k\cdot p}A_1(s,\alpha,\beta)\right)\\
&\times\frac{\hat{p}-\frac{e^2a^2}{4k\cdot p}\hat{k}+m}{p^2-m_*^2+i0}\,\mathrm{e}^{-ip\cdot(x-x')-ik\cdot(sx-s'x')}\\
&\times\left(A_0(s',\alpha,\beta)+\frac{ea\hat{\epsilon}\hat{k}}{2k\cdot p}A_1(s',\alpha,\beta)\right),
\end{aligned}
\tag{9}
$$

where in the last equality have used the specific form (4) of the vector potential, expanded the propagator into a product of two Fourier series, and finally changed variables $p_\mu \to p_\mu + e^2a^2k_\mu/(4k\cdot p)$. This transformation makes the appearance of the effective mass m_* in the propagator denominator explicit.

B. Matrix element and cross section

In our treatment, the final states of the electron and of the positron are described by Volkov states, and the Dirac-Volkov propagator is employed for the intermediate, virtual states, i.e. the interaction of all fermions with the laser field is taken into account to all orders. The effect of the Coulomb field of the nucleus and the gamma photon are calculated using perturbation theory. To this end, we introduce the vector potential $A^C_\mu(x)$ of the nucleus with atomic charge number $Z=1$ (the scaling with Z can later be restored easily) and the vector potential $A^\gamma_\mu(x)$ of the perturbative photon

$$
A^C_\mu(x)=\frac{-e\,\delta_{\mu 0}}{4\pi|\boldsymbol{x}|},\qquad A^\gamma_\mu(x)=\frac{1}{\sqrt{2\omega^\gamma}}\,\epsilon^\gamma_\mu\,e^{-ik^\gamma\cdot x}. \tag{10}
$$

Here, ω^γ denotes the frequency and k^γ_μ the μth component of the momentum four-vector of the gamma photon. Note the minus sign in the exponential in $A^\gamma_\mu(x)$, since photon absorption is the desired process. Expressions (2), (9), and (10) now permit us to write down the matrix element S for the production of one electron with effective momentum q_e and one positron with effective momentum q_p, by absorption of one photon k^γ, corresponding to both Feynman diagrams in Fig. 1:

$$
\begin{aligned}
S&=\sum_{n=-\infty}^{\infty}S_n\delta(Q_p+Q_e+n\omega-\omega^\gamma)\\
&=2\pi i\sum_{n,s=-\infty}^{\infty}\frac{e^3\,m}{\sqrt{2\omega^\gamma Q_pQ_e}}\frac{\delta(Q_p+Q_e+n\omega-\omega^\gamma)}{(\boldsymbol{q}_e+\boldsymbol{q}_p+n\,\boldsymbol{k}-\boldsymbol{k}^\gamma)^2}\\
&\times\bar{u}^-_{p_e}\left(F^s_{4334}(\hat{\epsilon}^\gamma)\frac{\hat{\tilde{p}}_e-\hat{k}e^2a^2/(4k\cdot\tilde{p}_e)+m}{\tilde{p}_e^2-m_*^2}F^{s-n}_{1313}(\gamma^0)\right.\\
&\left.+F^{s+n}_{4224}(\gamma^0)\frac{\hat{\tilde{p}}_p-\hat{k}e^2a^2/(4k\cdot\tilde{p}_p)+m}{\tilde{p}_p^2-m_*^2}F^s_{1212}(\hat{\epsilon}^\gamma)\right)u^+_{p_p},
\end{aligned}
\tag{11}
$$

where

$$
\begin{aligned}
F^m_{KLMN}(X)&=A_0(m,\alpha_K-\alpha_L,\beta_K-\beta_L)X\\
&+A_1(m,\alpha_K-\alpha_L,\beta_K-\beta_L)\left(\frac{Xea\hat{k}\hat{\epsilon}}{2k\cdot p_M}+\frac{ea\hat{\epsilon}\hat{k}X}{2k\cdot p_N}\right)\\
&+A_2(m,\alpha_K-\alpha_L,\beta_K-\beta_L)\frac{e^2\hat{a}\hat{k}X\hat{k}\hat{a}}{4k\cdot p_Mk\cdot p_N},
\end{aligned}
\tag{12}
$$

with $K,L,M,N\in\{1,2,3,4\}$, $X\in\{\hat{\epsilon}^\gamma,\gamma^0\}$,

$$
\alpha_K=ea\epsilon\cdot p_K/(k\cdot p_K),\qquad \beta_K=-e^2a^2/(8k\cdot p_K), \tag{13}
$$

$p_1=-q_p$, $p_2=\tilde{p}_p=-q_p+sk+k^\gamma$, $p_3=\tilde{p}_e=q_e+sk-k^\gamma$ and $p_4=q_e$. We recall that index e (p) is used to label the electron (positron) momentum vector. The expression (11) was first obtained in [27]. The first line in Eq. (11) implicitly defines the nth order matrix element S_n, and the argument of the delta function in Eq. (11) expresses energy conservation in terms of the effective energies Q_p and Q_e. The number $-n$ ($+n$) can be interpreted as the number of photons absorbed from (emitted into) the laser during the process. In particular, the threshold $\omega^\gamma - n\omega \geq 2m_*$ for pair creation is higher than the field-free case, due to the larger effective mass $m_* > m$. From the matrix element we obtain by the usual methods [43] the differential cross section $d\sigma$, averaged over the polarization of the gamma photon and summed over the spins of the electron and positron,

$$
\begin{aligned}
d\sigma=&\frac{1}{2}\sum_{\text{spin, pol.}}\frac{d^3q_p}{(2\pi)^3}\frac{d^3q_e}{(2\pi)^3}\,|S|^2\,\frac{1}{T}\\
=&\frac{1}{4\pi}\sum_{\substack{\text{spin, pol.}\\ n}}\frac{d^3q_p}{(2\pi)^3}\frac{d^3q_e}{(2\pi)^3}|S_n|^2\delta(Q_p+Q_e+n\omega-\omega^\gamma),
\end{aligned}
\tag{14}
$$

where in the last line the delta function is explicitly written out. The matrix element (11) is gauge invariant, both under the gauge transformation $\epsilon_\mu \to \epsilon_\mu + C_1k_\mu$ of the laser field and $\epsilon^\gamma_\mu \to \epsilon^\gamma_\mu + C_2k^\gamma_\mu$, where $C_{1,2}$ are constants. Gauge invariance, especially for the gamma photon field, provides a sensible numerical check of the computer code used to evaluate the

differential cross section (14). In principle, gauge invariance also makes it possible to use the replacement

$$\sum_{\text{polarization}} \epsilon_\mu^\gamma \epsilon_\nu^\gamma = -g_{\mu\nu}\,, \tag{15}$$

for the calculation of the polarization sum. However, numerically the polarization sum is more conveniently done using a specific representation of the polarization vectors. The sum over spins is written like a trace over Dirac gamma matrices, which is performed numerically. Quite counterintuitively, this procedure can be computationally advantageous for traces over Dirac gamma matrices occurring in laser-related problems, where the expressions obtained after taking the traces do not simplify as much as in typical problems from high-energy physics [31, 32].

Another numerical test of correctness is the behavior of the cross section at the apparent singularity when $k \cdot \tilde{p}_{e,p} \to 0$ in the F functions in the expression on the right-hand side of Eq. (11) (we recall that $p_2 = \tilde{p}_p$ and $p_3 = \tilde{p}_e$). The matrix element can be shown to be finite in this limit, but the calculation constitutes a test of numerical stability as the arguments of the generalized Bessel functions tend to infinity.

III. RESULTS AND DISCUSSION

In this section, we present results of a concrete numerical evaluation of the differential cross section (14). The frequency of the laser is taken to be $\omega = 1\,\text{keV}$, and the amplitude a is chosen such that the classical nonlinearity parameter $\xi = -ea/m$ is of order unity. Experimentally, this choice of parameters can be realized in either of the two following scenarios. For a high-power laser, operating at a photon energy of $1\,\text{eV}$ and intensity of 9×10^{17} W/cm^2, head-on collision with a relativistic nucleus with a Lorentz boost factor $\gamma \approx 500$ will give $\xi = 1$ and $\omega = 1$ keV in the rest frame of the nucleus. In an alternative scenario, a focused x-ray free electron laser [44] applied to a nucelus at rest may also give access to the parameters above. Here $\xi = 1$ and $\omega = 1$ keV in the laboratory frame requires an intensity of 9×10^{23} W/cm^2 at the focus of the laser. In this regime, the peak electric field of the laser is still much smaller than the critical field, $E_{\text{peak}}/E_c = -\xi e\omega/m \ll 1$. We will consider the case where the laser counter propagates with the gamma photon, and describe the direction of the produced electron and positron by an angle $\theta_{e,p}$, as depicted in Fig. 2.

A. Energy cutoff

In principle, since the sum over n in Eq. (11) extends from $-\infty$ to $+\infty$, the created pair can acquire arbitrarily high effective energies Q_p, Q_e. This should be compared to the field-free case, given by the Bethe-Heitler formula [33], where the cross section vanishes identically for positron (or electron) energies $E > \omega^\gamma - m$. In practice, however, an apparent cutoff will occur in the energy spectrum, and thereby limit the available energy for the produced pair. In the following, we will assume the directions $\boldsymbol{q}_e/|\boldsymbol{q}_e|$, $\boldsymbol{q}_p/|\boldsymbol{q}_p|$ of the positron and electron given, and consider the differential cross section (14) as a function of the effective energy Q_p of the positron. The effective energy Q_e of the electron is fixed by energy conservation for each n. It follows from the expression (11) that to find the energy cutoff, we should consider the behavior of the function

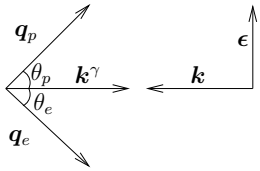

FIG. 2: The geometrical setup of the considered process. The photon with three-momentum $\boldsymbol{k}^\gamma$ collides head on with the laser beam with wave vector $\boldsymbol{k}$ and polarization vector $\boldsymbol{\epsilon}$, producing one positron with effective three-momentum $\boldsymbol{q}_p$, making an angle θ_p with the $\boldsymbol{k}^\gamma$-axis, and one electron with effective three-momentum $\boldsymbol{q}_e$ and angle θ_e. The vectors $\boldsymbol{q}_p$ and $\boldsymbol{q}_e$ lie in the plane spanned by $\boldsymbol{k}$ and $\boldsymbol{\epsilon}$.

$$H_n = \sum_{s=-\infty}^{\infty} \frac{A_0(s, \alpha_e - \tilde{\alpha}, \beta_e - \tilde{\beta})}{s + C} \times A_0(s - n, \alpha_p - \tilde{\alpha}, \beta_p - \tilde{\beta}) \tag{16}$$

as a function of n. As follows from the discussion in Sec. III B, we can assume that C is non-integer. As shown in the Appendix, the function (16) has the same cutoff properties as the generalized Bessel function

$$A_0(n, \alpha_e - \alpha_p, \beta_e - \beta_p), \tag{17}$$

provided C is larger than the cutoff index of the first of the A_0 in the numerator in Eq. (16). As $\beta_e - \beta_p = -[(k \cdot q_e)^{-1} + (k \cdot q_p)^{-1}]\, e^2 a^2/8 < 0$, and high values of Q_p are obtained by absorbing photons, that is, for negative n, it follows that Q_p^{cutoff} is the largest positron energy for which the inequality

$$n_{\text{pos. cutoff}} > |n|, \tag{18}$$

is still satisfied. The integer $n_{\text{pos. cutoff}}$ is defined in Eq. (A.1). Since the quantities $k \cdot q_e$ and $k \cdot q_p$ involve direction cosines, it becomes clear that the energy cutoff is direction dependent. In particular, this implies that the maximal energy Q_p^{cutoff} will depend not only on the direction of the positron, but also on the direction of the electron. In order to determine the direction-dependent energy cutoff, one therefore proceeds as follows. In the first step, one fixes the directions of the electron and positron, which defines $n_{\text{pos. cutoff}}$ as a function of n and Q_p. In the second step, one varies Q_p and in this way find the largest positron effective energy Q_p satisfying Eq. (18).

As a concrete example, we let the positron and electron be ejected at equal angles $\theta_p = \theta_e \equiv \theta$, and show in Fig. 3 the cutoff as a function of θ for different values of the intensity parameter ξ. The frequency of the single photon is

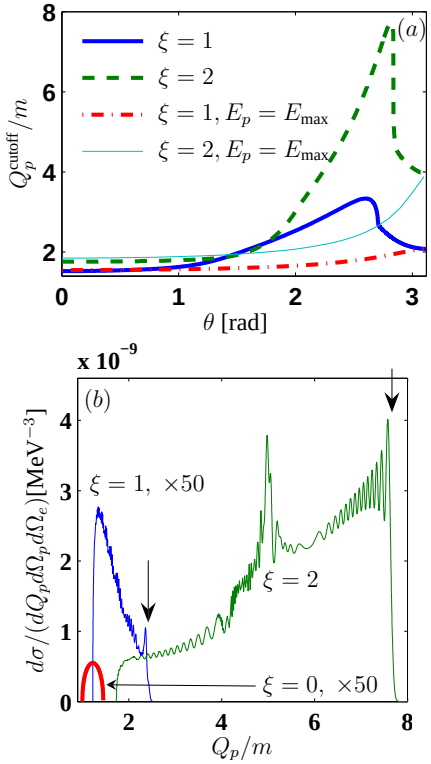

FIG. 3: (Color online) Upper panel: Effective energy cutoff as a function of the angle $\theta = \theta_p = \theta_e$, resulting from the solution of Eq. (18). For comparison, we also show the effective energy that would result if the positron were created with the largest available energy in absence of the laser, $E_p = E_{\max} = m - \omega^\gamma$, and then placed in the laser field with fixed direction of $\boldsymbol{q}_p$ (all curves are labeled accordingly). The difference of the latter two curves to the laser-dressed solution is because of the correlation between the electron and positron induced by the laser. This correlation was also observed in [22]. In the lower panel, we show a concrete example of the cross section, for $\theta = 2.8$ rad, chosen to maximize the cutoff for $\xi = 2$. The "laser-assisted" curves show a complex oscillatory behavior, with a peak just before the cutoff. The cutoffs predicted by Eq. (18) are indicated by arrows. Note that the curves for $\xi = 1$ and $\xi = 0$ were multiplied by a factor 50; the ordinate axis is kept on a linear scale.

$\omega^\gamma = \sqrt{6}\,m$, which corresponds exactly to the threshold value $2m_*$ for $\xi = 1$. In the same figure, we also show a concrete evaluation of the differential cross section for the corresponding parameters, compared to the laser-free case. The magnitude of the differential cross section is here significantly larger that the case without the laser, and also displays a complicated oscillatory behavior.

B. Resonances and competing processes

In principle, the matrix element (11) diverges if one of the intermediate momenta $\tilde{p}_e, \tilde{p}_p$ satisfies the on-shell condition

$$\tilde{p}_e = (q_e + sk - k^\gamma)^2 = m_*^2, \qquad \tilde{p}_p = (k^\gamma - q_p + sk)^2 = m_*^2 \tag{19}$$

for some s. Physically, this means that the considered second-order process splits up into two consecutive first-order processes, laser-induced pair creation by a gamma photon followed by Coulomb scattering of the electron or the positron. This phenomenon has been studied before in the context of laser-assisted electron-electron scattering [45–47] and laser-assisted bremsstrahlung [30–32, 48]. The usual way to regularize the matrix element, so that it remains finite also at the condition (19), is to add a small imaginary part to the energy of the electron (positron) [49], related to the total probability for the intermediate state to decay by Compton scattering. Finite values will results also if the finite extent of the laser field or the frequency width of the laser or photon beam is taken into account. In the current paper, however, we consider a regime of parameters where the resonances are strongly suppressed. Mathematically, this means that the value of s needed to satisfy the resonance condition (19) is larger than the corresponding cutoff index for the generalized Bessel function, and that the contribution from this index in the sum over s is negligible, once properly regularized. Physically speaking, we are dealing with laser parameters such that purely laser-induced processes, that cannot occur in the absence of the laser, have vanishingly small probability to occur. The basic requirement for laser-induced processes like pair creation by a photon [13] (at photon frequency $\omega^\gamma \approx 2m_*$) or pair creation by a nucleus [16] to have substantial probability is that the peak electric field $E_{\rm peak} = a\omega$ should be comparable to the critical field, $E_{\rm peak}/E_c \approx 1$, and, as mentioned before, we consider only laser parameters a, ω such that $E_{\rm peak} \ll E_c$. This also means that at the field strengths considered, there will be no competing processes, so that our process will indeed be the dominating one.

C. Angular distribution

For the field-free case, the pairs prefer to emerge at an angle $\theta \sim m/\omega^\gamma$ with the vector $\boldsymbol{k}^\gamma$ [33]. When the laser field is turned on, we expect to find more pairs in the direction of the laser wave vector $\boldsymbol{k}$. In Fig. 4, we display the differential cross section integrated over dQ_p and dQ_e, for $\xi = 1, 2$. The peak is seen to shift from the direction of the gamma photon to the direction of the laser wave.

D. Total cross section

The total cross section is obtained by integrating the differential cross section (14) over the energies Q_p, Q_e and solid

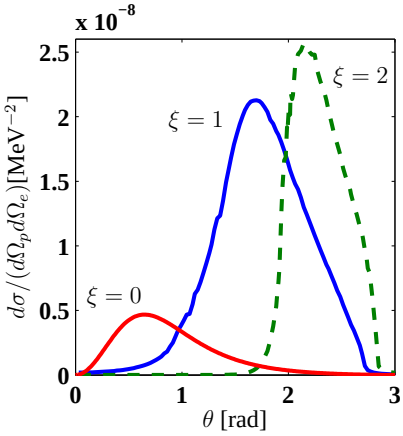

FIG. 4: (Color online) The differential cross section integrated over the effective energy $Q_{p,e}$, for $\xi = 0$ (solid red line), $\xi = 1$ (solid blue line) and for $\xi = 2$ (dashed green line). As in Fig. 3, $\omega^\gamma = \sqrt{6}\,m$. The pair is emitted at equal angles $\theta_p = \theta_e = \theta$ (see Fig. 2), in the plane spanned by $\boldsymbol{k}$ and $\boldsymbol{\epsilon}$. We note that the area under these curves are notably different, which implies that the presence of the laser enhances the number of pairs produced at $\theta_p = \theta_e$. The differential cross section integrated over all angles will however, as we will see later (see Fig. 5), be almost unchanged as compared to the laser free case.

angles Ω_e, Ω_p of the produced positron and electron:

$$\sigma_{\rm tot} = \int \frac{1}{2} \sum_{\substack{\text{spin, pol.} \\ n}} \frac{Q_p |\boldsymbol{q}_p| dQ_p d\Omega_p}{(2\pi)^3} \frac{Q_e |\boldsymbol{q}_e| dQ_e d\Omega_e}{(2\pi)^3} \times |S_n|^2 \delta(Q_p + Q_e + n\omega - \omega^\gamma). \quad (20)$$

Here, it is convenient to replace the sum over the number of exchanged photons n by an integral, and to evaluate this integral with the delta function so that n equals the integer closest to $(\omega^\gamma - Q_p - Q_e)/\omega$. This is a good approximation since $\omega \ll Q_{e,p}, \omega^\gamma$. The remaining six-fold integral has to be performed numerically (we employ a Monte Carlo method). We note that this method has been used before to obtain total rates for the production of pairs from a colliding laser beam and a nucleus [25, 26]. In general, Monte Carlo integration is the method of choice for integrals of high dimensionality where the accuracy demand is modest. The result of one such calculation is shown in Fig. 5, where we present the total cross section as a function of the frequency ω^γ of the perturbative photon. As expected, in the region where pair production is possible without the laser, the rates are almost indistinguishable.

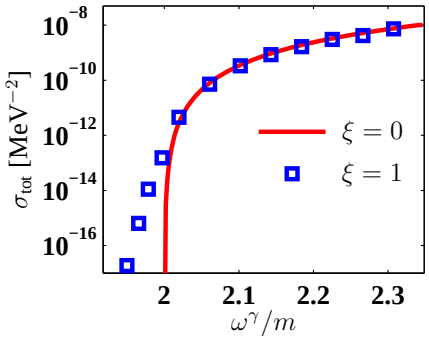

FIG. 5: (Color online) The total cross section as a function of the frequency ω^γ of the non-laser mode photon, compared with the case without the laser field. The laser frequency used is $\omega = 1$ keV. Due to the laser, there remains a finite probability of pair creation below the field-free threshold $\omega^\gamma = 2m$. However, the magnitude drops exponentially, as expected.

IV. CONCLUSIONS

In this paper, we have presented a calculation of the laser-assisted Bethe-Heitler process, i.e. pair production by a high-frequency photon in the presence of a nuclear Coulomb field and an intense laser field. The regime of parameters considered was for a subcritical laser field, that is the peak electric field of the laser was much smaller than the critical field $E_c = m^2/|e|$, but with a the nonlinear parameter ξ of order unity and the gamma photon frequency $\omega^\gamma > 2m$. In this regime, pair production is possible without the field, and as the laser field strength is below the critical field, it is expected that the total rates are almost unaffected by the laser. This was confirmed by evaluating the six-fold integral for the total cross section numerically (see Fig. 5). However, the differential cross section was found to be drastically altered by the presence of the laser wave, as shown in Fig. 4. Finally, we note that all cross sections shown here are evaluated for a nuclear charge number $Z = 1$ and scale as Z^2, since we have taken into account the Coulomb field in first-order perturbation theory.

Clear laser-assisted signatures are thus expected in the differential cross sections, and these might provide an opportunity for interesting experiments in the near future.

Acknowledgments

We thank A. Di Piazza for useful discussions. One of the authors (U.D.J.) acknowledges support by the Deutsche Forschungsgemeinschaft (Heisenberg program).

APPENDIX: CUTOFF PROPERTIES AND EVALUATION OF THE GENERALIZED BESSEL FUNCTIONS

1. Cutoff rules

Important for the understanding of physical processes expressed through generalized Bessel functions is the cutoff behavior. A rule is needed for how many terms should be included in sums like Eq. (11) to reach convergence. For the usual Bessel function $J_n(\alpha)$, the cutoff rule is well known: for $n > \alpha$ (positive n, α) the magnitude of $J_n(\alpha)$ will drop sharply as $J_n(\alpha) \sim \alpha^n/n^{n+\frac{1}{2}}$, and the cutoff is therefore $n \approx \alpha$. For the generalized Bessel function $A_0(n,\alpha,\beta)$, the correct rule reads for positive α and β

$$\begin{aligned} n_{\text{pos. cutoff}} &= \begin{cases} \alpha - 2\beta & \text{if } 8\beta < \alpha \\ 2\beta + \frac{\alpha^2}{16\beta} & \text{if } 8\beta > \alpha \end{cases}, \\ n_{\text{neg. cutoff}} &= -\alpha - 2\beta. \end{aligned} \tag{A.1}$$

For negative α, β we use the symmetries

$$\begin{aligned} A_0(n,\alpha,-\beta) &= (-1)^n A_0(-n,\alpha,\beta), \\ A_0(n,-\alpha,\beta) &= (-1)^n A_0(n,\alpha,\beta). \end{aligned} \tag{A.2}$$

Beyond the cutoff, $|A_0(n,\alpha,\beta)|$ will show inverse factorial decrease $\sim n^{-n-\frac{1}{2}}$, similar to $J_n(\alpha)$. An example of $A_0(n,\alpha,\beta)$ is displayed in Fig. 6. These cutoff rules can be derived from the asymptotic expansion by the saddle point method [13, 36, 50] or from the maximal and minimal value of the classically allowed energy for an electron moving in a plane electromagnetic wave [51].

2. The function H_n

Regarding the function H_n, as appeared in Eq. (16)

$$H_n = \sum_{s=-\infty}^{\infty} \frac{A_0(s,\alpha,\beta)\, A_0(s-n,\gamma,\delta)}{s+C}, \tag{A.3}$$

we can use the expansion

$$\frac{1}{s+C} = \frac{1}{C} - \frac{s}{C^2} + \frac{s^2}{C^3} + \ldots, \tag{A.4}$$

and then perform the sum over s with the addition theorem for generalized Bessel functions, for each term in the expansion (A.4). Provided C is larger than the cutoff index of the first of the generalized Bessel functions entering the sum in Eq. (A.3), we can then write

$$\begin{aligned} H_n(\alpha,\beta,\gamma,\delta) = &\frac{A_0(n,\alpha-\gamma,\beta-\delta)}{C} + \frac{W_2(n,\alpha,\beta,\gamma,\delta)}{C^2} \\ &+ \frac{W_3(n,\alpha,\beta,\gamma,\delta)}{C^3} + \ldots. \end{aligned} \tag{A.5}$$

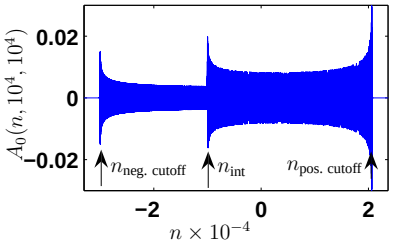

FIG. 6: (Color online) The generalized Bessel function $A_0(n,\alpha,\beta)$ as a function of n, with $\alpha = \beta = 10^4$. Indicated are the positive cutoff $n_{\text{pos. cutoff}} = 2\beta + \alpha^2/(16\beta) = 20625$, the negative cutoff $n_{\text{neg. cutoff}} = -2\beta - \alpha = -3 \times 10^4$ as well as the index for the transition to another "plateau", given by $n_{\text{int}} = -2\beta + \alpha = -10^4$.

We also give the expression for the first correction W_2:

$$\begin{aligned} W_2(n,\alpha,\beta,\gamma,\delta) = -\frac{\alpha}{2}&[A_0(n-1,\Gamma,\Delta) \\ &+ A_0(n+1,\Gamma,\Delta)] \\ &+\beta[A_0(n-2,\Gamma,\Delta) + A_0(n+2,\Gamma,\Delta)], \end{aligned} \tag{A.6}$$

where $\Gamma = \alpha - \gamma$ and $\Delta = \beta - \delta$. It is now clear that $H_n(\alpha,\beta,\gamma,\delta)$ will have the same cutoff behavior as $A_0(n,\alpha-\gamma,\beta-\delta)$, under the stated conditions.

3. Algorithm for numerical evaluation

In order to investigate the problem in the present paper numerically, a large number of generalized Bessel functions for different indices, but of the same arguments were needed, in particular to accurately evaluate functions like H_n discussed above. In analogy with the usual Bessel function, generalized Bessel functions satisfy a recursion relation, relating one index with its four neighbors:

$$\begin{aligned} 2nA_0(n,\alpha,\beta) = &\alpha\left[A_0(n-1,\alpha,\beta) + A_0(n+1,\alpha,\beta)\right] \\ &- 2\beta\left[A_0(n-2,\alpha,\beta) + A_0(n+2,\alpha,\beta)\right]. \end{aligned} \tag{A.7}$$

The recursion relation (A.7) is however numerically stable only for certain intervals of the index n, and cannot be used directly for a numerical evaluation. We have found that it is possible to make the recursion stable for arbitrary n, if we transform the recursion relation (A.7) into a third-order relation by letting each of the coefficients satisfy its own recursion relation. In the following, we describe the algorithm for positive n, the treatment of negative n is completely analogous. We also assume $\alpha \neq 0$. In the case $\alpha = 0$ the generalized Bessel function $A_0(n,\alpha,\beta)$ can be expressed as an ordinary Bessel function. After the transformation, the function $A_0(n,\alpha,\beta)$ will satisfy

$$2\beta A_0(n-1,\alpha,\beta) + \kappa_n A_0(n,\alpha,\beta) + \lambda_n A_0(n+1,\alpha,\beta) = 0, \tag{A.8}$$

if the coefficients κ_n and λ_n are defined recursively like

$$\begin{aligned} \kappa_n &= \zeta_n - \frac{2\beta\xi_n}{\lambda_{n+1}}, \\ \lambda_n &= \eta_n - \frac{\kappa_{n+1}\xi_n}{\lambda_{n+1}}, \end{aligned} \tag{A.9}$$

where ζ_n, η_n and ξ_n are again defined recursively as

$$\begin{aligned} \zeta_n &= -\alpha - \frac{4\beta^2}{\xi_{n+1}}, \\ \eta_n &= 2(n+1) - \frac{2\beta\zeta_{n+1}}{\xi_{n+1}}, \\ \xi_n &= -\alpha - \frac{2\beta\eta_{n+1}}{\xi_{n+1}}. \end{aligned} \tag{A.10}$$

The above definitions provide a numerically stable algorithm for calculating $A_0(n,\alpha,\beta)$ as follows. The recursion (A.9) for the coefficients is started at a large index $n_0 > n_{\text{pos. cutoff}}$ [see Eq. (A.1)] with non-zero but otherwise arbitrary initial conditions, in the downward direction for n. When the coefficients $\kappa_{n_0}, \kappa_{n_0-1}, \ldots, \kappa_1$ and $\lambda_{n_0}, \lambda_{n_0-1}, \ldots, \lambda_1$ are calculated, the recursion relation (A.8), this time applied in the direction of increasing n, together with two initial values $A_0(0,\alpha,\beta)$, $A_0(1,\alpha,\beta)$ is used to calculate the complete array $A_0(0 \le n \le n_0, \alpha, \beta)$. The two initial values are computed efficiently either from the definition (7), or for large values of the arguments α, β by an asymptotic expansion [36]. The described algorithm provides a very efficient way of calculating a large number of generalized Bessel function of the same arguments, but of different order. As far as the accuracy is concerned, essentially no significant figures are lost during the recursion, even for very high orders $n > n_{\text{pos. cutoff}}$. The accuracy is therefore limited by that of the initial values $A_0(0,\alpha,\beta)$, $A_0(1,\alpha,\beta)$. We also estimated numerically the minimum value of the quantity $N = n_0 - n_{\text{pos. cutoff}}$ needed to reach the precision of the initial values, and found $N_{\text{min}} \approx B(n_{\text{pos. cutoff}})^{0.3}$. Here B is a constant depending on α and β of the order $O(10)$.

[1] F. Sauter, Z. Phys **69**, 742 (1931).
[2] J. Schwinger, Phys. Rev. **82**, 664 (1951).
[3] E. Brezin and C. Itzykson, Phys. Rev. D **2**, 1191 (1970).
[4] V. S. Popov, Pis'ma v. Zh. Éksp. Teor. Fiz. **13**, 261 (1971) [JETP Lett. **13**, 185 (1971)].
[5] V. S. Popov, Pis'ma v. Zh. Éksp. Teor. Fiz. **74**, 151 (2001) [JETP Lett. **74**, 133 (2001)].
[6] V. N. Baĭer, V. M. Katkov, and V. M. Strakhovenko, Yad. Fiz. **14**, 1020 (1971) [Sov. J. Nucl. Phys **14**, 572 (1972)].
[7] V. N. Baĭer, V. M. Katkov, and V. M. Strakhovenko, Yad. Fiz. **53**, 1021 (1991) [Sov. J. Nucl. Phys **53**, 632 (1991)].
[8] S. S. Bulanov, N. B. Narozhny, V. D. Mur, and V. S. Popov, Zh. Éksp. Teor. Fiz. **129**, 14 (2006) [JETP **102**, 9 (2006)].
[9] H. K. Avetissian, A. K. Avetissian, G. F. Mkrtchian, and K. V. Sedrakian, Phys. Rev. E **66**, 016502 (2002).
[10] A. Di Piazza, Phys. Rev. D **70**, 053013 (2004).
[11] D. B. Blaschke, A. V. Prozorkevich, C. D. Roberts, S. M. Schmidt, and S. A. Smolyansky, Phys. Rev. Lett. **96**, 140402 (2006).
[12] H. R. Reiss, J. Math. Phys. **3**, 59 (1962).
[13] A. I. Nikishov and V. I. Ritus, Zh. Éksp. Teor. Fiz. **46**, 776 (1964) [Sov. Phys. JETP **19**, 529 (1964)].
[14] D. L. Burke, R. C. Field, G. Horton-Smith, J. E. Spencer, D. Walz, S. C. Berridge, W. M. Bugg, K. Shmakov, A. W. Weidemann, C. Bula, et al., Phys. Rev. Lett. **79**, 1626 (1997).
[15] C. Bamber, S. J. Boege, T. Koffas, T. Kotseroglou, A. C. Melissinos, D. D. Meyerhofer, D. A. Reis, W. Ragg, C. Bula, K. T. McDonald, et al., Phys. Rev. D **60**, 092004 (1999).
[16] V. P. Yakovlev, Zh. Éksp. Teor. Fiz. **49**, 318 (1965) [Sov. Phys. JETP **22**, 223 (1966)].
[17] M. H. Mittleman, Phys. Rev. A **35**, 4624 (1987).
[18] A. I. Milstein, C. Müller, K. Z. Hatsagortsyan, U. D. Jentschura, and C. H. Keitel, Phys. Rev. A **73**, 062106 (2006).
[19] M. Yu. Kuchiev and D. J. Robinson, Phys. Rev. A **76**, 012107 (2007).
[20] M. Yu. Kuchiev, Phys. Rev. Lett. **99**, 130404 (2007).
[21] C. Müller, A. B. Voitkiv, and N. Grün, Nucl. Instrum. Meth. Phys. Res. B **205**, 306 (2003).
[22] C. Müller, A. B. Voitkiv, and N. Grün, Phys. Rev. A **67**, 063407 (2003).
[23] C. Müller, A. B. Voitkiv, and N. Grün, Phys. Rev. Lett. **91**, 223601 (2003).
[24] C. Müller, A. B. Voitkiv, and N. Grün, Phys. Rev. A **70**, 023412 (2004).
[25] J. Z. Kamiński, K. Krajewska, and F. Ehlotzky, Phys. Rev. A **74**, 033402 (2006).
[26] P. Sieczka, K. Krajewska, J. Z. Kamiński, P. Panek, and F. Ehlotzky, Phys. Rev. A **73**, 053409 (2006).
[27] S. P. Roshchupkin, Izv. Vyssh. Uchebn. Zaved., Fiz. **26**, 12 (1983) [Rus. Phys. J. **26**, 683 (1983)].
[28] A. V. Borisov, O. G. Goryaga, and V. C. Zhukovskii Izv. Vyssh. Uchebn. Zaved., Fiz. **20**, 15 (1977) [Rus. Phys. J. **20**, 569 (1977)].
[29] A. V. Borisov, V. C. Zhukovskii, A. K. Nasirov, and P. A. Éminov Izv. Vyssh. Uchebn. Zaved., Fiz. **24**, 12 (1981), [Rus. Phys. J. **24**, 107 (1981)].
[30] S. P. Roshchupkin, Yad. Fiz. **41**, 1244 (1985) [Sov. J. Nucl. Phys. **41**, 796 (1985)].
[31] E. Lötstedt, U. D. Jentschura, and C. H. Keitel, Phys. Rev. Lett. **98**, 043002 (2007).
[32] S. Schnez, E. Lötstedt, U. D. Jentschura, and C. H. Keitel, Phys. Rev. A **75**, 053412 (2007).
[33] H. A. Bethe and W. Heitler, Proc. Roy. Soc. A **146**, 83 (1934).
[34] W. Becker, G. T. Moore, R. R. Schlicher, and M. O. Scully, Phys. Lett. A **94**, 131 (1983).
[35] D. M. Volkov, Z. Phys. **94**, 250 (1935).
[36] C. Leubner, Phys. Rev. A **23**, 2877 (1981).
[37] G. Dattoli, L. Giannessi, L. Mezi, and A. Torre, Nuovo Cim. **105 B**, 327 (1990).
[38] G. Dattoli, A. Torre, S. Lorenzutta, G. Maino, and C. Chiccoli, Nuovo Cim. **106 B**, 21 (1991).
[39] H. J. Korsch, A. Klumpp, and D. Witthaut, J. Phys. A **39**, 14947

(2006).
[40] H. R. Reiss and J. H. Eberly, Phys. Rev. **151**, 1058 (1966).
[41] H. Mitter, Acta Phys. Austriaca Suppl. **14**, 397 (1975).
[42] V. I. Ritus, Trud. Ord. Len. Fiz. Inst. im. P. N. Leb. Akad. Nauk SSSR **11**, 5 (1979) [J. Rus. Laser Res. **6**, 497 (1985)].
[43] W. Greiner and J. Reinhardt, *Quantenelektrodynamik (Band VII der Lehrbuchreihe über Theoretische Physik)* (Harry Deutsch, Frankfurt a. M., 1995), 2nd ed.
[44] A. Ringwald, Phys. Lett. B **510**, 107 (2001).
[45] V. P. Oleĭnik, Zh. Éksp. Teor. Fiz. **52**, 1049 (1967) [Sov. Phys. JETP **25**, 697 (1967)].
[46] J. Bös, W. Brock, H. Mitter, and T. Schott, J. Phys. A **12**, 715 (1979).
[47] P. Panek, J. Z. Kamiński, and F. Ehlotzky, Phys. Rev. A **69**, 013404 (2004).
[48] S. P. Roshchupkin, Laser Phys. **12**, 498 (2001).
[49] W. Becker and H. Mitter, J. Phys. A **9**, 2171 (1976).
[50] H. R. Reiss, Phys. Rev. A **22**, 1786 (1980).
[51] V. G. Bagrov and D. M. Gitman, *Exact Solutions of Relativistic Wave Equations* (Kluwer Academic Publishers, Dordrecht, 1990).

C.3 QED effects in strong laser fields

QED effects in strong laser fields

A. Di Piazza, E. Lötstedt, K. Z. Hatsagortsyan, U. D. Jentschura, and C. H. Keitel
Max-Planck-Institut für Kernphysik, D-69117 Heidelberg, Germany

Quantum electrodynamical processes occurring in the presence of a strong laser field are discussed. We review the processes of vacuum high-harmonic generation and light-by-light diffraction that we have studied recently as a means of testing vacuum polarization effects in a strong laser field. Then, we investigate in detail two processes which are more feasible experimentally: laser photon merging in laser-proton collisions and laser-assisted bremsstrahlung.

1 Introduction

Quantum Electrodynamics (QED) has been tested experimentally under very different conditions. Its predictions especially in atomic physics have been confirmed by experiments with very high accuracy like those on the anomalous magnetic moment of the electron or the Lamb shift (see the recent reviews [1, 2] and the references therein). However, many of these tests relate to perturbative QED in which the theoretical predictions are extracted starting from the Dyson expansion of the S-matrix with respect to the fine-structure constant $\alpha = e^2/4\pi \approx 1/137$ [3]. Here, we have introduced the electron charge $-e < 0$ and we have used, as throughout this Report, natural units with $\hbar = c = 1$. Experimental tests of QED in the presence of classical strong electromagnetic fields have so far been successful mostly in the case of strong Coulomb fields, i. e. the fields created by highly charged nuclei. In the context of QED the expression "highly charged nuclei" indicates nuclei with a charge number $Z \lesssim 1/\alpha \approx 137$. In fact, these nuclei produce an electric field of the order of the "critical" electric field $E_{cr} = m^2/e = 1.3 \times 10^{16}$ V/cm (m is the electron mass) at the typical QED length given by the Compton length $\lambda_c = 1/m$. In turn, an electric field of the order of the critical field E_{cr} is able to create electron-positron pairs in vacuum [4]. The Coulomb field produced by highly charged nuclei is so strong that higher orders in $Z\alpha$ contribute significantly to the QED predictions at the current level of experimental accuracy, even for low nuclear charge number (see the recent Refs. [5, 6, 7, 8, 9]). In some cases, as for the vacuum polarization effects induced by strong classical electromagnetic fields, even all orders in $Z\alpha$ have to be included because nonperturbative effects cannot be neglected. This has been experimentally tested in the case of the Delbrück scattering [10], i. e. the scattering of a photon by the Coulomb field of a heavy nucleus and of the photon splitting in a strong Coulomb field [11]. The theoretical predictions developed in [12, 13] have been confirmed.

Vacuum polarization effects in strong constant and uniform magnetic fields have also been studied theoretically. These effects become apparent in the presence of magnetic fields with an amplitude of the order of the so-called critical magnetic field $B_{cr} = m^2/e = 4.41 \times 10^{13}$ G [14, 15]. Such strong magnetic fields cannot be created in laboratory and this is why vacuum effects in the presence of strong magnetic fields can significantly occur only in astrophysical environments like around highly magnetized neutron stars [16, 17, 18].

The rapid development of laser technology allows for the use of intense laser fields even to probe QED in the presence of a strong wave field. Table-top multiterawatt lasers which are already available are employed to create new x-ray and γ-ray radiation sources [19], to accelerate electrons, protons and ions to high energies [20] and even to prime nuclear fusion reactions [21]. Moreover, theoretical proposals have been put forward to reach the critical electric field by focusing the high-order harmonics generated in the reflection of a strong laser beam by a plasma surface [22]. A laser field with an electric field amplitude E_{cr} would have an intensity of $I_{cr} = E_{cr}^2/8\pi = 2.3 \times 10^{29}$ W/cm^2. The most intense laser field ever produced in a laboratory has an intensity of "only" 7×10^{21} W/cm^2 [23]. Numerous Petawatt laser systems are under construction in different laboratories, as e. g. at GSI [24] and at Jena [25], capable, in principle, to attain an intensity of about 10^{23} W/cm^2 [26]. Also, the Extreme Light Infrastructure (ELI) is expected to reach unprecedented intensities of about 10^{25}-10^{26} W/cm^2 [27]. Although spontaneous pair creation in vacuum is exponentially suppressed at fields below the critical field, vacuum manifests nonlinear properties due to the presence of virtual electron-positron pairs (see the recent reviews [28, 29, 30]). However, the only successful experiment on vacuum nonlinearities induced by intense laser beams, so far was performed at SLAC where electron-positron pairs have been produced in the collision of a high-energy electron beam with a strong laser pulse [31].

In the following, we first review a few processes that have been considered in order to measure nonlinear vacuum polarization effects. Then, two examples which indicate the possibility of testing QED in the presence of strong laser beams are reported. In the first example we consider the possibility of laser photons merging when they interact with the electromagnetic field of a high-energy proton [32]. In the second one we study laser-assisted bremsstrahlung [33, 34].

2 Vacuum nonlinearities in strong laser fields

In this Section we shortly review a few processes that we have recently studied to detect the nonlinear properties of quantum vacuum in the presence of strong laser beams experimentally. In [35] we have investigated the possibility of observing high-harmonic generation in the collision in vacuum of two ultra-strong laser beams. We have found that nowadays only the scattering of two photons is experimentally feasible by making three lasers collide (laser-assisted

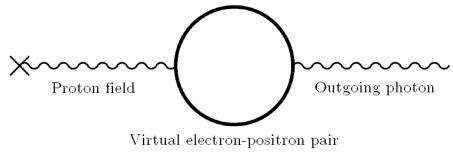

Figure 1: Feynman diagram corresponding to the process of laser photon merging in a proton field induced by vacuum polarization effects.

photon-photon scattering). This process seems to be the most promising to detect for the first time vacuum nonlinearities in a strong laser field and could, in principle, be observed with the next generation of Petawatt laser systems. In [36] we have investigated how a strong optical standing wave can "diffract" an x-ray probe beam that passes through it. The diffraction affects the polarization of the probe beam of an amount large enough that it could be measurable in the near future. Finally, in [37] we studied the process of photon splitting in a strong laser field of arbitrary shape and polarization. However, the experimental observation of this process is more problematic; more details can be found in [37].

3 QED effects in laser-proton collisions

In this section we investigate the vacuum polarization effects arising from the head-on collision of a high-energy proton and a strong laser beam. The proton has unique features that allow, as we will see, the detection of these effects. In fact, on the one hand, the proton is light enough to be accelerated to very high energies like up to 7 TeV at the Large Hadron Collider (LHC) [38]. This implies that the laser field in the rest frame of the proton is enhanced by a large factor compared to its value in the laboratory frame. On the other hand, the proton is heavy enough that the multiphoton Thomson scattering of the laser photons by the proton is negligible. This feature is very important because, in general, multiphoton Thomson scattering represents a background of our process. The Feynman diagram of the photon merging process is represented in Fig. 1. The diagram shows that the proton is considered, due to its large energy, as an external field. The thick electron-positron loop in Fig. 1 indicates that the propagators are calculated by exactly taking into account the presence of the laser field. From a physical point of view, the merging of the laser photons is mediated by the virtual electron-positron pair that absorbs a certain number of laser photons and emits only one. From the Furry theorem it can be inferred that only an even number of photons can be merged in the process [3]. The calculation of the rate $\mathcal{R}_{2n}$ of photons resulting from the merging of $2n$ ($n \geq 1$) laser photons follows the usual steps. One calculates the amplitude of the process according to the Feynman rules and then applies the Fermi golden rule [3]. The details of the calculations can be found in [32]. Below, we consider only the case of an ultra-relativistic optical laser field with amplitude E_0, intensity $I_0 = E_0^2/8\pi$ and frequency ω_0 such that the parameter $\xi = eE_0/m\omega_0$ is much larger than unity. We assume that the laser beam propagates along the positive y direction and that it is linearly polarized along the z direction. The proton moves with velocity β along the negative y direction. If ϑ is the angle between the outgoing photon and the y direction, it can be shown that the differential rate $d\mathcal{R}_{2n}/d\vartheta$ is given by

$$\frac{d\mathcal{R}_{2n}}{d\vartheta} = \frac{\alpha^3}{64\pi^2}\frac{(1+\beta)m^4}{\omega_0^3}\frac{\sin^3\vartheta}{(1-\cos\vartheta)^4}\frac{|c_{1,2n}|^2+|c_{2,2n}|^2}{n^3}. \tag{1}$$

In this expression we have introduced the coefficients $c_{j,2n}$

$$c_{j,2n} = e^{-i\pi/3}\int_0^1 dv \int_0^\infty \frac{d\lambda}{\lambda} e^{-\exp(i\pi/3)\lambda - x_{2n}} b_{j,2n} \tag{2}$$

where $j \in \{1,2\}$, $x_{2n} = \chi_{2n}^2\lambda^3(1-v^2)^2/96$ and where

$$b_{j,2n} = j\chi_{2n}^2\lambda^2\frac{1-v^{4/j}}{16}[I_n(x_{2n}) - I_n'(x_{2n})] + \frac{I_n(x_{2n})}{\lambda}, \tag{3}$$

with $I_n(x)$ being the modified Bessel function of order n and $I_n'(x)$ its derivative. As it is clear, the rate depends only on the parameter χ_{2n} which is given by

$$\chi_{2n} = \sqrt{\frac{I_0}{I_{cr}}}\frac{2n(1+\beta)\omega_0}{m}\frac{1-\cos\vartheta}{1+\beta\cos\vartheta}. \tag{4}$$

We consider below a numerical example illustrating the possibility of observing the process of photon merging experimentally. We consider the interaction between a proton bunch with parameters available at the LHC and a Petawatt laser pulse. We use the following laser parameters [39, 27]: a pulse energy of 5 J, a pulse duration of 5 fs at 10 Hz repetition rate and an intensity of $I_0 = 5\times10^{22}$ W/cm^2. The main parameters of the proton bunch are [38]: a proton energy of 7 TeV, a number of protons per bunch of 11.5×10^{10}, a bunch transversal radius of 16.6 μm, a bunch length of 7.55 cm. As we have mentioned, the $(2n)$-photon Thomson scattering of the laser photons by the proton beam is a competing process of $(2n)$-photon merging. In fact, it can be seen that the energies of the photons produced via $(2n)$-photon merging and via $(2n)$-photon Thomson scattering are equal. Then, the total photon rate has to be calculated by summing up the amplitudes of the two processes. In Fig. 2 we compare the differential rate $d\mathcal{W}^{(2)}/d\vartheta$ of the photons emitted only via 2-photon Thomson scattering with the total differential rate $d\mathcal{T}^{(2)}/d\vartheta$ which also includes the photons resulting from the merging (continuous line). The contribution of the vacuum effect is rather large. This becomes more apparent if we compare the total rate of photons emitted only via 2-photon Thomson scattering with the total rate of the two processes together. In fact, it can be shown that approximately 888 events per hour are obtained in the first case while about 1850 events are predicted per hour in the second case. The total rate of photons resulting only from 2-photon merging is about 1140 photons per hour. This implies a small, destructive interference effect between the two processes. Finally, it is evident in Fig. 2 that the values of the parameter χ_2 in the relevant region of the

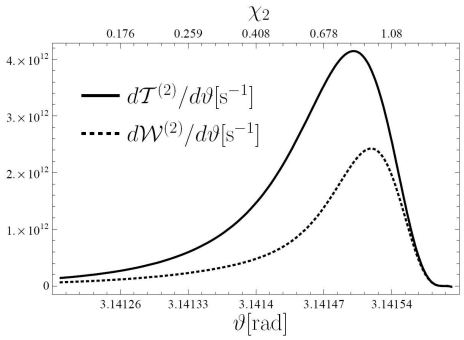

Figure 2: The rate per unit angle ϑ of photons emitted only via 2-photon Thomson scattering (dashed line) and via both 2-photon Thomson scattering and 2-photon merging (continuous line). The upper horizontal axis shows the parameter χ_2 as a function of ϑ [see also Eq. (4)].

spectrum are of the order of unity: the perturbative approach, which is valid as $\chi_2 \ll 1$, does not apply. Finally, one can also show that the rate of photons resulting from the merging of *four* laser photons amounts to 19.5 events per hour. In this case it can be seen that the 4-photon Thomson scattering is safely negligible due to its scaling as ξ_p^8, with $\xi_p = (m/M)\xi \approx 8.3 \times 10^{-2}$ (here M indicates the proton mass).

4 Laser-assisted bremsstrahlung

As we have mentioned in the Introduction, one of the goals of theoretical high-energy laser physics is to study the influence of a strong laser field on fundamental processes of QED. However, since the strong coupling to the laser field does not allow for the perturbation theory to be used, the formulas resulting from the theory tend to be complex and difficult to follow. Here, numerical work becomes important. Bremsstrahlung is the process of light emission from an electron scattering at the Coulomb potential of a nucleus. In the absence of the laser, the problem in the first Born approximation was solved by Bethe and Heitler. In [33, 34] we have studied and numerically evaluated the effect of an intense laser on the process of bremsstrahlung in a Coulomb field. The second order Feynman diagrams for this process are displayed in Fig. 3 and the resulting transition matrix element S_{fi} takes the form of a double sum over photon orders:

$$S_{fi} = \sum_{n,s=-\infty}^{\infty} \frac{\delta(Q_f - Q_i - n\omega_0 + \omega_b)}{\boldsymbol{q}^2 + \ell^{-2}} \times \left(\frac{A_f^{s,n}}{\tilde{p}_f^2 - m_*^2 + iM_f} + \frac{A_i^{s,n}}{\tilde{p}_i^2 - m_*^2 + iM_i} \right), \tag{5}$$

where $q_{i,f}^\mu = p_{i,f}^\mu + k_0^\mu m^2\xi^2/(4k_0\cdot p_{i,f})$ is the effective four-momentum of the electron in the laser field ($p_{i,f}$ is the electron four-momentum outside the laser field), where $k_0 = (\omega_0, \boldsymbol{k}_0)$ is the wave four-vector of the laser, $Q_{i,f} = q_{i,f}^0$ is the effective energy, $m_*^2 = q_{i,f}^2 = m^2(1+\xi^2/2)$ is the

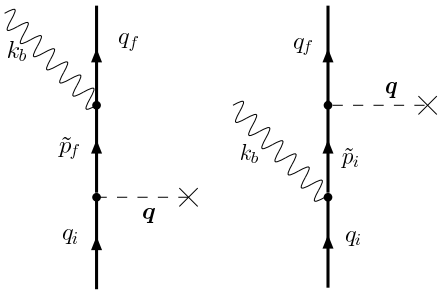

Figure 3: Feynman diagrams describing the process of laser-assisted bremsstrahlung. Thick lines indicate that Volkov wave functions and Volkov propagators are used for the electron, thus treating the electron-laser interaction nonperturbatively. The effective four-momentum of the initial (final) electron is q_i (q_f) and the four-momentum of the intermediate electron state is denoted by $\tilde{p}_{i,f}$. The virtual Coulomb photon with three-momentum $\boldsymbol{q}$ is drawn as a dashed line, and the emitted photon with momentum k_b as a wavy line.

squared effective electron mass, ω_b is the frequency of the bremsstrahlung photon, $\tilde{p}_{i,f} = q_{i,f} - sk_0 + k_b$ is the intermediate four-momentum, ℓ is a screening length, and $A_{i,f}^{s,n}$ are certain functions depending on the laser parameters. In a strong laser field, photon emission can occur even without a Coulomb field through laser-induced Compton scattering. This means that for values of ω_b satisfying the modified Compton formula, we may have $\tilde{p}_{i,f}^2 = m_*^2$, with a formally diverging matrix element as a result. This divergence can be rendered finite by the inclusion of an imaginary contribution to the electron energy, represented by the term $iM_{i,f}$ in the matrix element (5). We note that other methods, such as taking into account a finite space-time duration of the laser or energy spread of the initial electron also would produce finite results, and that our method is valid in the limit of long laser pulses. An example of a photon spectrum resulting from the matrix element (5), characterized by a large number of peaks, is shown in Fig. 4. This kind of resonances are absent in the nonrelativistic treatment of the problem [40] where the dipole approximation for the laser is employed.

5 Conclusion

In this Report we have considered two examples in which QED can be tested in the presence of strong laser fields. We have seen that even non-perturbative vacuum polarization effects can be detected in the collision of high-energy protons and strong laser fields. Also, the dramatic influence of the presence of a strong laser beam on the bremsstrahlung process has been pointed out.

References

[1] M. I. Eides, H. Grotch and V. A. Shelyuto, Phys. Rep. **342**, 63 (2001).

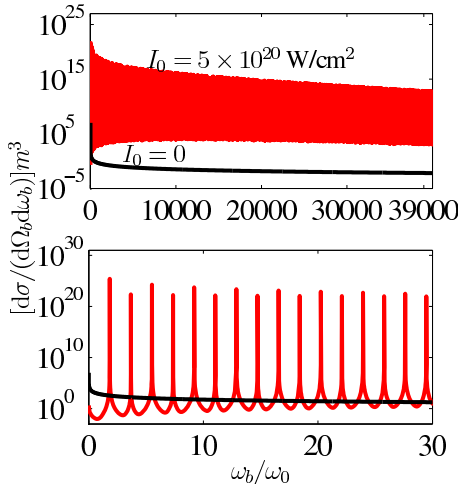

Figure 4: The cross section differential in the solid angle Ω_b and the frequency ω_b of the emitted photon, scaled with the cubed electron mass m^3. The calculation is performed for an initial electron with an energy $E_i = 5.11$ MeV, counterpropagating with a linearly polarized laser beam of frequency $\omega_0 = 1$ eV and intensity $I_0 = 5 \times 10^{20}$ W/cm^2. The photon is emitted at an angle of 1° with respect to the direction of the initial electron. The black line corresponds to the case without laser.

[2] S. G. Karshenboim, Phys. Rep. **422**, 1 (2005).

[3] V. B. Berestetskii, E. M. Lifshitz, and L. P. Pitaevskii, *Quantum Electrodynamics - 2nd Ed.* (Elsevier, Oxford, 1982).

[4] W. Greiner, B. Müller, and J. Rafelski, *Quantum electrodynamics of strong fields: with an introduction into modern relativistic quantum mechanics* (Springer, Berlin, 1985).

[5] A. Czarnecki, U. D. Jentschura, and K. Pachucki, Phys. Rev. Lett. **95**, 180404 (2005).

[6] U. D. Jentschura, A. Czarnecki, and K. Pachucki, Phys. Rev. A **72**, 062102 (2005).

[7] U. D. Jentschura *et al.*, Phys. Rev. Lett. **95**, 163003 (2005).

[8] U. D. Jentschura and V. A. Yerokhin, Phys. Rev. A **73**, 062503 (2006).

[9] U. D. Jentschura, Phys. Rev. A **74**, 062517 (2006).

[10] Sh. Zh. Akhmadaliev, et al., Phys. Rev. C **58**, (1998) 2844.

[11] Sh. Zh. Akhmadaliev *et al.*, Phys. Rev. Lett. **89**, (2002) 061802.

[12] R. N. Lee, A. I. Milstein, V. M. Strakhovenko, Zh. Eksp. Teor. Fiz. **112**, 1921 (1997) [JETP **85**, 1049 (1997)]; Phys. Rev. A **57**, 2325 (1998); Phys. Rev. A **58**, 1757 (1998).

[13] R. N. Lee *et al.*, Phys. Rep. **373**, 213 (2003).

[14] W. Dittrich and M. Reuter, *Effective Lagrangians in Quantum Electrodynamics* (Springer-Verlag, Berlin, 1985).

[15] W. Dittrich and H. Gies, *Probing the Quantum Vacuum* (Springer-Verlag, Berlin, 2000).

[16] S. L. Adler *et al.*, Phys. Rev. Lett. **25**, 1061 (1970).

[17] Z. Bialynicka-Birula and I. Bialynicki-Birula, Phys. Rev. D **2**, 2341 (1970).

[18] S. L. Adler, Ann. Phys. (N.Y.) **67**, 599 (1971).

[19] C. Rischel *et al.*, Nature **390**, 490 (1997); Ph. Zeitoun *et al.*, Nature **431**, 426 (2004); J. Seres *et al.*, Nature **433**, 596 (2004); A. L. Cavalieri *et al.*, Phys. Rev. Lett. **94**, 114801 (2005).

[20] G. Mourou and D. Umstadter, Sci. Am. **286**, 80 (1997); V. Malka *et al.*, Science **298**, 1596 (2002); Th. Katsouleas, Nature **431**, 515 (2004); P. D. Mangles *et al.*, Nature **431**, 535 (2004); C. G. R. Geddes *et al.*, Nature **431**, 538 (2004); J. Faure *et al.*, Nature **431**, 541 (2004); J. Fuchs *et al.*, Nature Phys. **2**, 48 (2006); B. M. Hegelich *et al.*, Nature **439**, 441 (2006); H. Schwoerer *et al.*, Nature **439**, 445 (2006).

[21] M. Tabak *et al.*, Phys. Plasmas **1**, 1626 (1994); P. Mulser and D. Bauer, Laser Part. Beams **22**, 5 (2004); S. Atzeni, J. Meyer-ter-Vehn, *The Physics of Inertial Fusion* (Clarendon Press, Oxford, 2004).

[22] T. Tajima and G. Mourou, Phys. Rev. ST Accel. Beams **5**, 031301 (2002); S. Gordienko, A. Pukhov, O. Shorokhov, and T. Baeva, Phys. Rev. Lett. **94**, 103903 (2005).

[23] S.-W. Bahk *et al.*, Opt. Lett. **29**, 2837 (2004).

[24] See the Phelix project homepage at http://www.gsi.de /forschung/phelix/.

[25] See the Polaris project homepage at http://www.physik.uni-jena.de/qe/Forschung/F-Deutsch/Petawatt/FP-Petawatt.html (in German).

[26] J. Norby, Laser Focus World, January 1 (2005).

[27] See the ELI proposal at http://www.extreme-light-infrastructure.eu/.

[28] Y. I. Salamin *et al.*, Phys. Rep. **427**, 41 (2006).

[29] G. A. Mourou, T. Tajima, and S. V. Bulanov, Rev. Mod. Phys. **78**, 309 (2006).

[30] M. Marklund and P. K. Shukla, Rev. Mod. Phys. **78**, 591 (2006).

[31] D. L. Burke *et al.*, Phys. Rev. Lett. **79**, 1626 (1997).

[32] A. Di Piazza, K. Z. Hatsagortsyan, and C. H. Keitel, Phys. Rev. Lett. (in press). See also arXiv:0708.0475 [hep-ph].

[33] E. Lötstedt, U. D. Jentschura, and C. H. Keitel, Phys. Rev. Lett. **98**, 043002 (2007).

[34] S. Schnez, E. Lötstedt, U. D. Jentschura, and C. H. Keitel, Phys. Rev. A **75**, 053412 (2007).

[35] A. Di Piazza, K. Z. Hatsagortsyan, and C. H. Keitel, Phys. Rev. D **72**, 085005 (2005).

[36] A. Di Piazza, K. Z. Hatsagortsyan, and C. H. Keitel, Phys. Rev. Lett. **97**, 083603 (2006).

[37] A. Di Piazza, A. I. Milstein, and C. H. Keitel, Phys. Rev. A **76**, 032103 (2007).

[38] W.-M. Yao *et al.*, J. Phys. G **33**, 1 (2006).

[39] See the petawatt field synthesizer homepage at http://www.attoworld.de/research/PFS.html.

[40] M. Dondera and V. Florescu, Rad. Phys. Chem. **75**, 1380 (2006).

Bibliography

[1] M Abramowitz and I. A. Stegun (eds.), *Handbook of mathematical functions with formulas, graphs, and mathematical tables*, Dover, New York, 1968, fifth Dover printing.

[2] Sh. Zh. Akhmadaliev, G. Ya. Kezerashvili, S. G. Klimenko, R. N. Lee, V. M. Malyshev, A. L. Maslennikov, A. M. Milov, A. I. Milstein, N. Yu. Muchnoi, A. I. Naumenkov, V. S. Panin, S. V. Peleganchuk, G. E. Pospelov, I. Ya. Protopopov, L. V. Romanov, A. G. Shamov, D. N. Shatilov, E. A. Simonov, V. M. Strakhovenko, and Yu. A. Tikhonov, *Experimental investigation of high-energy photon splitting in atomic fields*, Phys. Rev. Lett. **89** (2002), 061802 (1–4).

[3] Sh. Zh. Akhmadaliev, G. Ya. Kezerashvili, S. G. Klimenko, V. M. Malyshev, A. L. Maslennikov, A. M. Milov, A. I. Milstein, N. Yu. Muchnoi, A. I. Naumenkov, V. S. Panin, S. V. Peleganchuk, V. G. Popov, G. E. Pospelov, I. Ya. Protopopov, L. V. Romanov, A. G. Shamov, D. N. Shatilov, E. A. Simonov, and Yu. A. Tikhonov, *Delbrück scattering at energies of 140–450 MeV*, Phys. Rev. C **58** (1998), 2844–2850.

[4] E. Kh. Akhmedov, *β decay in the field of an intense electromagnetic wave*, Zh. Éksp. Teor. Fiz. **85** (1983), 1521–1531, [Sov. Phys. JETP **58**, 883 (1983)].

[5] H. K. Avetissian, A. K. Avetissian, G. F. Mkrtchian, and Kh. V. Sedrakian, *Electron-positron pair production in the field of superstrong oppositely directed laser beams*, Phys. Rev. E **66** (2002), 016502 (1–6).

[6] M. Babzien, I. Ben-Zvi, K. Kusche, I. V. Pavlishin, I. V. Pogorelsky, D. P. Siddons, V. Yakimenko, D. Cline, F. Zhou, T. Hirose, Y. Kamiya, T. Kumita, T. Omori, J. Urakawa, and K. Yokoya, *Observation of the second harmonic in Thomson scattering from relativistic electrons*, Phys. Rev. Lett. **96** (2006), 054802 (1–4).

[7] V. G. Bagrov and D. M. Gitman, *Exact solutions of relativistic wave equations*, Kluwer Academic Publishers, Dordrecht, 1990.

[8] S. W. Bahk, P. Rousseau, T. A. Planchon, V. Chvykov, G. Kalintchenko, A. Maksimchuk, G. A. Mourou, and V. Yanovsky, *Generation and characterization of the highest laser intensities (10^{22} W/cm^2)*, Opt. Lett. **29** (2004), 2837–2839.

[9] V. N. Baĭer, V. M. Katkov, and V. M. Strakhovenko, *Higher-order effects in external field: Pair production by a particle*, Yad. Fiz. **14** (1971), 1020–1026, [Sov. J. Nucl. Phys **14**, 572 (1972)].

[10] ———, *Operator approach to quantum electrodynamics in an external field: The mass operator*, Zh. Éksp. Teor. Fiz. **67** (1974), 453–470, [Sov. Phys. JETP **40**, 225 (1975)].

[11] ———, *Operator approach to quantum electrodynamics in an external field. Electron loops*, Zh. Éksp. Teor. Fiz. **68** (1975), 405–420, [Sov. Phys. JETP **41**, 198 (1975)].

[12] ———, *Electroproduction of e^+e^- pairs in an external field*, Yad. Fiz. **53** (1991), 1021–1029, [Sov. J. Nucl. Phys **53**, 632 (1991)].

[13] ———, *Electromagnetic processes at high energies in oriented single crystals*, first ed., World Scientific Publishing Co. Pte. Ltd., Singapore, 1998.

[14] V. N. Baĭer, A. I. Mil'steĭn, and V. M. Strakhovenko, *Interaction between a photon and an intense electromagnetic wave*, Zh. Éksp. Teor. Fiz. **69** (1975), 1893–1904, [Sov. Phys. JETP **42**, 961-965 (1976)].

[15] V. N. Baier and K. Yokoya, *Interaction of high energy electrons and photons with intense electromagnetic wave: linear collider applications*, Part. Acc. **44** (1994), 77–106.

[16] C. Bamber, S. J. Boege, T. Koffas, T. Kotseroglou, A. C. Melissinos, D. D. Meyerhofer, D. A. Reis, W. Ragg, C. Bula, K. T. McDonald, E. J. Prebys, D. L. Burke, R. C. Field, G. Horton-Smith, J. E. Spencer, D. Walz, S. C. Berridge, W. M. Bugg, K. Shmakov, and A. W. Weidemann, *Studies of nonlinear QED in collisions of 46.6 GeV electrons with intense laser pulses*, Phys. Rev. D **60** (1999), 092004 (1–43).

[17] D. Bauer, *Theory of intense laser-matter interaction*, Lecture notes, Univ. of Heidelberg, 2006.

[18] D. Bauer, D. B. Milošević, and W. Becker, *On the validity of the strong field approximation and simple man's theory*, J. Mod. Opt. **53** (2006), 135–147.

[19] G. Baur, K. Hencken, and D. Trautmann, *Electron-positron pair production in ultrarelativistic heavy ion collision*, Phys. Rep. **453** (2007), 1–27.

[20] W. Becker and H. Mitter, *Vacuum polarization in laser fields*, J. Phys. A **8** (1975), 1638–1657.

[21] ———, *Modification of the quasi-levels of an electron in a laser field due to radiative corrections*, J. Phys. A **9** (1976), 2171–2184.

[22] W. Becker, G. T. Moore, R. R. Schlicher, and M. O. Scully, *A note on total cross sections and decay rates in the presence of a laser field*, Phys. Lett. A **94** (1983), 131–134.

[23] I. V. Belusov, *On resonance Compton scattering in the field of an intense electromagnetic wave*, Opt. Commun. **20** (1977), 205–208.

[24] V. B. Berestetskii, E. M. Lifshitz, and L. P. Pitaevskii, *Quantum electrodynamics*, 2nd ed., vol. 4, Elsevier, Oxford, 1982.

[25] H. A. Bethe and W. Heitler, *On the stopping of fast particles and on the creation of positive electrons*, Proc. Roy. Soc. A **146** (1934), 83–112.

[26] W. G. Bickley, L. J. Comrie, J. C. P. Miller, D. H. Sadler, and A. J. Thompson, *Bessel functions, part II, functions of positive integer order*, Mathematical tables, vol. X, Cambridge University Press, Cambridge, 1960.

[27] D. Binosi and L. Theußl, *JaxoDraw: A graphical user interface for drawing Feynman diagrams*, Comput. Phys. Commun. **161** (2004), 76–86.

[28] J. D. Bjorken and S. D. Drell, *Relativistic quantum mechanics*, McGraw-Hill, New York, 1964.

[29] D. B. Blaschke, A. V. Prozorkevich, C. D. Roberts, S. M. Schmidt, and S. A. Smolyansky, *Pair production and optical lasers*, Phys. Rev. Lett. **96** (2006), 140402 (1–4).

[30] A. V. Borisov, O. G. Goryaga, and V. Ch. Zhukovskii, *Electron-positron pair formation in the field of a bichromatic plane electromagnetic wave*, Izv. Vyssh. Uchebn. Zaved., Fiz. **No. 2** (1977), 46–53, [Rus. Phys. J. **20**, 176 (1977)].

[31] ———, *Photoproduction of electron-positron pairs in the field of a nucleus and the field of a plane electromagnetic wave*, Izv. Vyssh. Uchebn. Zaved., Fiz. **No. 5** (1977), 15–20, [Rus. Phys. J. **20**, 569 (1977)].

[32] A. V. Borisov, O. G. Goryaga, V. Ch. Zhukovskii, and A. A. Sokolov, *Production of electron-positron pairs on nuclei in the field of a bichromatic plane electromagnetic wave*, Izv. Vyssh. Uchebn. Zaved., Fiz. **No. 9** (1978), 33–40, [Rus. Phys. J. **21**, 1136 (1978)].

[33] A. V. Borisov, V. Ch. Zhukovskiĭ, and P. A. Éminov, *Resonant electron-electron bremsstrahlung in the field of an electromagnetic wave*, Zh. Éksp. Teor. Fiz. **78** (1980), 530–537, [Sov. Phys. JETP **51**, 267 (1980)].

[34] A. V. Borisov, V. Ch. Zhukovskii, A. K. Nasirov, and P. A. Éminov, *Resonance two-photon pair production on nuclei and on electrons*, Izv. Vyssh. Uchebn. Zaved., Fiz. **No. 2** (1981), 12–15, [Rus. Phys. J. **24**, 107 (1981)].

[35] J. Bös, W. Brock, H. Mitter, and Th. Schott, *Intensity-dependent scattering energies in high-intensity Møller scattering*, J. Phys. A **12** (1979), 2573–2581.

[36] ———, *Resonances and intensity-dependent shifts of the Møller cross section in a strong laser field*, J. Phys. A **12** (1979), 715–731.

[37] E. Brézin and C. Itzykson, *Pair production in vacuum by an alternating field*, Phys. Rev. D **2** (1970), 1191–1199.

[38] L. S. Brown and T. W. B. Kibble, *Interaction of intense laser beams with electrons*, Phys. Rev. **133** (1964), A705–A719.

[39] C. Bula, K. T. McDonald, E. J. Prebys, C. Bamber, S. Boege, T. Kotseroglou, A. C. Melissinos, D. D. Meyerhofer, W. Ragg, D. L. Burke, R. C. Field, G. Horton-Smith, A. C. Odian, J. E. Spencer, D. Walz, S. C. Berridge, W. M. Bugg, K. Shmakov, and A. W. Weidemann, *Observation of nonlinear effects in Compton scattering*, Phys. Rev. Lett. **76** (1996), 3116–3119.

[40] S. S. Bulanov, N. B Narozhny, V. D. Mur, and V. S. Popov, *Electron-positron pair production by electromagnetic pulses*, Zh. Éksp. Teor. Fiz. **129** (2006), 14–29, [JETP **102**, 9 (2006)].

[41] D. L. Burke, R. C. Field, G. Horton-Smith, J. E. Spencer, D. Walz, S. C. Berridge, W. M. Bugg, K. Shmakov, A. W. Weidemann, C. Bula, K. T. McDonald, E. J. Prebys, C. Bamber, S. J. Boege, T. Koffas, T. Kotseroglou, A. C. Melissinos, D. D. Meyerhofer, D. A. Reis, and W. Ragg, *Positron production in multiphoton light-by-light scattering*, Phys. Rev. Lett. **79** (1997), 1626–1629.

[42] P. P. Corso, E. Fiordilino, and F. Persico, *The electron wavefunction in laser-assisted bremsstrahlung*, J. Phys. B **36** (2003), 2823–2835.

[43] R. E. Cutkosky, *Singularities and discontinuities of Feynman amplitudes*, J. Math. Phys. **1** (1960), 429–433.

[44] R. Daniele and E. Fiordilino, *Bremsstrahlung and harmonic generation in laser-assisted electron-nucleus collision*, Nuovo Cim. **18 D** (1996), 547–556.

[45] G. Dattoli, C. Chiccoli, S. Lorenzutta, G. Maino, M. Richetta, and A. Torre, *Generating functions of multivariable generalized Bessel functions and Jacobi-elliptic functions*, J. Math. Phys. **33** (1991), 25–36.

[46] ———, *Advances on the theory of generalized Bessel functions and applications to multiphoton processes*, J. Sci. Comp. **8** (1993), 69–109.

[47] G. Dattoli, C. Chiccoli, S. Lorenzutta, G. Maino, and A. Torre, *Generalized Bessel functions of the Anger type and applications to physical problems*, J. Math. Anal. App. **184** (1994), 201–221.

[48] G. Dattoli, L. Giannessi, L. Mezi, and A. Torre, *Theory of generalized Bessel functions*, Nuovo Cim. **105 B** (1990), 327–348.

[49] G. Dattoli, C. Mari, A. Torre, C. Chiccoli, S. Lorenzutta, and G. Maino, *Analytical and numerical results on M-variable generalized Bessel functions*, J. Sci. Comp. **7** (1992), 175–196.

[50] G. Dattoli, A. Torre, S. Lorenzutta, G. Maino, and C. Chiccoli, *Theory of generalized Bessel functions II*, Nuovo Cim. **106 B** (1991), 21–51.

[51] L. De Braeckeleer, E. G. Adelberger, and A. García, *Reexamination of an anomaly in near-threshold pair production*, Phys. Rev. A **46** (1992), R5324–R5326.

[52] M. M. Denisov and M. V. Fedorov, *Bremsstrahlung effect on relativistic electrons in a strong radiation field*, Zh. Éksp. Teor. Fiz. **53** (1967), 1340–1348, [Sov. Phys. JETP **26**, 779 (1968)].

[53] Deutsches Elektronen-Synchrotron (DESY), `http://hasylab.desy.de/`, Accessed 15-02-2008.

[54] A. Di Piazza, *Pair production at the focus of two equal and oppositely directed laser beams: The effect of the pulse shape*, Phys. Rev. D **70** (2004), 053013 (1–6).

[55] A. Di Piazza and G. Calucci, *Pair production in a rotating strong magnetic field*, Phys. Rev. D **65** (2002), 125019 (1–10).

[56] A. Di Piazza, K. Z. Hatsagortsyan, and C. H. Keitel, *Nonperturbative vacuum-polarization effects in proton-laser collisions*, Phys. Rev. Lett. **100** (2008), 010403 (1–4).

[57] A. Di Piazza, A. I. Milstein, and C. H. Keitel, *Photon splitting in a laser field*, Phys. Rev. A **76** (2007), 032103 (1–13).

[58] K. Dietz and M. Pröbsting, *The structure of the QED vacuum and electron-positron pair production in super-intense, pulsed laser fields*, J. Phys. B **31** (1998), L409–L414.

[59] M. Dondera and V. Florescu, *Laser modified electron bremsstrahlung revisited*, Romanian Reports in Physics **56** (2004), 623–636.

[60] ———, *Bremsstrahlung in the presence of a laser field*, Radiation Physics and Chemistry **75** (2006), 1380–1396.

[61] T. J. Englert and E. A. Rinehart, *Second-harmonic photons from the interaction of free electrons with intense laser radiation*, Phys. Rev. A **28** (1983), 1539–1545.

[62] H. En'yo, T. Numao, and T. Yamazaki, *Cross section of pair production near threshold*, Phys. Rev. A **21** (1980), 1439–1442.

[63] T. Erber, *High-energy electromagnetic conversion processes in magnetic fields*, Rev. Mod. Phys. **38** (1966), 626–659.

[64] G. A. Evans, *Two robust methods for irregular oscillatory integrals over a finite range*, Appl. Numer. Math. **14** (1994), 383–395.

[65] Extreme Light Infrastructure, `http://www.extreme-light-infrastructure.eu/`, Accessed 15-02-2008.

[66] R. P. Feynman, *Space-time approach to quantum electrodynamics*, Phys. Rev. **76** (1949), 769–789.

[67] ———, *The theory of positrons*, Phys. Rev. **76** (1949), 749–759.

[68] A. Florescu and V. Florescu, *Laser-modified electron bremsstrahlung in a Coulomb field*, Phys. Rev. A **61** (2000), 033406 (1–12).

[69] W. H. Furry, *On bound states and scattering in positron theory*, Phys. Rev. **81** (1951), 115–124.

[70] C. Gahn, G. D. Tsakiris, G. Pretzler, K. J. Witte, C. Delfin, C.-G. Wahlström, and D. Habs, *Generating positrons with femtosecond-laser pulses*, Appl. Phys. Lett. **77** (2000), 2662–2664.

[71] W. Gautschi, *Computational aspects of three-term recurrence relations*, SIAM Rev. **9** (1967), 24–82.

[72] R. L. Gluckstern and M. H. Hull, Jr., *Polarization dependence of the integrated bremsstrahlung cross section*, Phys. Rev. **90** (1953), 1030–1035.

[73] M. L. Goldberger and K. M. Watson, *Collision theory*, first ed., Wiley, New York, 1964.

[74] C. Graziani, *Strong-field cyclotron scattering. I. Scattering amplitudes and natural line width*, Astrophysical J. **412** (1993), 351–362.

[75] W. Greiner, B. Müller, and J. Rafelski, *Quantum electrodynamics of strong fields*, Springer, Berlin, Heidelberg, 1985.

[76] W. Greiner and J. Reinhardt, *Quantenelektrodynamik (Band VII der Lehrbuchreihe über theoretische Physik)*, second ed., Harry Deutsch, Frankfurt a. M., 1995.

[77] A. K. Harding, *The physics of gamma-ray bursts*, Phys. Rep. **206** (1991), 327–391.

[78] Z. Harman, I. I. Tupitsyn, A. N. Artemyev, U. D. Jentschura, C. H. Keitel, J. R. Crespo López-Urrutia, A. J. González Martínez, H. Tawara, and J. Ullrich, *Benchmarking high-field few-electron correlation and QED contributions in Hg^{75+} to Hg^{78+} ions. II. Theory*, Phys. Rev. A **73** (2006), 052711 (1–13).

[79] H. Herold, *Compton and Thomson scattering in strong magnetic fields*, Phys. Rev. D **19** (1979), 2868–2875.

[80] European High Power laser Energy Research facility, `http://www.hiper-laser.org`, Accessed 20-02-2008.

[81] M. Hosaka, H. Hama, K. Kimura, J. Yamazaki, and T. Kinoshita, *Observation of intra-cavity Compton backscattering of the UVSOR free electron laser*, Nucl. Instrum. Meth. **A 393** (1997), 525–529.

[82] A. Hsieh and E. Yehudai, *HIP: Symbolic high-energy physics calculations*, Comput. Phys. **6** (1992), 253–261.

[83] C. Itzykson and J.-B. Zuber, *Quantum field theory*, 2nd ed., Dover, New York, 2006.

[84] J. D. Jackson, *Classical electrodynamics*, first ed., J. Wiley & Sons, New York, 1965.

[85] G. Jarlskog, L. Jönsson, S. Prünster, H. D. Schulz, H. J. Willutzki, and G. G. Winter, *Measurement of Delbrück scattering and observation of photon splitting at high energies*, Phys. Rev. D **8** (1973), 3813–3823.

[86] U. D. Jentschura, K. Z. Hatsagortsyan, and C. H. Keitel, *Laser-assisted bremsstrahlung emission in a Coulomb field*, Internal report, 2003.

[87] U. D. Jentschura, S. Kotochigova, E.-O. Le Bigot, P. J. Mohr, and B. N. Taylor, *Precise calculation of transition frequencies of hydrogen and deuterium based on a least-squares analysis*, Phys. Rev. Lett. **95** (2005), 163003 (1–4).

[88] U. D. Jentschura and P. J. Mohr, *Electron self-energy for higher excited S levels*, Phys. Rev. A **69** (2004), 064103 (1–2).

[89] J. Z. Kamiński, K. Krajewska, and F. Ehlotzky, *Monte Carlo analysis of electron-positron pair creation by powerful laser-ion impact*, Phys. Rev. A **74** (2006), 033402 (1–8).

[90] R. V. Karapetyan and M. V. Fedorov, *Spontaneous bremsstrahlung of an electron in the field of an intense electromagnetic wave*, Zh. Éksp. Teor. Fiz. **75** (1978), 816–826, [Sov. Phys. JETP **48**, 412 (1978)].

[91] L. V. Keldysh, *Ionization in the field of a strong electromagnetic wave*, Zh. Éksp. Teor. Fiz. **47** (1964), 1945–1957, [Sov. Phys. JETP **20**, 1307 (1965)].

[92] T. W. B. Kibble, *Frequency shift in high-intensity Compton scattering*, Phys. Rev. **138** (1965), B740–B753.

[93] H. W. Koch and J. W. Motz, *Bremsstrahlung cross-section formulas and related data*, Rev. Mod. Phys. **31** (1959), 920–956.

[94] H. J. Korsch, A. Klumpp, and D. Witthaut, *On two-dimensional Bessel functions*, J. Phys. A **39** (2006), 14947–14964.

[95] M. Yu. Kuchiev, *Production of high-energy particles in laser and Coulomb fields and the e^+e^- antenna*, Phys. Rev. Lett. **99** (2007), 130404 (1–4).

[96] M. Yu. Kuchiev and D. J. Robinson, *Electron-positron pair creation by Coulomb and laser fields in the tunneling regime*, Phys. Rev. A **76** (2007), 012107 (1–15).

[97] T. Kumita, Y. Kamiya, M. Babzien, I. Ben-Zvi, K. Kusche, I. V. Pavlishin, I. V. Pogorelsky, D. P. Siddons, V. Yakimenko, T. Hirose, T. Omori, J. Urakawa, K. Yokoya, D. Cline, and F. Zhou, *Observation of the nonlinear effect in relativistic Thomson scattering of electrons and laser beams*, Laser Phys. **16** (2006), 267–271.

[98] L. D. Landau and E. M. Lifshitz, *The classical theory of fields*, revised second ed., Pergamon Press, Oxford, 1965.

[99] I. V. Lebedev, *Generation of harmonics due to electron retardation in the presence of an intensive light wave*, Opt. Spectrosk. **32** (1972), 120–122, [Opt. Spectrosc. (USSR) **32**, 59 (1972)].

[100] R. N. Lee, A. L. Maslennikov, A. I. Milstein, V. M. Strakhovenko, and Yu. A. Tikhonov, *Photon splitting in atomic fields*, Phys. Rep. **373** (2003), 213–246.

[101] C. Leubner, *The spectrum of nonlinear inverse Compton radiation by the method of steepest descents*, Astron. Astrophys. **69** (1978), 149–154.

[102] ———, *Uniform asymptotic expansion of a class of generalized Bessel functions occurring in the study of fundamental scattering processes in intense laser fields*, Phys. Rev. A **23** (1981), 2877–2890.

[103] C. Leubner and E. M. Strohmaier, *Analysis of intensity effects in laser electron-beam backscattering in terms of generalised Bessel functions*, J. Phys. A **14** (1981), 509–520.

[104] E. Lötstedt, U. D. Jentschura, and C. H. Keitel, *Evaluation of laser-assisted bremsstrahlung with Dirac-Volkov propagators*, Phys. Rev. Lett. **98** (2007), 043002 (1–4), also in Virtual Journal of Ultrafast Science, February 2007.

[105] V. A. Lyul'ka, *Quantum effects in an intense electromagnetic field*, Zh. Éksp. Teor. Fiz. **67** (1974), 1638–1646, [Sov. Phys. JETP **40**, 815 (1974)].

[106] A. Maquet and R. Grobe, *Atoms in strong laser fields: challenges in relativistic quantum mechanics*, J. Mod. Opt. **49** (2002), 2001–2018.

[107] A. J. González Martínez, J. R. Crespo López-Urrutia, J. Braun, G. Brenner, H. Bruhns, A. Lapierre, V. Mironov, R. Soria Orts, H. Tawara, M. Trinczek, J. Ullrich, A. N. Artemyev, Z. Harman, U. D. Jentschura, C. H. Keitel, J. H. Scofield, and I. I. Tupitsyn, *Benchmarking high-field few-electron correlation and QED contributions in Hg^{75+} to Hg^{78+} ions. I. Experiment*, Phys. Rev. A **73** (2006), 052710 (1–10).

[108] G. Matviyenko, *On the evaluation of Bessel functions*, Appl. Comp. Harm. Anal. **1** (1993), 116–135.

[109] J. W. Meyer, *Covariant classical motion of electron in a laser beam*, Phys. Rev. D **3** (1971), 621–622.

[110] D. D. Meyerhofer, *High-intensity-laser-electron scattering*, IEEE J. Quantum Electronics **33** (1997), 1935–1941.

[111] A. I. Mil'shtein and V. M. Strakhovenko, *Quasiclassical approach to the high-energy Delbrück scattering*, Phys. Lett. **95A** (1983), 135–138.

[112] A. I. Milstein, C. Müller, K. Z. Hatsagortsyan, U. D. Jentschura, and C. H. Keitel, *Polarization-operator approach to electron-positron pair production in combined laser and Coulomb fields*, Phys. Rev. A **73** (2006), 062106 (1–10).

[113] H. Mitter, *Quantum electrodynamics in laser fields*, Acta Phys. Austriaca Suppl. **14** (1975), 397–468.

[114] M. H. Mittleman, *Multiphoton pair creation*, Phys. Rev. A **35** (1987), 4624–4628.

[115] P. J. Mohr, *Numerical evaluation of the $1S_{1/2}$-state radiative level shift*, Ann. Phys. **88** (1974), 52–87.

[116] C. I. Moore, J. P. Knauer, and D. D. Meyerhofer, *Observation of the transition from Thomson to Compton scattering in multiphoton interactions with low-energy electrons*, Phys. Rev. Lett. **74** (1995), 2439–2442.

[117] D. A. Morozov and V. I. Ritus, *Elastic electron scattering in an intense field and two-photon emission*, Nucl. Phys. B **86** (1974), 309–332.

[118] J. W. Motz, H. A. Olsen, and H. W. Koch, *Pair production by photons*, Rev. Mod. Phys. **41** (1969), 581–639.

[119] G. A. Mourou, T. Tajima, and S. V. Bulanov, *Optics in the relativistic regime*, Reviews of Modern Physics **78** (2006), 309–371.

[120] C. Müller, K. Z. Hatsagortsyan, and C. H. Keitel, *Particle physics with a laser-driven positronium atom*, Phys. Lett. B **659** (2008), 209–213.

[121] C. Müller, A. B. Voitkiv, and N. Grün, *Differential rates for multiphoton pair production by an ultrarelativistic nucleus colliding with an intense laser beam*, Phys. Rev. A **67** (2003), 063407 (1–8).

[122] ———, *Multiphoton pair production by a highly charged ion in an intense laser field*, Nucl. Instrum. Meth. Phys. Res. B **205** (2003), 306–309.

[123] ———, *Nonlinear bound-free pair creation in the strong electromagnetic fields of a heavy nucleus and an intense x-ray laser*, Phys. Rev. Lett. **91** (2003), 223601 (1–4).

[124] ———, *Few-photon electron-positron pair creation in the collision of a relativistic nucleus and an intense x-ray laser beam*, Phys. Rev. A **70** (2004), 023412 (1–9).

[125] N. B. Narozhny and M. S. Fofanov, *Comment on "Quantum processes in the field of a two-frequency circularly polarized plane electromagnetic wave"*, Phys. Rev. E **60** (1999), 3443–3449.

[126] ———, *Quantum processes in a two-mode laser field*, Zh. Éksp. Teor. Fiz. **117** (1999), 476–488, [JETP **90**, 415 (2000)].

[127] N. B. Narozhnyĭ and M. S. Fofanov, *Photon emission by an electron in a collision with a short focused laser pulse*, Zh. Éksp. Teor. Fiz. **110** (1996), 26–46, [JETP **83**, 14 (1996)].

[128] H. H. Nickle and B. L. Beers, *Algebraic solution of the Klein-Gordon equation*, J. Phys. A **5** (1972), 1658–1663.

[129] A. I. Nikishov and V. I. Ritus, *Quantum processes in the field of a plane electromagnetic wave and in a constant field. I*, Zh. Éksp. Teor. Fiz. **46** (1964), 776–796, [Sov. Phys. JETP **19**, 529 (1964)].

[130] V. P. Oleĭnik, *Resonance effects in the field of an intense laser beam*, Zh. Éksp. Teor. Fiz. **52** (1967), 1049–1067, [Sov. Phys. JETP **25**, 697 (1967)].

[131] ———, *Resonance effects in the field of an intense laser ray II*, Zh. Éksp. Teor. Fiz. **53** (1967), 1997–2011, [Sov. Phys. JETP **26**, 1132 (1968)].

[132] J. Oliver, *The numerical solution of linear recurrence relations*, Num. Math. **11** (1968), 349–360.

[133] F. W. J. Olver, *Asymptotics and special functions*, A K Peters ed., A K Peters, Natick, Massachusetts, 1997.

[134] T. Omori, M. Fukuda, T. Hirose, Y. Kurihara, R. Kuroda, M. Nomura, A. Ohashi, T. Okugi, K. Sakaue, T. Saito, J. Urakawa, M. Washio, and I. Yamazaki, *Efficient propagation of polarization from laser photons to positrons through Compton scattering and electron-positron pair creation*, Phys. Rev. Lett. **96** (2006), 114801 (1–4).

[135] H. Onozawa, T. Mishima, T. Okamura, and H. Ishihara, *Quasinormal modes of maximally charged black holes*, Phys. Rev. D **53** (1996), 7033–7040.

[136] I. Øverbø, K. J. Mork, and H. A. Olsen, *Pair production by photons: Exact calculation for unscreened atomic field*, Phys. Rev. A **8** (1973), 668–685.

[137] W. A. Paciorek and G. Chapuis, *Generalized Bessel functions in incommensurate structure analysis*, Acta Cryst. **A50** (1994), 194–203.

[138] P. Panek, J. Z. Kamiński, and F. Ehlotzky, *Laser-induced Compton scattering at relativistically high radiation powers*, Phys. Rev. A **65** (2002), 022712 (1–8).

[139] ———, *Relativistic electron-atom scattering in an extremely powerful laser field: Relevance of spin effects*, Phys. Rev. A **65** (2002), 033408 (1–8).

[140] ———, *Analysis of resonances in Møller scattering in a laser field of relativistic radiation power*, Phys. Rev. A **69** (2004), 013404 (1–9).

[141] M. E. Peskin and D. V. Schroeder, *An introduction to quantum field theory*, Westview Press, 1995.

[142] V. S. Popov, *Production of e^+e^- pairs in an alternating external field*, Pis'ma v. Zh. Éksp. Teor. Fiz. **13** (1971), 261–263, [JETP Lett. **13**, 185 (1971)].

[143] ———, *Schwinger mechanism of electron-positron pair production by the field of optical and x-ray lasers in vacuum*, Pis'ma v. Zh. Éksp. Teor. Fiz. **74** (2001), 151–156, [JETP Lett. **74**, 133 (2001)].

[144] W. H. Press, B. P. Flannery, S. A. Teukolsky, and W. T. Vetterling, *Numerical Recipes: The art of scientific computing*, Cambridge University Press, Cambridge, 1986.

[145] L. Råde and B. Westergren, *Mathematics Handbook*, fourth ed., Studentlitteratur, Lund, Sweden, 1998.

[146] J. Rafelski, L. P. Fulcher, and A. Klein, *Fermions and bosons interacting with arbitrarily strong external fields*, Phys. Rep. **38** (1978), 227–361.

[147] H. R. Reiss, *Absorption of light by light*, J. Math. Phys. **3** (1962), 59–67.

[148] ———, *Effect of an intense electromagnetic field on a weakly bound system*, Phys. Rev. A **22** (1980), 1786–1813.

[149] H. R. Reiss and J. H. Eberly, *Green's function in intense-field electrodynamics*, Phys. Rev. **151** (1966), 1058–1066.

[150] H. R. Reiss and V. P. Krainov, *Generalized Bessel functions in tunneling ionization*, J. Phys. A **36** (2003), 5575–5585.

[151] A. Ringwald, *Pair production from vacuum at the focus of an X-ray free electron laser*, Phys. Lett. B **510** (2001), 107–116.

[152] V. I. Ritus, *Radiative corrections in quantum electrodynamics with intense field and their analytical properties*, Ann. Phys. (N.Y.) **69** (1972), 555–582.

[153] ———, *Vacuum polarization correction to elastic electron and muon scattering in an intense field and pair electro- and muoproduction*, Nucl. Phys. B **44** (1972), 236–252.

[154] ———, *Quantum effects of the interaction of elementary particles with an intense electromagnetic field*, Trud. Ord. Len. Fiz. Inst. im. P. N. Leb. Akad. Nauk SSSR **11** (1979), 5–151, [J. Rus. Laser Res. **6**, 497 (1985)].

[155] S. P. Roshchupkin, *Resonance effects with the photoproduction of electron-positron pairs in the field of a plane electromagnetic wave*, Izv. Vyssh. Uchebn. Zaved., Fiz. **No. 8** (1983), 12–15, [Rus. Phys. J. **26**, 683 (1983)].

[156] ———, *Spontaneous bremsstrahlung with electron scattering in the field of a plane electromagnetic wave*, Izv. Vyssh. Uchebn. Zaved., Fiz. **No. 4** (1983), 18–22, [Rus. Phys. J. **26**, 334 (1983)].

[157] ———, *Bremsstrahlung of a relativistic electron scattered by a nucleus in a strong electromagnetic field*, Yad. Fiz. **41** (1985), 1244–1257, [Sov. J. Nucl. Phys. **41**, 796 (1985)].

[158] ———, *Resonant effects in collision of relativistic electrons in the field of a light wave*, Laser Phys. **6** (1996), 837–858.

[159] ———, *Resonant spontaneous bremsstrahlung of an electron in the field of the nucleus and two light waves*, Laser Phys. **12** (2001), 498–503.

[160] S. P. Roshchupkin and O. B. Lysenko, *Spontaneous interference bremsstrahlung effect in the scattering of a relativistic electron by a nucleus in the field of two light waves*, Zh. Éksp. Teor. Fiz. **116** (1999), 1210–1240, [JETP **89**, 647 (1999)].

[161] Y. I. Salamin, S. X. Hu, K. Z. Hatsagortsyan, and C. H. Keitel, *Relativistic high-power laser-matter interactions*, Phys. Rep. **427** (2006), 41–155.

[162] F. Sauter, *Über das Verhalten eines Elektrons im homogenen elektrischen Feld nach der relativistischen Theorie Diracs*, Z. Phys **69** (1931), 742–764.

[163] S. Schnez, *Bremsstrahlung in a circularly polarized laser field*, Master's thesis, Univ. of Heidelberg, 2006.

[164] S. Schnez, E. Lötstedt, U. D. Jentschura, and C. H. Keitel, *Laser-assisted bremsstrahlung for circular and linear polarization*, Phys. Rev. A **75** (2007), 053412 (1–12), also in Virtual Journal of Ultrafast Science, June 2007.

[165] J. Schwinger, *On gauge invariance and vacuum polarization*, Phys. Rev. **82** (1951), 664–679.

[166] J. H. Shirley, *Solution of the Schrödinger equation with a Hamiltonian periodic in time*, Phys. Rev. **138** (1965), B979–B987.

[167] P. Sieczka, K. Krajewska, J. Z. Kamiński, P. Panek, and F. Ehlotzky, *Electron-positron pair creation by powerful laser-ion impact*, Phys. Rev. A **73** (2006), 053409 (1–9).

[168] N. Szpak, *On the problem of "spontaneous pair creation" in strong electric fields*, Nucl. Instrum. Meth. B **205** (2003), 30–35.

[169] C. Szymanowski, V. Véniard, R. Taïeb, A. Maquet, and C. H. Keitel, *Mott scattering in strong laser fields*, Phys. Rev. A **56** (1997), 3846–3859.

[170] G. J. Troup and H. S. Perlman, *Pair production in a vacuum by an alternating field*, Phys. Rev. D **6** (1972), 2299–2299.

[171] I. Tsohantjis, S. Moustaizis, and I. Ploumistakis, *On electron-positron pair production using a two level on resonant multiphoton approximation*, Phys. Lett. B **650** (2007), 249–256.

[172] D. M. Volkov, *Über eine Klasse von Lösungen der Diracschen Gleichung*, Z. Phys. **94** (1935), 250–260.

[173] Vulcan Glass Laser, `http://www.clf.rl.ac.uk/Facilities/vulcan/laser.htm`, Accessed 04-02-2008.

[174] G. N. Watson, *A treatise on the theory of Bessel functions*, second ed., Cambridge University Press, Cambridge, 1995.

[175] J. Wimp, *Computation with recurrence relations*, first ed., Pitman Advanced Publishing Program, Boston, London, Melbourne, 1984.

[176] V. P. Yakovlev, *Electron-positron pair production by a strong electromagnetic wave in the field of a nucleus*, Zh. Éksp. Teor. Fiz. **49** (1965), 318–328, [Sov. Phys. JETP **22**, 223 (1966)].

[177] ———, *Incoherent electromagnetic wave scattering in a Coulomb field*, Zh. Éksp. Teor. Fiz. **51** (1966), 619–627, [Sov. Phys. JETP **24**, 411 (1967)].

[178] T. Yamazaki and J. M. Hollander, *Measurement of pair-production cross section near threshold*, Phys. Rev. **140** (1965), B630–B637.

[179] V. Yanovsky, V. Chvykov, G. Kalinchenko, P. Rousseau, T. Planchon, T. Matsuoka, A. Maksimchuk, J. Nees, G. Cheriaux, G. Mourou, and K. Krushelnick, *Ultra-high intensity- 300-TW laser at 0.1 Hz repetition rate*, Opt. Express **16** (2008), 2109–2114.

[180] S. Zakowicz, *Square-integrable wave packets from the Volkov solutions*, J. Math. Phys. **46** (2005), 032304 (1–24).

[181] F. Zhou and L. Rosenberg, *Bremsstrahlung in laser-assisted scattering*, Phys. Rev. A **48** (1993), 505–515.

Acknowledgements

First of all I would like to express my gratitude to Professor Christoph H. Keitel for accepting me as a PhD student and letting me work in his group on the highly interesting topic of laser-matter interaction, and for stimulating discussions about physics, especially about the importance of intuitive explanations. The stimulating atmosphere in his group at the Max-Planck-Institute for Nuclear Physics (MPI-K) surely contributed to this thesis a lot. A close to perfect working environment, both in terms of computing facilities and of inspiring discussions with group members working in the same field was crucial to the completion of this thesis.

Secondly, I would like to thank Privatdozent Ulrich D. Jentschura for the continuous guidance and support during the whole period of PhD training. I never cease to be impressed by your scientific broadness.

Thanks to Mrityunjay for the curry and for all that you taught me about your clusters, thanks to Antonino Di Piazza for valuable comments on the thesis, to Antonino, Carsten Müller and Professor Alexander I. Milstein, for discussions about strong-field QED, thanks Peter Brunner for the support with the computers. I acknowledge Stephan Schnez for the collaboration on laser-assisted bremsstrahlung, and I am grateful to librarian Gernot Vogt for quickly providing all the books and articles I requested. The working atmosphere in our room was pleasant thanks to my room mates Atif, Henrik, Elmar, Hossein, Bastian, Carlus, Benedikt, and thanks also Ciprian Chirilă for first showing me the useful integration algorithm of Evans [64]. For typesetting the thesis the LaTeX template provided by Martin Haas was very helpful, thanks Martin also for the advice on the administrative procedures of the PhD exam.

Last, but not least, my family: Miyuki, Leo and Noah, and my mother and father. Thank you!